Electric Microfield Distributions and Structure Factors in Dense Plasmas

D I S S E R T A T I O N

zur Erlangung des akademischen Grades

doctor rerum naturalium
(Dr. rer. nat)
im Fach (Physik)

eingereicht an der
Mathematisch-Naturwissenschaftlichen Fakultät I
der Humboldt Universität zu Berlin

von
M. Sc. Saltanat Polatovna Sadykova

Präsident der der Humboldt Universität zu Berlin:
Prof. Dr. Jan-Hendrik Olbertz

Dekan der Mathematisch-Naturwissenschaftlichen Fakultät I:
Prof. Dr. Andreas Herrmann

Gutachter:
1. Prof. Dr. W. Ebeling
2. Prof. Dr. I. M. Sokolov
3. Acad. Prof. Dr. A. A. Rukhadze

eingereicht am: 03.01.2010
Tag der mündlichen Prüfung: 30.03.2011

I dedicate this Work
to my Family and my Friends

Abstract

In this Ph.D. thesis we study the electric microfield distributions (EMDs) and its tails for electron, electron-positron, hydrogen H^+ and single-ionized alkali (Li^+, Na^+, K^+, Rb^+, Cs^+) plasmas in a frame of different pseudopotential models. We also study the static and dynamic structure factors for alkali and Be^{2+} plasmas. We pay special attention to inclusion of the ion shell structure into the studied phenomena.

We have calculated the EMDs for electron-positron plasmas at the location of an electron and a neutral point, for hydrogen and single-ionized alkali two-component plasmas (TCP) at the location of an ion and for electron one-component plasmas (OCP) at the location of an electron and a neutral point. The theoretical methods used for calculation of EMDs are a coupling-parameter integration technique developed by C. A. Iglesias (Iglesias, 1983) for OCP and the generalized coupling-parameter integration technique proposed by J. Ortner et al. (Ortner et al., 2000) for TCP. We studied the EMDs in a frame of the screened Kelbg, Deutsch, Hellmann-Gurskii-Krasko (HGK) pseudopotential models which take into account quantum-mechanical (diffraction, quantum symmetry effects, Pauli exclusion principle) and screening effects. The screened HGK model takes into account the ion shell structure due to the Pauli exclusion principle (Sadykova et al., 2009a). The repulsive part of the HGK pseudopotential reflects important features of the ion shell structure. The screening effects were introduced on a base of Bogoljubov's works (Bogoljubov-Born-Green-Kirkwood-Yvon (BBGKY)) described in (Bogoljubov, 1946, 1962). We used the screened HGK pseudopotential in the Debye approximation as well as in a higher order screening approximation valid also for a moderately coupled plasma, both were derived in (Sadykova et al., 2009a). The moderately coupled plasma approximation compared to the Debye approximation makes a considerable improvement in the EMD calculation at moderate magnitudes of ion-ion coupling parameter Γ_{ii}. We have derived a new type of the screened HGK pseudopotential, where for electron-electron interaction we used the corrected Kelbg micro-pseudopotential instead of earlier applied Deutsch micro-pseudopotential. We have obtained the analytical expressions for the screened Deutsch pseudopotentials (Arkhipov et al., 2000) through the inverse Fourier transformation in "r"-space neglecting the symmetry effects and ionic screening. The influence of the coupling parameter on the EMD along with the ion shell structure was investigated. For comparison the corresponding EMDs for H^+-plasmas were given too. In this case no ion shell exists and we may see clearly the influence of the shell structure. We have performed the Molecular Dynamics and Monte-Carlo simulations of nonideal electron-positron, hydrogen and alkali TCPs as well as electron OCPs and determined the EMDs measured at an electron, ion and at a neutral point as depending on the electron-electron coupling parameter Γ_{ee} in the range $0.2 \leq \Gamma_{ee} \leq 2$ at $T = 30\,000$ K. The results were found in a good agreement with the Monte-Carlo and Molecular Dynamics simulation results. We pay a special attention to the behaviour of the distribution tails. We show that at low $\Gamma_{ee} \ll 1$ the tails of the EMDs at an electron in OCP, TCP and at an ion in TCP follow a pattern compatible with the Levy-type of distribution ($P(\beta) \sim \beta^{-\alpha-1}$). The tails of the EMDs at a neutral point at $\Gamma_{ee} \leq 2$ follow a pattern compatible with the Holtsmark one ($\alpha = 3/2$) also belonging to the Levy-type of distribution. At higher values of Γ_{ee} and higher fields $\beta >> 1$ the tails of EMDs at an electron in electron and electron-positron plasmas as well as at an ion in hydrogen plasma are considerably fatter and follow the modified power-exponential Potekhin form (Sadykova et al., 2009b) whereas in alkali plasmas the relatively fast decay is observed which follow the power-exponential Potekhin form (Potekhin et al., 2002). At values

$0.2 \leq \Gamma_{ee} \leq 1.2$ the tails measured at an electron in electron-positron plasma can be roughly approximated by the decay exponents ($\alpha' = \alpha + 1$) corresponding to the Levy-type of distribution changing from -2.2 to -1.8 with increasing Γ_{ee}.

Comparison of a synthetic Li^{2+}-Lyman spectrum at $T = 300\,000$ K and $n_e = 4 \cdot 10^{19}$ cm^{-3} (Lorenzen et al., 2008, 2009) with experimental data (Schriever et al., 1998a) as well as comparison of a synthetic Li^+ (Li II 548 nm) line at $T = 38\,527$ K and $n_e = 0.22 \cdot 10^{18}$ cm^{-3} (Koubiti et al., 2011) with the experimental data (Doria et al., 2006) allows us to conclude that the EMD, as an input value of the line profile, obtained in the present work on a base of C. A. Iglesias method for OCP within the HGK pseudopotential model and Molecular Dynamics, provides a good agreement with the experiment.

We have calculated the electron-electron, electron-ion, ion-ion and charge-charge static structure factors for alkali Li^+, Na^+, K^+, Rb^+, Cs^+ (at $T = 30\,000$ K, 60 000 K, $n_e = 0.7 \cdot 10^{21} \div 1.1 \cdot 10^{22}$ cm^{-3}) and Be^{2+} (at $T = 20$ eV, $n_e = 2.5 \cdot 10^{23}$ cm^{-3}) plasmas using the method described by G. Gregori et al. (Gregori et al., 2006b, 2007). We have calculated the dynamic structure factors for alkali plasmas at $T = 30\,000$K, $n_e = 1.74 \cdot 10^{20}$, $1.11 \cdot 10^{22}$ cm^{-3} using the method of moments developed by V. M. Adamyan et al. (Adamyan and Tkachenko, 1983; Adamjan et al., 1993). In both methods the screened HGK pseudopotential has been used. Our results on the static structure factors for Be^{2+} plasma deviate from the data obtained by G. Gregori et al., while our dynamic structure factors are in a reasonable agreement with those of S. V. Adamjan et al. determined within the Coulomb hydrogen-like point charges potential model: at higher values of k and with increasing k the curves damp down while at lower values of k, and especially at higher electron coupling, we observe sharp peaks also reported in the mentioned work. For lower electron coupling the dynamic structure factors of alkali plasmas do not differ while at higher electron coupling these curves split. As the number of shell electrons increases from Li^+ to Cs^+ the curves shift in the direction of low absolute value of ω and their heights diminish. We conclude that the short range forces, which we take into account by means of the HGK pseudopotential, which deviates from the Coulomb and Deutsch ones, influence the static and dynamic structure factors significantly.

Zusammenfassung

Diese Doktorarbeit widmet sich den elektrischen Mikrofeldverteilungen (EMDs) und ihren Auswüchsen in Elektron-, Elektron-Positron-, Wasserstoff-H^+ und einwertig ionisierten Alkaliplasmen (Li^+, Na^+, K^+, Rb^+, Cs^+) im Rahmen verschiedener Pseudopotentialmodelle. Außerdem untersuchen wir die statischen und dynamischen Strukturfaktoren in Alkali- und Be^{2+}-Plasmen. Wir konzentrieren uns insbesondere darauf, die Ionenrümpfe in die untersuchten Phänomene einzubeziehen.

Die EMDs sind für Elektron-Positron-Plasmen an der Stelle eines Elektrons und an einer neutralen Stelle, für Wasserstoff und einwertig ionisierte zweikomponentige (TCP) Alkaliplasmen an der Stelle eines Ions und für einkomponentige (OCP) Elektronenplasmen an der Stelle eines Elektrons und an einer neutralen Stelle berechnet worden. Die verwendeten theoretischen Verfahren zur Berechnung von EMDs gehen zurück auf die von C. A. Iglesias (Iglesias, 1983) entwickelte Kopplungsparameter Integrationstechnik für OCP und die von J. Ortner et al. (Ortner et al., 2000) vorgeschlagene verallgemeinerte Kopplungsparameter Integrationstechnik für TCP. EMDs wurden im Rahmen der abgeschirmten Kelbg-, Deutsch-, Hellmann-Gurskii-Krasko-Pseudopotenialmodelle untersucht, welche quantenmechanische (Beugung, quantensymmetrische Effekte, Paulisches Ausschlussprinzip) und Abschirmungseffekte berücksichtigen. Das abgeschirmte HGK-Pseudopotenialmodell berücksichtigt außerdem die Struktur der Ionenrümpfe auf Grund des Paulischen Ausschlussprinzips (Sadykova et al., 2009a). Der abstoßende Teil des HGK-Pseudopotenials spiegelt wichtige Eigenschaften der ionischen Rumpfstruktur wider. Die Abschirmungseffekte wurden auf Grundlage der Arbeiten von Bogoljubov (Bogoljubov-Born-Green-Kirkwood-Yvon (BBGKY)) eingeführt, in (Bogoljubov, 1946, 1962) beschrieben. Wir haben das abgeschirmte HGK-Pseudopotential in der Debye-Näherung sowie eine Abschirmungsnäherung in höherer Ordnung verwendet, welche auch für mäßig gekoppelte Plasmen gültig ist; beide sind in (Sadykova et al., 2009a) hergeleitet worden. Im Vergleich zur Debye-Näherung sorgt die mäßig gekoppelte Plasma-Näherung zu einer beträchtlichen Verbesserung in der EMD Berechnung bei mittelgroßen Ion-Ion-Kopplungsparametern Γ_{ii}. Wir haben eine neue Art von abgeschirmtem HGK-Pseudopotential hergeleitet, bei dem wir für die Elektron-Elektron-Wechselwirkung statt dem zuvor angewendeten Deutsch-Mikro-Pseudopotential das korrigierte Kelbg-Mikro-Pseudopotential verwendet haben. Für das abgeschirmte Deutsch-Pseudopotential (Arkhipov et al., 2000) haben wir die analytischen Ausdrücke durch inverse Fouriertransformation im "r"-Raum unter Vernachlässigung der Symmetrieeffekte und der ionischen Abschirmung erhalten. Der Einfluss des Kopplungsparameters auf die EMDs zusammen mit der ionischen Rumpfstruktur wurde untersucht. Zum Vergleich wurden auch die entsprechenden EMDs für H^+-Plasmen gezeigt. In diesem Fall existiert kein Ionenrumpf und wir können deutlich den Einfluss der Rumpfstruktur erkennen. Wir haben die Molekulardynamik und Monte-Carlo Simulationen von nicht idealen Elektron-Positron-, Wasserstoff- und Alkali-TCPs sowie Elektron-OCPs durchgeführt und die Abhängigheit vom Elektro-Elektron-Kopplungsparameter Γ_{ee} im Bereich $0.2 \leq \Gamma_{ee} \leq 2$ bei $T = 30\,000$ K der an der Stelle eines Elektrons, eines Ions und an einer neutralen Stelle gemessenen EMDs bestimmt. Die Ergebnisse stimmen mit den Simulationsergebnissen aus der Molekulardynamik und Monte-Carlo gut überein. Wir legen unseren Fokus insbesondere auf das Verhalten der Verteilungsauswüchse. Wir zeigen, daß für niedrige $\Gamma_{ee} \ll 1$ die Auswüchse der EMDs bei einem Elektron in OCP, TCP und bei einem Ion in TCP einem Muster folgen, welches zu den Levyformigen Verteilungen ($P(\beta) \sim \beta^{-\alpha-1}$) gehört. Die Auswüchse der EMDs an einer neutralen Stelle für $\Gamma_{ee} \leq 2$ folgen einem Muster, welches zu Holtsmark passt ($\alpha = 3/2$), das ebenfalls zu den Levyformigen

Verteilungen gehört. Für höhere Γ_{ee}-Werte und höhere Felder ($\beta >> 1$) die Auswüchse der EMDs bei einem Elektron in Elektron- und Elektron-Positron-Plasmen und einem Ion in Wasserstoffplasma beträchtlich dicker sind und der modifizierten Potenz-Exponential Potekhin-Form (Sadykova et al., 2009b) folgen, wohingegen in Alkaliplasmen ein relativ schneller Abfall beobachtet wird, welcher der Potenz-Exponential Potekhin-Form (Potekhin et al., 2002) folgt. Für $0.2 \leq \Gamma_{ee} \leq 1.2$-Werte können die bei einem Elektron in Elektron-Positron-Plasma gemessenen Auswüchse grob durch die Abfallexponenten ($\alpha' = \alpha + 1$) entsprechend der Levyformigen Verteilung genähert werden, welche sich von -2.2 bis -1.8 mit anwachsenden Γ_{ee} ändern.

Der Vergleich der experimentell gewonnenen Daten (Schriever et al., 1998a) mit sowohl einem synthetischen Li^{2+}-Lyman-Spektrum bei $T = 30\,0000$ K und $n_e = 4 \cdot 10^{19}$ cm^{-3} (Lorenzen et al., 2008, 2009) als auch mit einer synthetischen Li^+ (Li II 548 nm) Linie bei $T = 38\,527$ K und $n_e = 0.22 \cdot 10^{18}$ cm^{-3} (Koubiti et al., 2011) lassen den Schluss zu, daß die EMD als ein Eingabewert für das Linienprofil, welche in der vorliegenden Arbeit auf der Grundlage der Iglesias-Methode im HGK-Pseudopotentialmodell und der Molekulardynamik erhalten wurde, eine gute Übereinstimmung mit den experimentellen Werten liefert.

Die statischen Elektron-Elektron-, Elektron-Ion-, Ion-Ion-, und Ladung-Ladung-Strukturfaktoren wurden für Alkali- Li^+, Na^+, K^+, Rb^+,Cs^+ ($T = 30\,000$ K, $60\,000$ K, $n_e = 0.7 \cdot 10^{21} \div 1.1 \cdot 10^{22}$ cm^{-3}) und Be^{2+}- ($T = 20$ eV, $n_e = 2.5 \cdot 10^{23}$ cm^{-3}) Plasmen unter Verwendung der von G. Gregori et al. (Gregori et al., 2006b, 2007) beschriebenen Methode berechnet. Die dynamischen Strukturfaktoren für Alkaliplasmen wurden bei $T = 30\,000$K, $n_e = 1.74 \cdot 10^{20}$, $1.11 \cdot 10^{22}$ cm^{-3} unter Verwendung der durch V. M. Adamyan et al. (Adamyan and Tkachenko, 1983; Adamjan et al., 1993) entwickelten Methode der Momente berechnet. Bei beiden Methoden wurde das abgeschirmte HGK-Pseudopotential verwendet. Unsere Ergebnisse für die statischen Strukturfaktoren für Be^{2+}-Plasmen weichen von den Werten ab, die G. Gregori et al. erhalten haben, während unsere dynamischen Strukturfaktoren in ordentlicher Übereinstimmung mit denen von S.V. Adamjan et al., die auf der Basis des Coulombschen Wasserstoffähnlichen Punktladungsmodells bestimmt wurden, sind: fur höhere Werte von k und mit wachsenden k werden die Kurven gedämpft, während wir für niedrige Werte von k und insbesondere bei höherer Elektronenkopplung scharfe Spitzen beobachten, die auch in der besagten Arbeit erwähnt wurden. Bei niedrigerer Elektronenkopplung weichen die dynamischen Strukturfaktoren von Alkaliplasmen nicht ab, während sich bei höherer Elektronenkopplung diese Kurven aufteilen. Wenn die Anzahl an Rumpf-Elektronen von Li^+ to Cs^+ anwächst, verschieben sich die Kurven in Richtung kleiner absoluter ω-Werte und ihre Höhen verringern sich. Wir folgern, daß die kurzreichweitigen Kräfte, welche wir unter Zuhilfenahme des HGK-Pseudopotentials berücksichtigen, des von der Coulomb-Potential und Deutsch-Pseudopotential abweichenden HGK-Pseudopotentials die statischen und dynamischen Strukturfaktoren beträchtlich beeinflussen.

Contents

Contents **ix**

1 Introduction **1**
1.1 Some facts about plasma and its parameters 1
1.2 Electric microfield distributions 4
1.3 The static and dynamic structure factors 10

2 Electric microfield distributions **13**
2.1 Holtsmark distribution 13
2.1.1 One-component plasma 13
2.1.2 Two-component plasma 16
2.1.3 The second moment 17
2.1.4 The asymptotics of the Holtsmark distribution. The Holtsmark tail 17
2.2 One-component plasma model 18
2.2.1 The second moment 22
2.3 Two-component plasma model 24
2.3.1 The second moment 29
2.3.2 The tails 30

3 Electric microfield distributions in electron one-component plasmas and mass-symmetrical electron-positron two-component plasmas **33**
3.1 Pseudopotential models for point charges one-component and two-component plasmas. Screened Deutsch, Kelbg and generalized Kelbg models 33
3.2 EMDs at a charged and neutral particles in OCPs 46
3.3 Electric microfield distributions at a charged and a neutral particles in electron-positron two-component plasmas 47
3.3.1 Molecular dynamics simulations 49
3.4 The tails 54
3.5 Conclusions 56

4 Electric microfield distributions in electron-ion two-component plasmas with an account of the ion shell structure **59**
4.1 Taking into account the ion shell structure and plasma screening effects 59
4.1.1 Pseudopotential models taking into account the ion shell structure. Hellmann-Gurskii-Krasko pseudopotential 59
4.1.2 The screened Hellmann-Gurskii-Krasko pseudopotential obtained with the help of electron-electron Deutsch and electron-ion, ion-ion Hellmann-Gurskii-Krasko micro-pseudopotentials 66

4.1.3 The screened Hellmann-Gurskii-Krasko pseudopotential obtained with the help of electron-electron generalized Kelbg and electron-ion, ion-ion Hellmann-Gurskii-Krasko micro-pseudopotentials . . 73
4.2 Electric microfield distributions at an ion in alkali two-component plasmas with an account of the ion shell structure 76
4.2.1 The tails 79
4.3 Electric microfield distributions in a moderately coupled plasma approximation 86
4.4 Conclusions 87

5 Comparison of electric microfield distributions with the experimental optic Li^{2+} and Li^{+} data 91
5.1 Theory of line broadening for Li^{2+} plasma 92
5.2 Formalism of Stark broadening for Li^{+} plasma 94
5.3 Comparison with measurements from laser-produced plasmas 95

6 Static and dynamic structure factors with an account of the ion shell structure for high-temperature alkali and alkaline earth plasmas 101
6.1 Static structure factors 101
6.1.1 Thermal equilibrium plasmas 101
6.1.2 Static structure factors for two temperature plasmas 102
6.2 The dynamic structure factor: the moment approach 105
6.2.1 Taking into account the ion shell structure 110
6.3 Conclusions 113

7 Summary 117

Appendix 123

Bibliography 129

List of Figures 139

List of Tables 143

1 Introduction

1.1 Some facts about plasma and its parameters

Plasma is called the fourth state of matter. The other states are solids, liquids, and gases. Over 99% of the universe is believed to be plasma. Atoms and molecules, constituting the ordinary matter, are made up of nuclei and electrons. An electron has a negative charge ($e = 1.602176487(40) \cdot 10^{-19}$ Coulombs (C)). Ions produced by removing some or all of the orbital electrons become positively charged. A system of many such free charged particles forms a plasma.

Matter in the plasma state spans a wide range of physical regimes and phenomena including *electric discharges*, metals, semiconductors, the core, corona of the sun, white dwarfs, interstellar space, magnetic and inertial fusion, ionosphere etc. Plasmas can be produced in the laboratory by electric discharge. When a strong electric field is applied to an ordinary gas, charged particles in it get accelerated and ionize these neutral particles. Those newly born ions and electrons in its turn ionize other neutral particles by collisions leading to an avalanche. The electric discharge is found commonly in our daily life such as in the fluorescent lamp, neon tube, and arc welding.

Without using an electric discharge, a plasma state may be attained by simply raising the temperature of a neutral gas and thermal ionization occurs.

Metals or *semiconductors* contain relatively mobile free charged particles. For instance, one can find conduction electrons in metal forming a quantum-mechanically degenerate plasma at a density of approximately 10^{23} cm^{-3}. A semiconductor contains substantially smaller number of mobile electrons and holes compared to metals.

Today, there is a high interest in the *controlled thermonuclear fusion* induced by the search for a new alternative source of energy. There are two types of it: *inertial confinement fusion* (ICF) and *magnetic confinement fusion* (MCF) (Tokamak, Stellarator). The energy can be produced through the release of energy during the fusion process between light nuclei of hydrogen isotopes such as deuterium and tritium. In order to induce the nuclear fusion reactions, the Coulomb repulsive forces must be overcome by vigorous collisions between the nuclei. The minimum conditions for net production of energy by a magnetic confinement scheme are estimated to be dense, high-temperature plasmas of 10^{14} to 10^{15} cm^{-3} and $\sim 10^8$ K held for more than one second (Ichimaru, 1992).

Above the surface of the Earth, layers of ionized gas, called the *ionosphere*, exist at altitude of 70 to 500 km over the stratosphere. The highest electron density can be found at the upper layers and its value is approximately 10^6 cm^{-3}, and electron temperature is about 2000 K. However, these values depend on seasons and solar activities.

The Sun itself is an important source of plasma. It has a region containing *solar atmosphere* called the *chromosphere* ($\sim$ 2000 km in depth). The average electron density of such plasma is from 10^{10} cm^{-3} to 10^{11} cm^{-3} and temperature $\sim$ 6000 K. Above the chromosphere a large region of corona extends. At 10^5 km from the solar surface, the

electron density and temperature are estimated as 10^8 cm^{-3} and 10^6 K; at 10^6 km, they are 10^6 cm^{-3} and 10^6 K respectively.

The interior of a *white dwarfs*, one of the final stages of stellar evolution, consists of dense matter with electron density 10^{25} cm^{-3} to 10^{32} cm^{-3}, and temperature 10^7 to 10^8 K. At such high density the plasma is degenerate and strongly correlated.

Finally, we mention the *interstellar space* among the stars. This plasma is dilute and the typical electron densities range is from 10^{-2} cm^{-3} to 10^1 cm^{-3}, and the temperature $\sim 10^4$ K.

As a summary we show a schematic presentation of the parameter domains for described above plasmas in Fig. 1.1.

As we have overviewed above, the plasmas found in nature or in the laboratory are characterized by a wide range of temperature and density parameters revealing various physical properties. Plasma is considered to consist of nonrelativistic electrons (density n_e, mass m_e, temperature T_e) and $z-$times charged ions (density n_i, mass m_i, temperature T_i). Short range interactions effects as well as radiation effects are not taken into account. Let the plasma be fully ionized, enclosed in a volume Ω and be in a thermal equillibrium with temperature T. Let us define a *Coulomb coupling* constant or *nonideality parameter* of a plasma as a ratio of an overage Coulomb- interaction energy to an average kinetic energy, here the word "Coulomb" is usually skipped. There are different types of the coupling parameters like electron-electron coupling representing the ratio of average electron potential energy $e^2/(4\pi\varepsilon_0 r_{ee})$ to average kinetic energy $k_B T$ for electrons separated by the mean electron-electron distance r_{ee} or the Wigner-Seitz radius. The temperature is assumed to be the same for every species. Correspondingly, the ion-ion and electron-ion coupling parameters represent the ratio of average potential energy $z^2e^2/(4\pi\varepsilon_0 r_{ii})$, $ze^2/(4\pi\varepsilon_0 r_{ei})$ to average kinetic energy $k_B T$ for ions and electron-ions separated by the mean ion-ion, electron-ion distances r_{ii}, r_{ei}. Concluding, the generalized form of the Coulomb coupling parameter takes the form

$$\Gamma_{ab} = \frac{|z_a e \cdot z_b e|}{4\pi\varepsilon_0 r_{ab} k_B T}, \tag{1.1}$$

where the the Wigner-Seitz radius defined as

$$r_{ab} = \left(\frac{4\pi n_a}{3}\right)^{-1/3}, \tag{1.2}$$

a, $b = e$, i, $z_e = -1$, $z_i = z$ and for r_{ei} the total density $n = n_e + n_i$ is considered. Those plasmas with values $\Gamma_{ab} << 1$ may be called weakly coupled or ideal plasmas. Plasmas in this regime have weak particle-particle correlations and are dominated by the thermal properties. For example, the gaseous-discharge plasma, a controlled thermonuclear-fusion experiment and the solar corona have $\Gamma_{ii} \approx 10^{-3}$, 10^{-5}. Moderately coupled plasmas are characterized by $\Gamma_{ab} \lesssim 1$, whereas the strongly coupled plasmas - by $\Gamma_{ab} > 1$. In this regime, the particle correlations play a crucial role. Strong ion-ion and electron-ion correlations influence the dynamical properties that can affect important atomic, radiative, and nuclear processes in the medium (Kraeft et al., 1986). Such plasmas can be found in interiors of highly evolved stars like white dwarfs, neutron stars ($\Gamma_{ii} = 10$ to 200).

One of the common classical plasma length is the *Landau length*

$$l = \frac{e^2}{4\pi\varepsilon_0 k_B T}. \tag{1.3}$$

In plasma this length plays a role of the effective interaction radius, i.e. the distance at which two electrons have a potential energy equal to a thermal one.

Another very useful parameter representing the ratio between the Wigner-Seitz radius for electrons r_{ee} and Bohr radius $r_B = 4\pi\varepsilon_0\hbar^2/(m_e e^2) \approx 0.53\,10^{-10}$ m is a Brueckner parameter: $r_s = r_{ee}/r_B$, $\hbar = h/2\pi = 1.054571628(53)\cdot 10^{-34}$ J·s is the Planck's constant.

We shall also consider parameters describing the extents to which the quantum-mechanical effects are involved in a plasma. The lines

$$n_i\Lambda_i = 1 \text{ or } n_e\Lambda_e = 1 \tag{1.4}$$

with the thermal de Broglie wavelengths Λ_a

$$\Lambda_i = \frac{h}{\sqrt{2\pi m_i k_B T}} \text{ and } \Lambda_e = \frac{h}{\sqrt{2\pi m_e k_B T}} \tag{1.5}$$

divide the diagram Fig. 1.1 into degenerate ($n_{e(i)}\Lambda_{e(i)} >> 1$), where the system must be considered quantum-mechanically, and nondegenerate classical regions ($n_{e(i)}\Lambda_{e(i)} << 1$).

For high-density electron system such as conduction electrons in metal or matters with the corresponding density, one uses the Fermi energy $E_F = \hbar^2(3\pi^2 n_e)^{2/3}/2m_e$. Since E_F is an increasing function of n_e, $E_F >> k_B T$ can be realized in a high-density electron system.

Consider now one of the most important plasma parameters - *Debye screening length.* Debye screening illuminates the collective phenomena typical for a plasma. Consider a point charge ze located at the origin ($r = 0$) : in vacuum it produces a potential field $\varphi = ze/(4\pi\varepsilon_0 r)$. In the plasma such a potential field disturbs the spatial distribution of charged particles. The field induced around the point charge in turn produces an extra potential field, which should be added to the original potential φ; a new *effective* potential Φ is thus obtained. A calculation along these lines was originally made by Debye and Hückel (Debye and Hückel, 1923) in connection with the theory of strong electrolytes.

The Poisson equation for the total field is thus the following

$$\nabla^2\Phi(\vec{r}) = -4\pi(ze\delta(\vec{r}) + ze < \delta n(\vec{r}) >), \tag{1.6}$$

where $\delta(\vec{r})$ is the three-dimensional delta function. The average density variation $< \delta n(\vec{r}) >$ is calculated using the Boltzmann distribution:

$$< \delta n(\vec{r}) >= n \exp\left(\frac{-ze\Phi(\vec{r})}{k_B T}\right) - n, \tag{1.7}$$

where n refers to the uniform, average number density of the particles. The exponent $ze\Phi(\vec{r})/(k_B T)$ represents the ionic coupling parameter Γ_{ii} presented above. When

$\Gamma_{ii} << 1$ then we can expand the Eq. (1.7) as $< \delta n(\vec{r}) >= -zen\Phi(\vec{r})/(k_BT)$. Substitution of this into Eq. (1.6) yields a differential equation for determination of the effective potential $\Phi(\vec{r})$:

$$-\nabla^2\Phi(\vec{r}) + \frac{4\pi n z^2 e^2}{k_BT}\Phi(\vec{r}) = 4\pi ze\delta(\vec{r}), \tag{1.8}$$

The solution to this equation with the boundary condition $\Phi(\vec{r}) \to 0$, when $r \to \infty$ is

$$\Phi(r) = \frac{ze}{r}\exp\left(-\frac{r}{r_{Di}}\right) \tag{1.9}$$

The parameter

$$r_{Di} = \sqrt{\frac{4\pi\varepsilon_0 k_B T}{4\pi n_i z^2 e^2}}. \tag{1.10}$$

is called the ionic Debye length. The meaning of Eq. (1.9) is clear by comparison with the bare Coulomb potential. For distance smaller than r_{Di}, the effective potential is virtually identical to the Coulomb potential, whereas for distances $r >> r_{Di}$, $\Phi(r) \approx 0$. In other words, the potential field around a point charge is effectively screened out by the induced field for distances greater than the Debye length. If we consider only the electrons on a uniform positive background then the Debye screening length will take the following view

$$r_{De} = \sqrt{\frac{4\pi\varepsilon_0 k_B T}{4\pi n_e e^2}}. \tag{1.11}$$

The calculation of the Debye screening can be extended to cases that involve a more than one mobile charged component. Let us consider the electron-ion system. If we use a subscript a to distinguish between the species of the plasma with charges $z_a e$ and density n_a, the total Debye length of such plasma is expressed as

$$r_D = \sqrt{\frac{\varepsilon_0 k_B T}{\sum_{a=e,i} {z_a}^2 e^2 n_a}}. \tag{1.12}$$

with $z_e = -1$, $z_i = z$.

1.2 Electric microfield distributions

The Electric Microfield Distribution (EMD) is determined by the sum of elementary Coulomb fields ($\vec{E}$) created by a very large number of elementary charges at a fixed charged or neutral point contained in a fixed volume.

The distribution of electric microfields influences many elementary processes in plasma (ionization, recombination and dissociation) as well as governs a number of its optic properties. In particular, EMD at the radiating atom or ion (*radiator*) determines the Stark broadening of spectral lines, an effect widely applied in plasma diagnostics to evaluate plasma densities in stellar atmosphere or in laboratory (Griem, 1974).

The problem of determining of the electric microfield distributions (EMD) is conventionally divided into two parts due to the existence of two different time scales in a plasma. On the time scales comparable to the electron relaxation time the plasma

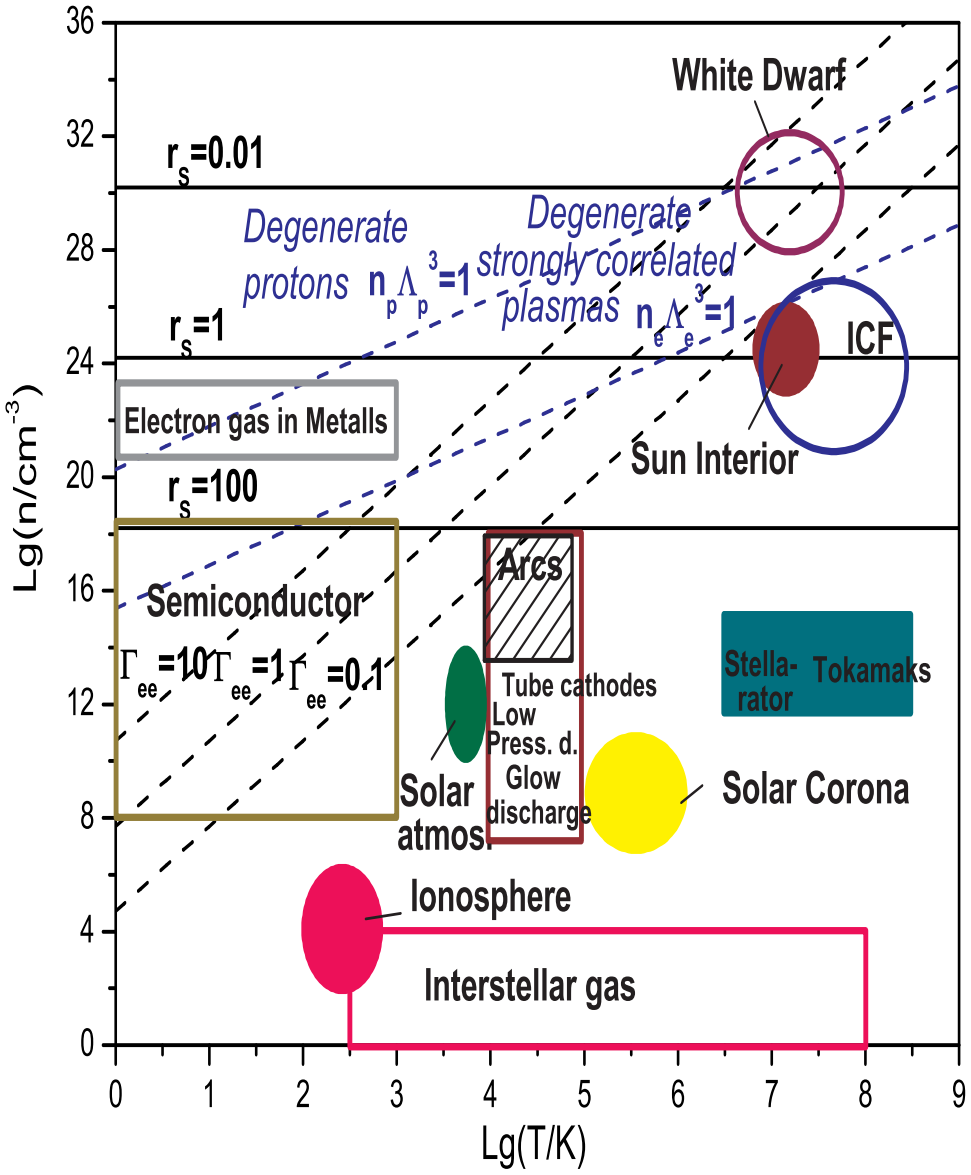

Figure 1.1: Density-temperature diagram for various plasmas in a double decimal logarithmic scale (Ichimaru, 1992), (Ebeling et al., 1976)

medium may be considered as a gas of electrons immersed in a positively charged neutralizing background of ions and, thus, the Coulomb forces act at the observation point to generate the microfield distribution. This distribution is called the *high-frequency component* of the microfield since the electron relaxation time is dramatically less in magnitude then that one of the ions. The *low-frequency component*, appearing on the scale of the ion relaxation time, is then introduced by noting that it is governed by the dynamics of ions, surrounded by electron clouds, and, consequently, the shielded Coulomb forces at the observation point should thoroughly be considered. In recent works it is argued that the low-frequency component of electric microfield also influences the fusion rates (Romanovsky and Ebeling, 1998, 2004) and the rates for the three-body electron-ion recombination in dense plasmas. For details of these applications concerning the low frequency component we refer to the recent survey in this journal (Romanovsky and Ebeling, 2006).

J. Holtsmark was the first who studied in 1919 the EMD in a plasma (Holtsmark, 1919). He considered a one-component model and completely neglected correlations between particles. The Holtsmark distribution gives the probability to find a definite value E of the electric microfield at a fixed given location in an ideal plasma. The EMD is determined by the sum of elementary fields created by a very large number of elementary point charges at a fixed neutral point. The main features of the Holtsmark distribution are the long tail with the asymptotic drop proportional to $E^{-5/2}$ and the absence of the second EMD moment which stresses the role of extreme events.

Since the pioneering work of Holtsmark who studied *one-component model* and completely neglected correlations between particles much of the efforts has been concentrated on a theory of the microfield distribution including the collective events in a plasma. In 1943 S. Chandrasekhar and von Neumann considered the probability of a stationary force in an infinite homogeneous gravitational system which is also described by the Holtsmark distribution (Chandrasekhar, 1943). S. Chandrasekhar also showed analytically that this distribution has asymptotic behaviour for E similar to the one of the field of the nearest-neighbor galaxy, which stresses that the possible non-random structure of the system would influence EMD strongly. The first remarkable advance was made by M. Baranger and B. Mozer (Baranger and Mozer, 1959; Mozer and Baranger, 1960) who wrote the distributions of high- and low-frequency components of the microfield distribution as expansions with respect to the correlation functions which then had been terminated at the pair correlation. However, it was argued that such an approach is valid only for low density, high-temperature plasmas where deviations from Holtsmark's original distribution, corresponding to the first term in the series, are not large. Afterwards, Hooper and Tighe (Hooper, 1966; Tighe and Hooper, 1976, 1977) reformulated this expansion in terms of other functions by introducing a free parameter. The disadvantage of this method is the choice of a free parameter on the basis of the vague argument arriving at a plateau where there is no dependence on the free parameter itself. To improve these results Iglesias and Hooper (Iglesias and Hooper, 1982) included in the analysis the Debye chain cluster expansion similar to that of Ursel and Mayer (Mayer and Mayer, 1940). Quite an analogous approach, now known as adjustable-parameter approximation model (APEX), was proposed by Iglesias, Lebowitz et. al. (Iglesias et al., 1983; Iglesias and Lebowitz, 1984; Iglesias et al., 1985) but the free parameter, called adjustable, had been chosen to satisfy the second moment rule for the electric field strength. In the early 1980's, following the idea of Morita on the similarity of the

representation of the microfield distribution to that of the excess chemical potential, Iglesias virtually reduced the problem to the determination of the radial distribution function (RDF) for a fictious system with an imaginary part of the interaction potential energy (Iglesias, 1983). This technique has the advantage that the knowledge of the two-body function gives the Fourier transform of the microfield distribution exactly without knowing many-body functions (Baranger and Mozer, 1959; Hooper, 1966; Tighe and Hooper, 1977). This method was used for the calculation of the high-frequency component for the so called semiclassical Deutsch model, where not only the quantum-mechanical effects of diffraction but also screening field effects were taken into account (Sadykova et al., 2004). Employing Iglesias's idea, Lado developed an integral-equation technique for calculation of the RDF and a good agreement with computer simulations was obtained. Another point of interest is the inclusion of quantum-mechanical effects. This was done by Held and co-workers at high temperatures when the Landau length (l) is smaller than the thermal de Broglie wavelength of electrons (Held et al., 1982b,a, 1985). The pseudopotential and the corresponding correlation functions were then used in the framework of the Baranger-Mozer expansion to find both a very rich picture for the microfield distribution behaviour, depending on plasma parameters region, and agreement with other approaches as well (Boercker and Dufty, 1983).

Within most of the previous calculations of electric microfield distribution, created by only one of the components, the influence of the second component was totally neglected. For the ion subsystem, in a first approximation, the electrons are assumed to move freely through the plasma. Since the electrons are much faster than ions, they are treated as a smeared negative charged background. For simplicity, this system is assumed to be in thermal equilibrium, uniform in the density and macroscopically neutral. A more realistic model should also take into account the variation of the background charge density. A background charge distribution which differs from a uniform distribution results in a screening of the ion charge, the screening strength is generally frequency dependent, meaning that it depends on the ion velocity. In a first approximation one can neglect the frequency dependence of the screening. Then one can talk of an one-component plasma model (**OCP**) model on a polarization background POCP, which is used for the description of the low frequency part (Baranger and Mozer, 1959; Mozer and Baranger, 1960; Ecker, 1957; Ecker and Müller, 1958; Gombert, 2002). However, both these models fail to include correctly the correlations between the electron and the ion subsystem. To include these correlations the *two-component plasma* model (**TCP**) will be used here.

We study here the two-component model where the correlations between the electron and the ion subsystems is taken into account. TCP model was studied earlier in works of J. Ortner et al. (Ortner et al., 2000) using the parameter integration technique in the Debye approximation, X.-Z. Yan (Yan and Ichimaru, 1986) for partially degenerate electrons, H. B. Nersisyan (Nersisyan et al., 2005, 2008) for strongly coupled plasmas. In works (Yan and Ichimaru, 1986; Nersisyan et al., 2005, 2008) the EMD at a charged and neutral particles were studied on a base of the potential-of-mean-force (PMF) approximation for electron-highly-charged-ion plasmas which exactly satisfies the second-moment sum rule without use of adjustable parameters.

Beyond new possible applications we would like to point out the following important principal statement: In any classical many-component plasma model with discrete positive and negative charged components the microfield distribution is divergent. This is due to the divergence of the fields between positive and negative point charges at

small distances. This problem can be resolved only by including quantum-mechanical effects, this will be done here based on the ideas of Kelbg, Deutsch, Krasko, Gurskii and coworkers. As a result it will be shown that the resulting distributions for the total electric field are quite similar to the Holtsmark distribution. However, to conclude that this demonstrates the irrelevance of the heavy components is completely unjustified. On the contrary, one should accept, that the one-component model, so-called OCP, is an unphysical model which describes at best limiting cases. Deviations from the Holtsmark theory we observe mainly in the region of high fields. This is exactly the region where the quantum effects incorporated into the potentials at small distances lead to a modification of the fields. We consider these arguments as a justification to concentrate on the investigation of the total field created by electrons and ions.

In this paper the free electrons and ions are also simulated numerically by a semiclassical Monte-Carlo (MC) and Molecular Dynamics methods with interactions described by pseudopotentials. The semiclassical methods allow to include the quantum-mechanical effects (the Heisenberg and the Pauli principle) by appropriate pseudopotentials which resolve divergency problem of the electric fields at small distances. This method was pioneered by Kelbg, Dunn, Broyles, Deutsch and others (Kelbg, 1964a; Dunn and Broyles, 1967; Deutsch, 1977; Minoo et al., 1981) and later significantly improved (Ebeling et al., 1999; Filinov et al., 2003; Wagenknecht et al., 2001). A number of simulations of equillibrium two-component plasmas were made (Zamalin et al., 1977; Hansen and McDonald, 1981; Pierleoni et al., 1994; Klakow et al., 1994b,a; Penman et al., 1995). These models are valid for highly temperature plasmas when the ions are bare or there is no significant influence of the *ion shell structure*. In order to correctly describe *alkali plasmas* at moderate temperatures one needs to take into account the ion shell structure. For example, for the behaviour of alkali plasmas the short range forces between the charged particles are of great importance. For alkali plasmas at small distances between the particles deviations from Coulomb law are observed which are mainly due to the influence of the core (shell) electrons. The method of model pseudopotentials describing the ion structure was pioneered by Hellmann. Hellmann demonstrated, using the Thomas-Fermi model, that the Pauli exclusion principle for the valence electrons can be replaced by a nonclassical repulsive potential (Hellmann, 1935a,b, 1936; Hellmann and Kassatotschkin, 1936). This method was later rediscovered and further developed for metals by Heine, Abarenkov and Animalu (Heine and Abarenkov, 1964; Harrison, 1966; Heine et al., 1973). Heine, Abarenkov proposed a model, where one considers two types of interaction: outside of the shell, where the interaction potential is Coulomb and inside, where it is the constant. Parameters of this model potentials were determined using the spectroscopic data. Later on the different pseudopotential models were proposed. For the more detailed review we refer a reader to (Heine et al., 1973; Heine, 1970). All these models have one disadvantage. Their Fourier transforms (formfactor) are not sufficiently convergent when the Fourier space coordinate goes to infinity. Gurskii and Krasko (Krasko and Gurskii, 1969) proposed a model potential which eliminates this problem and provides smoothness of the pseuopotential inside the shell giving its finite value at small distances. First attempt to construct the model for alkali plasmas taking into account ion structure was made in works (Ebeling et al., 1976; Zimdahl and Ebeling, 1977; Ebeling et al., 1977, 1979) where the Hellmann type pseudopotentials were used. In this work we use *Hellmann-Gurskii-Krasko pseudopotential* (HGK) pseudopotential model for electron-ion interactions and its modified version of ion-ion interactions. Notice also that there

is a high interest in the construction of a pseudopotential model of particle interactions in *dense plasmas* (high density); this model is to take into account not only the quantum-mechanical effects including the ion shell structure at short distances, but also the screening field effects. The screened Hellmann-Gurskii-Krasko pseudopotential was derived in (Sadykova et al., 2009a) using Bogoljubov's method (Bogoljubov-Born-Green-Kirkwood-Yvon (BBGKY)) as described e.g. in (Bogoljubov, 1946, 1962), (Falkenhagen, 1971), (Baimbetov et al., 1995). This method is based on an expansion of the correlation functions with respect to the Bogoljubov plasma parameter $\mu = e^2/4\pi\varepsilon_0 k_B T r_D$ where r_D is the Debye radius. Strictly speaking, the approach outlined here is based on the Bogoljubov expansion which includes only linear in μ terms and is valid only for weakly and moderately coupled plasmas with $\Gamma_{ii} \lesssim 1$. Several calculations for $\Gamma_{ii} > 1$ are also presented but these results should be considered as mere extrapolations.

The thermodynamic properties and in particular the critical data of alkali plasmas are of basic interest and of importance for high-temperature technical applications like inertial confinement fusion. Over the past years a considerable amount of effort has been concentrated on the experimental (Hensel, 1977; Hensel et al., 1985; Freyland, 1979), (Juengst et al., 1985; Winter et al., 1988) and theoretical (Mott, 1974; Goldstein and Ashcroft, 1985; Ebeling et al., 1988; Hess, 1992) investigation of the behavior of alkali metals in the liquid and plasma state expanded by heating toward the liquid-vapor critical point. Near the critical point the materials are in the thermodynamic state of a strongly coupled plasma. The plasma phase transition (Mott transition) is a high-temperature modification of the insulator-metal transition (Ebeling et al., 1976). Here we will go far beyond the critical point to the region of nearly fully ionized plasmas where the temperature $T \approx 30\,000$ K where most of valency electrons are ionized but the rest core electrons are still tightly bound. In the table 1.1 the ionization energies of alkali atoms are presented. The investigation of thermodynamic properties in alkali plasmas under extreme conditions is not only important for basic research, but is also of high interest and importance for high-temperature technical applications, e.g. in material sciences for production of hydrocarbon superconductors with the help of alkali metals (Rosseinsky and Prassides, 2010), for various industrial applications of alkali metal adsorption on metals and semiconductors (Bonzel et al., 1989), geophysics and astrophysics for the applications in geocosmical alkali plasma research (Klyucharev et al., 2007). There are many applications, e.g. in material sciences, geophysics and astrophysics. Furthermore, these studies throw light on the complex picture of phase transitions in metal vapors which play an outstanding role in technology. Furthermore, these our studies throw some light on the complex picture of phase transitions in metal vapors which play an outstanding role in technological applications.

High-temperature alkali plasmas are widely applied in many technical projects. For instance, Li is an alkali metal of considerable technological interest. Lithium is planned to be used in inertial confinement fusion, solar power plants, electrochemical energy storage, magnetohydrodynamic power generators and in a lot of further applications. Recent advances in the field of extreme ultraviolet EUV lithography have revealed that laser-produced Li plasmas are source candidates for next-generation microelectronics (Sizyuk et al., 2006). For this reason we believe that the study of basic properties of alkali plasmas, like the microfield distributions are of interest.

We consider electron-positron and alkali (Li^+, Na^+, K^+, Rb^+, Cs^+), H^+ TCP and OCP cases. The electron-positron and alkali plasmas are anti-symmetric with respect

Table 1.1: The ionisation energies (eV) of alkali atoms (Ebeling et al., 1976)

	H	Li	Na	K	Rb	Cs	Be
First electron	13.595	5.39	5.138	4.339	4.176	3.893	9.306
Second electron	-	75.62	47.29	31.81	27.5	25.1	18.187

to the charges $ze_- = -e_+$ ($z = 1$) and symmetrical with respect to the densities $n_i = n_e$ while symmetric and anti-symmetric correspondingly with respect to the masses $m_i >> m_e$. We will calculate here the distributions of electric microfields acting on ions and electrons in TCP, and on electrons in OCP, taking into account quantum effects with the help of Kelbg, Deutsch potentials and the ion shell structure using HGK pseudopotential and find the corresponding radial distribution functions. For determination of the radial distribution functions we use the screened and screened Deutsch (Arkhipov et al., 2000), Kelbg (Sadykova and Ebeling, 2007) potentials and HGK pseudopotential in the Debye and moderately coupled plasma approximation (only for TCP) (Sadykova et al., 2009a). The methods which are used for the calculation are the coupling-parameter integration technique for OCP developed by C. A. Iglesias (Iglesias, 1983) and quantum TCP generalized by Ortner et al. (Ortner et al., 2000). We would like to underline again that the inclusion of both components into the theory and a correct account of the short-range electron-ion interactions, is very essential for an understanding of the high field wing of the electric microfields in the plasma. Therefore we will pay special attention to this point.

1.3 The static and dynamic structure factors

As one of possible applications of our new screened HGK pseudopotentials we see the structure factors because for determination of the *static* and *dynamic structure factors* one needs to have a screened pseudopotential as an essential input value. The structure and thermodynamic properties of Alkali and earth-alkali plasmas are of basic interest and of importance for high-temperature technical applications.

On the other hand, recently, *X-ray scattering* has proven to be a powerful tool which permits to measure density, temperature, charge states and simultaneously resolve the non-collective (particle) spectral characteristics of beryllium (Glenzer et al., 2003), carbon (Gregori et al., 2006a) and shock-compressed aluminium (Riley et al., 2000), in the warm dense matter regime.

In inertial confinement fusion and laboratory experiments related to astrophysics, Coulomb systems demonstrate a variety of plasma regimes and we are interested here in moderately and strongly coupled plasmas with $\Gamma_{ii} \geq 1$. Such regimes often manifest themselves during plasma-to-solid phase transitions. Recent experiments with solid density Be plasmas presumably showed a significant level of ion-ion coupling effects (Glenzer, 2007). In the present study of the two-component plasma static (SSF) and dynamic (DSF) structure factors we go beyond the random-phase approximation (RPA) and do not use the Mermin model also based on the RPA. The method of moments we apply accounts for the the ion-ion and ion-electron correlations through the fourth

power frequency moment of the loss function (the module of the imaginary part of the inverse dielectric function divided by frequency), the f-sum rule and other exact relations automatically, by construction, and the correlations are taken into account by the static characteristics we estimate. Notice also that the moments (sum-rules) are calculated specifically for the pseudopotential we employ and, that since the electrons are main contributors to the scattering process, the charge-charge dynamic structure factor, $S_{zz}(k,\omega)$, we calculate is directly related to the electron DSF and the differential scattering cross section,

$$\frac{d^2\sigma}{d\Omega d\omega} = \sigma_T \frac{k_1}{k_0} S_{ee}(k,\omega), \tag{1.13}$$

where $\sigma_T = 8\pi r_e^2/3$ is the total Thomson cross section with the classical electron radius r_e. The difference between the energy of the in- and outcoming photons which contribute to this intensity, is the energy of the collective mode generated in the plasma, i.e., effectively, the frequency ω the scattering intensity (1.13) depends on, while the corresponding wavenumber k is the module of the transfered momentum, $k = |\vec{k_1} - \vec{k_0}| = 4\pi \sin(\theta/2)/\lambda_0$, where θ is the scattering angle and λ_0 photon wavelength, presumed to be invariable in the scattering process (Sheffield, 1975).

For example, under the characteristic experimental conditions of the free electron laser facility at DESY (FLASH) (Höll et al., 2007), for $\theta = \pi/2$, $\lambda_0 = 15\ nm$ ($\approx 50\ eV$) $n_e = 10^{21} - 10^{22}\ cm^{-3}$, $T \sim 10eV$, $k = 3.6 \cdot 10^6\ cm^{-1}$ and the scattering parameter (Sheffield, 1975) $\alpha = k_{De}/k \gtrsim 3.8$ correspond to the"collective" scattering. On the other hand, the electronic Debye radius k_{De}^{-1} is of the order of the interparticle distance so that the Debye approximation is hardly applicable.

It is clear that the method of moments reduces the knowledge of the DSF to that of the static characteristics, precisely, the SSF, see, e.g., (Arkhipov et al., 2007) and (Arkhipov et al., 2010). In the case of weakly coupled plasmas the latter can be obtained within the Debye-Hückel theory or the RPA, while at moderate coupling the RPA fails to describe the spatial correlations correctly. However, in recent works by Gregori et al. (Gregori et al., 2006b), (Gregori et al., 2007) it was shown that in moderately coupled plasmas the BBGKY technique of expansion with respect to the plasma coupling parameter developed in the classical work of Bogoljubov provides sufficiently reliable expressions for the SSFs. In (Arkhipov et al., 2007) this was shown for hydrogen plasmas, representing the singly charged point charges, by comparison with MD-based results of Hansen and McDonald (Hansen et al., 1974). We consider here mainly moderately coupled plasmas and in our study of the SSFs we follow here this relatively simple and analytical route based on Bogoljubov expansions and consider it as an alternative to methods based on *ab initio* molecular dynamic simulations applying quantum density functional theory (DFT), hypernetted-chain (HNC) methods, quantum Monte-Carlo etc. which need in part high numerical efforts and are computer time consuming (Schwarz et al., 2009), (Gericke et al., 2009), (Bernu and Ceperley, 1999).

We consider Li^+, Na^+, K^+, Rb^+, Cs^+ and Be^{2+} plasmas of a TCP with the charges $ze_- = -e_+$ and masses $m_i >> m_e$ and the densities $n_e = zn_i$ ($z = 1, 2$). For simplicity, we neglect other ionization states for these plasmas and consider the temperatures $T \approx 30\,000$ K for alkali plasmas and $T \approx 100\,000$ K for Be^+ plasmas where most of valency electrons except the core electrons are ionized. We calculate the TCP correla-

tion functions, static and dynamic structure factors; we include into our consideration quantum effects and the ion shell structure using the screened Hellmann-Gurskii-Krasko pseudopotential obtained in (Sadykova et al., 2009a). The method which is used for the calculation of the SSFs of alkali and alkaline earth plasmas is essentially the TCP HNC approximation developed for the case of absence of the local thermodynamic equilibrium (LTE) by Seuferling et al. (Seuferling et al., 1989) and further discussed and extended for the SSFs by Gregori et al. (Gregori et al., 2006b), (Gregori et al., 2007); while to determine the DSFs we employ the method of moments developed by the V.M. Adamyan et al. as applied to two-component Hydrogen-like point charges (HLPC) plasmas where the charged particles were considered without an account of the ion shell structure as point-like electron and singly ionized ion system (Adamyan and Tkachenko, 1983; Adamyan et al., 1985; Adamjan et al., 1993). We would like to underline again that the inclusion of both components into the theory and a correct account of short-range electron-ion interactions, is essential for the understanding of the structure factors in plasmas.

2 Electric microfield distributions

2.1 Holtsmark distribution

2.1.1 One-component plasma

J. Holtsmark was the first who studied the Electric Microfield Distribution in a plasma in 1919 (Holtsmark, 1919). He considered one-component model consisting of N_i ions and completely neglected correlations between particles. Define $Q(\vec{\epsilon})$ as the probability density of finding an electric field $\vec{\epsilon}$ at a neutral point, located at $\vec{r}_0$, at the origin. This system is described by classical statistical mechanics in a canonical ensemble of N_i particles and temperature T. Note, that if the charge of the radiator is not equal to 0, then it should be taken into account and since we put the radiator at the origin, then there will be no dependence on the $\vec{r}_0$. The normalized probability density of the microfield $\vec{\epsilon}$ is in the thermodynamic limit is then given by

$$\begin{aligned} Q(\vec{\epsilon}) &= \left\langle \delta(\vec{\epsilon} - \vec{E}) \right\rangle \\ &\equiv \frac{1}{Z} \int_{\Omega} \exp(-\beta U(\tilde{R}^{(i)}, \vec{r}_0)) \delta(\vec{\epsilon} - \vec{E}(\tilde{R}^{(i)}), \vec{r}_0) d\vec{r}_0 d\tilde{R}^{(i)} \end{aligned} \tag{2.1}$$

where the angular brackets symbolize averaging over the distribution function of the positions of all ions and $\beta = 1/k_B T$, $\tilde{R}^{(i)} = \{\vec{r}_1^{(i)}, \vec{r}_2^{(i)}, ..., \vec{r}_{N_i}^{(i)}\}$ are the coordinates of ions. Here

$$Z = \int_{\Omega} \exp(-\beta U(\tilde{R}^{(i)}, \vec{r}_0) d\vec{r}_0 d\tilde{R}^{(i)} \tag{2.2}$$

is the canonical partition function and $U(\tilde{R}^{(i)}, \vec{r}_0)$ is the potential energy of the ionic interactions:

$$U(\tilde{R}^{(i)}, \vec{r}_0) = U_{ii}(\tilde{R}^{(i)}) + U_{iR}(\tilde{R}^{(i)}, \vec{r}_0) \tag{2.3}$$

As it was mentioned above, Holtsmark considered no interactions among the particles and since the radiator is a neutral point then the interaction term in (2.3) can be represented as

$$U_{ii}(\tilde{R}^{(i)}) = \frac{1}{2} \sum_{j \neq k=1}^{N_i} u_{ii}(|\vec{r}_j^{(i)} - \vec{r}_k^{(i)}|) = 0 \tag{2.4}$$

$$U_{iR}(\tilde{R}^{(i)}, \vec{r}_0) = \sum_{j=1}^{N_i} u_{iR}(|\vec{r}_0 - \vec{r}_j^{(i)}|) = 0 \tag{2.5}$$

The total electric field $\vec{E}(\tilde{R}^{(i)}, \vec{r}_0)$ acting on the radiator is given by the superposition of ionic single-particle Coulomb fields

$$\vec{E}(\tilde{R}^{(i)}, \vec{r}_0) = \vec{E}^{(i)}(\tilde{R}^{(i)}, \vec{r}_0) \tag{2.6}$$

with

$$\vec{E}^{(i)}(\tilde{R}^{(i)},\vec{r}_0)=\sum_{j=1}^{N_i}\vec{E}_i(\vec{r}_0-\vec{r}_j^{(i)})=\sum_{j=1}^{N_i}\frac{ze}{4\pi\varepsilon_0|\vec{r}_0-\vec{r}_j^{(i)}|^2}\hat{r}_{0j}, \tag{2.7}$$

where $\hat{r}_{0j}$ is a unit vector in the direction of $\vec{r}_0-\vec{r}_j^{(i)}$.

The spherical symmetric interaction between plasma particles and the isotropy of the system allows to introduce the normalized microfield distribution $P(\epsilon)=4\pi Q(\vec{\epsilon})\epsilon^2$. $P(\epsilon)$ can be expressed in terms of the Fourier transform of $Q(\epsilon)$, which $T(k)$, is through

$$P(\epsilon)=\frac{2\epsilon}{\pi}\int_0^\infty kT(k)\sin(\epsilon k)dk, \tag{2.8}$$

where

$$T(\vec{k})=\int Q(\vec{\epsilon})\exp(\imath\vec{k}\vec{\epsilon})d\vec{\epsilon}=<\exp(\imath\vec{k}\cdot\vec{E})>, \tag{2.9}$$

where $\imath$ denotes an imaginary unit with $\imath^2=-1$ and $<\cdots>$ is a statistical average, or

$$T(\vec{k})=\frac{1}{Z}\int_\Omega\exp[\imath\vec{k}\cdot\vec{E}(\tilde{R}^{(i)},\vec{r}_0)]e^{-\beta U(\tilde{R}^{(i)},\vec{r}_0)}d\vec{r}_0d\tilde{R}^{(i)}, \tag{2.10}$$

The coefficients of the expansion of the function $T(k)$ at $k\to 0$ yield the even moments of the microfield distribution,

$$T(k)=1-\frac{k^2}{6}<E^2>+\frac{k^4}{120}<E^4>-\cdots. \tag{2.11}$$

A similar expansion for the function $L(k)$ defined by $T(k)=\exp(-L(k))$ yields

$$L(k)=\frac{k^2}{6}<E^2>+\frac{k^4}{72}[<E^2>^2-\frac{3}{5}<E^4>]+\cdots. \tag{2.12}$$

As one can see, the Fourier transform of the EMD can be interpreted as a generating function of microfield even moments. Equations (2.1)-(2.12) describe the EMD at the position $\vec{r}_0$ of the radiator generated by the statistically distributed ions of the OCP. Since we are interested in calculating the EMD, (2.8), in a infinite system, the statistical average of any quantity becomes translationally invariant with respect to $\vec{r}_0$ and the location of the test charge can be chosen as the origin $\vec{r}_0=0$ without loss of generality.

For determination of the Fourier transform of EMD for OCP (2.10) Baranger and Mozer developed the cluster expansion technique (Baranger and Mozer, 1959; Mozer and Baranger, 1960) using the following transformation:

$$\chi_j{}^{(i)}(\vec{k})=e^{\imath\vec{k}\cdot\vec{E}_i(\vec{r_j})}-1, \tag{2.13}$$

Using this transformation the exponential factor in Eq. (2.10) becomes

$$\begin{aligned}\exp[\imath\vec{k}\cdot\vec{E}(\tilde{R}^{(i)})]&=\Pi_{j=1}^{N_i}[1+\chi_j{}^{(i)}(\vec{k})]\\&=1+\sum_1\chi_n{}^{(i)}(\vec{k})+\sum_2\chi_m{}^{(i)}(\vec{k})\chi_n{}^{(i)}(\vec{k})+\cdots,\end{aligned} \tag{2.14}$$

where $\sum_1$ means the sum over all particles, $\sum_2$ the sum over all pairs, etc. This transformation is similar to the use of Mayer's functions for thermodynamic properties of gases (Mayer and Mayer, 1940). Substituting Eq. (2.14) into (2.10) leads in the thermodynamic limit $N, \Omega \to \infty$ when $n = N/\Omega$ remains constant directly to the series

$$T(\vec{k}) = \exp\{\sum_{j=1}^{\infty} \frac{n^j}{j!} {h_j}^{(i)}(\vec{k})\}. \tag{2.15}$$

Here ${h_j}^{(i)}(\vec{k})$ is given by

$${h_j}^{(i)}(\vec{k}) = \int {\chi_1}^{(i)}(\vec{k}){\chi_2}^{(i)}(\vec{k}) \cdots {\chi_j}^{(i)}(\vec{k}){\bar{g}_j}^{(i)}(\vec{R}_j^{\,(i)})d\vec{R}_j^{\,(i)}, \tag{2.16}$$

and ${\bar{g}_j}^{(i)}(\vec{R}_j^{\,(i)})$ is the single-particle Ursell cluster function (Mayer and Mayer, 1940) for OCP expressed by the ordinary pair correlation function between radiator R and "j" plasma particles (ions) at $\vec{r}_1^{\,(i)}, \vec{r}_2^{\,(i)}, ..., \vec{r}_j^{\,(i)}$, ${\bar{g}_j}^{(i)}(\vec{r}) = g_{iR}(r) \simeq \exp(-U^*_{iR}(r)/k_BT)$ in a weakly coupled limit with $U^*_{iR}(r)$ being the screened interaction potential. Since we do not consider any correlations among the particles as well as with the radiator then ${\bar{g}_j}^{(i)} = g_{iR}(r) = 1$. The integration range in (2.16) is controlled by both the ${\chi_j}^{(i)}(\vec{k})$ and the Ursell functions because for completely uncorrelated systems of particles the many-body functions $g_{iR}(r)$ tend to unity while ${\bar{g}_j}^{(i)} \to 0$ beginning with ${\bar{g}_2}^{(i)}$. One should notice that j determines the order of the correlation function. For more detailed review we refer a reader to (Ecker, 1972).
Equations (2.15), (2.16) together with the relation $T(\vec{k}) = e^{-L(\vec{k})}$ constitutes the generalization of the Baranger-Mozer cluster expansion technique to the OCPs.

For ideal OCPs, the Holtsmark limit, all terms at $j \geq 2$ in (2.15) in the sum vanish, and only the term with $j = 1$ contributes to the EMD. Having taken into account all the described above, the expression (2.15) will turn into the following

$$T(k) = \exp\{n \int \chi_1(\vec{k})d\vec{r}_1\}, \tag{2.17}$$

where $\chi_1(\vec{k}) = e^{\imath\vec{k}\cdot\vec{E}_i(\vec{r_1})} - 1$, here "$i$" is skipped. If we skip the index and insert the definition for χ_1 we get:

$$T(k) = \exp\{n \int (e^{\imath\vec{k}\cdot\vec{E}_i(\vec{r})} - 1)d\vec{r}\}, \tag{2.18}$$

Introducing the polar coordinates we can easily estimate the integral entering the equation 2.18:

$$T(k) = \exp\{n \int_0^{\infty}\int_0^{\pi}\int_0^{2\pi} \left[e^{\imath k \frac{ze}{4\pi\varepsilon_0 r^2}\cos\theta} - 1\right] \sin\theta d\varphi d\theta r^2 dr\} =$$

$$4\pi n \int_0^{\infty} \left[j_0\left(k\frac{ze}{4\pi\varepsilon_0 r^2}\right) - 1\right] r^2 dr = \exp(-k^{*3/2}\frac{2}{5}\sqrt{2\pi}), \tag{2.19}$$

where $j_0 = \sin(x)/x$ is the spherical Bessel function of order zero and $k^* = kE_0$, $E_0 = \frac{ze}{4\pi\varepsilon_0 {r_{ii}}^2}$ with r_{ii} being the ion-ion spacing. For the detailed derivation see in the Appendix 7. The final formula for the Holtsmark distribution is the following:

$$P(\beta)_H = \frac{2\beta}{\pi} \int_0^\infty k^* \exp(-{k^*}^{3/2} \frac{2}{5}\sqrt{2\pi}) \sin(\beta k^*) dk^*. \tag{2.20}$$

One should note that if one measures the field in electron OCP in $E_0 = \frac{e}{4\pi\varepsilon_0 {r_{ee}}^2}$ with r_{ee} being the electron-electron spacing and in ion OCP in $E_0 = \frac{ze}{4\pi\varepsilon_0 {r_{ii}}^2}$ then the Holtsmark distribution remains invariant, its form does not change. In the Figure 2.1 the Holtsmark distribution is shown.

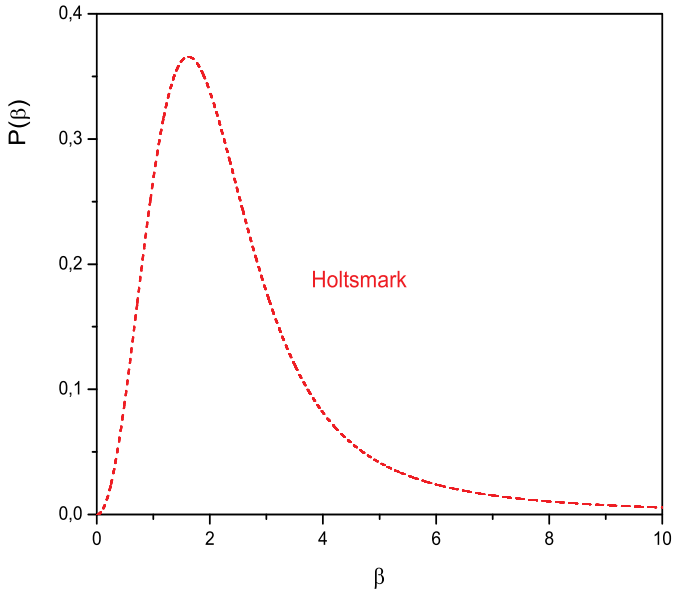

Figure 2.1: The Holtsmark electric microfield distribution for hydrogen-like plasma $z = 1$

2.1.2 Two-component plasma

In Two-component electron-ion plasma the Fourier transform will turn into:

$$T(k) = \exp\{\sum_{\alpha=i,e} n_a \int_0^\infty \int_0^\pi \int_0^{2\pi} \left[e^{\imath k \frac{z_\alpha e}{4\pi\varepsilon_0 r^2} \cos\theta} - 1 \right] \sin\theta d\varphi d\theta r^2 dr\} = \exp(-{k^*}^{3/2} \frac{2}{5}\sqrt{2\pi}), \tag{2.21}$$

where $k^* = kE_0$, $E_0 = \frac{z_{eff} e}{4\pi\varepsilon_0 {r_{ei}}^2}$ with $z_{eff} = \left(\frac{z(1+\sqrt{z})}{(1+z)}\right)^{2/3}$. In this case the Holtsmark distribution will have the same functional form (2.20) as either ionic or the electronic OCP. However, when one measures the field in other units different from mentioned above then the OCP and TCP Holtsmark distributions may strongly differ from each other.

It is important to stress that the Holtsmark distribution is a good approximation for high-temperature and low density plasma. That is why at such conditions any theory considering the pair correlations should lead to the Holtsmark distribution.

2.1.3 The second moment

It is very useful to have a knowledge of moment sum rules for developing approximation schemes for fluids and plasmas. The EMD moments fix the shape of the distribution and contains useful information about the system. Here, we derive exact expressions for the second moment of the EMD at a neutral point.

Let us write the exact expressions for the second moment of the EMD at a neutral point in the one-component plasma. The second moment can be found from (2.19)in the limit $k \to 0$.

$$\lim_{k\to 0} T(k) = 1 - \frac{k^2}{6} 4\pi n \int\limits_0^\infty \frac{z^2 e^2}{(4\pi\varepsilon_0)^2 r^2} dr \tag{2.22}$$

Taking into account that $T(k)$ at $k \to 0$ yields the even moments (2.11) we get

$$\begin{aligned} < E^2 > = 4\pi n \int\limits_0^\infty \frac{z^2 e^2}{(4\pi\varepsilon_0)^2 r^2} dr = \\ - 4\pi n \frac{z^2 e^2}{(4\pi\varepsilon_0)^2 r} \,|_0^\infty \to \infty \end{aligned} \tag{2.23}$$

As we can see the second moment of the Holtsmark microfield distribution in OCP does not exist.

Let us now consider the second moment for the TCP. From (2.21) follows

$$\begin{aligned} < E^2 > = 4\pi n_e \int\limits_0^\infty \frac{e^2}{(4\pi\varepsilon_0)^2 r^2} + 4\pi n_i \int\limits_0^\infty \frac{z^2 e^2}{(4\pi\varepsilon_0)^2 r^2} dr = \\ - 4\pi n_e (1+z) \frac{e^2}{(4\pi\varepsilon_0)^2 r} \,|_0^\infty \to \infty \end{aligned} \tag{2.24}$$

The second moment of the Holtsmark distribution in the TCP also does not exist.

2.1.4 The asymptotics of the Holtsmark distribution. The Holtsmark tail

Let's now derive the asymptotics of the Holtsmark distribution at $\boldsymbol{\beta \to \infty}$ conventionally defined as a tail of the distribution. Returning to the introduced Holtsmark integral

(2.20):

$$\lim_{\beta\to\infty} P(\beta) = \lim_{\beta\to\infty} \frac{2\beta}{\pi} \int_0^\infty k^* \exp(-k^{*3/2}\frac{2}{5}\sqrt{2\pi}) \sin(\beta k^*) dk^* =$$

$$\lim_{\beta\to\infty} -\frac{2\beta}{\pi} \int_0^\infty \frac{\partial}{\partial\beta} \exp(-k^{*3/2}\frac{2}{5}\sqrt{2\pi}) \cos(\beta k^*) dk^* =$$

Taking into an account that at $\beta \to \infty$ the stationary phase limit can be applied, meaning negligibly small $l^* \Longrightarrow k^* \to 0$, we get:

$$\lim_{\beta\to\infty} -\frac{2\beta}{\pi}\frac{\partial}{\partial\beta} \int_0^\infty (1 - k^{*3/2}\frac{2}{5}\sqrt{2\pi}) \cos(\beta k^*) dk^* \approx \frac{3}{2}\beta^{-5/2} \tag{2.25}$$

For the detailed derivation see in the Appendix 7.

In the Figure 2.2 the Holtsmark distribution (2.20) compared to its asymptote (2.25) at $1 < \beta < 161$ is shown. As one can see, the Holtsmark tail starts to converge to its asymptote at $\beta \simeq 16$.
At $\boldsymbol{\beta \to 0}$, we get:

$$\lim_{\beta\to 0} P(\beta) = \lim_{\beta\to\infty} \frac{2\beta}{\pi} \int_0^\infty k^* \exp(-k^{*3/2}\frac{2}{5}\sqrt{2\pi}) \sin(\beta k^*) dk^* =$$

$$\lim_{\beta\to 0} -\frac{2\beta^2}{\pi} \int_0^\infty k^{*2} \exp(-k^{*3/2}\frac{2}{5}\sqrt{2\pi}) dk^* \approx \frac{25}{6\pi^2}\beta^2 \tag{2.26}$$

2.2 One-component plasma model

Define $Q(\vec{\epsilon})$ as the probability density of finding an electric field $\vec{E} = \vec{\epsilon}$ produced by N_α ($\alpha = e$ or i) particles moving in a neutralizing background at a charged point $z_R e$ ($z_R > 0$) located at $\vec{r}_0$, at the origin. This system is described by classical statistical mechanics in a canonical ensemble of $N_\alpha + 1$ particles contained in a volume Ω and temperature T. Note, that if the charge of the radiator is not equal to 0, then it should be taken into account. The total system is assumed to be in thermal equilibrium and macroscopically neutral. The definition of the normalized probability density (2.1) of the microfield $\vec{E}$ together with the normalized microfield distribution $P(\epsilon)$ (2.8) was introduced above in the Sec. 2.1 for the Holtsmark distribution with the following changes. Here, we do consider the particle correlations including correlations between the plasma particle and the radiator:

$$U(\tilde{R}^{(\alpha)}, \vec{r}_0) = U_{\alpha\alpha}(\tilde{R}^{(\alpha)}) + U_{\alpha R}(\tilde{R}^{(\alpha)}, \vec{r}_0) + V_B \tag{2.27}$$

with either electron-electron, electron-radiator or ion-ion, ion-radiator terms respectively, $\alpha = e$ or i. V_B is the contribution to the potential energy due to the background. Assuming spherical symmetric interactions between the particles the interaction terms

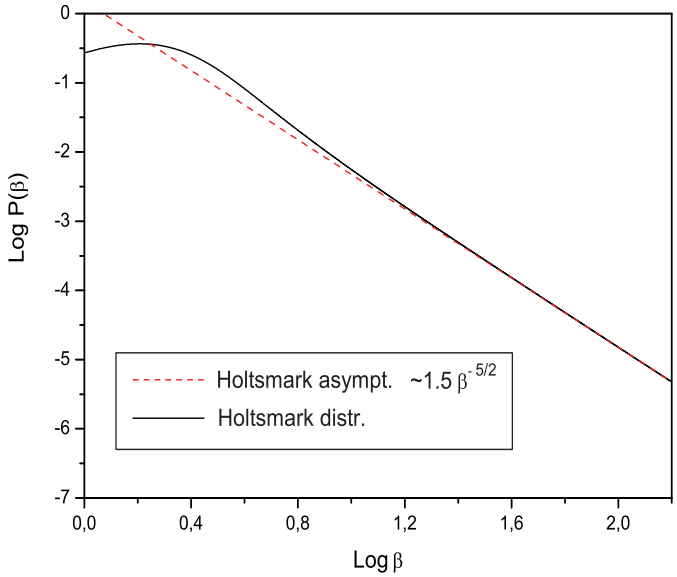

Figure 2.2: The Holtsmark electric microfield distribution and its asymptote at $\beta \to \infty$ for hydrogen-like plasma $z = 1$ in a double decadic logarithmic scale

in (2.27) can be represented as

$$U_{\alpha\alpha}(\tilde{R}^{(\alpha)}) = \frac{1}{2} \sum_{(j \neq k=1)}^{N_\alpha} u_{\alpha\alpha}(|\vec{r}_j^{\,(\alpha)} - \vec{r}_k^{\,(\alpha)}|), \tag{2.28}$$

$$U_{\alpha R}(\tilde{R}^{(\alpha)}, \vec{r}_0) = \sum_{j=1}^{N_\alpha} u_{\alpha R}(|\vec{r}_0 - \vec{r}_j^{\,\alpha}|) \tag{2.29}$$

in terms of the pair interaction potentials $u_{\alpha\alpha}(r)$ and $u_{\alpha R}(r)$. The total electric field $\vec{E}(\tilde{R}^{(\alpha)}, \vec{r}_0)$ acting on the radiator is given by the superposition of all the ionic or electron single-particle microfields

$$\begin{aligned} \vec{E}(\tilde{R}^{(\alpha)}, \vec{r}_0) = -\frac{\vec{\nabla}_0 U}{z_R e} &= \sum_{j=1}^{N_\alpha} \vec{E}_\alpha(\vec{r}_0 - \vec{r}_j^{\,(\alpha)}) + \vec{E}_B \\ &= \sum_{j=1}^{N_\alpha} \frac{z_\alpha e}{4\pi\varepsilon_0 |\vec{r}_0 - r_j{}^{(\alpha)}|^2} \hat{r}_{0j}^{(\alpha)} + \vec{E}_B, \end{aligned} \tag{2.30}$$

where $\hat{r}_{0j}^{(\alpha)}$ is a unit vector in the direction of $\vec{r}_0 - \vec{r}_j^{\,(\alpha)}$. $\vec{\nabla}_0$ is the gradient with respect to $\vec{r}_0$.

This system models what is usually referred to as the high-frequency component of the field when $\alpha = e$ or low-frequency component when $\alpha = i$ in a real plasma. As it was mentioned above, since we are interested in calculating the EMD, (2.8), in a infinite

system, the statistical average of any quantity becomes translationally invariant with respect to $\vec{r}_0$ and the location of the test charge can be chosen as the origin $\vec{r}_0 = 0$ without loss of generality.

In this work we apply the coupling parameter integration method proposed by C. A. Iglesias in (Iglesias, 1983). This approach is based on recognizing the similarity between the formal expressions for the excess chemical potential[1] and the Fourier transform of $Q(\vec{\epsilon})$.

The Fourier transform of $Q(\vec{\epsilon})$ is then expressed, without any approximation, in terms of a two-body function which could be interpreted as a "generalized" radial distribution function (RDF) $\mathcal{G}(\vec{r}, \vec{k})$ involving the radiator and one of the plasma particles. This is in a contrast to previous developments which require knowledge of many-body functions (Baranger and Mozer, 1959; Mozer and Baranger, 1960), (Hooper, 1966), (Iglesias and Hooper, 1982; Hooper, 1966).

Following the (2.10) the Fourier transform of the EMD probability density can be alternatively represented as:

$$T_{\alpha R}(\vec{k}) = \frac{Z_{\alpha R}(\vec{k})}{Z_{\alpha R}}, \tag{2.31}$$

where

$$Z_{\alpha R}(\vec{k}) = \int_\Omega e^{-\beta U(\tilde{R}^{(\alpha)}, \vec{k})} d\tilde{R}^{(\alpha)}, \tag{2.32}$$

and $Z_{\alpha R}$ is introduced as Z above in Eq. (2.2). The subscripts $s\alpha R$ denote the α species producing the electric field at a radiator R. The function can be interpreted as the generalized configurational partition function for a system with "potential energy" $U(\tilde{R}^{(\alpha)}, \vec{k}) = U(\tilde{R}^{(\alpha)}) - \imath k_B T(\vec{k} \cdot \vec{E})$. To accomplish this we introduce the parameter λ which is defined as the magnitude of the vector $\vec{k} = \lambda \hat{k}$, where $\hat{k}$ is a unit vector in the direction of $\vec{k}$.

From the definition of $T_\alpha(\vec{k})$ in Eq. (2.31) we may write

$$\begin{aligned} \ln T_{\alpha R}(\vec{k}) &= \ln[Z_{\alpha R}(\lambda = \vec{k}) / Z_{\alpha R}(\lambda = 0)] \\ &= \int_0^k d\lambda \frac{\partial \ln Z_{\alpha R}(\vec{k})}{\partial \lambda} = \int_0^k d\lambda \frac{< (\imath \hat{k} \cdot \vec{E}) \exp(\imath \vec{k} \cdot \vec{E}) >}{< \exp(\imath \vec{k} \cdot \vec{E}) >} \\ &= \imath \hat{k} n_\alpha \int_0^k d\lambda \int d\vec{r} E_\alpha(\vec{r}) [\mathcal{G}_{\alpha R}(\vec{r}, \lambda \hat{k}) - 1]. \end{aligned} \tag{2.33}$$

Here $\vec{k} = \hat{k}\lambda$, $\vec{E}_\alpha(\vec{r}) = z_\alpha e \hat{r} / 4\pi\varepsilon_0 (r^{(\alpha)})^2$ with $z_e = -1$, $z_i = z$ is the single particle either ionic or electrical fields. $\mathcal{G}_{\alpha R}(\vec{r}, \vec{k})$ represents the pair correlation functions between the radiator and the plasma particles in a fictitious system whose interaction potential is given by the complex quantity $U(\tilde{R}^{(\alpha)}, \vec{k})$, i.e.,

$$\mathcal{G}_{\alpha R}(\vec{r}_1, \vec{k}) = \frac{\Omega^2}{Z(\vec{k})} \int_\Omega e^{-\beta U(\tilde{R}^{(\alpha)}, \vec{k})} d\tilde{R}_1^{(\alpha)}. \tag{2.34}$$

[1] The excess (ex.) chemical potential (CP) is defined as the difference b/w the CP of a given species and that of an ideal (id.) gas under the same condition (pressure, temperature, etc.). $\mu = -k_B T \ln Z_{N+1}/Z_N = \mu_{id} + \mu_{ex}$. Here Z_N, Z_{N+1} are the partition functions of N and $N+1$ particles respectively.

Here $\tilde{R}_s^{(\alpha)} = \Pi_{a=s+1}^{N_\alpha} d\vec{r}_a^{(\alpha)}$ is the reduced volume element in a phase space which does not involve the particles $1, 2, \cdots, s$ of plasma species α. At $\vec{k} \to 0$ they coincide with the actual RDF $g_{\alpha R}$:

$$g_{\alpha R}(\vec{r}_1^{(\alpha)}) = \frac{\Omega^2}{Z} \int_\Omega e^{-\beta U(\tilde{R}^{(\alpha)})} d\tilde{R}_1^{(\alpha)}. \tag{2.35}$$

Here, $U(\tilde{R}^{(\alpha)})$ does not depend on $\vec{r}_0$. The pair correlation functions given by Eq. (2.35) describe coupling between the radiator (ion) and plasma particles. When the coupling between the radiator and particles vanishes, e.g. radiator is a neutral point, the pair correlation function behaves like $g_{\alpha R} \to 1$. If the radiator is a particle of plasma species β these correlation function coincide with the RDF of bulk plasma, $g_{\alpha R} \equiv g_{\alpha\beta}$.

The central problem is now the evaluation of $\mathcal{G}_{\alpha R}(\vec{r}, \vec{k})$. This complex correlation function must be known in the interval from 0 to k. Usually approximation schemes of the type commonly employed in the liquid theory are applied.

Many of these schemes are based on "thermodynamic perturbation theory" (Zwanzig, 1954). Here we apply the exponential approximation (Iglesias et al., 1985; Iglesias and Lebowitz, 1984; Iglesias et al., 1983; Iglesias, 1983), (Andersen and Chandler, 1972). The system with potential $U(k = 0) = U$ is chosen as a reference system and its structure is assumed to be known to a good approximation. The perturbation potential is then given by $U_1 = -\imath(k_B T)(\vec{k} \cdot \vec{E})$ and we expand the correlation functions (2.34) with respect to U_1. Within first order we obtain $\mathcal{G}_{\alpha R}(\vec{r}, k) \approx g_{\alpha R}(r)[1 + \imath\vec{k} \cdot \vec{\mathcal{E}}_\alpha]$. Here $g_{\alpha R}(r)$ are the actual RDF in the real system (2.35), and $\vec{\mathcal{E}}_\alpha = \vec{\mathcal{E}}_\alpha^{\,0}(\vec{r}, 0)$. The electric fields $\vec{\mathcal{E}}_\alpha(\vec{r})$ may be interpreted as effective electric fields in the fictitious system which have no dependence on $\vec{k}$. Taking into account that $< \vec{E} >= 0$ we obtain

$$\vec{\mathcal{E}}_\alpha = \vec{E}_\alpha + n_\beta \int d\vec{r}_1 \vec{E}_\beta(\vec{r}_1)[g_{\alpha\beta}(|\vec{r} - \vec{r}_1|) - 1]. \tag{2.36}$$

Since $g_{\alpha R}(r)$ depends only on $|\vec{r} - \vec{r}_1|$ the effective electric fields in (2.36) can be represented as $\vec{\mathcal{E}}_\alpha(\vec{r}) = \hat{r}\mathcal{E}_\alpha$. The single particle electric fields can be written as $\vec{E}_\alpha = \hat{r}E_\alpha$. In the weak coupling regime ($\Gamma_{ii} \to 0$) the pair correlation function (RDF) in the ionic OCP is given by the linear Debye-Hückel approximation

$$g_{iR}(r) \approx 1 - \frac{z z_R e^2}{k_B T r} \exp(-r/r_D). \tag{2.37}$$

Inserting Eq. (2.37) into (2.36) we get the following effective Debye screened field

$$\mathcal{E}_i(r) = \frac{ze}{r^2}(1 + \chi r) \exp(-\chi r). \tag{2.38}$$

with

$$\chi = \frac{1}{r_D} = \left(\sum_{a=e,i} \frac{4\pi n_a {e_a}^2}{4\pi\varepsilon_0 k_B T} \right)^{1/2}, \tag{2.39}$$

r_D being the total Debye radius.
We would like to point out that the use of Debye-Hückel form (2.38) for $g_{\alpha R}(r)$ and effective electronic fields should be questioned when the quantum-mechanical diffraction effects play a significant role in their correlations. That is why in our works for particle

interactions we used the quantum-mechanical Deutsch and Kelbg pseudopotentials which allow to avoid such difficulties. Whereas for the screened interactions we have used the screened Deutsch (Sadykova et al., 2004), Kelbg (Sadykova and Ebeling, 2007), (Sadykova et al., 2005) pseudopotentials and derived the screened Hellmann-Gurskii-Krasko pseudopotentials, described later in Subsec. 4.1.2 and in Sec. 3.1 on the p. 42, which in addition to the quantum diffraction effects and symmetry take into account the ion shell structure (Sadykova et al., 2009a,b). In the work (Sadykova et al., 2009a,b) we applied the classical approach based on the BBGKY chain of Bogoljubov equations (Bogoljubov, 1946, 1962) to get these effective fields directly from the screened pseudopotentials.

$$\vec{\mathcal{E}}_\alpha = -\frac{1}{z_R e}\vec{\nabla}_r \Phi_{\alpha R}(r), \tag{2.40}$$

here for $\Phi_{\alpha R}(r)$ ($\alpha = e$ or i) the equations (4.24) in the Sec. 4.1.2 are used. Alternatively this can be done on the basis of the potential of mean force approximation (PMF) with the help of logarithmic derivative of the actual RDF (Yan and Ichimaru, 1986), (Nersisyan et al., 2005).

We now use the exponential approximation (Iglesias et al., 1983) and make the ansatz

$$\mathcal{G}_{\alpha R}(\vec{r}, \vec{k}) = g_{\alpha R}(r) \exp[\imath \vec{k} \cdot \vec{\mathcal{E}}_\alpha(r)] \tag{2.41}$$

and integrate (2.33) with respect to λ and the angles to find

$$\ln T_{\alpha R}(k) = 4\pi n_\alpha \int_0^\infty E_\alpha(r) \left[\frac{j_0\left(k\mathcal{E}_\alpha(r)\right) - 1}{\mathcal{E}_\alpha(r)}\right] g_{\alpha R}(r) r^2 dr, \tag{2.42}$$

j_0 is the spherical Bessel function of order zero. Equation (2.42) is the main results of C.A. Iglesias (Iglesias, 1983). $g_{\alpha R}(r)$ represents the radial distribution function for a screened either ion or electron subsystems in OCP case. In this work, the actual radial distribution function is estimated as following (Kraeft et al., 1986)

$$g_{\alpha R}(r) = \exp\left(-\frac{\Phi_{\alpha R}(r)}{k_B T}\right) \tag{2.43}$$

If the radiator represents one of the ions $z_R > 0$ then $\Phi_{\alpha R}$ corresponds to $\Phi_{\alpha i}$.
It is now possible to evaluate $T_{\alpha R}(k)$ from Eqs. (2.42) in terms of the radial distribution function (2.43), screened Deutsch pseudopotentials (3.18-3.20) in the Sec. 3.1 (Sadykova et al., 2004), screened Kelbg pseudopotential (3.45), (3.46) in the Sec. 3.1 and the effective fields (2.40).

2.2.1 The second moment

As it has been mentioned above a knowledge of moment sum rule is often useful in developing approximation schemes for fluids and liquids. For example, in the APEX method the exact second moment was incorporated into the EMD calculations.

The second moment within the exponential approximation (2.41) can be found from

(2.42) in the limit $k \to 0$. It yields

$$< E^2 >= 4\pi n_\alpha \int_0^\infty E_\alpha(r)\mathcal{E}_\alpha(r)g_{\alpha R}(r)r^2 dr, \tag{2.44}$$

Let us consider now the exact expression for the second moment of the microfield distribution in OCP and for a charged radiator. The second moment can be written as following

$$< E^2 >= \frac{1}{(z_R e)^2} < \vec{\nabla}_0 U \cdot \vec{\nabla}_0 U >, \tag{2.45}$$

where $\vec{\nabla}_0$ is the gradient with respect to $\vec{r}_0$ and the average is taken over the canonical ensemble defined in (2.1). Noting that $e^{-U/k_BT}(\vec{\nabla}_0 U) = -k_BT(\vec{\nabla}_0 e^{-U/k_BT})$, substituting this into (2.45), integrating by parts, and setting the surface terms equal to zero yields

$$< E^2 >= \frac{k_BT}{(z_R e)^2} < {\nabla_0}^2 U >= -\frac{k_BT}{z_R e} < \vec{\nabla}_0 \cdot \vec{E} > \tag{2.46}$$

Inserting (2.30) and $\vec{\nabla} \cdot \vec{E}_\alpha(\vec{r}) = -(1/r^2)[r^2 u'_{\alpha R}(r)/z_R e]'$ into (2.46), taking advantage of Poisson's equation and using the translational symmetry, we have

$$< E^2 >= \frac{k_BTn_B}{\varepsilon_0 z_R} - \frac{k_BT4\pi n_\alpha}{z_R^2 e^2} \int_0^\infty [r^2 u'_{\alpha R}]' g_{\alpha R}(r) dr, \tag{2.47}$$

where n_B represents the background charge density. The functions $g_{\alpha R}(r)$ have been described above, see Eq. (2.35), where $n_\alpha g_{\alpha R}(r)$ is the density of plasma particles α at a distance r from the radiator. The interaction potential $U(\tilde{R}^{(\alpha)})$ does not depend on $\vec{r}_0$. The exact second moment of the EMD (2.47) must be fulfilled by (2.44).

To get the effective fields we apply the classical approach based on the BBGKY chain (Bogoljubov, 1946, 1962) for the Hellmann-Gurskii-Krasko pseudopotential model (Krasko and Gurskii, 1969) in TCP. The screened HGK pseudopotential model takes into account not only the quantum-mechanical, screening effects but also the ion shell structure. We also used the screened Deutsch pseudopotentials for OCP obtained with the help of the same Bogoljubov approach in (Arkhipov et al., 2000) and the screened Kelbg pseudopotential model derived in (Sadykova and Ebeling, 2007) on a base of the method described by Falkenhagen in (Falkenhagen, 1971), which is primarily based on Bogoljubov's works (Bogoljubov, 1962). The method applied provides with the quite good results at $\Gamma_{ii} \lesssim 1$. Using Eq. (2.43) we can represent this field as

$$\mathcal{E}_\alpha = \frac{k_BT}{z_R e}\frac{\partial}{\partial r}[\ln g_{\alpha R}(r)]. \tag{2.48}$$

Inserting Eq. (2.48) into (2.44) automatically satisfies the sum rule (2.47) without any adjustable parameter. Summarizing all the said above, we can calculate the EMDs with the exact second moment using Eq. (2.8) or the following equation

$$P(\beta) = \frac{2\beta}{\pi} \int_0^\infty k^* T_R(k^*) \sin(\beta k^*) dk^* \tag{2.49}$$

represented in dimensionless electric field form, where $\beta = E/E_0$ and $k^* = kE_0$, $E_0 = \frac{ze}{4\pi\varepsilon_0 r_{\alpha\alpha}{}^2}$ with $r_{\alpha\alpha}$ being the electron-electron spacing and using Eqs. (2.42), (2.43) and (2.40). This approach is based on integral-equation method, exponential approximation (2.41) and classical Bogoljubov approach (BBGKY) for the screened pseudopotentials.

The ionic Coulomb system

Let us consider now the ionic OCP model. If the interaction between ions is described by the classical bare Coulomb potential, then taking advantage of Poisson's equation we can write

$$\nabla_0{}^2 U = \frac{zz_R e^2}{\varepsilon_0}(n_i - \sum_{j=1}^{N_i} \delta(\vec{r}_j)), \tag{2.50}$$

where $zn_i = n_e$ and $-en_e = \vec{\nabla}_0 \cdot \vec{E}_B/4\pi$ is the background charge density, which remains unchanged in the thermodynamic limit. Inserting this equation into (2.46) and taking into account Eq. (2.47) we get

$$\begin{aligned} < E^2 >_{OCP} &= \frac{k_B T n_e}{\varepsilon_0 z_R} - \frac{k_B T z n_i}{\varepsilon_0 z_R} \int_0^\infty \delta(r) g_{iR}(r) dr \\ &= \frac{k_B T n_e}{z_R \varepsilon_0} - \frac{k_B T z n_i}{\varepsilon_0 z_R} g_{iR}(0) = \frac{k_B T n_e}{z_R \varepsilon_0}, \end{aligned} \tag{2.51}$$

Here is assumed that for $z_R > 0$, $n_e = zn_i$ and $g_{iR}(0) = 0$, Eq. (2.35), if quantum-diffraction effects are negligible for the ions.

2.3 Two-component plasma model

Define $Q(\vec{\epsilon})$ as the probability density of finding an electric field $\vec{E} = \vec{\epsilon}$ produced at a charged point $z_R e$ by N_i ions and N_e electrons moving in a neutralizing background ($z_R > 0$) located at $\vec{r}_0$, at the origin. This system is described by classical statistical mechanics in a canonical ensemble of $N_i + N_e + 1$ particles contained in a volume Ω and temperature T. Note, that if the charge of the radiator is not equal to 0, then it should be taken into account. The total system is assumed to be in thermal equilibrium and macroscopically neutral. The definition of the normalized probability density (2.1) of the microfield $\vec{E}$ is then given by (Yan and Ichimaru, 1986; Ortner et al., 2000)

$$\begin{aligned} Q(\vec{\epsilon})_{TCP} &= \left\langle \delta(\vec{\epsilon} - \vec{E}) \right\rangle \\ &\equiv \frac{1}{Z} \int_\Omega \exp(-\beta U(\tilde{R}^{(i)}, \tilde{R}^{(e)}, \vec{r}_0)) \delta(\vec{\epsilon} - \vec{E}(\tilde{R}^{(i)}, \tilde{R}^{(e)}, \vec{r}_0)) d\vec{r}_0 d\tilde{R}^{(i)} d\tilde{R}^{(e)} \end{aligned} \tag{2.52}$$

where the angular brackets symbolize statistical averaging over the distribution function of the positions of all ions and electrons, $\beta = 1/k_B T$, $\tilde{R}^{(i)} = \{\vec{r}_1^{(i)}, \vec{r}_2^{(i)}, ..., \vec{r}_{N_i}^{(i)}\}$ are the coordinates of ions, $\tilde{R}^{(e)} = \{\vec{r}_1^{(e)}, \vec{r}_2^{(e)}, ..., \vec{r}_{N_e}^{(e)}\}$ - the coordinates of electrons. Here

$$Z = \int_\Omega \exp(-\beta U(\tilde{R}^{(i)}, \tilde{R}^{(e)}, \vec{r}_0) d\vec{r}_0 d\tilde{R}^{(i)} d\tilde{R}^{(e)} \tag{2.53}$$

Z is the canonical partition function and $U(\tilde{R}^{(i)}, \vec{r}_0)$ is the potential energy of the configuration given here by:

$$U(\tilde{R}^{(i)}, \tilde{R}^{(e)}, \vec{r}_0) = \frac{1}{2} \sum_{(j \neq k)=1,\, \alpha,\beta} u_{\alpha\beta}(|\vec{r}_j^{(\alpha)} - \vec{r}_k^{(\beta)}|) + \sum_{\alpha,j} u_{\alpha R}(|\vec{r}_0 - \vec{r}_j^{\alpha}|) \tag{2.54}$$

in terms of the pair interaction potentials $u_{\alpha\beta}(r)$ and $u_{\alpha R}(r)$. Here, the spherical symmetry of interactions between the particles is assumed. The total electric field $\vec{E}(\tilde{R}^{(i)}, \tilde{R}^{(e)}, \vec{r}_0)$ acting on the radiator is given by the superposition of all the ionic and electronic single-particle microfields

$$\begin{aligned} \vec{E}(\tilde{R}^{(i)}, \tilde{R}^{(e)}, \vec{r}_0) = -\frac{\vec{\nabla}_0 U}{z_R e} &= \sum_{j=1}^{N_i} \vec{E}_i(\vec{r}_0 - \vec{r}_j^{\,(i)}) + \sum_{j=1}^{N_e} \vec{E}_e(\vec{r}_0 - \vec{r}_j^{\,(e)}) \\ &= \sum_{j=1}^{N_i} \frac{ze}{4\pi\varepsilon_0 |\vec{r}_0 - r_j{}^{(i)}|^2} \hat{r}_{0j}^{i} - \sum_{j=1}^{N_e} \frac{e}{4\pi\varepsilon_0 |\vec{r}_0 - r_j{}^{(e)}|^2} \hat{r}_{0j}^{e}, \end{aligned} \tag{2.55}$$

where $\hat{r}_{0j}^{\alpha}$ is a unit vector in the direction of $\vec{r}_0 - \vec{r}_j^{(\alpha)}$, $\alpha = e,\, i$. $\vec{\nabla}_0$ is the gradient with respect to $\vec{r}_0$.
This system takes into account both components including the electron-ion correlations in a real plasma. As it was mentioned above, since we are interested in calculating the EMD, (2.8), in a infinite system, the statistical average of any quantity becomes translationally invariant with respect to $\vec{r}_0$ and the location of the test charge can be chosen as the origin $\vec{r}_0 = 0$ without loss of generality.

In this work we apply the coupling parameter integration technique for a quantum TCP generalized by Ortner et al. (Sadykova et al., 2011a) on a base of the method earlier proposed by C. A. Iglesias for OCP in works (Iglesias, 1983; Iglesias and Lebowitz, 1984) and later. This approach is based on recognizing the similarity between the formal expressions for the excess chemical potential and the Fourier transform of $Q(\vec{\epsilon})$, and exponential approximation. The Fourier transform of $Q(\vec{\epsilon})$ is then expressed, without any approximation, in terms of a two-body function which could be interpreted as a "generalized" radial distribution function (RDF) $\mathcal{G}(\vec{r}, \vec{k})$ involving the radiator and one of the plasma particles. This is in a contrast to previous developments which require knowledge of many-body functions (Baranger and Mozer, 1959; Mozer and Baranger, 1960), (Hooper, 1966), (Iglesias and Hooper, 1982; Hooper, 1966).

The normalized microfield distribution $P(\epsilon)$ (2.8) was introduced above in the Sec. 2.1 for the Holtsmark distribution. It has been expressed in terms of the Fourier transform of $Q(E)$ through

$$P(\epsilon) = \frac{2\epsilon}{\pi} \int_0^{\infty} k T_R(k) \sin(\epsilon k) dk, \tag{2.56}$$

and

$$T_R(\vec{k}) = \frac{1}{Z} \int_{\Omega} \exp[\imath \vec{k} \cdot \vec{E}(\tilde{R}^{(i)}, \tilde{R}^{(e)}, \vec{r}_0)] e^{-\beta U(\tilde{R}^{(i)}, \tilde{R}^{(e)}, \vec{r}_0)} d\vec{r}_0 d\tilde{R}^{(i)} d\tilde{R}^{(e)}. \tag{2.57}$$

here R denotes the fact that the TCP electric field is produced at a radiator R.

Following the (2.57) the Fourier transform of the EMD probability density can be alternatively represented as:

$$T_R(\vec{k}) = \frac{Z_R(\vec{k})}{Z}, \tag{2.58}$$

where

$$Z_R(\vec{k}) = \int_\Omega e^{-\beta U(\tilde{R}^{(i)},\tilde{R}^{(e)},\vec{k})} d\tilde{R}^{(i)} d\tilde{R}^{(e)}, \tag{2.59}$$

here Z is defined in Eq.(2.53). The function can be interpreted as the generalized configurational partition function for a system with "potential energy" $U(\tilde{R}^{(i)}, \tilde{R}^{(e)}, \vec{k}) = U(\tilde{R}^{(i)}, \tilde{R}^{(e)}) - \imath k_B T(\vec{k} \cdot \vec{E})$. To accomplish this we introduce the parameter λ which is defined as the magnitude of the vector $\vec{k} = \lambda \hat{k}$, where $\hat{k}$ is a unit vector in the direction of $\vec{k}$.

From the definition of $T(\vec{k})$ in Eq. (2.58) we may write

$$\begin{aligned} \ln T_R(\vec{k}) &= \ln[Z_R(\lambda = \vec{k}) / Z_R(\lambda = 0)] \\ &= \int_0^k d\lambda \frac{\partial \ln Z_R(\vec{k})}{\partial \lambda} = \int_0^k d\lambda \frac{< (\imath \hat{k} \cdot \vec{E}) \exp(\imath \vec{k} \cdot \vec{E}) >}{< \exp(\imath \vec{k} \cdot \vec{E}) >} \\ &= \imath \hat{k} \sum_\alpha n_\alpha \int_0^k d\lambda \int d\vec{r} \vec{E}_\alpha(\vec{r}) [\mathcal{G}_{\alpha R}(\vec{r}, \lambda \hat{k}) - 1]. \end{aligned} \tag{2.60}$$

Here $\vec{k} = \hat{k}\lambda$, $\vec{E}_\alpha(\vec{r}) = z_\alpha e \hat{r} / 4\pi\varepsilon_0 (r^{(\alpha)})^2$ with $z_e = -1$, $z_i = z$ is the single particle either ionic or electrical fields. Inserting the electric fields into the Eq. (2.60) we will get a more simplified view

$$\ln T_R(\vec{k}) = \imath \hat{k} n_e \int_0^k d\lambda \int d\vec{r} \vec{E}_e(\vec{r}) [\mathcal{G}_{iR}(\vec{r}, \vec{k}) - \mathcal{G}_{eR}(\vec{r}, \vec{k})]. \tag{2.61}$$

$\mathcal{G}_{\alpha R}(\vec{r}, \vec{k})$ represents the pair correlation functions between the radiator and the plasma particles in a fictitious system whose interaction potential is given by the complex quantity $U(\tilde{R}^{(i)}, \tilde{R}^{(e)}, \vec{k})$, i.e.,

$$\mathcal{G}_{iR}(\vec{r}_1, \vec{k}) = \frac{\Omega^2}{Z_R(\vec{k})} \int_\Omega e^{-\beta U(\tilde{R}^{(i)},\tilde{R}^{(e)},\vec{k})} d\tilde{R}_1^{(i)} d\tilde{R}^{(e)}, \tag{2.62}$$

$$\mathcal{G}_{eR}(\vec{r}_1, \vec{k}) = \frac{\Omega^2}{Z_R(\vec{k})} \int_\Omega e^{-\beta U(\tilde{R}^{(i)},\tilde{R}^{(e)},\vec{k})} d\tilde{R}_1^{(e)} d\tilde{R}^{(i)}. \tag{2.63}$$

Here $\tilde{R}_s^{(\alpha)} = \Pi_{a=s+1}^{N_\alpha} d\vec{r}_a^{(\alpha)}$ is the reduced volume element in a phase space which does not involve the particles $1, 2, \cdots, s$ of plasma species α. At $\vec{k} \to 0$ they coincide with the actual RDF $g_{\alpha R}$:

$$g_{\alpha R}(\vec{r}_1) = \frac{\Omega^2}{Z} \int_\Omega e^{-\beta U(\tilde{R}^{(i)},\tilde{R}^{(e)})} d\tilde{R}_1^{(\alpha)} d\tilde{R}^{(\alpha^*)}. \tag{2.64}$$

Here, $U(\tilde{R}^{(i)}, \tilde{R}^{(e)})$ does not depend on $\vec{r}_0$, $\alpha^* = i$ if $\alpha = e$ and $\alpha^* = e$ if $\alpha = i$. The pair correlation functions given by Eq. (2.64) describe coupling between the radiator (ion)

and plasma particles. When the coupling between the radiator and particles vanishes, e.g. radiator is a neutral point, the pair correlation function behaves like $g_{\alpha R} \to 1$. If the radiator is a particle of plasma species β these correlation functions coincide with the RDF of bulk plasma, $g_{\alpha R} \equiv g_{\alpha\beta}$.

The central problem is now the evaluation of $\mathcal{G}_{\alpha R}(\vec{r}, \vec{k})$. This complex correlation function must be known in the interval from 0 to k. Usually approximation schemes of the type commonly employed in the liquid theory are applied.

As it was mentioned in Sec. 2.2, many of these schemes are based on "thermodynamic perturbation theory" (Zwanzig, 1954). Here we apply the exponential approximation (Iglesias et al., 1985; Iglesias and Lebowitz, 1984; Iglesias et al., 1983; Iglesias, 1983), (Andersen and Chandler, 1972). In TCP case, the electric fields $\vec{\mathcal{E}}_\alpha(\vec{r})$ may be interpreted as effective electric fields in the fictitious TCP system which have no dependence on $\vec{k}$. Taking into account that $< \vec{E} >= 0$ we obtain

$$\vec{\mathcal{E}}_\alpha = \vec{E}_\alpha + \sum_\beta n_\beta \int d\vec{r}_1 \vec{E}_\beta(\vec{r}_1)[g_{\alpha\beta}(|\vec{r} - \vec{r}_1|) - 1]. \tag{2.65}$$

Since $g_{\alpha R}(r)$ depends only on $|\vec{r} - \vec{r}_1|$ the effective electric fields in (2.65) can be represented as $\vec{\mathcal{E}}_\alpha(\vec{r}) = \hat{r}\mathcal{E}_\alpha$. The single particle electric fields can be written as $\vec{E}_\alpha = \hat{r}E_\alpha$. In the weak or moderately coupling regime ($\Gamma_{ii} \to 0$) the pair correlation function (RDF) in the TCP can be given by the linear Debye-Hückel approximation (Kraeft et al., 1986)

$$g_{\alpha R}(r) \approx 1 - \frac{z_\alpha z_R e^2}{k_B T r} \exp(-r/r_D). \tag{2.66}$$

Inserting Eq. (2.66) into (2.65) we get the following effective Debye screened field

$$\mathcal{E}_\alpha(r) = \frac{z_\alpha e}{r^2}(1 + \chi r) \exp(-\chi r). \tag{2.67}$$

here $\alpha = e, i$. We would like to point out that the use of Debye-Hückel form (2.38) for $g_{\alpha R}(r)$ and electronic effective fields at high Γ_{ii} should be questioned when the quantum-mechanical diffraction effects and ion shell structure play a significant role in their correlations. That is why in our works for screened particle interactions we used the screened Deutsch (Sadykova et al., 2004), Kelbg (Sadykova and Ebeling, 2007), (Sadykova et al., 2005) potentials and derived the screened Hellmann-Gurskii-Krasko pseudopotentials which in addition to the quantum diffraction effects and symmetry take into account the ion shell structure (Sadykova et al., 2009a,b). The derivation of HGK pseudopotential is described later in Subsec. 4.1.2 and in Sec. 3.1 on P. 42.
Alternatively this can be done on the basis of the potential of mean force approximation (PMF) with the help of logarithmic derivative of the actual RDF (Yan and Ichimaru, 1986), (Nersisyan et al., 2005).

We now use the exponential approximation (Iglesias et al., 1983) and make the ansatz

$$\mathcal{G}_{\alpha R}(\vec{r}, \vec{k}) = g_{\alpha R}(r) \exp[\imath \vec{k} \cdot \vec{\mathcal{E}}_\alpha(r)] \tag{2.68}$$

and integrate (2.60) with respect to λ to find

$$\ln T_R(k) = \sum_\alpha 4\pi n_\alpha \int_0^\infty E_\alpha(r) \left[\frac{j_0\left(k\mathcal{E}_\alpha(r)\right) - 1}{\mathcal{E}_\alpha(r)}\right] g_{\alpha R}(r) r^2 dr, \tag{2.69}$$

j_0 is the spherical Bessel function of order zero and the integrations over the parameter λ and the angles have been done. Equation (2.69) is the main results of Ortner et al. (Ortner et al., 2000). $g_{\alpha R}(r)$ represents the radial distribution function for a screened ion and electron subsystems in TCP case. In this work we instead apply the classical approach based on the BBGKY chain of Bogoljubov equations (Bogoljubov, 1946, 1962) to get screened fields directly from the screened Hellmann-Gurskii-Krasko pseudopotentials. Correspondingly, the actual radial distribution function is estimated as following

$$g_{\alpha R}(r) = \exp\left(-\frac{\Phi_{\alpha R}(r)}{k_B T}\right) \tag{2.70}$$

where $\Phi_{\alpha R}(r)$ represents either the screened Hellmann-Gurskii-Krasko pseudopotential in a weakly and moderately coupled plasma approximation Eqs. (4.15-4.19) in the Sec. 4.1.2 or the screened Kelbg Eq. (4.24) in the Sec. 3.1. If the radiator represents one of the ions $z_R > 0$ then $\Phi_{\alpha R}$ corresponds to $\Phi_{\alpha i}$. Inserting (2.70) and (2.67) into (2.68) the generalized RDF will take the following view

$$\mathcal{G}_{\alpha R}(\vec{r}, \vec{k}) = \exp\left(-\frac{\Phi_{\alpha R}(r)}{k_B T}\right) \exp[\imath\vec{k}\cdot\hat{r}\frac{z_\alpha e}{r^2}(1+\chi r)\exp(-\chi r)] \tag{2.71}$$

In our works (Sadykova and Ebeling, 2007; Sadykova et al., 2009a,b, 2011a) we used the Eqs. (2.61), (2.71).
In order to improve the results in moderately and stronger coupled plasma approximation we substituted the expressions for the screened fields (4.24) by the Eqs. (4.15-4.19) in the Sec. 4.1.2 (Sadykova et al., 2011a), whereas the effective fields can be calculated as following

$$\vec{\mathcal{E}}_\alpha = -\frac{1}{z_R e}\vec{\nabla}_r \Phi_{\alpha R}(r), \tag{2.72}$$

here for better improvement the $\Phi_{\alpha R}(r)$ ($\alpha = e$ or i) the equations (4.15)- (4.19) in the Sec. 4.1.2 should be used.
It is now possible to evaluate $T_R(k)$ from Eqs. (2.69) in terms of the radial distribution function (2.70), screened Hellmann-Gurskii-Krasko pseudopotentials (4.24) (Sadykova et al., 2009a) in Sec. 4.1.2, screened Kelbg Eqs. (4.15-4.19) in the Sec. 3.1 and effective fields (2.67).

Let us say few words about the APEX approach. Iglesias, Lebowitz and MacGowan proposed the APEX scheme for the classical OCP with bare Coulomb interaction. In order to fulfill the exact second moment $< E^2 >_{OCP} = k_B T n_e / z_R \varepsilon_0$, Eq. (2.44) must take the form

$$\int_0^\infty \mathcal{E}_i(r) g_{iR}(r) dr = \frac{k_B T}{z_R e}, \tag{2.73}$$

where $\mathcal{E}_i$ is assumed to take the Debye-Hückel-type screened interaction with the free adjustable parameter satisfying the relation (2.73). The resulting curves showed excellent

agreement with the computer simulation MD and MC data even at high Γ_{ee}. However, one encounters the difficulties when this method is applied for a TCP plasma, by treating the Debye-Hückel-type interaction separately for the electrons and ions and introducing two adjustable parameters. Then the second moment rule (2.73)for TCP becomes ambiguous since it allows for many different choices of the adjustable screening lengths. This problem can be solved for ionic mixtures by requiring that the second moment rule is satisfied satisfied species by species (Iglesias and Lebowitz, 1984; Iglesias et al., 1985).

2.3.1 The second moment

As it has been mentioned above a knowledge of moment sum rule is often useful in developing approximation schemes for fluids and liquids.

The second moment within the exponential approximation (2.68) can be found from (2.69) in the limit $k \to 0$. It yields (Yan and Ichimaru, 1986)

$$< E^2 >_{TCP} = \sum_{\alpha} 4\pi n_{\alpha} \int_0^{\infty} E_{\alpha}(r)\mathcal{E}_{\alpha}(r)g_{\alpha R}(r)r^2 dr, \tag{2.74}$$

Let us consider now the exact expression for the second moment of the microfield distribution in TCP and for a charged radiator. The second moment can be written as following

$$< E^2 >= \frac{1}{(z_R e)^2} < \vec{\nabla}_0 U \cdot \vec{\nabla}_0 U >, \tag{2.75}$$

where $\vec{\nabla}_0$ is the gradient with respect to $\vec{r}_0$ and the average is taken over the canonical ensemble defined in (2.1). Noting that $e^{-U/k_B T}(\vec{\nabla}_0 U) = -k_B T(\vec{\nabla}_0 e^{-U/k_B T})$, substituting this into Eq. (2.75), integrating by parts, and setting the surface terms equal to zero yields

$$< E^2 >= \frac{k_B T}{(z_R e)^2} < {\nabla_0}^2 U >= -\frac{k_B T}{z_R e} < \vec{\nabla}_0 \cdot \vec{E} > \tag{2.76}$$

Inserting (2.55) and $\vec{\nabla} \cdot \vec{E}_{\alpha}(\vec{r}) = -(1/r^2)[r^2 u'_{\alpha R}/z_R e]'$ into (2.76), taking advantage of Poisson's equation and using the translational symmetry, we have (Nersisyan et al., 2005)

$$< E^2 >= -\frac{k_B T 4\pi}{z_R^2 e^2} \left(\int_0^{\infty} [r^2 u'_{iR}]' n_i g_{iR}(r) + \int_0^{\infty} [r^2 u'_{eR}]' n_e g_{eR}(r) \right) dr, \tag{2.77}$$

The functions $g_{\alpha R}(r)$ have been described above, see Eq. (2.64), where $n_{\alpha} g_{\alpha R}(r)$ is the density of plasma particles α at a distance r from the radiator. The interaction potential $U(\tilde{R}^{(\alpha)})$ does not depend on $\vec{r}_0$. The exact second moment of the EMD (2.77) must be fulfilled by (2.74).

To get the effective fields for TCP we applied the Debye-Hückel ansatz (2.67) which provides a quite good agreement with the computer simulation data for weakly or moderately coupled plasma when the coupling parameter $\Gamma_{ii} \lesssim 1$. Using Eq. (2.70) we can represent this field as

$$\mathcal{E}_{\alpha} = \frac{k_B T}{z_R e} \frac{\partial}{\partial r} [\ln g_{\alpha R}(r)]. \tag{2.78}$$

Inserting Eq. (2.78) into (2.74) automatically satisfies the sum rule (2.77) without any adjustable parameter. Summarizing all the said above, we can calculate the EMDs with

the exact second moment using the Eq. (2.56). In dimensionless electric field units we get

$$P(\beta) = \frac{2\beta}{\pi} \int_0^\infty k^* T_R(k^*) \sin(\beta k^*) dk^*,$$

where $\beta = E/E_0$ and $k^* = kE_0$, $E_0 = \frac{ze}{4\pi\varepsilon_0 {r_{ei}}^2}$ with r_{ei} being the electron-ion spacing and Eqs. (2.56), (2.69), (2.70) and (2.67). This approach is based on integral-equation method, exponential approximation (2.68) and classical Bogoljubov approach (BBGKY) for screened Hellmann-Gurskii-Krasko pseudopotentials (4.24) (Sadykova et al., 2009a) in Sec. 4.1.2, screened Kelbg Eqs. (4.15-4.19) in the Sec. 3.1.

The TCP Coulomb system

Let us consider now the ionic TCP model. If the interaction between particles is described by the classical bare Coulomb potential, then taking advantage of Poisson's equation we can write

$$\nabla_0{}^2 U = \frac{z_R e^2}{\varepsilon_0} \left(\sum_{l=1}^{N_e} \delta(\vec{r}_l) - z \sum_{j=1}^{N_i} \delta(\vec{r}_j)\right) \tag{2.79}$$

Inserting this equation into (2.76) and taking into account Eq. (2.77) we get

$$\begin{aligned} < E^2 >_{TCP} &= \frac{k_B T n_e}{\varepsilon_0 z_R} \int_0^\infty \delta(r) g_{eR}(r) dr - \frac{k_B T z n_i}{\varepsilon_0 z_R} \int_0^\infty \delta(r) g_{iR}(r) dr \\ &= \frac{k_B T n_e}{\varepsilon_0 z_R} (g_{eR}(0) - g_{iR}(0)), \end{aligned} \tag{2.80}$$

Here is assumed that for $z_R > 0$, $g_{iR}(0) = 0$, Eq. (2.64), if quantum-diffraction effects are negligible for the ions, whereas $g_{eR}(r)$ diverges at small distances for a bare Coulomb potential. This shows that the second moment of the microfield distribution does not exist for a classical Coulomb TCP. But in the OCP limit $g_{eR}(0) = 1$ one recovers the result $< E^2 >_{OCP} = k_B T n_e / z_R \varepsilon_0$ for classical ionic OCP.

2.3.2 The tails

As it was shown above in the section 2.1, when the correlation between the particles are not taken into account, i.e. $\Gamma = 0$, then in the case of very strong fields at $\beta \to \infty$, the Holtsmark distribution has the asymptote $P(\beta) \approx 1.5\beta^{-5/2}$, which is close to the asymptote of the nearest neighbor field distribution obtained by Lewis and Margenau for low-frequency model at an ion (Lewis and Margenau, 1958)

$$P(\beta) = C\beta^{-5/2} \exp\left(-\Gamma_{ii}\sqrt{\beta}\right) \left[1 + \frac{C}{12}\frac{\Gamma_{ii}}{\beta} + \cdots\right], \tag{2.81}$$

where $C = \sqrt{\frac{2}{\pi}}\frac{15}{8}$.
Later on, M. Baranger and B. Mozer introduced the pair correlations at $\Gamma \lesssim 1$ into the high-frequency model at a neutral point and got the following asymptote (Baranger and

Mozer, 1959)

$$P(\beta) = P_H(\beta)|_{\beta\to\infty} - (r_{ee}/r_{De})\beta^{-7/2}(0.5453(r_{ee}/r_{De}) + 11.78\beta^{-1} + 114.6\beta^{-5/2} + \cdots). \tag{2.82}$$

where $P_H(\beta)|_{\beta\to\infty}$ represents the Holtsmark asymptote.
In the opposite limit of extremely strong correlations $\Gamma \to \infty$, the Mayer model is applicable, in which every ion is assumed to oscillate independently of the others around its equilibrium position at the ion-sphere center (Mayer, 1947), (Broyles, 1957, 1955). The model for the charged radiator yields

$$P(\beta) = \frac{1}{2\sqrt{\pi}A^{3/2}}{\Gamma_{ii}}^{3/2}\beta^2 \exp\left(-\frac{\beta^2\Gamma_{ii}}{4A}\right), \tag{2.83}$$

where $A = \frac{15}{4}\sqrt{\frac{2}{\pi}}\frac{1}{3!}$. The Mayer model fails in the strong-field limit, because in this case one should consider a test ion that lies at a very short distance $r \propto \beta^{-1/2}$ from the nearest perturbing ion. Then the geometrical and Boltzmann factors give at $\beta \to \infty$ $P(\beta) \sim \beta^{-5/2}\exp(-\Gamma_{ii}\sqrt{\beta})$. A. Y. Potekhin et. al. derived a more accurate functional form of the asymptotic behavior of $P(\beta)$ at large β (Potekhin et al., 2002)

$$P(\beta) \sim B\beta^{-5/2}\exp\left(-C\beta^{1/2} - \beta^{-3/2}\right). \tag{2.84}$$

with the adjustable parameters (C, B). These parameters can be fitted using the computer simulation tools like Molecular Dynamics and Monte-Carlo.
Let us consider now the limit $lim_{\beta\to\infty}P(\beta)$. In this case the stationary phase limit can be applied (Feller, 1970), meaning that l^* are negligibly small . Then, consider the term (2.69) at the limit $k \to 0$:

$$\lim_{k\to 0} \ln T = -\frac{k^2}{6} < E^2 >_{TCP}, \tag{2.85}$$

here $< E^2 >_{TCP}$ is the second moment of the TCP defined by Eq. (2.74). Inserting Eq. (2.85) into the Eq. (2.56), skipping "TCP"-subscript and integrating over k we get the following asymptote

$$\lim_{\beta\to\infty} P(\beta) = 3\sqrt{\frac{6}{\pi}}\frac{\beta^2}{< \beta^2 >^{3/2}} \exp\left(-\frac{3}{2}\frac{\beta^2}{< \beta^2 >}\right), \tag{2.86}$$

where the integral $\int_0^\infty x \cdot e^{-p^2x^2} sin(ax)dx = \frac{a\sqrt{\pi}}{4p^3}e^{\frac{-a^2}{4p^2}}$ have been used (Gradstejn and Ryzhik, 1971) and the expression $P(\beta) = E_0P(E)$ has been taken into account.

3 Electric microfield distributions in electron one-component plasmas and mass-symmetrical electron-positron two-component plasmas

In calculations of the electric microfield distributions interaction potentials play a crucial role. Usually, for simplicity, one considers the charges in a plasma medium as points and do not take into account the ion shell structure.

3.1 Pseudopotential models for point charges one-component and two-component plasmas. Screened Deutsch, Kelbg and generalized Kelbg models

Coulomb potential

Often, the Coulomb potential is used.

$$\varphi_{ab}(r) = \frac{e_a e_b}{4\pi\varepsilon_0}\frac{1}{r}, \tag{3.1}$$

where e_a, e_b are the electric charges of the interacting particles. There is a well known difficulty in determination of various properties of dense plasma connected with the long-range character of bare Coulomb interacting particles. This difficulty (singularity) can be avoided by taking into account the collective effects connected with the great number of interacting particles, i.e. screening effects.

Debye potential

The screening is a fundamental property of a plasma. The Coulomb potential of a charged particle immersed into a plasma is shielded out at the distance of the order of Debye length

$$\frac{1}{r_D^2} = \sum_{a=e,i}\frac{4\pi n_a {z_a}^2 e^2}{4\pi\varepsilon_0 k_B T}, \tag{3.2}$$

resulting in a well known screened Debye-Hückel potential (Falkenhagen, 1971):

$$\Phi_{ab}(r) = \frac{e_a e_b}{4\pi\varepsilon_0}\frac{e^{-r/r_D}}{r}. \tag{3.3}$$

In the Figure 3.1 the Coulomb potential compared to the screened Debye-Hückel potential. As one can easily see at large distances the potentials start to deviate from each other describing in this way the screening effect and the screening is effectively completed over a distance of the order of $2r_B \approx r_D$. One should notice, the Coulomb and Deutsch potential do make no difference between the types of interactions except the direction of interaction, i.e $|\Phi_{ei}(r)| = |\Phi_{ee}(r)| = |\Phi_{ii}(r)|$. Furthermore, we would like to point out that for alkali and Be^{2+} plasmas, studied in this work, the Coulombic law is not applicable, since there are strong deviations from Coulomb law at small distances due to the influence of the core electrons.

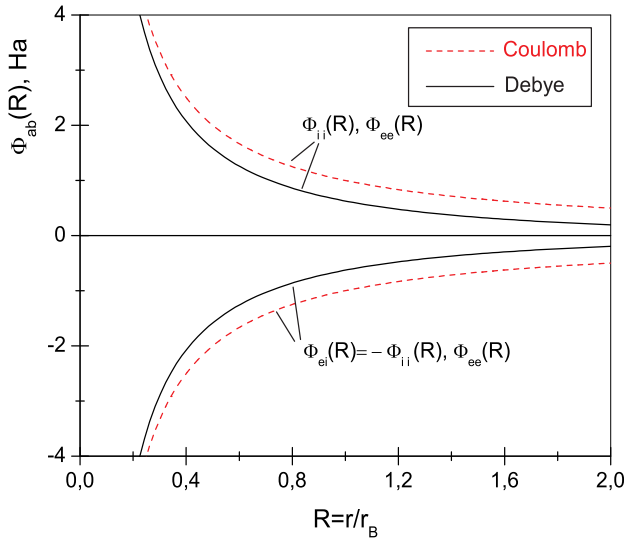

Figure 3.1: Comparison between the Coulomb and Debye electron-electron Φ_{ee}, electron-ion Φ_{ei} and ion-ion Φ_{ii} potentials of semiclassical Hydrogen-like point charges plasma against the dimensionless distance $R = r/r_B$ at $T = 30000$ K, $1 \cdot 10^{28}$ m^{-3}, $\Gamma_{ii} = 2$.

Deutsch pseudopotential

When plasma density increases the ratio between the Landau length and the thermal de Broglie wave length decreases and the quantum-mechanical effects begin to play an important role. To determine the thermodynamic and transport properties of semiclassical fully ionized plasmas effective potentials (pseudopotentials) simulating quantum effects of diffraction and symmetry are widely used (Kraeft et al., 1986), (Hansen and McDonald, 1981, 1990). In Particular, C. Deutsch obtained the following pseudopotential taking into account diffraction (Deutsch, 1977):

$$\varphi_{ab} = \frac{e_a e_b}{4\pi\varepsilon_0 r}\left[1 - \exp\left(-\frac{r}{\lambda_{ab}}\right)\right], \tag{3.4}$$

where $\lambda_{ab} = \hbar/\sqrt{2\pi\mu_{ab}k_BT}$ is the electron thermal de-Broglie wavelength, $\mu_{ab} = m_a m_b/(m_a + m_b)$ is the reduced mass of $a-b$ pair. This pseudopotential was improved later taking into account the symmetry affects as well (Minoo et al., 1981):

$$\varphi_{ab} = \frac{e_a e_b}{4\pi\varepsilon_0 r}\left[1 - \exp\left(-\frac{r}{\lambda_{ab}}\right)\right] + \delta_{ae}\delta_{be}k_BT\ln 2\exp\left(-\frac{r^2}{\lambda_{ee}^2\pi\ln 2}\right), \tag{3.5}$$

where δ_{ab} is the Kronecker delta.

Screened Deutsch pseudopotential

It is of high interest to construct a pseudopotential model of particle interaction in the dense high-temperature plasma, taking into account both the quantum-mechanical effects at short distances and the field screening effects at large distances. In (Arkhipov et al., 2000) the authors developed the approach based on the classical Bogoljubov-Born-Green-Kirkwood-Yvon (BBGKY) chain (Bogoljubov, 1946, 1962) for the equilibrium distribution functions where the pseudopotential (3.5) was taken as a micro-pseudopotential. Following (Ecker, 1972), the authors (Arkhipov et al., 2000) deduced the following system of integral-differential equations for the pseudopotential Φ_{ab} in the framework of the pair correlation approximation:

$$\Delta_i\Phi_{ab}(\vec{r}_i^{\,a}, \vec{r}_j^{\,b}) = \Delta_i\varphi_{ab}(\vec{r}_i^{\,a}, \vec{r}_j^{\,b}) - \sum_{c=e,i}\frac{n_c}{k_BT}\int d\vec{r}_m^{\,c}\Delta_i\varphi_{ac}(\vec{r}_i^{\,a}, \vec{r}_j^{\,c})\Phi_{cb}(\vec{r}_m^{\,c}, \vec{r}_j^{\,b}) \tag{3.6}$$

Here Δ_i denotes the Laplace operator acting on the coordinates of the ith particle. $\varphi_{ab}(r)$ represents the Deutsch pseudopotential.

In Fourier space this system of integral-differential equations (3.6) turns into a system of linear algebraic equations:

$$\Phi_{ab}(k) = \varphi_{ab}(k) - \frac{1}{k_BT}\left[n_e\varphi_{ae}(k)\Phi_{eb}(k) + n_i\varphi_{ai}(k)\Phi_{ib}(k)\right] \tag{3.7}$$

where $a, b = i, e$. Solving the system (3.7) for two-component plasma one can derive the following expressions for the Fourier transform $\Phi_{ab}(k)$ of the pseudopotential $\Phi_{ab}(r)$:

$$\Phi_{ei}(k) = \frac{ze^2}{\varepsilon_0\Delta}\frac{1}{k^2(1 + k^2\lambda_{ei}^2)}, \tag{3.8}$$

$$\begin{aligned}\Phi_{ee}(k) =& \frac{e^2}{\varepsilon_0\Delta}\left\{\frac{1}{k^2(1 + k^2{\lambda_{ee}}^2)}\right.\\ &+ \frac{1}{k^4{r_{Di}}^2}\left[\frac{1}{(1 + k^2{\lambda_{ee}}^2)(1 + k^2{\lambda_{ii}}^2)} - \frac{1}{(1 + k^2{\lambda_{ei}}^2)^2}\right]\\ &\left.+ A\left(1 + \frac{1}{k^2{r_{Di}}^2(1 + k^2{\lambda_{ii}}^2)}\right)\exp\left(-\frac{k^2}{4b}\right)\right\},\end{aligned} \tag{3.9}$$

$$\begin{aligned}\Phi_{ii}(k) =& \frac{z^2e^2}{\varepsilon_0\Delta}\left\{\frac{1}{k^2(1+k^2{\lambda_{ii}}^2)}\right.\\ &+\frac{1}{k^4{r_{De}}^2}\left[\frac{1}{(1+k^2{\lambda_{ee}}^2)(1+k^2{\lambda_{ii}}^2)}-\frac{1}{(1+k^2{\lambda_{ei}}^2)^2}\right]\\ &\left.++\frac{A}{k^2{r_{De}}^2(1+k^2{\lambda_{ii}}^2)}\exp\left(-\frac{k^2}{4b}\right)\right\}. \end{aligned} \tag{3.10}$$

Here r_{De}, r_{Di} are the Debye radius of electrons and ions respectively, with $1/{r_{Di}}^2 = z^2e^2n_i/(\varepsilon_0k_BT)$,$1/{r_{De}}^2 = e^2n_e/(\varepsilon_0k_BT)$, $b = ({\lambda_{ee}}^2\pi\ln 2)^{-1}$, $A = k_BT\ln 2\pi^{3/2}b^{-3/2}\cdot$ $\cdot\varepsilon_0/e^2$ and

$$\begin{aligned}\Delta =& 1+\frac{1}{k^2{r_{De}}^2(1+k^2{\lambda_{ee}}^2)}+\frac{1}{k^2{r_{Di}}^2(1+k^2{\lambda_{ii}}^2)}\\ &+\frac{1}{k^4{r_{De}}^2{r_{Di}}^2}\left[\frac{1}{(1+k^2{\lambda_{ee}}^2)(1+k^2{\lambda_{ii}}^2)}-\frac{1}{(1+k^2{\lambda_{ei}}^2)^2}\right]\\ &+\frac{A}{{r_{De}}^2}\left(1+\frac{1}{k^2{r_{Di}}^2(1+k^2{\lambda_{ii}}^2)}\right)\exp\left(-\frac{k^2}{4b}\right). \end{aligned} \tag{3.11}$$

The pseudopotential $\Phi_{ab}(r)$ can be restored from (3.8-3.11) by Fourier transformation

$$\Phi_{ab}(r) = \frac{1}{2\pi^2r}\int\Phi_{ab}(k)k\sin(kr)dk \tag{3.12}$$

Let us consider the limiting cases of the expressions (3.8-3.9).

A. If r_{De}, $r_{Di}\to\infty$, then

$$\Phi_{ab}(r) = \varphi_{ab}(r) \tag{3.13}$$

When the screening effects are negligible, the pseudopotential $\Phi_{ab}(r)$ coincides with the pseudopotential (3.5).

B. If λ_{ee}, λ_{ei}, $\lambda_{ii}\to 0$, then

$$\Phi_{ab}(r) = \frac{e_ae_b}{4\pi\varepsilon_0}\frac{e^{-r/r_D}}{r}, \tag{3.14}$$

where

$$\frac{1}{{r_D}^2} = \sum_{c=e,i}\frac{{e_c}^2n_c}{\varepsilon_0k_BT}. \tag{3.15}$$

Eq. (3.14) means when quantum-mechanical effects are negligible, then the pseudopotential $\Phi_{ab}(r)$ coincides with the Debye-Hückel one.

C. If r_{De}, $r_{Di}\to\infty$, λ_{ee}, λ_{ei}, $\lambda_{ii}\to 0$, then

$$\Phi_{ab}(r) = \frac{e_ae_b}{4\pi\varepsilon_0r}. \tag{3.16}$$

When the quantum-mechanical and screening field effects are negligible, then the

pseudopotential $\Phi_{ab}(r)$ coincides with the Coulomb potential.

D. If $\lambda_{ee}, \lambda_{ei}, \lambda_{ii} \ll r_{De}, r_{Di}$, then for $e-i$ and $i-i$

$$\Phi_{ab}(r) = \frac{e_a e_b}{4\pi\varepsilon_0 r}\left[e^{-r/r_D} - e^{-r/\lambda_{ab}}\right] + \delta_{ae}\delta_{be}k_B T \ln 2 \exp\left(-\frac{r^2}{\lambda_{ee}^2 \pi \ln 2}\right). \quad (3.17)$$

These expressions differ from the potentials (3.5) in the presence of the term $\exp(-r/r_D)$ term in the brackets instead of 1. This case corresponds to the weakly coupled plasmas when $\Gamma \ll 1$. The derived expressions (3.8-3.11) differ from the bare pseudopotentials (3.5) due to the screening terms. The present approximation is restricted to the constraint $\Gamma \lesssim 1$ due to the use of linearization process at the derivation of integral-differential equation (3.6).

In the Figure 3.2 the screened Deutsch pseudopotential (3.8-3.11) compared to the Deutsch (3.5) pseudopotential, Coulomb (3.1) and Debye (3.3) potentials are shown. One can easily see that there is a considerable difference between the Coulomb, Debye and Deutsch pseudo-potentials. First of all, the Deutsch pseudopotential in comparison with the Debye and Coulomb potentials is not symmetric with respect to the type of interactions, i.e. $|\Phi_{ee}(r)| \neq |\Phi_{ei}(r)| \neq |\Phi_{ii}(r)|$. The Coulomb and Debye pseudopotentials are infinite at $r = 0$, whereas the Deutsch and screened Deutsch pseudopotentials due to the quantum-mechanical effects of diffraction are finite. At large distances the Coulomb and Deutsch pseudo-potentials coincide. The same is applied to the Debye and screened Deutsch pseudo-potentials. At the high value of Γ there is a considerable difference between the Coulomb and Debye pseudo-potentials as well as between the Deutsch and screened Deutsch pseudopotentials. This can be explained by that fact that at high Γ the screening taken into account in the Debye and screened Deutsch pseudopotentials starts to play a significant role.

Let us now restore the screened $a-b$ Deutsch pseudopotentials $\Phi_{ab}(r)$ by the Fourier transformation (3.12) and neglect the symmetry effects, ionic screening $r_{Di} \to \infty$ for simplicity, see the Appendix 7. Then, the $\Phi_{ab}(r)$ will split into three types of pseudopotentials in dependence on the parameter range of consideration (Sadykova et al., 2004). For the $\Phi_{ee}(r)$ we have:

1. When $\boldsymbol{C_1 = \frac{r_{De}}{\lambda_{ee}} < 2}$ or $\Gamma_{ee} > \frac{1}{2}\frac{\pi r_s}{3}$

$$\Phi_{ee}(r) = \frac{e^2 C_1^2}{4\pi\varepsilon_0 2ab}\frac{e^{-a\frac{r}{r_{De}}}\sin\left(b\frac{r}{r_{De}}\right)}{r}, \quad (3.18)$$

where $a = \frac{\sqrt{C_1}\sqrt{2+C_1}}{2}$, $b = \frac{\sqrt{C_1}\sqrt{2-C_1}}{2}$.

2. When $\boldsymbol{C_1 = \frac{r_{De}}{\lambda_{ee}} = 2}$ or $\boldsymbol{\Gamma_{ee} = \frac{1}{2}\frac{ß r_s}{3}}$

$$\Phi_{ee}(r) = \frac{\sqrt{2}e^2}{4\pi\varepsilon_0 r_{De}} e^{-\sqrt{2}\frac{r}{r_{De}}}, \quad (3.19)$$

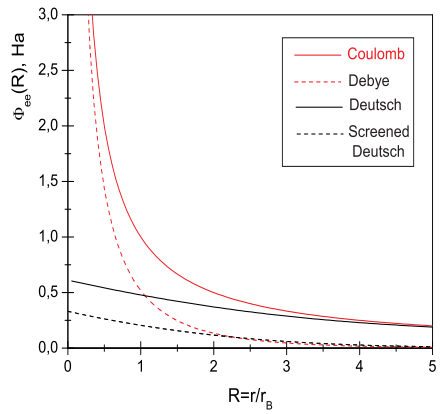

a)

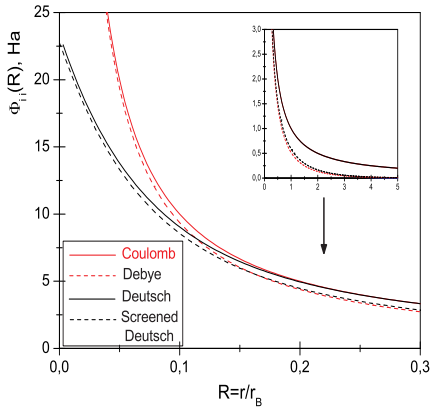

c)

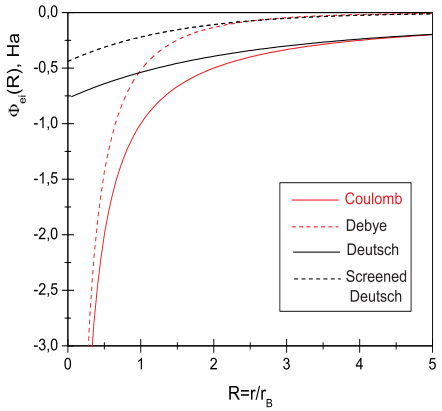

b)

Figure 3.2: Comparison between electron-electron (a), electron-ion (b), ion-ion (c) Coulomb (3.1), Debye (3.3) potentials, Deutsch (3.5) and Screened Deutsch (3.8-3.11) pseudopotentials in Hartree units of semiclassical Hydrogen plasma against the dimensionless distance $R = r/r_B$ at $T = 30000$ K, $1 \cdot 10^28$ m^{-3}, $\Gamma_{ii} = 2$.

3. When $\boldsymbol{C_1 = \frac{r_{De}}{\lambda_{ee}} > 2}$ or $\boldsymbol{\Gamma_{ee} < \frac{1}{2}\frac{\pi r_s}{3}}$

$$\Phi_{ee}(r) = \frac{e^2 C_1^2}{4\pi\varepsilon_0 {r_{De}}^2 (A_1 - A_2)} \frac{e^{-\sqrt{A_1}r} - e^{-\sqrt{A_2}r}}{r}, \tag{3.20}$$

where $A_1 = \frac{C_1(C_1+\sqrt{C_1^2-4})}{2{r_{De}}^2}$, $A_2 = \frac{C_1(C_1-\sqrt{C_1^2-4})}{2{r_{De}}^2}$.

Eq. 3.18 possesses the oscillating $\sin(r)$ function what demonstrates that at higher plasma density or low r_s the local minima and maxima arise which are due to the short-range formation as a result of competition between the quantum-mechanical and screening field effects when the scales of their action are comparable. This is demonstrated in the Figure 3.3, where the fully restored $\Phi_{ee}(r)$ pseudopotential (3.9), (3.12) at $C_1 = \frac{r_{De}}{\lambda_{ee}} < 2$ is plotted. As one can easily see, the Debye potential does not reflect such short-order formation.

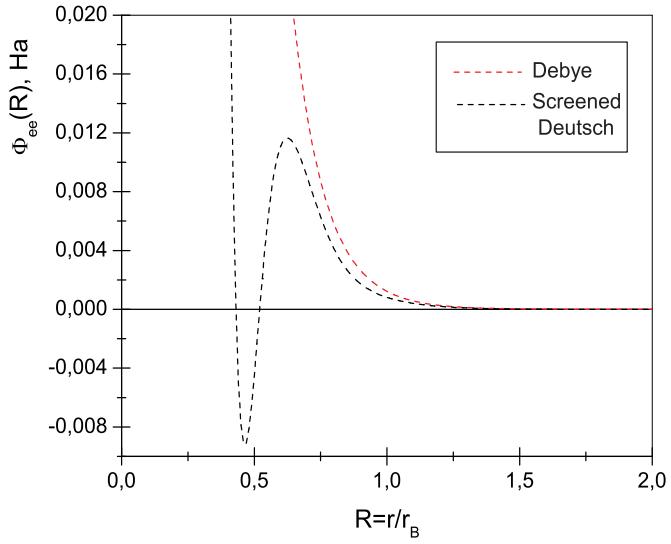

Figure 3.3: Comparison between the Debye (3.3) and Screened Deutsch (3.9), (3.12) pseudopotentials of semiclassical Hydrogen-like point charges plasma against the dimensionless distance $R = r/r_B$ at $T = 5248578$ K and $n_e = 0.2 \cdot 10^{27}$ cm^{-3}.

For the $\Phi_{ii}(r)$ we have:

1. When $\boldsymbol{C_1 = \frac{r_{De}}{\lambda_{ee}} < 2}$ or $\boldsymbol{\Gamma_{ee} > \frac{1}{2}\frac{\pi r_s}{3}}$

$$\begin{aligned}\Phi_{ii}(r) =& \frac{2z^2e^2}{4\pi\varepsilon_0 r} - \frac{z^2e^2}{4\pi\varepsilon_0 r}e^{-\frac{r}{\lambda_{ii}}} - \alpha\frac{z^2e^2}{4\pi\varepsilon_0 r}e^{-\frac{r}{\lambda_{ei}}} - \beta\frac{z^2e^2}{8\pi\varepsilon_0\lambda_{ei}}e^{-\frac{r}{\lambda_{ei}}} \\ &+ \gamma\frac{z^2e^2}{4\pi\varepsilon_0 r}e^{-a\frac{r}{r_{De}}}\sin\left(b\frac{r}{r_{De}}\right) + \theta\frac{z^2e^2}{4\pi\varepsilon_0 r}e^{-a\frac{r}{r_{De}}}\cos\left(b\frac{r}{r_{De}}\right), \end{aligned} \tag{3.21}$$

where $a = \frac{\sqrt{C_1}\sqrt{2+C_1}}{2}$, $b = \frac{\sqrt{C_1}\sqrt{2-C_1}}{2}$, $\alpha = \frac{{C_1}^4-2{C_3}^2({C_3}^2-{C_1}^2)^2}{({C_3}^4-{C_1}^2{C_3}^2+{C_1}^2)^2}$, $\beta = \frac{{C_1}^2-{C_3}^2}{{C_3}^4-{C_1}^2{C_3}^2+{C_1}^2}$, $\gamma = \frac{C_1}{\sqrt{4-{C_1}^2}}\left(\frac{{C_1}^2({C_2}^2-1)}{{C_2}^4-{C_1}^2{C_2}^2+{C_1}^2} + \frac{(2{C_3}^4(2-{C_1}^2)+4{C_3}^2{C_1}^2({C_1}^2-3)+{C_1}^2(-{C_1}^4+5{C_1}^2-4))C_3^4}{2{C_1}^4({C_3}^4-{C_1}^2{C_3}^2+{C_1}^2)^2}\right)$ and $\theta = \frac{(-{C_3}^4+2{C_3}^2({C_1}^2-1)+{C_1}^2(2-{C_1}^2))C_3^4}{{C_1}^2({C_3}^4-{C_1}^2{C_3}^2+{C_1}^2)^2}$ with $C_2 = \frac{r_{De}}{\lambda_{ii}}$, $C_3 = \frac{r_{De}}{\lambda_{ei}}$.

2. When $\boldsymbol{C_1 = \frac{r_{De}}{\lambda_{ee}} = 2}$ or $\boldsymbol{\Gamma_{ee} = \frac{1}{2}\frac{\pi r_s}{3}}$

$$\begin{aligned}\Phi_{ii}(r) =& \frac{2z^2e^2}{4\pi\varepsilon_0 r} - \frac{z^2e^2}{4\pi\varepsilon_0 r}e^{-\frac{r}{\lambda_{ii}}} - \alpha\frac{z^2e^2}{4\pi\varepsilon_0 r}e^{-\frac{r}{\lambda_{ei}}} - \beta\frac{z^2e^2}{8\pi\varepsilon_0\lambda_{ei}}e^{-\frac{r}{\lambda_{ei}}} \\ &+ \gamma\frac{\sqrt{2}z^2e^2}{8\pi\varepsilon_0 r_{De}}e^{-\frac{\sqrt{2}r}{r_{De}}} - \theta\frac{z^2e^2}{4\pi\varepsilon_0 r}e^{-\frac{\sqrt{2}r}{r_{De}}}, \end{aligned} \tag{3.22}$$

where $\alpha = \frac{2(8-{C_3}^2({C_3}^2-4)^2)}{({C_3}^2-2)^4}$, $\beta = \frac{4-{C_3}^2}{({C_3}^2-2)^2}$, $\gamma = \left(\frac{4({C_2}^2-1)}{({C_2}^2-2)^2} + \frac{{C_3}^6(4-{C_3}^2)}{8({C_3}^2-2)^4}\right)$ and $\theta = \frac{{C_3}^2-4}{({C_3}^2-2)^3}$ with $C_2 = \frac{r_{De}}{\lambda_{ii}}$, $C_3 = \frac{r_{De}}{\lambda_{ei}}$.

3. When $\boldsymbol{C_1 = \frac{r_{De}}{\lambda_{ee}} > 2}$ or $\boldsymbol{\Gamma_{ee} < \frac{1}{2}\frac{\pi r_s}{3}}$

$$\begin{aligned}\Phi_{ii}(r) =& \frac{2z^2e^2}{4\pi\varepsilon_0 r} - \frac{z^2e^2}{4\pi\varepsilon_0 r}e^{-\frac{r}{\lambda_{ii}}} - \alpha\frac{z^2e^2}{4\pi\varepsilon_0 r}e^{-\frac{r}{\lambda_{ei}}} - \beta\frac{z^2e^2}{8\pi\varepsilon_0\lambda_{ei}}e^{-\frac{r}{\lambda_{ei}}} \\ &+ \gamma\frac{z^2e^2}{4\pi\varepsilon_0 r}e^{-\sqrt{A_1}r} - \theta\frac{z^2e^2}{4\pi\varepsilon_0 r}e^{-\sqrt{A_2}r}, \end{aligned} \tag{3.23}$$

where $A_1 = \frac{C_1(C_1+\sqrt{C_1^2-4})}{2{r_{De}}^2}$, $A_2 = \frac{C_1(C_1-\sqrt{C_1^2-4})}{2{r_{De}}^2}$, $\alpha = \frac{-2{C_3}^6+4{C_3}^4{C_1}^2-2{C_3}^2{C_1}^4+{C_1}^4}{({C_3}^4-{C_1}^2{C_3}^2+{C_1}^2)^2}$, $\beta = \frac{{C_1}^2-{C_3}^2}{{C_3}^4-{C_1}^2{C_3}^2+{C_1}^2}$, $\gamma = \frac{2A_2}{{\lambda_{ei}}^2A_1(A_1-A_2)(1-{\lambda_{ei}}^2A_1)}$ and $\theta = \frac{2A_1}{{\lambda_{ei}}^2A_2(A_1-A_2)(1-{\lambda_{ei}}^2A_2)}$ with $C_3 = \frac{r_{De}}{\lambda_{ei}}$.

For the $\Phi_{ei}(r)$ we have:

1. When $\boldsymbol{C_1 = \frac{r_{De}}{\lambda_{ee}} < 2}$ or $\boldsymbol{\Gamma_{ee} > \frac{1}{2}\frac{\pi r_s}{3}}$

$$\begin{aligned}\Phi_{ei}(r) =& -\alpha\frac{z^2e^2}{4\pi\varepsilon_0 r}e^{-\frac{r}{\lambda_{ei}}} \\ &- \beta\frac{z^2e^2}{4\pi\varepsilon_0 r}e^{-a\frac{r}{r_{De}}}\sin\left(b\frac{r}{r_{De}}\right) - \gamma\frac{z^2e^2}{4\pi\varepsilon_0 r}e^{-a\frac{r}{r_{De}}}\cos\left(b\frac{r}{r_{De}}\right), \end{aligned} \tag{3.24}$$

where $a = \frac{\sqrt{C_1}\sqrt{2+C_1}}{2}$, $b = \frac{\sqrt{C_1}\sqrt{2-C_1}}{2}$, $C_2 = \frac{r_{De}}{\lambda_{ii}}$, $\alpha = \frac{{C_3}^2({C_1}^2-{C_3}^2)}{({C_3}^4-{C_1}^2{C_3}^2+{C_1}^2)^2}$, $\beta =$

$\frac{C_1}{\sqrt{4-{C_1}^2}}\left(1+\frac{2-{C_1}^2}{{C_3}^2}\right)$ and $\gamma = 1-\frac{{C_1}^2}{{C_3}^2}$ with $C_3 = \frac{r_{De}}{\lambda_{ei}}$.

2. When $\boldsymbol{C_1 = \frac{r_{De}}{\lambda_{ee}} = 2}$ or $\boldsymbol{\Gamma_{ee} = \frac{1}{2}\frac{\pi r_s}{3}}$

$$\Phi_{ei}(r) = -\alpha\frac{z^2e^2}{4\pi\varepsilon_0 r}e^{-\frac{r}{\lambda_{ei}}} - \beta\frac{\sqrt{2}z^2e^2}{8\pi\varepsilon_0 r_{De}}e^{-\frac{\sqrt{2}r}{r_{De}}} - \gamma\frac{z^2e^2}{4\pi\varepsilon_0 r}e^{-\frac{\sqrt{2}r}{r_{De}}}, \tag{3.25}$$

where $\alpha = \frac{{C_3}^2(4-{C_3}^2)}{({C_3}^2-2)^2}$, $\beta = \frac{{C_3}^2}{{C_3}^2-2}$, and $\gamma = \frac{{C_3}^2({C_3}^2-4)}{({C_3}^2-2)^2}$ with $C_3 = \frac{r_{De}}{\lambda_{ei}}$.

3. When $\boldsymbol{C_1 = \frac{r_{De}}{\lambda_{ee}} > 2}$ or $\boldsymbol{\Gamma_{ee} < \frac{1}{2}\frac{\pi r_s}{3}}$

$$\Phi_{ei}(r) = -\alpha\frac{z^2e^2}{4\pi\varepsilon_0 r}e^{-\frac{r}{\lambda_{ei}}} - \beta\frac{z^2e^2}{4\pi\varepsilon_0 r}e^{-\sqrt{A_1}r} + \gamma\frac{z^2e^2}{4\pi\varepsilon_0 r}e^{-\sqrt{A_2}r}, \tag{3.26}$$

where $A_1 = \frac{C_1(C_1+\sqrt{C_1^2-4})}{2{r_{De}}^2}$, $A_2 = \frac{C_1(C_1-\sqrt{C_1^2-4})}{2{r_{De}}^2}$, $\alpha = \frac{{C_3}^2({C_1}^2-{C_3}^2)}{{C_3}^4-{C_1}^2{C_3}^2+{C_1}^2}$, $\beta = \frac{A_2}{(A_1-A_2)(-1+{\lambda_{ei}}^2A_1)}$ and $\gamma = \frac{A_1}{(A_1-A_2)(-1+{\lambda_{ei}}^2A_2)}$ with $C_3 = \frac{r_{De}}{\lambda_{ei}}$.

We would like to note that the expressions (3.21-3.23) and (3.24-3.24) were for the first time derived in this work.

Kelbg pseudopotential

Frequently the Kelbg pseudopotential, obtained by perturbational theory, is used:

$$\varphi_{ab}(r) = \frac{e_a e_b}{4\pi\varepsilon_0}\left(\frac{1-e^{-r^2/\lambda_{ab}^2}}{r} + \frac{\sqrt{\pi}}{\lambda_{ab}}(1-erf(r/\lambda_{ab}))\right), \tag{3.27}$$

where $\lambda_{ab} = \hbar/\sqrt{2m_{ab}k_BT}$ is De Broglie wave length of relative motion of $(a, b = e, i)$, $\hbar$ is the Planck constant and k_B is the Boltzmann constant.

The Kelbg pseudopotential is a good approximation in the case of small interaction parameters $\xi_{ab} = -(e_a e_b)/(4\pi\varepsilon_0 k_B T\lambda_{ab})$ if the interparticle distance r is sufficiently large. In order to attain the correct behaviour also at small distances the corrected (generalized) Kelbg pseudopotential defined in (Ebeling et al., 1999), (Wagenknecht et al., 2001) should be used:

$$\varphi_{ab}(r) = \frac{e_a e_b}{4\pi\varepsilon_0}\frac{1-e^{-r^2/\lambda_{ab}^2}}{r} + \frac{e_a e_b}{4\pi\varepsilon_0}\frac{\sqrt{\pi}}{\lambda_{ab}}(1-erf(r/\lambda_{ab})) - k_BT\tilde{A}_{ab}(\xi_{ab})\exp(-(r/\lambda_{ab})^2) \tag{3.28}$$

The corresponding coefficients for the electron-electron and for the electron-ion interaction read:

$$\begin{aligned}
\tilde{A}_{ee} &= \sqrt{\pi}\,|\xi_{ee}| + \ln\left[2\sqrt{\pi}\,|\xi_{ee}|\int_0^\infty \frac{dyy\exp(-y^2)}{\exp(\pi\,|\xi_{ee}|\,/y)-1}\right] \\
\tilde{A}_{ei} &= -\sqrt{\pi}\,|\xi_{ei}| + \ln\left[\sqrt{\pi}\xi_{ei}^3(\varsigma(3)+\varsigma(5)\xi_{ei}^2) + 4\sqrt{\pi}\xi_{ei}\int_0^\infty \frac{dyy\exp(-y^2)}{1-\exp(\pi\xi_{ei}/y)}\right].
\end{aligned} \tag{3.29}$$

Here $\varsigma(x)$ denotes Riemann's Zeta-function.

Screened Kelbg pseudopotential

It is of great interest to get an analytical expression for the corrected screened Kelbg pseudopotential $\Phi_{ab}(r)$, which takes into account both quantum-mechanical effects of diffraction as well as symmetry, coming from the different spin directions of particles, and screening effects. In this work we apply again the Bogoljubov-Born-Green-Kirkwood-Yvon method described in (Falkenhagen, 1971), which is primarily based on Bogoljubov's works (Bogoljubov, 1962). In the work (Sadykova et al., 2004) following H. Falkenhagen we derived the screened Kelbg pseudopotential (3.27) in the framework of the classical Bogoljubov approach for equillibrium distribution functions described on P. 42. Following the derivation procedure of H. Falkenhagen, we write the BBGKY chain of Bogoljubov RDF equations for a system of charged particles of species a_i as following

$$k_B T \frac{\partial}{\partial \vec{r}_l} g_{a_1 \cdots a_s} + \mu g_{a_1 \cdots a_s} \frac{\partial}{\partial \vec{r}_l} \sum_{1 \le i \le j \le s} \varphi_{a_i a_j} + \sum_{a_{s+1}} n_{a_{s+1}} \int \frac{\partial \varphi_{a_l a_{s+1}}}{\partial \vec{r}_l} g_{a_1 \cdots a_{s+1}} d\vec{r}_{s+1} = 0. \tag{3.30}$$

Here the charged particles located at $\vec{r}_1, \cdot\cdot, \vec{r}_s$ belong to the species $a_1, \cdot\cdot, a_s$ and $g_{a_1 \cdots a_s}$ means RDF (2.64), $\varphi_{a_l a_{s+1}}$ is a pair interaction potential between the particles (micro-pseudo-potential). The equation (3.30) satisfies the equillibrium condition for the forces. In the equation (3.30) the first term means a diffusion force, the second - a direct force and the third one - the force taking into account the collective effects into account, all acting on a l-th particle. In accordance with the Bogoljubov's approach H. Falkenhagen introduced the parameter $\mu = 1$ at the second term which in dimensionless form of (3.30) turns into $\mu = e^2/(4\pi\varepsilon_0 r_D k_B T)$ and at the small densities $\mu \le 1$ with r_D being the Debye radius. That is why Bogoljubov suggested to expand the RDF with respect to this parameter. Let us introduce the irreducible correlation functions $\gamma_a, \gamma_{ab}, \gamma_{abc}$:

$$\begin{aligned} & g_a = \gamma_a, \;\; g_{ab} = \gamma_a \gamma_b + \mu \gamma_{ab} \\ & g_{abc} = \gamma_a \gamma_b \gamma_c + \mu(\gamma_{ab}\gamma_c + \gamma_{ac}\gamma_b + \gamma_{bc}\gamma_a) + \mu^2 \gamma_{abc}, \\ & g_{a_1 \cdots a_s} = \gamma_{a_1}\gamma_{a_2} \cdots \gamma_{a_s} + \mu(\gamma_{a_1 a_2}\gamma_{a_3} \cdots \gamma_{a_s} + \cdots) + \cdots + \mu^s \gamma_{a_1 \cdots a_s}. \end{aligned} \tag{3.31}$$

For homogeneous systems $g_a(\vec{r}) = \gamma_a(\vec{r}) = 1$. We restrict ourselves only to the first equation of the chain and put $l = 1$ then we have

$$k_B T \frac{\partial g_{ab}}{\partial \vec{r}_1} + \mu g_{ab} \frac{\partial \varphi_{ab}}{\partial \vec{r}_1} + \sum_c n_c \int \frac{\partial \varphi_{ac}}{\partial \vec{r}_1} g_{abc} d\vec{r}_3 = 0. \tag{3.32}$$

Here $a_1 = a$, $a_2 = b$, $a_3 = c, \cdots$. Inserting the irreducible correlation functions into Eq. (3.32) we get

$$k_B T \frac{\partial \gamma_{ab}}{\partial \vec{r}_1} + (1 + \mu\gamma_{ab}) \frac{\partial \varphi_{ab}}{\partial \vec{r}_1} + \sum_c n_c \int \frac{\partial \varphi_{ac}}{\partial \vec{r}_1} (\gamma_{ab} + \gamma_{ac} + \gamma_{bc} + \mu\gamma_{abc}) d\vec{r}_3 = 0. \tag{3.33}$$

Taking into account that $\lim_{|r_i-r_j|\to\infty}\gamma_{ab}(\vec{r}_1,\vec{r}_2)\to 0$, $\lim_{|r_i-r_j|\to\infty}\gamma_{ac}(\vec{r}_1,\vec{r}_2)\to 0$ and $\lim_{|r_i-r_j|\to\infty}\gamma_{abc}(\vec{r}_1,\vec{r}_2,\vec{r}_3)\to 0$ we obtain the following

$$k_BT\frac{\partial\gamma_{ab}}{\partial\vec{r}_1}+(1+\mu\gamma_{ab})\frac{\partial\varphi_{ab}}{\partial\vec{r}_1}+\sum_c n_c\int\frac{\partial\varphi_{ac}}{\partial\vec{r}_1}(\gamma_{bc}+\mu\gamma_{abc})d\vec{r}_3=0. \tag{3.34}$$

Similarly one can get the equations of the higher approximation order of correlation functions.

Let us expand the irreducible correlation functions with respect to the parameter μ:

$$\begin{aligned}\gamma_{ab}&=\gamma_{ab}^{(0)}+\mu\gamma_{ab}^{(1)}+\mu^2\gamma_{ab}^{(2)},\\ \gamma_{a_1\cdots a_s}&=\gamma_{a_1\cdots a_s}^{(0)}+\mu\gamma_{a_1\cdots a_s}^{(1)}+\cdots\end{aligned} \tag{3.35}$$

In the first approximation order of correlation function when $\mu\to 0$ the equation (3.34) will turn into

$$k_BT\frac{\partial\gamma_{ab}^{(0)}}{\partial\vec{r}_1}+\frac{\partial\varphi_{ab}}{\partial\vec{r}_1}+\sum_c n_c\int\frac{\partial\varphi_{ac}}{\partial\vec{r}_1}\gamma_{bc}^{(0)}d\vec{r}_3=0. \tag{3.36}$$

After integration, Eq. (3.36) will take the following look

$$k_BT\gamma_{ab}^{(0)}(\vec{r}_1,\vec{r}_2)+\varphi_{ab}(\vec{r}_1,\vec{r}_2)+\sum_c n_c\int\varphi_{ac}(\vec{r}_1,\vec{r}_3)\gamma_{bc}^{(0)}(\vec{r}_2,\vec{r}_3)d\vec{r}_3=0. \tag{3.37}$$

Since the correlation functions depend only on the relative distance between the particles we get

$$\gamma_{ab}(\vec{r}_1,\vec{r}_2)=\gamma_{ab}(\vec{r}_2-\vec{r}_1).$$

Introducing $\vec{r}=\vec{r}_2-\vec{r}_1$, $\vec{r}'=\vec{r}_3-\vec{r}_2$ we obtain

$$k_BT\gamma_{ab}^{(0)}(\vec{r})+\varphi_{ab}(\vec{r})+\sum_c n_c\int\varphi_{ac}(\vec{r}'+\vec{r})\gamma_{bc}^{(0)}(\vec{r}')d\vec{r}'=0. \tag{3.38}$$

In order to solve this set of equations we will make the Foutier-ansatz:

$$\begin{aligned}\gamma_{ab}^{(0)}(\vec{r})&=\frac{1}{(2\pi)^3}\int e^{\imath\vec{k}\cdot\vec{r}}\gamma_{ab}^{(0)}(\vec{k})d\vec{k},\\ \varphi_{ab}(|\vec{r}|)&=\frac{1}{(2\pi)^3}\int e^{\imath\vec{k}\cdot\vec{r}}\varphi_{ab}(\vec{k})d\vec{k}.\end{aligned} \tag{3.39}$$

Inserting the latter we get

$$\frac{1}{(2\pi)^3}\int e^{\imath\vec{k}\cdot\vec{r}}\{k_BT\gamma_{ab}^{(0)}(\vec{k})+\varphi_{ab}(\vec{k})\}d\vec{k}+\sum_c n_c\int\int e^{\imath\vec{k}\cdot(\vec{r}'+\vec{r})}\varphi_{ac}(\vec{k})\gamma_{bc}^{(0)}(\vec{r}')d\vec{k}dr'=0. \tag{3.40}$$

Taking into account

$$\gamma_{bc}^{(0)}(\vec{k})=\int e^{-\imath\vec{k}\cdot\vec{r}}\gamma_{bc}^{(0)}(\vec{r})d\vec{r}, \tag{3.41}$$

and $\gamma_{bc}^{(0)}(-\vec{r}'') = \gamma_{cb}^{(0)}(\vec{r}'')$, making a transformation of the coordinates $r'' = -r'$ we become

$$\frac{1}{(2\pi)^3}\int e^{\imath\vec{k}\cdot\vec{r}}\{k_BT\gamma_{ab}^{(0)}(\vec{k}) + \varphi_{ab}(\vec{k}) + \sum_c n_c\varphi_{ac}(\vec{k})\gamma_{cb}^{(0)}(\vec{k})\} = 0. \tag{3.42}$$

Since r is arbitrary we can write

$$k_BT\gamma_{ab}^{(0)}(\vec{k}) + \varphi_{ab}(\vec{k}) + \sum_c n_c\varphi_{ac}(\vec{k})\gamma_{cb}^{(0)}(\vec{k}) = 0. \tag{3.43}$$

This is the main result of the BBGKY's chains.

In a weakly coupled limit the effective potentials taking into account the collective effects can be obtained from the RDF (2.70), similarly to (2.66)

$$g_{ab}(r) \approx 1 - \frac{\Phi_{ab}(r)}{k_BT}. \tag{3.44}$$

Having compared this equation with (3.31) we find that $\Phi_{ab}(r) = -\gamma_{ab}^{(0)}(r)\cdot k_BT$ or $\Phi_{ab}(k) = -\gamma_{ab}^{(0)}(k)\cdot k_BT$. Inserting this into Eq. (3.43), presuming that $\gamma_{ab}^{(0)}(r) = e_ae_b\gamma^{(0)}(r)$, $\varphi_{ab}^{(0)}(r) = e_ae_b\varphi^{(0)}(r)$ and making the inverse Fourier transformation we'll get

$$\Phi_{ab}(r) = \frac{e_ae_b}{4\pi\varepsilon_0}\frac{1}{2\pi^2 r}\int_0^\infty \frac{4\pi k\varphi_{ab}(k)\sin(kr)}{4\pi + \chi^2\varphi_{ab}(k)}dk, \tag{3.45}$$

with

$$\varphi_{ab}(k) = \frac{8\pi}{k^3\lambda_{ab}}\exp(-\lambda_{ab}^2k^2/4)\int_0^{k\lambda_{ab}/2}\exp(t^2)dt, \tag{3.46}$$

and

$$\chi^2 = \frac{1}{r_D^2} = \sum_a \frac{n_ae_a^2}{\varepsilon_0k_BT}, a = e, i. \tag{3.47}$$

Here $\varphi_{ab}(k)$ represents the Fourier transformation of $4\pi\varepsilon_0\varphi_{ab}(r)/(e_ae_b)$ where $\varphi_{ab}(r)$ is the Kelbg pseudopotential (3.27) and r_D is the Debye screening radius. This screened Kelbg pseudopotential can be calculated numerically.

Unfortunately, this method does not take into account the difference between λ_{ee} and λ_{ei}. In order to take these differences into account for electron-ion system taking into account three particle correlations we get the following system of linear algebraic equations

$$\Phi_{ab}(\vec{k}) = \varphi_{ab}(\vec{k}) - \frac{1}{k_BT}\left[n_e\varphi_{ae}(\vec{k})\Phi_{eb}(\vec{k}) + n_i\varphi_{ai}(\vec{k})\Phi_{ib}(\vec{k})\right]. \tag{3.48}$$

This system of equations is identical with (3.7) which follows from (3.6). The system of equations (3.6) was deduced in accordance with the Bogoljubov's approach using the continuity equation for the RDF of a system being in a thermodynamic equillibrium.

In the Figure 3.4 the comparison among the Kelbg (3.27), Corrected Kelbg 3.28 and Screened Kelbg (3.45) pseudopotentials is shown. It should be noticed that the

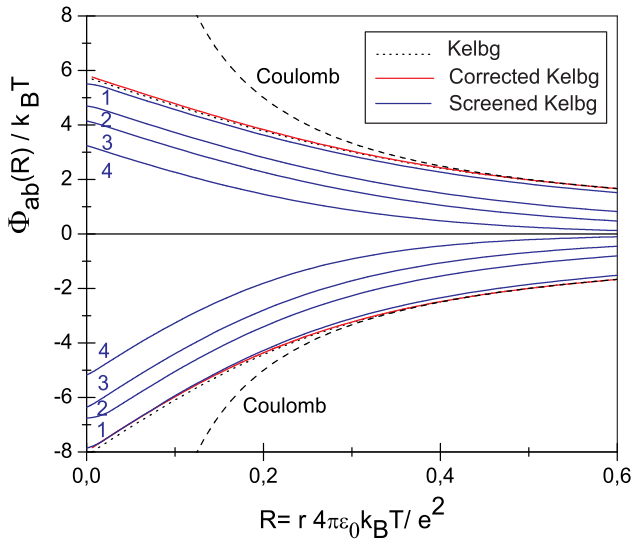

Figure 3.4: Comparison between the Kelbg (3.27), Corrected Kelbg 3.28 and Screened Kelbg (3.45) pseudopotentials of semiclassical Hydrogen-like point charges plasma against the dimensionless distance $R = r/r_L$ at $T = 30000$ K and various concentrations: 1: $n_e = 10^{19}$ cm^{-3}, $\Gamma_{ee} = 0.2$; 2: $n_e = 0.7 \cdot 10^{21}$ cm^{-3}, $\Gamma_{ee} = 0.8$; 3: $n_e = 2.4 \cdot 10^{21}$ cm^{-3}, $\Gamma_{ee} = 1.2$; 4: $n_e = 10^{22}$ cm^{-3}, $\Gamma_{ee} = 2$.

pseudopotential is not symmetric, i.e. $|\Phi_{ee}(r)| \neq |\Phi_{ei}(r)|$. At such a high temperature there is no observable difference between the Kelbg, corrected Kelbg and screened Kelbg at the low $\Gamma_{ee} = 0.2$ pseudopotentials, whereas the screened Kelbg pseudopotential deviates from them with an increase of the density and coupling parameter Γ_{ee}. This can be explained by that fact that with an increase of the density the screening effects start to play a significant role.

3.2 Electric microfield distributions at a charged and neutral particles in one-component plasmas

For simplicity we restrict ourselves to the case of a high-frequency OCP with the electron density $n_- = n_e$. We will calculate here the electric microfield acting on electrons in OCP including quantum effects. The method which is used for the calculation is coupling-parameter integration technique proposed by Iglesias (Iglesias, 1983). The method is described in the section 2.2. In the semiclassical system the quantum system is modelled by effective potential $\varphi_{ab}(r)$, where the short range part of the effective potential $\varphi_{ab}(r)$ Eq. (3.27) cuts the short-range divergency of the Coulomb potential. We would like to underline that a correct account of the short-range electron-ion interactions is very essential for an understanding and especially of the high field tail of the electric microfields in the plasma. Usually one considers the microfield on a place in vacuum and assumes that this is at least approximately valid also at the place of an atom or molecule. Here we locate an electron at the place where the field is calculated. However there is an open problem: We can not make in our framework an explicit difference between free and bound electrons.

The final calculation equation derived in the section 2.2 on the page 22 for the microfield probability distribution function (2.49) at an electron is

$$P(\beta) = \frac{2\beta}{\pi} \int_0^\infty k^* T_e(k^*) \sin(\beta k^*) dk^*.$$

Here $T_e(l)$ is the Fourier transform of the electric microfield distribution $Q =< \exp(\imath\vec{k} \cdot \vec{E}) >$ with $\vec{E}$ being the electronic electric microfield, $\beta = \epsilon/\epsilon_0$, $k^* = k\epsilon_0$, $\epsilon_0 = e/(4\pi\varepsilon_0 r_{ee}^2) = e n_e^{2/3}/((36\pi)^{1/3}\varepsilon_0)$.

The Fourier transform of the electric microfield distribution $T_e(l)$ is calculated using Eq. (2.33) or (2.42) where the generalized two-body correlation function $\mathcal{G}(\vec{r}, \vec{k})$ entering $T_e(l)$ is calculated using Eqs. (2.41) with (2.43) and (2.40). The pair correlation function $g_{\alpha R}(r)$ was determined with the help of the expressions (3.45) in the Sec. 3.1 for the screened Kelbg pseudopotential obtained in (Sadykova and Ebeling, 2007).

The results of EMD calculations based on (2.49) for the parameter sets shown in the Table 3.1 are presented in Figs. 3.5. These parameters are beyond the degeneration border ($n_e \cdot \Lambda_{ee}^3 < 1$) and can be treated classically. It is clearly seen in Fig. 3.5 that at relatively small nonideality $\Gamma_{ee} = 0.4$ and density there is a small deviation between the curve obtained in the framework of the Iglesias model and Molecular Dynamics simulation (MD) made using the corrected Kelbg pseudopotential. At such low densities and high temperatures the contribution of correlation and quantum effects is negligible.

Table 3.1: Plasma Parameters of consideration

r_s	2	2	2
Γ_{ee}	0.1	0.2	0.4
$n_e = n_i, 10^{23}$ cm^{-3}	2	2	2
$T, 10^4$K	160	78.83	39.4

The Kelbg pseudopotential deviates slightly from the screened one as to be seen in Fig. 3.4. However, the curves are still shifted toward the lower field direction with respect to the Holtsmark distribution. When density and nonideality increase, correlation effects start to play an important role leading to the shift in a direction of lower fields. This fact one can explain by repulsive forces with an increase of interactive forces, i.e. Γ_{ee}. The EMD curves measured at an neutral point is presented for comparison. As one can see it is less pronounced and has a fatter tail (region of high fields). Such tail behaviour can be explained by that fact that electron can approach the neutral point closer than the electron leading to a higher field.

We also made study of the EMDs measured at an electron in electron OCP in the framework of the screened Deutsch model (3.18-3.20) described in the Sec. 3.1, see (Sadykova et al., 2004). The study showed similar behaviour of EMDs with respect to the increase of Γ_{ee}: increase of the plasma density and coupling parameter leads to considerable shifts of EMDs' peaks toward the weaker fields as well as to increase of their magnitudes. However, when either plasma density or coupling parameter is fixed and small enough while another one changes in a range of low magnitudes, the shifts are not essentially large (Sadykova et al., 2005).

3.3 Electric microfield distributions at a charged and a neutral particles in electron-positron two-component plasmas

For simplicity we restrict ourselves to the case of a TCP which is anti-symmetric with respect to the charges $e_- = -e_+$ and symmetrical with respect to the densities $n_+ = n_p = n_- = n_e$ and masses $m_- = m_e = m_+ = m_p$. We will calculate here the electric microfield acting on electrons in TCP including quantum effects in comparison to the corresponding high-frequency OCP case. The method which is used for the calculation is the generalized coupling-parameter integration technique for two-component semi-classical plasmas introduced by Ortner et al. (Ortner et al., 2000) described in the section 2.3. In the semiclassical system the quantum system is modelled by effective potential $\varphi_{ab}(r)$, where the short range part of the effective potential $\varphi_{ab}(r)$ Eq. (3.27) cuts the short-range divergency of the Coulomb potential. We would like to underline again that the inclusion of both components into the theory and a correct account of the short-range electron-positron interactions, is very essential for an understanding of the high field tail of the electric microfields in the plasma. Usually one considers the microfield on a place in vacuum and assumes that this is at least approximately valid also at the place of an atom or molecule. Here we locate an electron at the place where the field is calculated. However there is an open problem: We can not make in our

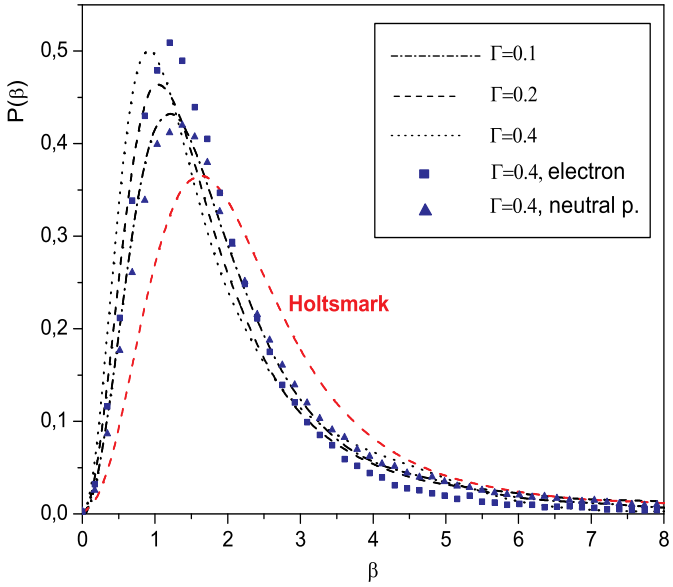

Figure 3.5: Electric microfield distributions an electron for OCP plasmas at $T = 394\,000$ K and $\Gamma_{ee} = 0.1$, 0.2, 0.4. The EMD curve measured at an electron at $\Gamma_{ee} = 0.4$ and $T = 394\,000$ K (Sadykova and Ebeling, 2007) is compared to MD results at an electron and neutral point obtained in the present work. The Holtsmark distribution is also shown for comparison.

framework an explicit difference between free and bound electrons.

The final calculation formular derived in the section 2.3 on the page 24 for the microfield probability distribution function at an electron (2.49) is

$$P(\beta) = \frac{2\beta}{\pi} \int_0^\infty k^* T_e(k^*) \sin(\beta k^*) dk^*$$

Here $T_e(k)$ is the Fourier transform of the electric microfield distribution $Q =< \exp(\imath \vec{k} \cdot \vec{E}) >$ with $\vec{E}$ being the total electric microfield, $\beta = \epsilon/\epsilon_0$, $k^* = k\epsilon_0$, $\epsilon_0 = e/(4\pi\varepsilon_0 r_{ei}^2) = en^{2/3}/((36\pi)^{1/3}\varepsilon_0)$, where $n = n_e + n_i$.

The EMD studied in the work (Sadykova and Ebeling, 2007) is given by the Debye screening approximation described by the generalized two-body correlation function $\mathcal{G}(\vec{r}, \vec{k})$ (2.71). The Fourier transform of the electric microfield distribution $T_e(l)$ is calculated using Eq. (2.69) with Debye-Hückel effective fields (2.67) and pair correlation function $g_{\alpha R}(r)$ (2.70) where for determination of pair correlation functions the expressions (3.45) in the Sec. 3.1 for the screened Kelbg pseudopotential obtained in (Sadykova and Ebeling, 2007) have been used.

As mentioned above, we do not distinguish between free and bound electrons. The results of calculations for the parameter sets shown in the Table 3.2 are presented in Figs. 3.6 a, b and 3.7. These parameters are beyond the degeneration border ($n_e \cdot \Lambda_{ee}^3 < 1$) and can be treated classically.

Table 3.2: Plasma Parameters of consideration

r_s	52.55	13.13	8.76
Γ_{ee}	0.2	0.8	1.2
$n_e = n_i, 10^{21}$ cm^{-3}	0.01	0.7	2.4
$T, 10^4$K	3	3	3

It is clearly seen in Fig. 3.6 a that at small nonidealities and densities the curves almost coincide with those obtained by Molecular Dynamics simulation (MD) presented in (Ortner et al., 2000) and Ortner's et al. theoretical results (Ortner et al., 2000) where for the pair distribution function of the pair (e, a) $g_{ea}(\vec{r})$ the corrected Kelbg pseudopotential in Debye screening approximation was used, as described in the previous section 3.1. At such low densities and high temperatures the contribution of correlation and quantum effects is negligible. The pseudopotentials also are similar as to be seen in Fig. 3.4. However, the curves are still shifted toward the lower field direction with respect to the Holtsmark distribution.

When density and nonideality increase, correlation effects begin to play an important role. One can see in Fig. 3.6 b, 3.7 that the curves are shifted with respect to each other. The curve obtained in the present work is always located between the MD and the Holtsmark curves and slightly differs from Ortner's curve. The parameters $\Gamma = 2$, $r_s \simeq 5.25$ correspond to degenerated area. Therefore this case was not considered here.

3.3.1 Molecular dynamics simulations

The theoretical discussion and Molecular Dynamics simulations in (Ortner et al., 2000), (Sadykova et al., 2010b,a), (Sadykova and Ebeling, 2007) have shown that the distributions for the electric microfield in TCP plasma are quite similar in their shapes to the Holtsmark distribution. Deviations from the Holtsmark result are mainly observed in the region of high fields leading to "fatter" tail. The second moment of TCP microfield distribution formed by discrete positive and negative charged components diverges. This high field domain is exactly the region where the quantum effects incorporated into the Kelbg pseudopotential at small distances play the role. The distribution obtained for the electric microfield in two component plasmas leads to a good agreement of atomic line wing shapes with experiment (Klimontovich, 1983). We note however that quantum-effects may lead to an effective cut-off in the far tail eliminating the divergence of the second moment (Ortner et al., 2000). As we see, the analytical theory of EMD in TCP is still far from being complete.

This makes it interesting to calculate EMD without making additional simplifications with the help of powerful computers using Molecular Dynamics (MD) or Monte-Carlo approach. MD allows to follow the system's time evolution in different plasma parameters domains. In what follows we report the results of MD simulations of EMD for several values of nonideality parameter Γ_{ee} and fixed temperature T. We consider the TCP electron-positron plasma which is anti-symmetric with respect to the charges and symmetric with respect to the masses and densities. This special model allows for more effective computer simulations and also delivers a simpler case for further theoretical

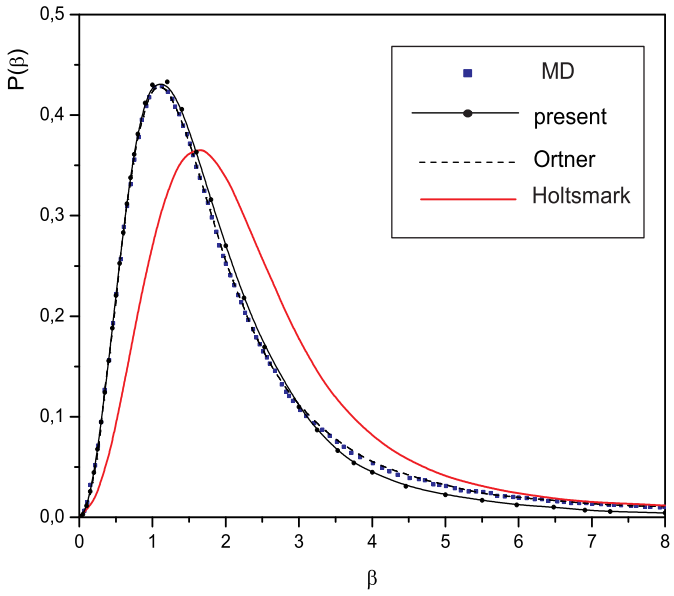

a)

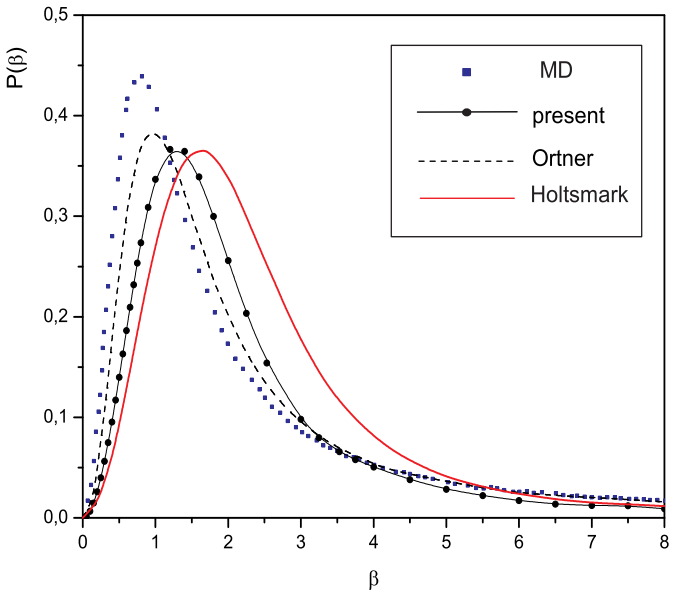

b)

Figure 3.6: Electric microfield distributions at an electron for TCP electron-positron plasmas at $T = 30000$ K and a) $\Gamma_{ee} = 0.2$, b) $\Gamma_{ee} = 0.8$. MD results have been taken from (Ortner et al., 2000). The Holtsmark distribution is also shown for comparison.

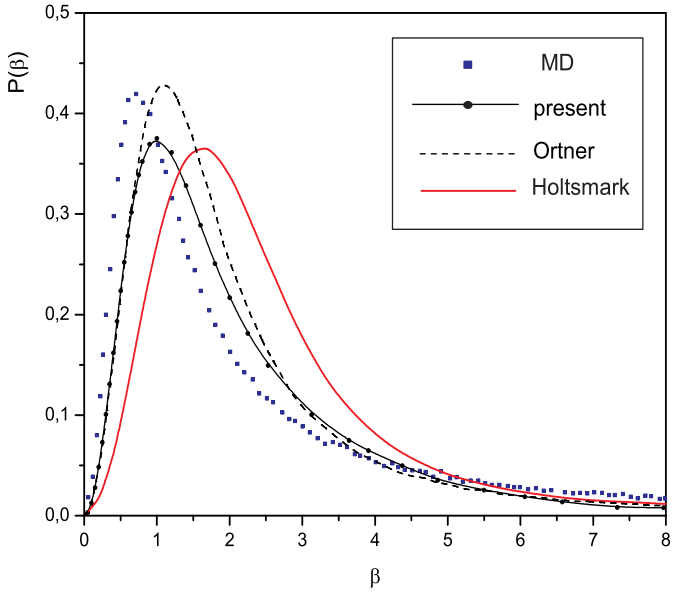

Figure 3.7: Electric microfield distribution at an electron for TCP electron-positron plasma at $T = 30000$ K, $\Gamma_{ee} = 1.2$ (Sadykova and Ebeling, 2007). MD results have been taken from (Ortner et al., 2000). The Holtsmark distribution is also shown for comparison.

studies.

We have performed a series of molecular dynamic simulations. The leap-frog variant of the so-called Verlet algorithm was used to integrate numerically the equations of motion in the corrected Kelbg pseudopotential of Eq. (3.28). The algorithm was first utilized by L. Verlet (1967). The following equations constitute this algorithm:

$$\vec{x}_i^{(n+1)} = 2\vec{x}_i^{(n)} - \vec{x}_i^{(n-1)} + [\vec{F}_i^{(n)}/M](\Delta t)^2, \tag{3.49}$$

$$\vec{v}_i^{(n)} = [\vec{x}_i^{(n+1)} - \vec{x}_i^{(n-1)}]/2(\Delta t), \tag{3.50}$$

where $\vec{x}_i^{(n)} = \vec{x}_i(t_n)$ and $\vec{v}_i^{(n)} = \vec{v}_i(t_n)$ are the position and the velocity of the i-th particle correspondingly at time t_n with $t_n = n(\Delta t)$, Δt - time interval, $\vec{F}_i^{(n)} = \vec{F}_i(t_n) = (d^2\vec{x}_i/dt^2)_{t_n}$ is the total force acting on the i-th particle with a mass M at time t_n. In order to use the Verlet algorithm one needs to know two sets of positions, namely, $\{\vec{x}_i^{(0)}\}$ and $\{\vec{x}_i^{(1)}\}$, from which all subsequent positions can be determined by using the recursion relations (3.49). To get the positions $\{\vec{x}_i^{(0)}\}$ one sets up a lattice with the given particles; the locations of the lattice sites are used as $\{\vec{x}_i^{(0)}\}$. One also assigns velocities $\{\vec{v}_i^{(0)}\}$ to the particles by drawing these randomly from the Maxwell-Boltzmann distribution.

Then, to get $\{\vec{x}_i^{(1)}\}$ one uses the Taylor expansion

$$\vec{x}_i^{(1)} = \vec{x}_i^{(0)} + \vec{v}_i^{(0)}(\Delta t) + (1/2!)[\vec{F}_i^{(0)}/M](\Delta t)^2 + \cdots. \tag{3.51}$$

Then, using these sets, namely, $\{\vec{v}_i^{(0)}\}$ and $\{\vec{x}_i^{(1)}\}$, one can use the equations (3.49), (3.50) for all subsequent calculations of the positions and velocities of the particles.

The simulations were performed using a 200-particle system of electrons and positrons with the minimum-image (closest-image) convention of periodic boundary conditions (PBC) in a cubic cell of the volume selected according to the plasma coupling parameter Γ_{ee} varied from weak coupling ($\Gamma_{ee} = 0.2$) up to moderate coupling ($\Gamma_{ee} = 1.2$), see Fig. 3.8. The temperature of the system was chosen as $T = 30000K$. In computer simulations, PBC are a set of boundary conditions that are often used to simulate a large system by modeling a small part that is far from its edge. When using PBC, particles are enclosed in a box, and this box is replicated to infinity by rigid translation in all the three cartesian directions, completely filling the space. The replicated copies of the box are called images, of which there are infinitely many. During the simulation, only the properties of the box need to be recorded and propagated. The simulation box is defined in such a way that when a particle passes through one face of the box, it reappears on the opposite face with the same velocity. The key point is that each particle i in the box should be thought as interacting not only with other particles j in the box, but also with their images in nearby boxes. That is, interactions can "go through" box boundaries. The minimum-image convention is a common form of PBC in which each individual particle in the simulation interacts with the closest image of the remaining particles in the system. The pairwise electron-positron, positron-positron and electron-electron interactions are set to the corresponding unscreened corrected Kelbg pseudopotentials. The Metropolis algorithm as a type of Monte Carlo technique is used to calculate thermodynamic averages of a system at finite temperatures. This method samples phase space via a random walk. Steps in this random walk are only taken if the energy remains low enough to contribute a significant amount to the average. Random single-particle displacements with adjustable amplitude are used to keep the Metropolis algorithm acceptance ratio around 0.5, which is the fraction of proposed samples that is accepted in a window of the last N samples. The instantaneous microfields are numerically obtained by calculating direct Coulomb interaction contributions from all particles (electrons and positrons) at a set of measurement points. The measurement points can be placed either at random locations: neutral (for microfields at a neutral point) or at plasma positrons (for microfields at an positron) or at electrons (for microfields at an electron). In order to save a computer time in some cases we made MD runs not with the Langevin source but using MC procedures to establish thermal equilibrium in the system, both methods have led to the same results. The distributions are composed for $10^6 - 4 \cdot 10^7$ MC steps after the system equilibration. Long MC simulation runs are required to obtain the distribution tails for $\beta > 10$ (see Figures 3.9). We note that the microfield distributions can be simulated in a similar way by the semiclassical Monte-Carlo method.

The results of the simulation are shown in the Fig. 3.8 a for an EMD at an electron and in Fig. 3.8 b for an EMD at a neutral point in TCP (Sadykova et al., 2010b,a). The high-frequency OCP curves are given for comparison. In all cases the distributions are considerably different from the Holtsmark one both for the field at an electron and at

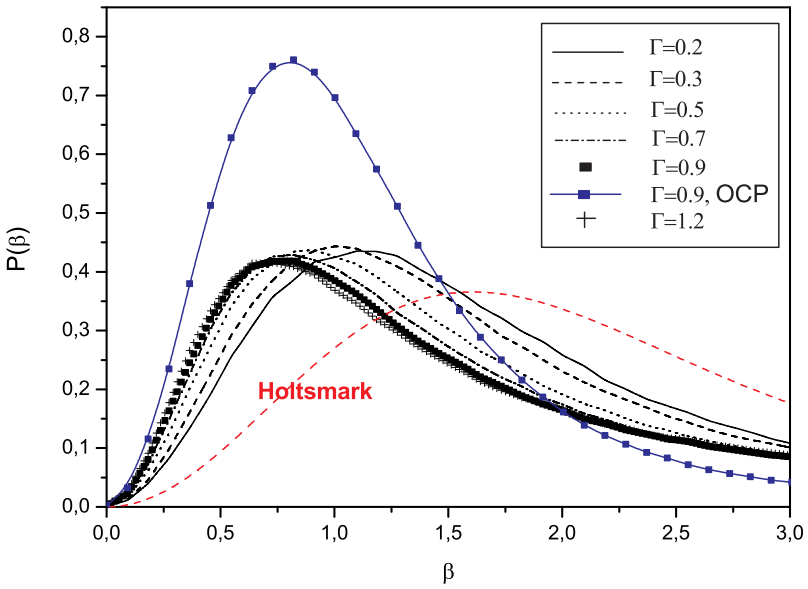

a)

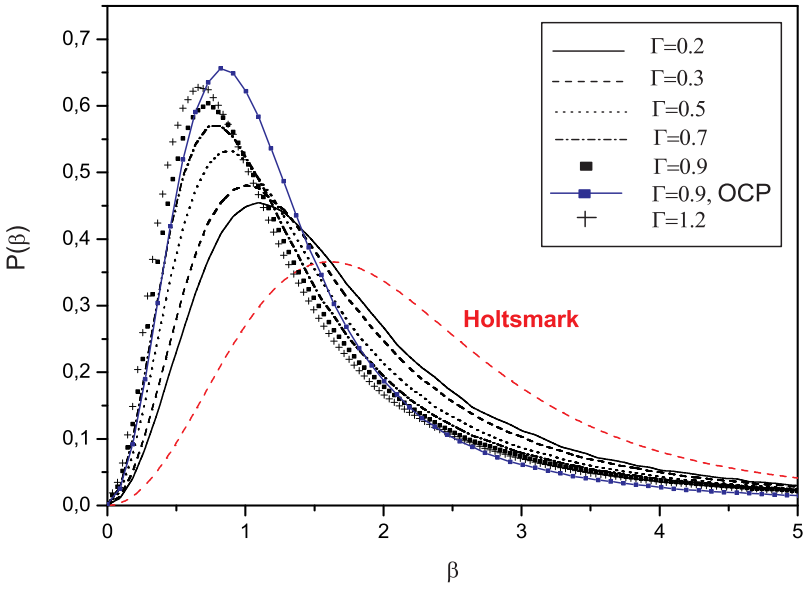

b)

Figure 3.8: Electric microfield distributions obtained with the help of MD for TCP electron-positron plasmas at $T = 30000$ K and various Γ. EMD are measured at a) an electron, b) a neutral point (Sadykova et al., 2010b,a). In both figures the EMDs are compared to the high-frequency OCP case at $\Gamma_{ee} = 0.9$ obtained in the present work. The Holtsmark distribution is also shown for comparison.

a neutral point. The curves are stronger peaked and the position of their maximum is shifted to the lower fields. Moreover, the results of simulations show that with increasing nonideality parameter the position of a peak for both cases, EMD at an electron and neutral point, shifts to the lower fields.

The height of the peak of EMD at a neutral point increases monotonically with the increase of Γ_{ee}. For the case of EMD at an electron this height diminishes monotonically only for $\Gamma_{ee} > 0.3$ and dependence on Γ_{ee} is not significant. The maximum of the curve lays below the one for $\Gamma_{ee} = 0.3$, which shows that the curves do not scale, i.e. their overall form is changing with Γ_{ee}. The similar results for nonsymmetric plasma were reported in (Kurilenkov and Filinov, 1980). Compared to their results the EMD at an electron in our case are much stronger peaked (peaks higher than one of the Holtsmark distribution), while the peaks observed in the work of Kurilenkov et al. for similar value of Γ_{ee} are lower than the ones of the Holtsmark distribution.

The qualitative explanation of our findings with respect to the position of the peak of EMD are the following: it can be explained by that fact that with the increasing of relative interaction strength between particles the typical field strength at a charge decreases due to the repulsion of equally charged particles. The explanation of the behaviour of the field at a neutral point is more involved since it depends on three-body correlations (Kurilenkov and Filinov, 1980). In the case of EMD at an electron the probability of finding very strong fields increases due to the attraction of oppositely charged particles, leading to a fatter tail compared to the one of the Holtsmark distribution and EMD measured at a neutral point. The quantitative theoretical description of these effects is still missing and will be the aim of out future work.

In Fig. 3.8 a, b the curves for TCP and electron OCP models at $\Gamma_{ee} = 0.9$ are compared. The TCP curve referred to an electron is less pronounced than the OCP one. This can be explained by that fact that in TCP case two components (electron and positron) are taken into account leading to the attraction between the opposite charges and stronger fields in average. That is why the probability of lower fields in TCP is lower than that in OCP. The tails are considered in detail the next section.

3.4 The tails

Let us now turn to the behaviour of tails of EMDs. Table 3.3 illustrates the behaviour of electric microfield distributions, obtained with the help of MD, in two-component plasma showing position of the peaks as well as the power law fits to their tails α_e, α_n (Sadykova et al., 2010b,a). The value of α_e and α_n for various values of Γ_{ee} are listed in the Table. 3.3. The figure 3.9 shows the tails of the corresponding EMDs in Two-component and One-component plasmas for $\Gamma_{ee} = 0.9$ in a double decimal logarithmic scale. One readily infers that the behaviour of the EMD for strong fields follows power laws $P(\beta) = A\beta^{-\alpha}$ with the parameter α depending on whether the field is measured at a charge (α_e) or at a neutral point (α_n) and which plasma parameters are considered. The behaviour of the field at a neutral point and any Γ_{ee} and a charge at low values of $\Gamma_{ee} << 1$ is compatible with $\alpha = 2.5$ as characterizing the Holtsmark distribution. The field at a charge at $\Gamma_{ee} = 0.4$ shows a different decay pattern characterized by $\alpha_e \approx -1.74$, i.e. follows the distribution with a considerably fatter tail than the Holtsmark one and lacking not only the second but also the first moment. This fact can be explained by an increase of the

Table 3.3: Nonideality parameter Γ_{ee}, magnitude of the most probable electric field measured at an electron and neutral point in TCP and power of the tail asymptote $\beta^{-\alpha}$ (Sadykova et al., 2010b,a).

Γ_{ee}	Neutral point		Electron	
	$\beta \vert P_{max}(\beta)$	α_n	$\beta \vert P_{max}(\beta)$	α_e
0.2	1.094	−2.565	1.094	−2.229
0.3	1.003	−2.538	1.003	−1.939
0.4	0.912	−2.498	0.912	−1.741
0.5	0.912	−2.497	0.912	−1.652
0.6	0.820	−2.461	0.820	−1.624
0.7	0.747	−2.444	0.820	−1.661
0.8	0.729	−2.446	0.820	−1.696
0.9	0.729	−2.407	0.820	−1.739
1	0.729	−2.409	0.729	−1.761
1.1	0.729	−2.402	0.729	−1.802
1.2	0.638	−2.380	0.729	−1.856

probability of high field at an electron as the result of attraction between the opposite charges. This finding however is only probably pertinent to the intermediate behaviour and at large fields there might be a cut off. The asymptotic errors are of 0.05% for α and 0.3% for the A.

With an increase of Γ_{ee} the values of α_n are very close to the Holtsmark's and are only slightly decreasing. The values of α_e exhibit a nonmonotonic behaviour: they first decrease and then start increasing with Γ_{ee}.

We would like to refer a reader also to the work (Sadykova et al., 2009b) where we have shown that at high fields $\beta >> 1$, when Γ_{ee} increases and becomes moderately high, the ion shell structure starts to play a big role and leads to the different decay pattern namely A. Y. Potekhin et al. form (2.84) (Potekhin et al., 2002) defined by

$$P(\beta) = B\beta^{-5/2} \exp(-C\beta^{1/2} - \beta^{-3/2}).$$

with the different parameters (C, B) in dependence on which type of alkali plasma is considered. However, for Hydrogen plasma this law for EMD measured at a proton, where no ion structure is taken into account, does not work satisfactorily. We have found another asymptote which better describes the H^+ plasma at high fields, we call it the modified Potekhin form :

$$P(\beta) = B\beta^{\mu} \exp(-C\beta^{1/2} - \beta^{-3/2}). \tag{3.52}$$

We came to the conclusion that in this case the ion structure should be thoroughly taken into account. We took the ion structure into account with the help of so called Hellmann-Gurskii-Krasko pseudopotential (Krasko and Gurskii, 1969).

In the figure 3.9 one can see that the behaviour of tails in TCP case and OCP case are different. For electron-positron plasma at higher Γ_{ee} and $\beta >> 1$ the Potekhin form is not a good approximation for the tail's asymptote measured at an electron as well. A better asymptote is provided by the modified Potekhin form (3.52) with $B = 0.55$, $C = 0.12$, $\mu = -1.505$ for TCP plasma and $B = 2.3$, $C = -0.56$, $\mu = -4.28$ for OCP plasma (asymptot. error $\approx 0.5\%$). In TCP case the EMD tail at an electron is fatter about $\alpha_e \approx 1.74$ (in a power law approx.) and longer than that of OCP $\alpha_e \approx 3.28$ (in a power law approx.). This fact can be explained by an increase of the probability of high field for TCP models as the result of attraction between the opposite charges and decreasing in the case of OCP model due to repulsion of particles with the same charges. The distribution at high fields is influenced by quantum effects which are modelled by the Kelbg pseudopotential. The tails measured at a neutral point exhibit similar to the Holtsmark distribution behaviour $\alpha_n \approx 2.5$. One should take into account that in Fig. 3.9 the EMD curves in OCP and TCP are measured in $E_0 = e/(4\pi\varepsilon_0 {r_{ei}}^2)$ units leading, as it was explained above in Sec. 2.1, to shifting of the tails of EMD curves with respect to each other and OCP case refered to the Holtsmark distribution.

Fig. 3.9 also shows the comparison to the results for asymptotic field distributions proposed by other models than the Holtsmark's one (2.20) on the page 13 of the Sec. 2.1: like Lewis-Margenau model for low-frequency OCP at an ion ($z = 1$) proposing (Lewis and Margenau, 1958) when $\beta >> 1$, $\Gamma_{ee}\sqrt{(\beta)} >> 1$ (2.81)

$$P(\beta) = C\beta^{-5/2}\exp(-\Gamma_{ii}\sqrt{\beta})\left[1 + \frac{C}{12}\frac{\Gamma_{ii}}{\beta} + \cdots\right],$$

where $C = \sqrt{\frac{2}{\pi}}\frac{15}{8}$ and Baranger-Mozer (Baranger and Mozer, 1959) model for high-frequency OCP at a neutral point (2.82) with

$$P(\beta) = P_H(\beta)|_{\beta\to\infty} - (r_{ee}/r_{De})\beta^{-7/2}(0.5453(r_{ee}/r_{De}) + 11.78\beta^{-1} + 114.6\beta^{-5/2} + \cdots),$$

where $P_H(\beta)|_{\beta\to\infty}$ represents the Holtsmark asymptote.

The comparison shows that both Holtsmark and Baranger-Mozer distributions reasonably describe the decay in the tail of EMD at a neutral point while the Margenau-Lewis distribution fails, at least for the value of Γ_{ee} used. The Lewis-Margenau, Holtsmark and Baranger-Mozer distributions when $z = 1$ remain the same in TCP case, whereas when $z \neq 1$ the curves modify. None of these distributions describes adequately the EMD at an electron.

3.5 Conclusions

The electric microfield distributions have been calculated at an electron and at a neutral point using a coupling-parameter integration technique for one-component plasmas proposed by C. A. Iglesias and the generalized coupling-parameter integration technique for two-component plasmas proposed by J. Ortner et al. . Electric microfield distributions are studied in the framework of the Kelbg pseudopotential model, taking

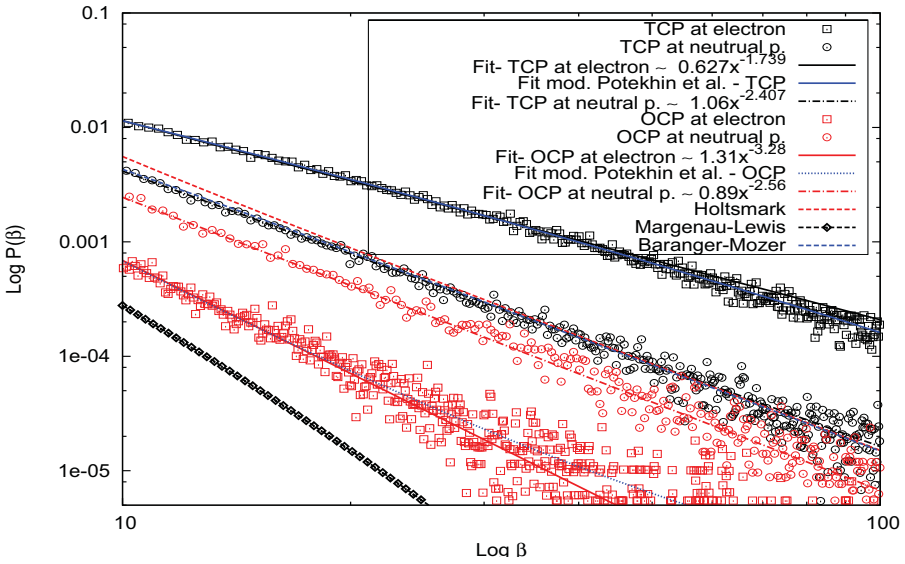

Figure 3.9: The tails of electric microfield distributions at electron in a electron-positron plasma, neutral point at $\Gamma_{ee} = 0.9$, $T = 30000$ K, $n_e = 10^{27}$ m^{-3} in comparison with Margenau-Lewis (2.81), Baranger-Mozer (2.82), Holtsmark (2.25) and modified Potekhin approximations (3.52) (Sadykova et al., 2010b,a).

into account quantum-mechanical effects (diffraction, quantum symmetry effects) and screening effects. The screening effects were introduced on a base of Bogoljubov's works (BBGKY) described by H. Falkenhagen. The screened pseudopotential is represented in a numerically approximated form. The results were found in a good approximation with Molecular Dynamics simulation results.

We performed the MD simulations of nonideal TCP and high-frequency OCP symmetrical plasma and concentrated on electric microfield distributions measured at an electron and at a neutral point as depending on the coupling parameter Γ_{ee} in the range $0.2 \leq \Gamma_{ee} \leq 1.2$ at $T = 30000K$ (Sadykova et al., 2010b,a). We show that with the increase of Γ_{ee} the most probable field shifts to the lower values. The height of the peak of the corresponding probability density in a case of EMD at an electron decreases with Γ_{ee} for $\Gamma_{ee} > 0.3$. The height of the peak of the corresponding probability density in a case of EMD at a neutral point increases monotonically with Γ_{ee}. The tails of EMD measured either at a neutral point or electron and low Γ_{ee} were found to obey to the power-laws. The tails of the EMD distribution at a neutral point and an electron at low Γ_{ee} follow a pattern compatible with the Holtsmark one while at higher values of Γ_{ee} and higher fileds $\beta >> 1$ the tails of EMD at an electron are considerably fatter and follow the modified Potekhin form ($P(\beta) = B\beta^{\mu} \exp(-C\beta^{1/2} - \beta^{-3/2})$). The TCP curves referred to either an electron or neutral point are less pronounced than the OCP one and their tails are fatter. This can be explained by that fact that in TCP case two components (electron and positron) are taken into account leading to the attraction between the opposite charges and stronger fields in average. These results can serve as a

benchmark for our further theoretical work.

4 Electric microfield distributions in electron-ion two-component plasmas with an account of the ion shell structure

As we have mentioned above, in order to correctly describe alkali plasmas which is of our interest at moderate temperatures one needs to take into account the ion shell structure. For example, for the behaviour of alkali plasmas the short range forces between the charged particles are of great importance. For alkali plasmas at small distances between the particles deviations from Coulomb law are observed which are mainly due to the influence of the shell electrons. Thus, the ion shell structure should be taken into account.

4.1 Taking into account the ion shell structure and plasma screening effects

4.1.1 Pseudopotential models taking into account the ion shell structure. Hellmann-Gurskii-Krasko pseudopotential

For the calculations of the microfields acting on a charged particle we need as an essential input quantity the pair distribution functions of the plasma particles (Ecker, 1972). Indeed it is evident from the point of view of the physics that the distribution of the electrical fields acting on a particle is determined by the distribution of the charged particles surrounding it. On the other hand the distribution is determined by the effective interactions between the charges. In particular, the Kelbg (Kelbg, 1964a; Ebeling et al., 1999) and the Deutsch (Deutsch, 1977; Minoo et al., 1981) potentials, obtained by perturbational theory, are frequently used. Clearly, the Coulomb law as well as the Kelbg or Deutsch potentials are not applicable to the forces between the charges in alkali plasmas since there are strong deviations at small distances due to the influence of core electrons.

The *pseudopotential* is an attempt to replace the complicated effects of the motion of the core (i.e. non-valence) electrons of an atom and its nucleus with an effective potential, or pseudopotential, so that the Schrödinger equation contains a modified effective potential term instead of the Coulomb potential term for core electrons normally found in the Schrödinger equation. The pseudopotential approximation was first introduced by Hans Hellmann in the 1930s. By construction of this pseudopotential, the valence wavefunction generated is also guaranteed to be orthogonal to all the core states. In a short, the pseudopotential is an effective potential constructed to replace the atomic all-electron potential such that core states are eliminated and the valence electrons are described by nodeless pseudo-wavefunctions.

The Method of model pseudopotentials describing the ion shell structure in metals was developed by Heine, Abarenkov and Animalu (Heine and Abarenkov, 1964), (Harrison,

1966), (Heine, 1970), (Heine et al., 1973). This method suggests that a pseudopotential $\hat{U}$ is defined as following:

$$\hat{U} = \sum_j w(\vec{r} - \vec{R}_j), \tag{4.1}$$

where $w(\vec{r})$ is a pseudopotential related to an ion. Then the problem of determination of $\hat{U}$ potential is reduced to the determination of electron pseudopotential in a field of the free ion.

Heine, Abarenkov (Heine and Abarenkov, 1964) proposed the following method of determination of the ionic model pseudopotential. One considers two types of interactions: outside of the shell of radius r_0, where the interaction potential is equal to $-ze^2/r$ with z being the ionic charge and inside, where it is the constant $A_l(E)$ (independent of r) which varies slowly with energy E of the incident conduction electron as well as with the chosen r_0. This constant is chosen in such a way, that the corresponding solution inside the sphere $j_l(kr)$ (here $k = (2m(E + A_l(E))/\hbar^2)^{1/2}$) would have on the shell surface the same logarithmic derivative as outside at a fixed eigenvalue of energy. Then, outside the shell the wave function defined through the model potential will have the same view as the wavefunction of the true potential and, thus, the same eigenvalue. For the more detailed review we refer a reader to (Heine et al., 1973), (Kovalenko et al., 2001). The model Heine-Abarenkov potential has the following form:

$$U_{HAei} = \begin{cases} -\sum_l A_l(E)\hat{P}_l, & r < r_0 \\ -ze^2/r, & r > r_0 \end{cases}, \tag{4.2}$$

where P_l is a projection operator which picks out the lth spherical harmonic component of the incident wave function and A_l, r_0 are the fitting parameters. Thus U_{HAei} is not simply a function of r but an $l-$ and $E-$ dependent operator.

It is worth to mention the more simple model pseudopotential of Cohen-Abarenkov-Heine:

$$U_{CAHei} = \begin{cases} ze^2u/r_0, & r < r_0 \\ -ze^2/r, & r > r_0 \end{cases}, \tag{4.3}$$

the adjustment parameters u and r_0 are usually determined through comparative analysis of theoretical and experimental data of statistical properties of metals. This pseudopotential reduces to the Ashkroft pseudopotential (Ashcroft, 1968) when $u = 0$ which is used for study of kinetic properties of metals. If one assumes that $u = 1$ then it turns into the Shaw pseudopotential which is used for study of thermodynamical properties of metals.

However, all pseudopotentials listed above have one *drawback*. They are usually described in $\vec{r}$ space by a discontinous function. As a result, their Fourier-transforms (formfactors) at $q \to \infty$ do not provide the sufficient convergence of series and integrals of the perturbation theory. Consequently, Abarenkov and Heine modified the Cohen-Abarenkov-Heine pseudopotential with the help of the arbitrary exponential damping factor for $q \to \infty$ (Vaks et al., 1977).

Another model is the Hard-Core Model (HC) describing the ion-ion interaction:

$$U_{HCii} = \begin{cases} \infty, & r < r_0 \\ z^2e^2/r, & r > r_0 \end{cases}, \tag{4.4}$$

The disadvantage of the Hard-Core Model as well as the Cohen-Abarenkov-Heine pseudopotential model is that at the radius r_0 the derivative (i.e forces) becomes infinite and their Fourier-transforms (formfactors) at $k \to \infty$ do not provide the sufficient convergence of series and integrals of the perturbation theory.

In many problems of atomic and molecular physics one can divide the electrons of the system into valence and core electrons. Often the important physical properties are determined by the valence electrons. In a series of pioneering papers Hellmann attempted to develop a computational model in which the treatment of such atoms and molecules is reduced to the treatment of valence electrons (Hellmann, 1935b,a, 1936), (Hellmann and Kassatotschkin, 1936). Hellmann demonstrated that the Pauli exclusion principle for the valence electrons can be replaced by a nonclassical potential (*Abstossungspotential*) which is now called the *pseudopotential*. Hellmann's idea was to replace the requirement of orthogonality of valence orbital to the core orbitals by the pseudopotential what made the respective mathematical calculations much simpler.

For the actual purpose of atomic and molecular calculations Hellmann suggested a simple analytic formula. Let φ be the sum of electrostatic, exchange, and polarisation potentials, representing the interaction between a valence electron and the core of an atom. Let φ_p be the *Abstossungspotential*. The potential $\varphi^H = \varphi + \varphi_p$ may be expressed:

$$\varphi^H{}_{ei}(r) = -\frac{ze^2}{4\pi\varepsilon_0 r} + \frac{ze^2}{4\pi\varepsilon_0}\frac{Ae^{-\alpha r}}{r}, \tag{4.5}$$

Here z is the ionic charge of the core; that is, if the nucleus contains Z positive charges and the core contains N electrons then $z = Z - N$. The constants A and α are determined from the requirement that the potential φ^H should reproduce the energy spectrum of the valence electron as accurately as possible.

The physical meaning of Eq. (4.5) can be understood from Figures 4.1. In Figure 4.1a we have plotted φ^H for the valence electron of the Na atom ($A = 10.09, \alpha = 2.004$ in a.u.) and in the Figure 4.1b for the Cs atom ($A = 1.584, \alpha = 0.562$ in a.u.). As we see in the Figure 4.1a for Na, in contrast to the Coulomb potential, which is an everywhere negative, attractive potential, the potential φ^H has a positive potential barrier at about $R \approx 0.12$ a deep negative well between $R \approx 0.1$ and $R \approx 0.3$, and is Coulombic for large R. Later on several modifications were introduced by Schwarz, Bardsley etc. into the determination of the Hellmann potential parameters without changing the basic analytic form of the potential (Szasz, 1985). For instance, Schwarz improved the determination of the potential parameters for neutral atoms Be, Mg, Ca, Sr, Zn of the second and negative ions Li, Na, K, Rb and Cu of the first family of the periodic system considerably obtaining the better fit to the empirical energy levels (Schwarz, 1968a), (Schwarz, 1968b), (Schwarz, 1969).

However, all the mentioned above pseudopotentials have one drawback. They are usually described in $\vec{r}$ space by a discontinous function or have a relatively hard core as in a case of Hellmann potential. As a result, their Fourier-transforms (formfactors) at $k \to \infty$ do not provide the sufficient convergence of series and integrals of the perturbation theory. Alternatively, Gurskii and Krasko constructed a pseudopotential model excluding the mentioned shortcoming by introducing a continuous in $\vec{r}$ space pseudopotential. On a base of smoothness of the obtained electron density distribution in an atom, Gurskii and Krasko proposed the following electron-ion model pseudopotential (Krasko and Gurskii,

1969), (Kovalenko et al., 2001):

$$\varphi^{HGK}{}_{ei}(r) = -\frac{ze^2}{4\pi\varepsilon_0}\frac{1-e^{-r/R_C}}{r} + \frac{ze^2}{4\pi\varepsilon_0}\frac{a}{R_C}e^{-r/R_C}, \tag{4.6}$$

where $z-$ valency, $R_C = r_C r_B$ and a are determined experimentally using the ionisation potential and the formfactor of the screened pseudopotential at the first sites of the reciprocal lattice. The parameter r_C is defined as a certain radius characterizing the size of the region of internal electron shells. If such measurements are not available, the second condition is replaced by the constraint that $P = 0$ at $T = 0$ in the equilibrium lattice. The magnitudes are given in SI system of units. In this work values of a, r_C are taken from (Gurskii and Krasko, 1971). We note that the first term is identical with the potential of Hellmann (Hellmann, 1935b,a, 1936), (Hellmann and Kassatotschkin, 1936). Due to this fact we call this pseudopotential as Hellmann-Gurskii-Krasko potential. The results of calculation of bound energy and phonon spectra with the help of Hellmann-Gurskii-Krasko (HGK) potential were found in a good agreement with the experimental data and can be used in a wide range of invetsigation of thermodynamic properties of alkali plasmas. We underline however that the HGK potential includes just some rough global effects of ion shell structure by means of a repulsive potential contribution. In the Fig. 4.1a and 4.1b the comparison between the electron-ion Hellmann, HGK and Coulomb potentials for Na^+ and Cs^+plasmas are shown. One can easily see that HGK has a more soft core compared to the Hellmann potential. In the Fig. 4.2a one can see the comparison between the different pseudopotential $\varphi^{HGK}{}_{ei}(r)$ of different alkali plasmas, where the electron-ion Hellmann-Gurskii-Krasko potential possess a minimum.

Unfortunately there are no available HGK parameters for the Be^{2+} ion. That is why for Be^{2+} we use the alternative Fiolhais et al. pseudopotential, for which the parameters are known in this case:

$$\begin{aligned}\varphi^{F}{}_{ei}(r) = &-\frac{ze^2}{4\pi\varepsilon_0 r}\left[1-\left(1+\beta\frac{r}{R_C}\right)\exp\left(-\alpha\frac{r}{R_C}\right)\right] \\ &+\frac{ze^2}{4\pi\varepsilon_0}\frac{A}{R_C}\exp\left(-\frac{r}{R_C}\right).\end{aligned} \tag{4.7}$$

Here R_C is the core decay length, $\alpha > 0$, $\beta = (\alpha^3 - 2\alpha)/4(\alpha^2 - 1)$ and $A = \alpha^2/2 - \alpha\beta$. In (Fiolhais et al., 1995) two possible choices of parameters are suggested: the "universal" and the "individual". We made a fit of the parameters of HGK potential to the "universal"one of Fiolhais et al. pseudopotential, which are $a = 3.72$, $r_C = 0.22$. In (Fiolhais et al., 1995) the universal parameters were chosen to obtain the best agreement between calculated and measured structure factors of alkali metals. In Fig. 4.3 the electron-ion Fiolhais et al., HGK and Coulomb potentials for Be^{2+} plasmas are compared. One can easily see that the HGK potential almost coincides with the Fiolhais et al. one.

The Hellmann type pseudopotentials were proposed to be used for alkali plasma in works (Ebeling et al., 1976; Zimdahl and Ebeling, 1977), (Ebeling et al., 1977, 1979) . Pseudopotentials for the ion-ion interaction are not well known. That is why we decided to use here the Hellmann-Gurskii-Krasko model with an adapted length parameter R_{Cii}.

The Hellmann-Gurskii-Krasko model for an ion-ion interaction shown in Fig. 4.2b

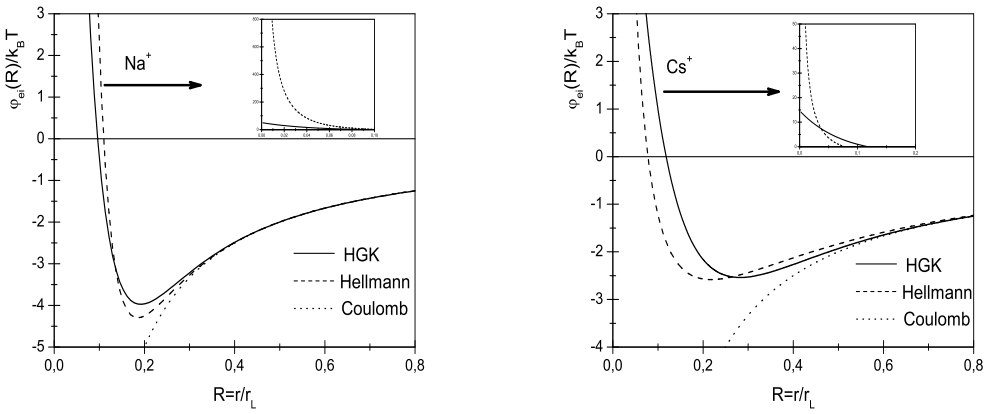

Figure 4.1: Comparisons among the $e-i$ HGK, Hellmann and Coulomb potentials at $T = 30000$ K for (a) Na^+ and (b) Cs^+ plasmas. The insets show the softness of the HGK potential compared to the Hellmann potential. As the length scale we use the Landau length $r_L = e^2/(4\pi\varepsilon_0 k_B T)$, $r_L \simeq 10.5 r_B$ and $k_B T \simeq 0.1$ Ha.

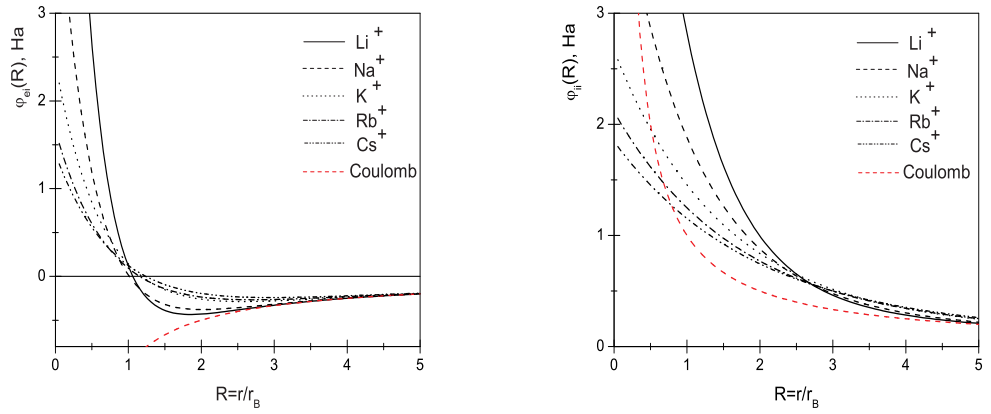

Figure 4.2: The HGK potential for different alkali plasmas (in atomic units).

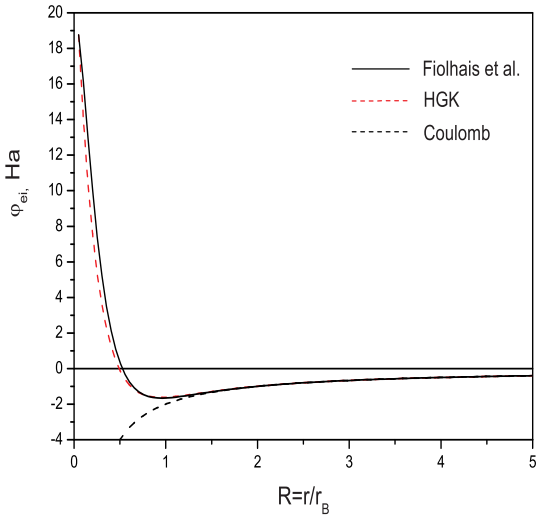

Figure 4.3: Comparisons among the $e-i$ HGK, Fiolhais et al. and Coulomb potentials for Be^{2+} (in atomic units).

for alkali plasmas is the following:

$$\varphi^{HGK}{}_{ii}(r) = \frac{z^2e^2}{4\pi\varepsilon_0}\frac{1-e^{-r/R_{Cii}}}{r} + \frac{z^2e^2}{4\pi\varepsilon_0}\frac{a_{ii}}{R_{Cii}}e^{-r/R_{Cii}}, \tag{4.8}$$

Since values of r_{Cii}, a are not given in literature. r_{Cii} is taken hypothetically as the doubled value of that taken for $e-i$ interaction $r_{Cii} = 2r_C$ taking in this way both ions cores (closed shells) into account and $a_{ii} = a$. In Fig. 4.2b we display the HGK pseudopotentials $\varphi^{HGK}{}_{ii}(r)$ for different alkali plasmas. We will study this in more detail and compare with the hard-core potential described in (Ebeling et al., 1976; Zimdahl and Ebeling, 1977), (Ebeling et al., 1977, 1979). In Table 4.1 the parameters of the Hellmann-Gurskii-Krasko potential for alkali elements and the elements of the second periodic family are presented. We note that $\varphi^{HGK}{}_{ei}(r)$ potential describes the interaction of a valence electron with the corresponding ion core of a charge z and radius R_{Cei}, while $\varphi^{HGK}{}_{ii}(r)$ describes the interaction between two ion cores of a charge z with the same radius R_{Cei}.
In (Ebeling et al., 1979) it was proposed to describe the electron-ion interaction by the Hellmann-potential and the ion-ion interaction by the model of charged hard cores with the crystallographic radii R_i. The electrical part of the ion-ion interaction is described by a pseudopotential:

$$\varphi^{HC}{}_{ii}(r) = \begin{cases} \frac{z^2e^2}{4\pi\varepsilon_0 r}, & r > 2R_i \\ \infty, & r < 2R_i \end{cases} \tag{4.9}$$

In principle the choice of the parameters for the ion-ion interaction should be based on methods similar to those in (Gurskii and Krasko, 1971). Alternatively, we propose to

Table 4.1: The parameters of the Hellmann-Gurskii-Krasko potential in atomic units (Gurskii and Krasko, 1971). In the case $z = 2$ the parameters correspond to the interaction of an ion with the charge $2e$ with an electron. rc_{ei} and rc_{ii} are measured in r_B units.

	Li	Na	K	Rb	Cs	Be	Mg	Ca	Sr	Br
z	1	1	1	1	1	2	2	2	2	2
a	5.954	3.362	2.671	2.293	2.214	3.72	2.588	2.745	2.575	2.870
rc_{ei}	0.365	0.487	0.689	0.779	0.871	0.22	0.427	0.571	0.644	0.698
rc_{ii}	0.73	0.974	1.948	1.558	1.742	0.44	0.854	1.142	1.288	1.396

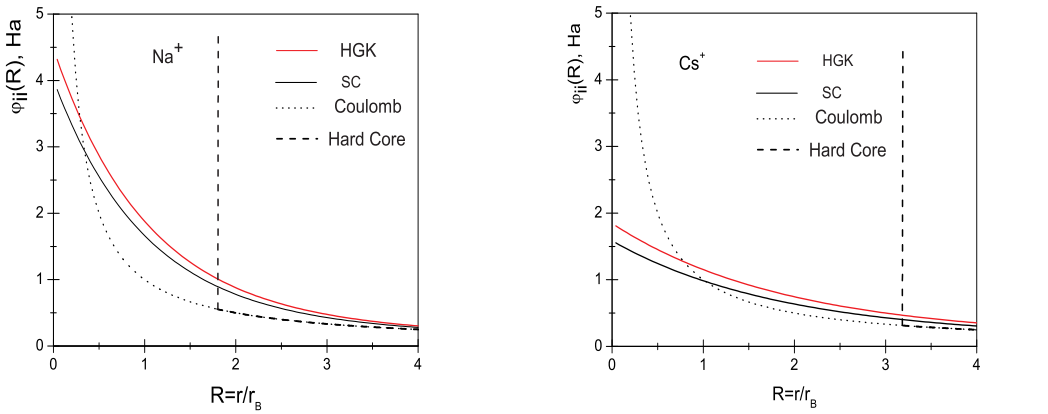

a) b)

Figure 4.4: The $i - i$ HGK, hard core, soft core and Coulomb potentials for (a) Na^+ and (b) Cs^+ plasmas (in atomic units).

use the following soft core potential:

$$\varphi^{SC}{}_{ii}(r) = \frac{z^2e^2}{4\pi\varepsilon_0}\frac{1-e^{-r/R_i}}{r} + \frac{z^2e^2}{4\pi\varepsilon_0}\frac{a}{R_{Cii}}e^{-r/R_{Cii}}, \tag{4.10}$$

As another simple approximation we propose to use the crystallographic ion radii R_i (Ebert, 1967) in the first constituent of the potential. The procedure of introducing crystallographic radii into the (first) Hellmann term was already quite successfully applied in the theory of ionic solutions (Falkenhagen, 1971). Furthermore, on a base of our calculations we came to the conclusion that the results are not sensitive with respect to the a parameter of the ion-ion interaction. That is why a is taken the same as for electron-ion interaction. In Figures 4.4a, b the comparison among the HGK, Hard-Core (HC) (Ebeling et al., 1979) and soft core (SC) eq. (4.10) models is presented.

The pseudopotentials which are used in our calculations were originally developed for applications in the electronic band structure and binding energies in alkali metals. However the derivation used by Hellmann and his followers is basically working with

wave functions of a few electrons and not the ionic all-electron wave functions like in the solid state. For this reason we can not see strong arguments against applications to the two-particle interactions in the plasma state. Definitely, this is a working assumption which needs further justification. Nevertheless we are convinced that application of pseudopotentials of Hellmann-type is much nearer to reality than the use of pure Coulomb potentials or hard-core potentials. Further we would like to argue that the experimental investigations of alkali metals near to the critical point did not show the existence of deep differences between the two particle interactions in the liquid and the gaseous state (Hensel, 1977; Hensel et al., 1985). What is clearly different are the multi-particle interactions, however multi-particle effects are less relevant at the low densities and relatively high temperatures we consider here.

4.1.2 The screened Hellmann-Gurskii-Krasko pseudopotential obtained with the help of electron-electron Deutsch and electron-ion, ion-ion Hellmann-Gurskii-Krasko micro-pseudopotentials

There are two main well-known difficulties in determination of thermodynamic and transport properties of dense high-temperature plasmas. The first one is induced by the long-range character of bare Coulomb interaction of charged particles. Conventionally, this difficulty is avoided by taking into account collective effects connected with the great number of interacting particles, i.e. screening effects. On the other hand, when plasma density increases the ratio between the Landau length and the thermal de Broglie wave length decreases and the quantum-mechanical effects begin to play an important role. In this regard, it is of high interest to construct a pseudopotential model of particle interaction in the dense high-temperature plasma, taking into account both the quantum-mechanical effects at short distances and the field screening effects at large distances.

To determine the thermodynamic and transport properties of semiclassical fully ionized plasma effective potentials simulating quantum effects of diffraction and symmetry are widely used (Kelbg, 1964a,b; Deutsch, 1977; Minoo et al., 1981) and later significantly improved (Ebeling et al., 1999; Wagenknecht et al., 2001; Filinov et al., 2003). In particular, Deutsch and co-workers (Deutsch, 1977), (Minoo et al., 1981) have obtained the following form of effective $e-e$ interaction potential of charged particles in plasma medium:

$$\varphi_{ee} = \frac{e^2}{4\pi\varepsilon_0 r}\left[1-\exp\left(-\frac{r}{\lambda_{ee}}\right)\right] + k_B T \ln 2 \exp\left(-\frac{r^2}{\pi\lambda_{ee}^2 \ln 2}\right), \tag{4.11}$$

where e is the elementary electronic charge of interacting particles, $\lambda_{ee} = \hbar/\sqrt{\pi m_e k_B T}$ is the thermal de-Broglie wavelength. The pseudopotential (4.11) does not take into account collective events in plasmas and can be applied only for highly ionized plasmas. Since most experimental data available refer to partially ionized plasmas at moderate temperatures when the ions partially retain their inner shell, it is of a high interest to construct the pseudopotential model which takes into account not only the quantum-mechanical and screening field effects but also the ion shell structure. We will use here the Deutsch pseudopotential (4.11) for the electron-electron interaction and the Hellmann-Gurskii-Krasko (HGK) pseudopotential for the electron-ion and ion-ion interactions. First the pseudopotentials have to be screened. In this work we applied the method

developed in (Falkenhagen, 1971) and (Arkhipov et al., 2000). In (Arkhipov et al., 2000) the authors developed the classical approach based on the BBGKY chain of Bogoljubov equations (Bogoljubov, 1946, 1962) for the equilibrium radial distribution functions where the $a-b=e,i$ Deutsch pseudopotentials (Deutsch, 1977), (Minoo et al., 1981) were taken as micro-pseudopotentials. In our paper we use the HGK pseudopotentials ${\varphi^{HGK}}_{ei}(r)$ (4.6), ${\varphi^{HGK}}_{ii}(r)$ (4.8) and Deutsch pseudopotential (4.11) as micro-pseudopotentials. Following (Ecker, 1957; Ecker and Müller, 1958), the authors (Arkhipov et al., 2000) deduced the following system of integral-differential equations for the pseudopotential Φ_{ab} in a framework of the pair correlation approximation:

$$\Delta_i\Phi_{ab}(\vec{r}_i^{\,a},\vec{r}_j^{\,b})=\Delta_i\varphi_{ab}(\vec{r}_i^{\,a},\vec{r}_j^{\,b})-\sum_{c=e,i}\frac{n_c}{k_BT}\int d\vec{r}_m^{\,c}\Delta_i\varphi_{ac}(\vec{r}_i^{\,a},\vec{r}_j^{\,c})\Phi_{cb}(\vec{r}_m^{\,c},\vec{r}_j^{\,b}). \tag{4.12}$$

Here Δ_i denotes the Laplace operator acting on the coordinates of the ith particle. $\varphi_{ei}(r)$, $\varphi_{ii}(r)$ in the sect. 4.1.1 (we skip here and further the "HGK"superscript) represent the HGK pseudopotentials which can be rewritten in SI system as following:

$$\varphi_{ab}(r)=\frac{e_ae_b}{4\pi\varepsilon_0}\left(\frac{1-e^{-r/R_{cab}}}{r}\right)+\frac{|e_ae_b|}{4\pi\varepsilon_0}\frac{a}{R_{cab}}e^{-r/R_{cab}}, \tag{4.13}$$

where $R_{Cab}=r_{cab}r_B$. Parameters r_{cei} can be taken from the tabl. 4.1 in the sect. 4.1.1, whereas $r_{cii}=2r_{cei}$. For the $e-e$ interaction the Deutsch pseudopotential (4.11) has been used.

In Fourier space this system (4.12) of integral-differential equations (4.12) turns into a system of linear algebraic equations:

$$\Phi_{ab}(k)=\varphi_{ab}(k)-\frac{1}{k_BT}\left[n_e\varphi_{ae}(k)\Phi_{eb}(k)+n_i\varphi_{ai}(k)\Phi_{ib}(k)\right] \tag{4.14}$$

where $a,b=i,e$. Solving the system (4.14) for two-component plasma one can derive the following expressions for the Fourier transform $\Phi_{ab}(k)$ of the pseudopotential $\Phi_{ab}(r)$:

$$\Phi_{ei}(k)=\frac{ze^2}{\varepsilon_0\Delta}\frac{(2a-1){R_{cei}}^2k^2-1}{k^2(1+k^2{R_{cei}}^2)^2}, \tag{4.15}$$

$$\begin{aligned}\Phi_{ee}(k)=&\frac{e^2}{\varepsilon_0\Delta}\left\{\frac{1}{k^2(1+k^2{\lambda_{ee}}^2)}\right.\\&+\frac{1}{k^4{r_{Di}}^2}\left[\frac{(2a+1){R_{cii}}^2k^2+1}{(1+k^2{\lambda_{ee}}^2)(1+k^2{R_{cii}}^2)^2}-\left(\frac{(2a-1){R_{cei}}^2k^2-1}{(1+k^2{R_{cei}}^2)^2}\right)^2\right]\\&\left.+A\left(1+\frac{(2a+1){R_{cii}}^2k^2+1}{k^2{r_{Di}}^2(1+k^2{R_{cii}}^2)^2}\right)\exp\left(-\frac{k^2}{4b}\right)\right\},\end{aligned} \tag{4.16}$$

$$\Phi_{ii}(k) = \frac{z^2e^2}{\varepsilon_0\Delta}\left\{\frac{(2a+1){R_{cii}}^2k^2+1}{k^2(1+k^2{R_{cii}}^2)^2}\right.$$
$$+\frac{1}{k^4{r_{De}}^2}\left[\frac{(2a+1){R_{cii}}^2k^2+1}{(1+k^2{\lambda_{ee}}^2)(1+k^2{R_{cii}}^2)^2}-\left(\frac{(2a-1){R_{cei}}^2k^2-1}{(1+k^2{R_{cei}}^2)^2}\right)^2\right]$$
$$\left.+A\frac{(2a+1){R_{cii}}^2k^2+1}{k^2{r_{De}}^2(1+k^2{R_{cii}}^2)^2}\exp\left(-\frac{k^2}{4b}\right)\right\}. \tag{4.17}$$

Here r_{De}, r_{Di} are the Debye radius of electrons and ions respectively, with $1/{r_{Di}}^2 = z^2e^2n_i/(\varepsilon_0k_BT)$, $1/{r_{De}}^2 = e^2n_e/(\varepsilon_0k_BT)$, $b = ({\lambda_{ee}}^2\pi\ln 2)^{-1}$, $A = k_BT\ln 2\pi^{3/2}b^{-3/2}\cdot$ $\cdot\varepsilon_0/e^2$ and

$$\Delta = 1+\frac{1}{k^2{r_{De}}^2(1+k^2{\lambda_{ee}}^2)}+\frac{(2a+1){R_{cii}}^2k^2+1}{k^2{r_{Di}}^2(1+k^2{R_{cii}}^2)^2}$$
$$+\frac{1}{k^4{r_{De}}^2{r_{Di}}^2}\left[\frac{(2a+1){R_{cii}}^2k^2+1}{(1+k^2{\lambda_{ee}}^2)(1+k^2{R_{cii}}^2)^2}-\left(\frac{(2a-1){R_{cei}}^2k^2-1}{(1+k^2{R_{cei}}^2)^2}\right)^2\right]$$
$$+\frac{A}{{r_{De}}^2}\left(1+\frac{(2a+1){R_{cii}}^2k^2+1}{k^2{r_{Di}}^2(1+k^2{R_{cii}}^2)^2}\right)\exp\left(-\frac{k^2}{4b}\right). \tag{4.18}$$

The pseudopotential $\Phi_{ab}(r)$ can be restored from (4.15-4.18) by Fourier transformation

$$\Phi_{ab}(r) = \frac{1}{2\pi^2r}\int\Phi_{ab}(k)k\sin(kr)dk \tag{4.19}$$

Let us consider the limiting cases of the expressions (4.15-4.16).

A. If r_{De}, $r_{Di}\to\infty$, then

$$\Phi_{ab}(r) = \varphi_{ab}(r) \tag{4.20}$$

When the screening effects are negligible, the pseudopotential $\Phi_{ab}(r)$ coincides with the potentials (4.11), (4.13).

B. If λ_{ee}, R_{cei}, $R_{cii}\to 0$, then

$$\Phi_{ab}(r) = \frac{e_ae_b}{4\pi\varepsilon_0}\frac{e^{-r/r_D}}{r}, \tag{4.21}$$

where

$$\frac{1}{{r_D}^2} = \sum_{c=e,i}\frac{{e_c}^2n_c}{\varepsilon_0k_BT}. \tag{4.22}$$

Eq. (4.21) means when quantum-mechanical effects are negligible, then the pseudopotential $\Phi_{ab}(r)$ coincides with the Debye-Hückel one.

C. If r_{De}, $r_{Di} \to \infty$, λ_{ee}, R_{cei}, $R_{cii} \to 0$, then

$$\Phi_{ab}(r) = \frac{e_a e_b}{4\pi\varepsilon_0 r}. \tag{4.23}$$

When the quantum-mechanical and screening field effects are negligible, then the pseudopotential $\Phi_{ab}(r)$ coincides with the Coulomb potential.

D. If $\lambda_{ee}, R_{cei}, R_{cii} \ll r_{De}, r_{Di}$, then for $e-i$ and $i-i$

$$\Phi_{ib}(r) = \frac{e_a e_b}{4\pi\varepsilon_0 r}\left[e^{-r/r_D} - e^{-r/R_{cab}}\right] + \frac{|e_a e_b|}{4\pi\varepsilon_0}\frac{a}{R_{cab}}e^{-r/R_{cab}}, \tag{4.24}$$

where $b = e, i$, whereas for $e-e$ interaction we have:

$$\Phi_{ee}(r) = \frac{e^2}{4\pi\varepsilon_0 r}\left[e^{-r/r_D} - e^{-r/\lambda_{ee}}\right] + k_B T \ln 2 e^{-r^2/\lambda_{ee}^2 ln2}. \tag{4.25}$$

These expressions differ from the pseudopotentials (4.11), (4.13) in the presence of the term $\exp(-r/r_D)$ term in the brackets instead of 1. This case corresponds to the weakly coupled plasmas when $\Gamma \ll 1$. The derived expressions (4.15-4.18) differ from the bare pseudopotentials (4.11), (4.13) due to the screening terms. The present approximation is restricted to the constraint $\Gamma_{ii} \lesssim 1$, $\Gamma_{ii} = z^2 e^2/(4\pi\varepsilon_0 k_B T r_{ii})$ with r_{ii} being the average ionic interparticle distance, i.e. for weakly and moderately coupled plasmas, due to the use of linearization process at the derivation of integral-differential equation (4.12).

The comparative plots among the HGK (4.11), (4.13) and screened HGK (4.15-4.19) pseudopotentials for $e-i$, $i-i$, $e-e$ together with their Radial distribution functions $g_{ab} = \exp(-\Phi_{ab}(r)/k_B T)$ are given in Figures 4.5-4.9. In Table. 4.2 the parameter regions for the calculated pseudopotentials are presented, where $r_L = e^2/(4\pi\varepsilon_0 k_B T)$, $r_s = r_{ee}/r_B$ (r_{ee} being the average electronic interparticle distance, $r_B = 0.53 \cdot 10^{-10} m$ - Bohr radius), $z = 1$. These parameters are beyond the degeneration border ($n_e \cdot \lambda_{ee}^3 < 1$) and can be treated classically ($r_L/\lambda_{ee} > 1$, λ_{ee} is the electron de Broglie wave length). In the Figure 4.5, one can easily see that at low Γ_{ii} the difference between the $e-e$ screened HGK pseudopotential (4.19) and Deutsch pseudopotential (4.11) is not significant, whereas when Γ_{ii} increases the difference becomes considerable. It is worth, to note that the Debye-Hückel screening approximation of the pseudopotential (4.25) describes quite well behaviour of the screened HGK pseudopotential at low Γ_{ii}. At the moderate magnitude of Γ_{ii} one can observe small discrepancy from the screened pseudopotential at the small distances $R = r/r_L$. In the Figure 4.6, in the case of $e-i$ interaction, at the small R when $r < r_B$ the curves almost coincide and at $r > r_B$ when R increases they begin to diverge. This can be explained by that fact that the screening effects at Bohr radius are absent and when R and Γ_{ii} increase they begin to play significant role. In the case of $i-i$ pseudopotential shown in Figure 4.7 one can see the similar behaviour as for $e-i$ interaction: at low Γ_{ii} the difference between the pseudopotentials is negligible, whereas when Γ_{ii} increases the screening effects begin to play significant role and the difference grows with R. The pseudopotentials (4.24) as for $e-i$, $i-i$ interactions describe quite well behaviour of the screened HGK pseudopotential even when Γ_{ii} is moderate. However, when one considers either extreme high temperatures $T \gtrsim 10^6 K$

Table 4.2: Plasma Parameters of consideration

r_s	52.55	13.13	8.76	5.25
Γ_{ii}	0.2	0.8	1.2	2
$n_e = n_i, 10^{21}$ cm^{-3}	0.01	0.7	2.4	10
$T, 10^4$K	3 ($k_BT \simeq 0.1$Ha)	3	3	3
$r_L, 10^{-9}$m	0.55 ($\simeq 10.5r_B$)	0.55	0.55	0.55

and densities $r_{ee} \approx r_B$ or high Γ_{ii} then the discrepancy between the pseudopotentials increases significantly. One can observe also local minima and maxima as it is shown in Figure 4.8 a, b for electron-ion pseudopotential. These oscillations one can see more clearly in the enlarged scale. This effect can be explained by competition between the quantum-mechanical and screening field effects when their scales become similar leading to the short-range order formation. The similar results have been reported in (Arkhipov et al., 2000) for $r_s = 0.1 \cdot r_B$ and $T = 10^6 K$. Strictly speaking, such extreme conditions as shown in the Figure 4.8 a can not be realized for Li^+ plasma that is why this example serves only as a demonstration of behaviour of the pseudopotential whereas in the case of 4.8 b - parameter region lies close to that of the laser produced plasma.

In the figures 4.9 a, the $e-e$, $i-i$ radial distribution functions are plotted, as one can see, the $i-i$ radial distribution function is zero at a distance approximately equal to the size of electron shell meaning that electron can not approach the nucleus at the smaller distance while another electron can. The $e-i$ radial distribution function in the Figure 4.9 b possesses a maximum showing the greatest probability of location of the electron at the distance approximately equal to the size of electron shell.

In order to compare with the alternative screened $i-i$ pseudopotential models we considered the Dalgic et al. pseudopotential, which determines the screened ion-ion pseudopotential (Dalgic et al., 2002) on the basis of the second order pseudopotential perturbation theory using the Fiolhais et al. pseudopotential ${\varphi^F}_{ei}(r)$:

$$\Phi^D_{ii}(k) = \frac{4\pi z^2 e^2}{4\pi\varepsilon_0 k^2} + \chi(k)|{\varphi^F}_{ei}(k)|^2, \tag{4.26}$$

where ${\varphi^F}_{ei}(k)$ is the pseudopotential local form factor. Here, we use instead of the Fiolhais pseudopotential the HGK $\Phi^{HGK}_{ii}(k)$ pseudopotential with the parameters fitted to those of Fiolhais et al. pseudopotential. Notice that $\chi(k)$ is the electron gas response function, where the Lindhard response of the ideal degenerate electron gas $\chi^0(k)$ and the local field correction (LFC) $G(k)$ enter the expression in the standard way. We used the LFC which satisfies the compressibility sum rule at finite temperatures obtained by Gregori et al. for the strong coupling regime (Gregori et al., 2007). Similar calculations have also been carried out by Apfelbaum who used the pseudopotential described by Dalgic et al. to calculate the SSF of Cs and Rb in the realm of the liquid-plasma transition (Apfelbaum, 2010) in agreement with the measured SSF.

In Fig. 4.10 the $e-i$ and $i-i$ HGK, screened HGK and $i-i$ Dalgic et al. pseudopotentials are presented for comparison. We presume that the curves shift, with the

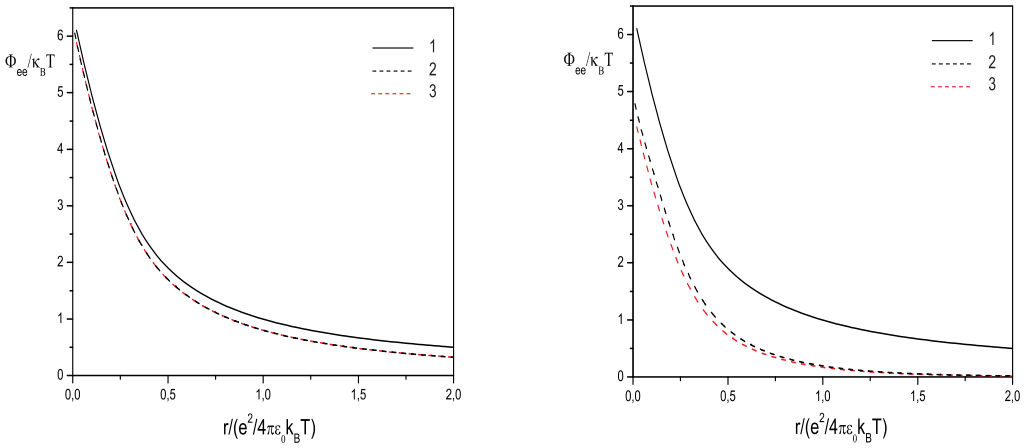

Figure 4.5: Comparison between the different $e-e$ pseudopotentials of semiclassical Li^+ plasma against the dimensionless distance $R = r/r_L$ at $T = 30000$ K, (a) $\Gamma_{ii} = 0.2$ and (b) $\Gamma_{ii} = 0.8$; 1: Electron-electron Deutsch pseudopotential (4.11); 2: Screened electron-electron Hellmann-Gurskii-Krasko pseudopotential (4.16), (4.19); 3: pseudopotential (4.25) (Sadykova et al., 2009a).

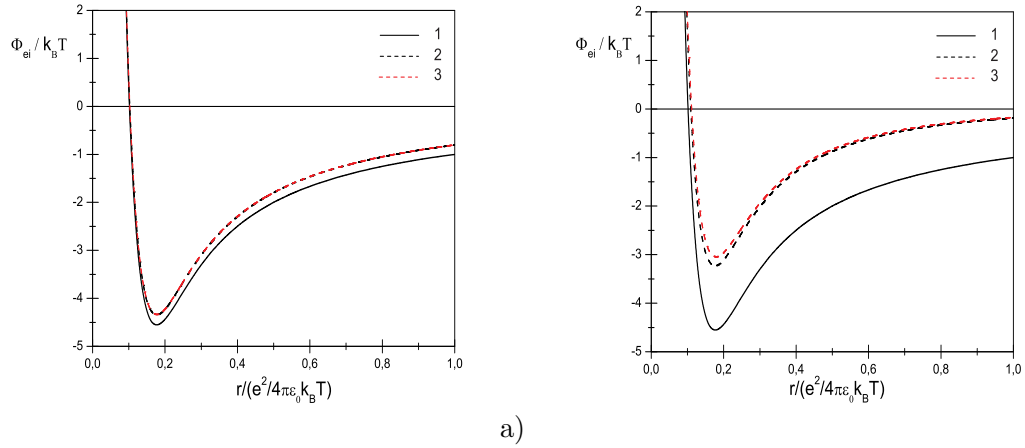

Figure 4.6: Comparison between the different $e-i$ pseudopotentials of semiclassical Li^+ plasma against the dimensionless distance $R = r/r_L$ at $T = 30000$ K, (a) $\Gamma_{ii} = 0.2$ and (b) $\Gamma_{ii} = 0.8$; 1: Electron-ion Hellmann-Gurskii-Krasko pseudopotential (4.13); 2: Screened electron-ion Hellmann-Gurskii-Krasko pseudopotential (4.15), (4.19); 3: pseudopotential (4.24) (Sadykova et al., 2009a).

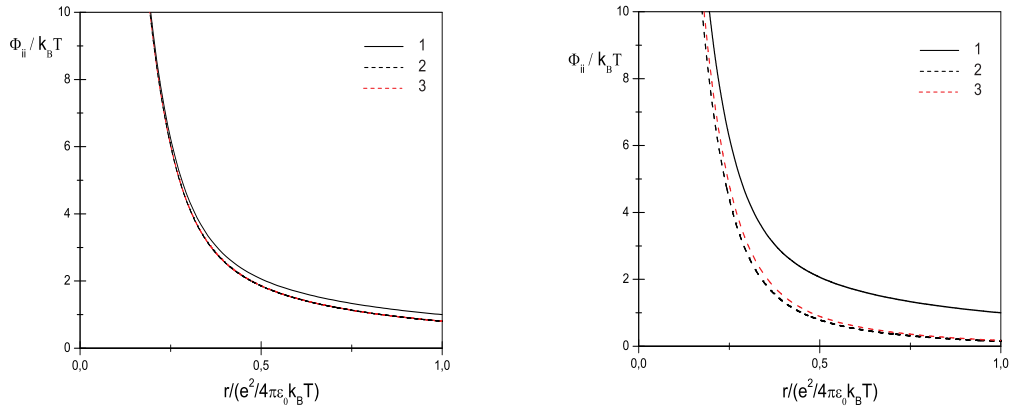

Figure 4.7: Comparison among the different $i-i$ pseudopotentials of semiclassical Li^+ plasma against the dimensionless distance $R = r/r_L$ at $T = 30000$ K, (a) $\Gamma_{ii} = 0.2$ and (b) $\Gamma_{ii} = 0.8$; 1: Ion-ion Hellmann-Gurskii-Krasko pseudopotential (4.13); 2: Screened ion-ion Hellmann-Gurskii-Krasko pseudopotential (4.17), (4.19); 3: pseudopotential (4.24) (Sadykova et al., 2009a).

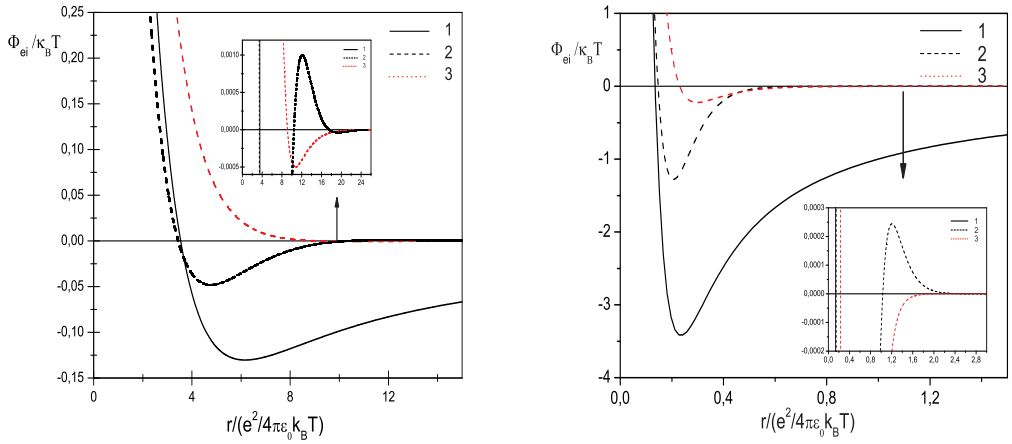

Figure 4.8: Electron-ion screened Hellmann-Gurskii-Krasko pseudopotentials of semiclassical Li^+ plasma against the dimensionless distance $R = r/r_L$ at (a) $\Gamma_{ii} = 0.3$, $T = 1049715$ K, $n_e = 1.6 \cdot 10^{24}$ cm^{-3} and (b) $\Gamma_{ii} = 2$, $T = 40000$ K, $n_e = 0.26 \cdot 10^{23}$ cm^{-3}; Solid line: Hellmann-Gurskii-Krasko pseudopotential (4.13); Black dashed line: Screened Hellmann-Gurskii-Krasko pseudopotential (4.19); Red dashed line: pseudopotential (4.24) (Sadykova et al., 2009a).

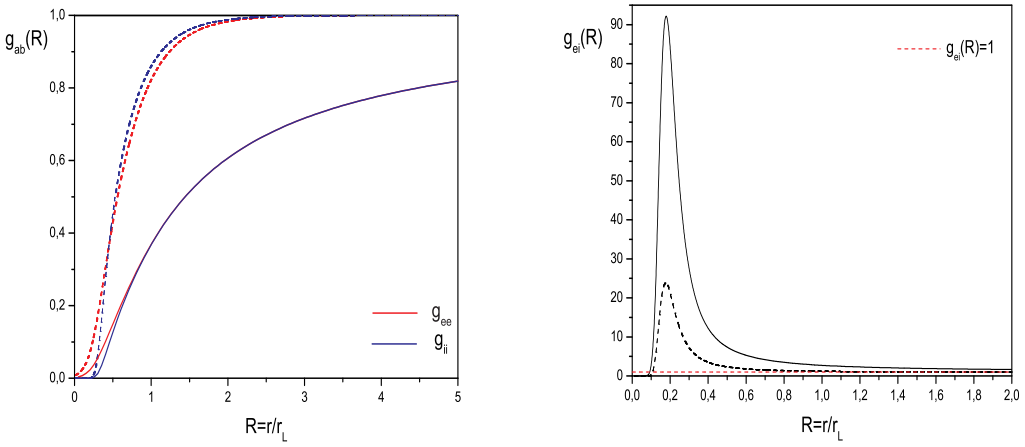

a) b)

Figure 4.9: Electron-electron, ion-ion (a) and electron-ion (b) Radial distribution functions of the screened Hellmann-Gurskii-Krasko pseudopotential of semiclassical Li^+ plasma against the dimensionless distance $R = r/r_L$ at $T = 30000$ K, $\Gamma_{ii} = 0.8$; Solid line: Hellmann-Gurski-Krasko pseudopotential (4.13) and (4.11); Dashed line: Screened Hellmann-Gurski-Krasko pseudopotentials (4.15)-(4.17), (4.19) (Sadykova et al., 2009a).

growth of Γ_{ee} (defined in the subsection 6.1.2 on the page 102), in the direction of its low absolute values, due to the increasing role of screening effects.

4.1.3 The screened Hellmann-Gurskii-Krasko pseudopotential obtained with the help of electron-electron generalized Kelbg and electron-ion, ion-ion Hellmann-Gurskii-Krasko micro-pseudopotentials

As it has been described above in the Sec. 4.1.2, it is of a high interest to construct the pseudopotential model which takes into account not only the quantum-mechanical and the ion shell structure but also the screening field effects. We follow the method described in the Sec. 4.1.2. In our paper (Sadykova et al., 2011a) we used the same Hellmann-Gurskii-Krasko pseudopotentials ${\varphi^{HGK}}_{ei}(r)$ (4.6), ${\varphi^{HGK}}_{ii}(r)$ (4.8) but instead of the earlier employed $e-e$ Deutsch pseudopotential (4.11) we used the corrected $e-e$ Kelbg pseudopotential. The motivation for doing so is that the corrected Kelbg pseudopotential provides better results at the low temperatures when quantum effects start to play a significant role. The corrected Kelbg pseudopotential has the following form:

$$\varphi_{ee}(r) = \frac{e^2}{4\pi\varepsilon_0}\left\{\frac{1-e^{-r^2/\lambda_{ee}^2}}{r} + \frac{\sqrt{\pi}}{\lambda_{ee}}(1-erf(r/\lambda_{ee}))\right\} - k_B T \tilde{A}_{ee}(\xi_{ee}) e^{-r^2/\lambda_{ee}^2} \quad (4.27)$$

with $\tilde{A}_{ee} = \sqrt{\pi}\,|\xi_{ee}| + \ln\left[2\sqrt{\pi}\,|\xi_{ee}| \int\limits_0^\infty dy y \exp(-y^2)/(\exp(\pi\,|\xi_{ee}|\,/y) - 1)\right]$, where $\lambda_{ee} = \hbar/\sqrt{m_e k_B T}$ is De Broglie wave length of relative motion, here m_e is the electron mass, $\hbar$ is the Planck constant and k_B is the Boltzmann constant. Here $\xi_{ee} = -e^2/(4\pi\varepsilon_0 k_B T \lambda_{ee})$ is the interaction parameter.

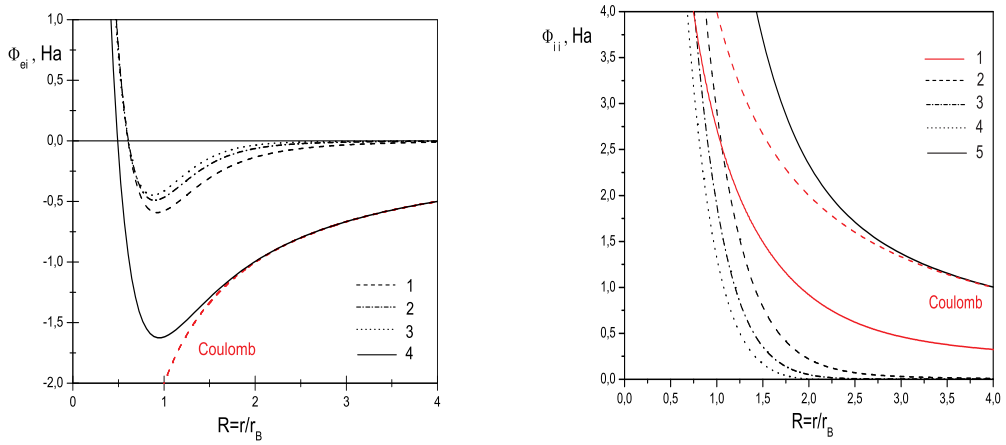

a) b)

Figure 4.10: Comparison among the different $e-i$ HGK pseudopotentials Φ_{ei} and $i-i$ pseudopotentials Φ_{ii} for beryllium plasmas (Be^{2+}) (in atomic units). **a)**1: Screened HGK (4.15), (4.19) at $T_e = T_i = 40$ eV ,$T_e' = 42.17$ eV, $\Gamma_{ee} = 0.346$; 2: Screened HGK at $T_e = T_i = 20$ eV , $T_e' = 24.06$ eV, $\Gamma_{ee} = 0.606$, 3: Screened HGK at $T_e = T_i = 13$ eV , $T_e' = 18.65$ eV, $\Gamma_{ee} = 0.782$, 4: HGK; **b)** 1: Dalgic et al. pseudopotential at $T_e = T_i = 13$ eV, $T_e' = 18.65$ eV, $\Gamma_{ee} = 0.782$, 2: Screened HGK at $T_e = T_i = 40$ eV, $T_e' = 42.17$ eV, $\Gamma_{ee} = 0.346$; 3: Screened HGK at $T_e = T_i = 20$ eV, $T_e' = 24.06$ eV, $\Gamma_{ee} = 0.606$, 4: Screened HGK (4.17) at $T_e = T_i = 13$ eV, $T_e' = 18.65$ eV, $\Gamma_{ee} = 0.782$, 5: HGK. The plasma parameters are described in the subsection 6.1.1 on the page 101 (Sadykova et al., 2011b).

We solve in Fourier space the following system of linear algebraic equations:

$$\Phi_{ab}(k) = \varphi_{ab}(k) - \frac{1}{k_B T}\left[n_e \varphi_{ae}(k)\Phi_{eb}(k) + n_i \varphi_{ai}(k)\Phi_{ib}(k)\right] \tag{4.28}$$

where $a, b = i, e$, $\varphi_{ab}(k)$ are the Fourier transforms of (4.27), (4.6), (4.8). The solution of the system (4.28) reads:

$$\Phi_{ei}(k) = \frac{Ze^2}{\varepsilon_0 \Delta}\frac{(2a-1){R_{cei}}^2 k^2 - 1}{k^2(1+k^2{R_{cei}}^2)^2}, \tag{4.29}$$

$$\begin{aligned}\Phi_{ee}(k) = &\frac{e^2}{\varepsilon_0\Delta}\left\{\frac{2\exp\left(-\frac{k^2\lambda_{ee}^2}{4}\right)}{k^3\lambda_{ee}}\int_0^{k\lambda_{ee}/2} e^{t^2}dt + \right.\\ &\frac{1}{k^4 {r_{Di}}^2}\left[\exp\left(-\frac{k^2\lambda_{ee}^2}{4}\right)\frac{2((2a+1){R_{cii}}^2k^2+1)}{k\lambda_{ee}(1+k^2{R_{cii}}^2)^2}\int_0^{k\lambda_{ee}/2} e^{t^2}dt - \right.\\ &\left.\left.\left(\frac{(2a-1){R_{cei}}^2k^2-1}{(1+k^2{R_{cei}}^2)^2}\right)^2\right] -\end{aligned}$$

$$A\tilde{A}_{ee}(\xi_{ee})\left(1+\frac{(2a+1){R_{cii}}^2k^2+1}{k^2{r_{Di}}^2(1+k^2{R_{cii}}^2)^2}\right)\exp\left(-\frac{k^2\lambda_{ee}^2}{4}\right)\Bigg\}, \tag{4.30}$$

$$\begin{aligned}\Phi_{ii}(k) =&\frac{Z^2e^2}{\varepsilon_0\Delta}\left\{\frac{(2a+1){R_{cii}}^2k^2+1}{k^2(1+k^2{R_{cii}}^2)^2}+\right.\\ &\frac{1}{k^4{r_{De}}^2}\left[\exp\left(-\frac{k^2\lambda_{ee}^2}{4}\right)\frac{2((2a+1){R_{cii}}^2k^2+1)}{k\lambda_{ee}(1+k^2{R_{cii}}^2)^2}\int_0^{k\lambda_{ee}/2}e^{t^2}dt-\right.\\ &\left.\left(\frac{(2a-1){R_{cei}}^2k^2-1}{(1+k^2{R_{cei}}^2)^2}\right)^2\right]-\\ &\left.A\tilde{A}_{ee}(\xi_{ee})\frac{(2a+1){R_{cii}}^2k^2+1}{k^2{r_{De}}^2(1+k^2{R_{cii}}^2)^2}\exp\left(-\frac{k^2\lambda_{ee}^2}{4}\right)\right\},\end{aligned} \tag{4.31}$$

here r_{De}, r_{Di} are the Debye radius for electrons and ions respectively, where $1/{r_{Di}}^2 = z^2e^2n_i/(\varepsilon_0k_BT)$, $1/{r_{De}}^2 = e^2n_e/(\varepsilon_0k_BT)$, $A = k_BT\pi^{3/2}\lambda_{ee}^3\varepsilon_0/e^2$ and Δ is:

$$\begin{aligned}\Delta =&1+\frac{2\exp\left(-\frac{k^2\lambda_{ee}^2}{4}\right)}{k^3{r_{De}}^2\lambda_{ee}}\int_0^{k\lambda_{ee}/2}e^{t^2}dt+\frac{(2a+1){R_{cii}}^2k^2+1}{k^2{r_{Di}}^2(1+k^2{R_{cii}}^2)^2}+\\ &\frac{1}{k^4{r_{De}}^2{r_{Di}}^2}\left[\exp\left(-\frac{k^2\lambda_{ee}^2}{4}\right)\frac{2((2a+1){R_{cii}}^2k^2+1)}{k\lambda_{ee}(1+k^2{R_{cii}}^2)^2}\int_0^{k\lambda_{ee}/2}e^{t^2}dt-\right.\\ &\left.\left(\frac{(2a-1){R_{cei}}^2k^2-1}{(1+k^2{R_{cei}}^2)^2}\right)^2\right]-\\ &\frac{A\tilde{A}_{ee}(\xi_{ee})}{{r_{De}}^2}\left(1+\frac{(2a+1){R_{cii}}^2k^2+1}{k^2{r_{Di}}^2(1+k^2{R_{cii}}^2)^2}\right)\exp\left(-\frac{k^2\lambda_{ee}^2}{4}\right),\end{aligned} \tag{4.32}$$

The present approximation is restricted to the constraint $\Gamma_{ii} \lesssim 1$. The pseudopotential $\Phi_{ab}(r)$ can be restored from (4.29-4.32) by Fourier transformation

$$\Phi_{ab}(r) = \frac{1}{2\pi^2 r}\int\Phi_{ab}(k)k\sin(kr)dk.$$

In a weakly coupled regime the equation (4.30) turns into the following:

$$\Phi_{ee}(r) = \frac{e^2}{4\pi\varepsilon_0}\left\{\frac{e^{-r/r_D}-e^{-r^2/\lambda_{ee}^2}}{r}+\frac{\sqrt{\pi}}{\lambda_{ee}}(1-erf(r/\lambda_{ee}))\right\}-k_BT\tilde{A}_{ee}(\xi_{ee})e^{-r^2/\lambda_{ee}^2} \tag{4.33}$$

with $1/{r_D}^2 = \sum_{c=e,i}{e_c}^2n_c/(\varepsilon_0k_BT)$. As one can clearly see from the Figures 4.11 a, b, c and d at high Γ_{ii} the difference between the screened HGK pseudopotentials with $e-e$ corrected Kelbg pseudopotential (4.29-4.19), $e-e$ Deutsch pseudopotential (4.15-4.19) and corresponding unscreened pseudopotentials (4.27), (4.11) and (4.6), (4.8) is quite large, whereas when Γ_{ii} decreases the difference becomes not so much considerable as shown in the Figure 4.11 d. In a case for $e-e$ interaction at relatively low temperature $T = 8000K$, higher Γ_{ii} and small distances the difference between the corrected Kelbg and the Deutsch pseudopotentials as well as between them and their corresponding

screened pseudopotentials is significant, whereas for $e-i$ and $i-i$ interactions the difference between the HGK pseudopotentials with the corrected Kelbg and the Deutsch micro-pseudopotentials is almost negligible. This can be explained by that fact that, as mentioned earlier, at low temperatures and high densities the screening and quantum effects start to play a big role especially for $e-e$ interactions. It is worth to note that the Debye screening approximation of the pseudopotentials (4.24), (4.25), (4.33) at $r/r_L > 0.7$ describes quite well behaviour of the screened HGK pseudopotential at low Γ_{ii} as shown in Fig. 4.11 d, b. However, at the moderately high Γ_{ii} one can see that the difference between these pseudopotentials and the screened HGK pseudopotentials at the small distances $R = r/r_L$ is quite considerable, especially for $e-e$ potentials in the Fig. 4.11 b.

4.2 Electric microfield distributions at an ion in alkali two-component plasmas with an account of the ion shell structure

We consider the two-component electron-ion Li^+, Na^+, K^+, Rb^+, Cs^+ thermally equillibrium and isotropic plasma ($Ze_- = -e_+$ ($Z = 1$) and masses $m_i >> m_e$) consisting of $N = N_e + N_i + N_R$ ($N_e = N_i, N_R = 1$) charged particles and a radiator (ion) at a temperature T in a volume Ω. The method which is used for the calculation is the generalized coupling-parameter integration technique for two-component plasmas introduced by Ortner et al. (Ortner et al., 1999). The final calculation formular derived in the section 2.3 on the page 24 for the microfield probability distribution function at an ion is

$$P(\beta) = \frac{2\beta}{\pi} \int_0^\infty k^* T_i(k^*) \sin(\beta k^*) dk^*.$$

Here $T_i(k)$ is the Fourier transform of the electric microfield distribution $Q =< \exp(\imath \vec{k} \cdot \vec{E}) >$ with $\vec{E}$ being the total electric microfield, $\beta = \epsilon/\epsilon_0$, $k^* = k\epsilon_0$, $\epsilon_0 = e/(4\pi\varepsilon_0 r_{ei}^2) = en^{2/3}/((36\pi)^{1/3}\varepsilon_0)$, where $n = n_e + n_i$.

The EMD studied in the work (Sadykova et al., 2009b,a) is given by the Debye screening approximation described by the generalized two-body correlation function $\mathcal{G}(\vec{r}, \vec{k})$ (2.71). The Fourier transform of the electric microfield distribution $T_i(l)$ is calculated using Eq. (2.61) or (2.69) with Debye-Hückel effective fields (2.67) and pair correlation function (RDF) $g_{\alpha R}(r)$ (2.70) where for determination of RDFs the expressions (4.24) in Sec. 4.1.2 for the screened Hellmann-Gurskii-Krasko pseudopotential in the Debye screening approximation obtained in (Sadykova et al., 2009a) are used.

To validate calculations of the microfield distributions obtained for the HGK interaction model by the Ortner et al. method we use direct semiclassical Monte-Carlo simulations with the HGK pseudopotentials. Since the MC simulation automatically takes the plasma screening effects into account, the comparison allows us to estimate the accuracy of the Debye screening approximation in our theory, remaining within the same interaction model (Ebeling et al., 1999), (Zamalin et al., 1977). We use a system of $N_e + N_i = 400$ electrons and ions in a cubic cell of the volume selected according to the plasma coupling parameter Γ_{ii}. The minimum-image convention of periodic boundary conditions is applied to the simulation cell. The pairwise electron-ion and

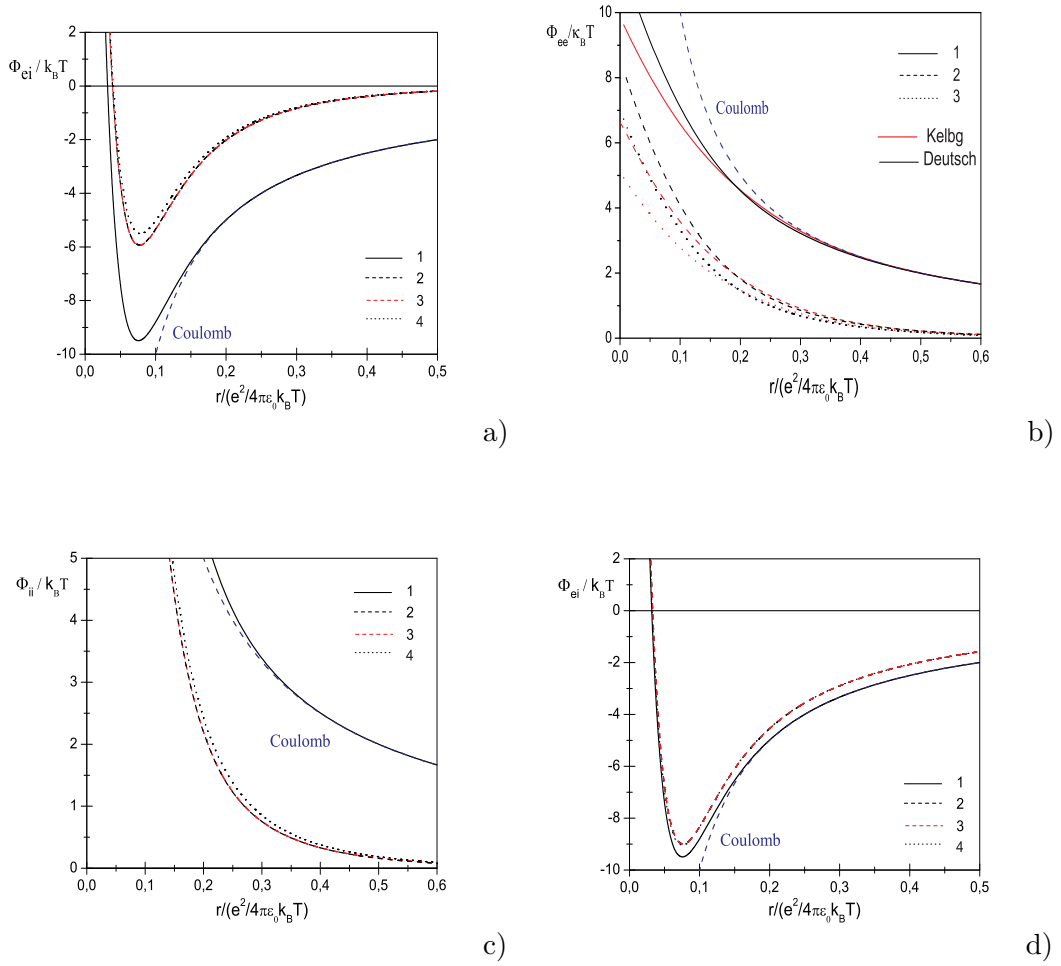

Figure 4.11: Comparison among the various $e-i$ **(a)**, $e-e$ **(b)**, $i-i$ **(c)** pseudopotentials at $\Gamma_{ii} \approx 1.56$, $T = 8000$ K, $n_e = 10^{26}$ m^{-3} and $e-i$ pseudopotential **(d)** at $\Gamma_{ii} \approx 0.335$, $T = 8000$ K, $n_e = 10^{24}$ m^{-3} of Cs^+ plasma against the dimensionless distance $R = r/r_L$. **(a)** 1: $e-i$ HGK pseudopotential (4.6); 2: $e-i$ Screened HGK pseudopotential with the $e-e$ Deutsch pseudopotential as a micro-pseudopotential (4.15); 3: $e-i$ Screened HGK pseudopotential (4.29) with the $e-e$ corrected Kelbg pseudopotential (4.27) as a micro-pseudopotential; 4: $e-i$ Screened HGK pseudopotential in the Debye screening approximation (4.24); **(b)** The $e-e$ corrected Kelbg (red) and Deutsch (black) sets of pseudopotentials. 1: Corrected Kelbg (4.27) or Deutsch pseudopotential (4.11); 2: Screened HGK pseudopotential with the $e-e$ corrected Kelbg (4.30) or Deutsch pseudopotentials as micro-pseudopotentials (4.16); 3: $e-e$ Screened HGK pseudopotential in the Debye screening approximation with $e-e$ Deutsch (4.25) or corrected Kelbg pseudopotentials (4.33) as micro-pseudopotentials; **(c)** 1: $i-i$ HGK pseudopotential (4.8); 2: $i-i$ Screened HGK pseudopotential with the $e-e$ Deutsch pseudopotential as micro-pseudopotential (4.17); 3: $i-i$ Screened HGK pseudopotential (4.31) with the $e-e$ corrected Kelbg pseudopotential (4.27) as micro-pseudopotential ; 4: $i-i$ Screened HGK in the Debye screening approximation (4.24); **(d)** Description of the legend is the same as in the Fig. 4.11 a (Sadykova et al., 2011a). Here $r_L \simeq 39.4 r_B$ and $k_B T \simeq 0.025$ Ha.

ion-ion interactions are set to the corresponding unscreened HGK pseudopotentials. The electron-electron interaction potential, not provided by the unscreened HGK model, is chosen to be of the corrected Kelbg type (Ortner et al., 1999). Random single-particle displacements with adjustable amplitude are used to keep the Metropolis algorithm acceptance ratio around 0.5. The instantaneous microfields are numerically obtained by calculating direct Coulomb interaction contributions from all particles (electrons and ions) at a set of measurement points. The measurement points can be placed either at random locations (for microfields at a neutral point) or at plasma ions (for microfields at an ion) or at electrons (for microfields at an electron). The electric microfield distributions are obtained from $10^6 - 4 \cdot 10^7$ MC steps after the system equilibration. Long MC simulation runs are required to obtain the distribution tails for $\beta > 10$ (see Figures 4.21 a and b. We note that the microfield distributions can be simulated in a similar way by the semiclassical Molecular Dynamics method. Since the dynamical properties of the microfields were not required, MC appeared to be more efficient numerically.

In the Figures 4.12-4.16 a, b the comparative MC results for EMD calculation for H^+ hydrogen and singly ionized Li^+, Na^+, K^+, Rb^+, Cs^+ plasmas in the framework of the Hellmann-Gurskii-Krasko pseudopotential model at the temperature $T = 30000K$ and different $\Gamma_{ii} = e^2/(4\pi\varepsilon_0 k_B T r_{ii})$ ($\Gamma_{ii} = 0.2$ and $\Gamma_{ii} = 2$ respectively) are shown (here $r_{ii} = (3/(4\pi n_i))^{1/3}$ is the average distance of the electrons, with n_i being ion density). In the Figures 4.12-4.16 a there is a good agreement between the theory and MC, MD simulations as well as between the EMD curves for alkali plasmas and H^+ plasma which can be explained by that fact that at low $\Gamma_{ii} = 0.2$ the screening, quantum effects and the influence of the ion shell structure are negligible. However at higher $\Gamma_{ii} = 2$ the difference between the alkali and hydrogen EMDs is quite big which demonstrates the influence of the ion shell structure on the EMD shape. The EMD curves (2.49) obtained on a base of theoretical model and the curves obtained from MC simulations are shifted toward the lower fields in comparison with the Holtsmark distribution. In the Figures 4.12 a, 4.18 the curves present two models: one within the $e-i$, $i-i$ screened HGK model described by (4.24) and another within the $e-i$ screened HGK model and $i-i$ screened Hard-Sphere (Core) (Hard-Sphere - Debye-Hückel) model described by $e-i$ (4.24) and $i-i$ (4.9), (3.3) on the page 64 correspondingly. As one can see, at low $\Gamma_{ii} = 0.2$ the curves representing different pseudopotential models almost coincide whereas at higher $\Gamma_{ii} = 1.2$ we observe a slight difference meaning that at low and moderate Γ_{ii} there is no substantial difference between the $i-i$ HGK and HS models. The present results have been found in an excellent agreement with the MC simulations even at moderate $\Gamma_{ii} = 0.8$ for Cs^+ and Li^+ plasmas shown in Figure 4.17 a, b. One can see that with the increasing Γ_{ii} the deviation from MC increases as it is shown in Figure 4.18 for Li^+ plasma at Γ_{ii}=1.2 and the peaks of EMDs shift toward the lower fields and their magnitude increases shown in Fig. 4.19 a and 4.19 b. The agreement between the improved Molecular Dynamics and the theory appeared to be better at $\Gamma_{ii} = 0.8$, while at higher $\Gamma_{ii} = 1.2$ the agreement is relatively good. This can be explained by that fact that the Ortner et al. method provides reliable results only for low and moderate Γ_{ii}. We should note that Eq. (2.70) represents the pair distribution function of the screened Hellmann-Gurskii-Kasko pseudopotential in the Debye screening approximation (4.24) which enters the expression for EMD (2.49). Hence, we can make a conclusion that these pseudopotentials (4.24) can be successfully used even at moderate Γ_{ii} allowing to avoid the inverse transformation of huge expressions of the screened

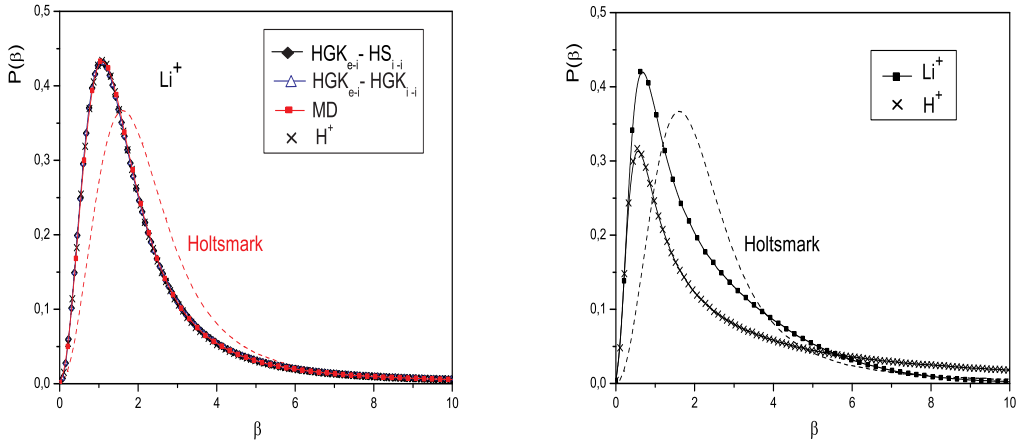

Figure 4.12: EMDs in the framework of the Hellmann-Gurskii-Krasko pseudopotential model for a K^+ and H^+ plasma at $T = 30000$ K and (a) $\Gamma_{ii} = 0.2$, (b) $\Gamma_{ii} = 2$ (MC) (Sadykova et al., 2009b).

Hellmann-Gurskii-Kasko pseudopotentials (Sadykova et al., 2009a). Taking into account that singly ionized alkali and hydrogen plasmas have the same macroscopic plasma parameters: Z, Γ_{ii}, n, T, one can expect that the curves will coincide in the framework of the pseudopotential models where the ion shell structure is not considered or when the influence of plasma parameters on ion shell structure is negligible, what we can observe in the figures 4.12-4.16 a. However, if we take a look at the Figure 4.20, where the comparison among the hydrogen H^+ where no ion shell exists and singly ionized alkali Li^+, Na^+, K^+, Rb^+, Cs^+ plasmas obtained from MC at $\Gamma_{ii} = 2$ is shown, we can see that at this value of Γ_{ii} the difference among curves is significant demonstrating again the influence of the ion shell structure. We expect that with increasing of Γ_{ii} the difference becomes even more significant. Moreover the tails (high field regions) of alkali plasmas compared to that of the hydrogen become less "heavier" (longer) at higher fields meaning that the attractive forces between the particles of opposite charges become weaker, i.e. the fields weaker, due to the ion shell screening effects.

The EMD studied in the present work is constrained to the Debye screening approximation given by (2.71), (4.24). Due to this fact we extended calculations of EMD to the case of moderately coupled plasma in the framework of the screened Hellmann-Gurskii-Krasko pseudopotentials (4.15), (4.17), (4.19) in the higher-order screening approximation compared to the screened Hellmann-Gurskii-Krasko pseudopotentials in the Debye screening approximation as recently published in (Sadykova et al., 2009b).

4.2.1 The tails

In the Figure 4.21 a, b the comparison between the tails of Na^+, Cs^+, H^+ plasmas at $\Gamma_{ii} = 0.2$ and $\Gamma_{ii} = 2$ respectively and $T = 30000K$ are shown. We have found that the behaviour of EMD for strong fields obeys either to the power law

$$P(\beta) \sim A\beta^{-\alpha-1} \tag{4.34}$$

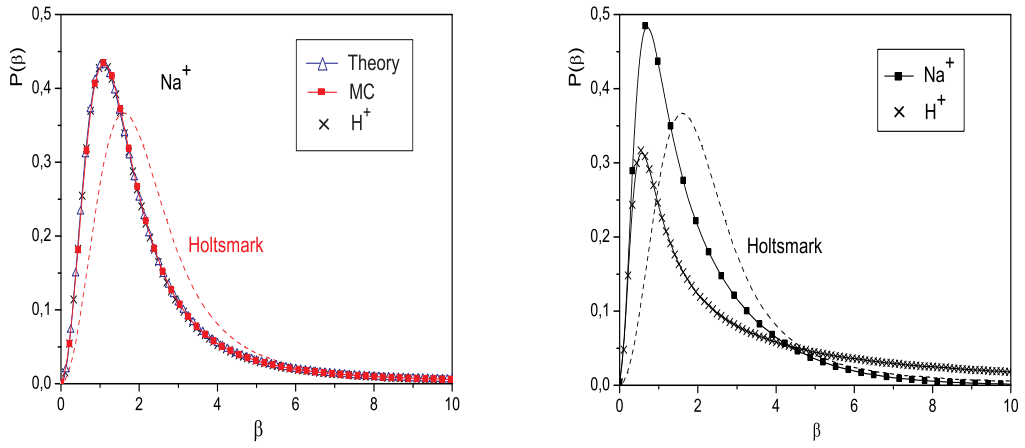

Figure 4.13: EMDs in the framework of the Hellmann-Gurskii-Krasko pseudopotential model for a Na^+ and H^+ plasma at $T = 30000$ K and (a) $\Gamma_{ii} = 0.2$, (b) $\Gamma_{ii} = 2$ (MC) (Sadykova et al., 2009b).

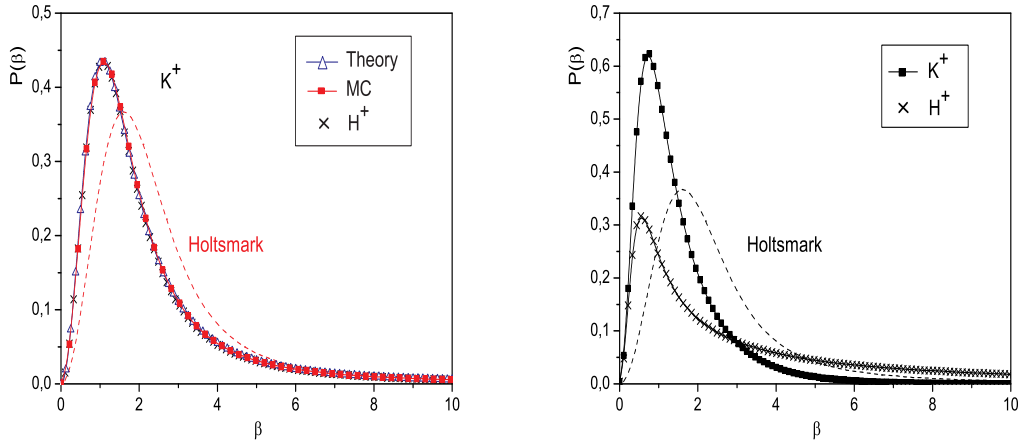

Figure 4.14: EMDs in the framework of the Hellmann-Gurskii-Krasko pseudopotential model for a K^+ and H^+ plasma at $T = 30000$ K and (a) $\Gamma_{ii} = 0.2$, (b) $\Gamma_{ii} = 2$ (MC) (Sadykova et al., 2009b).

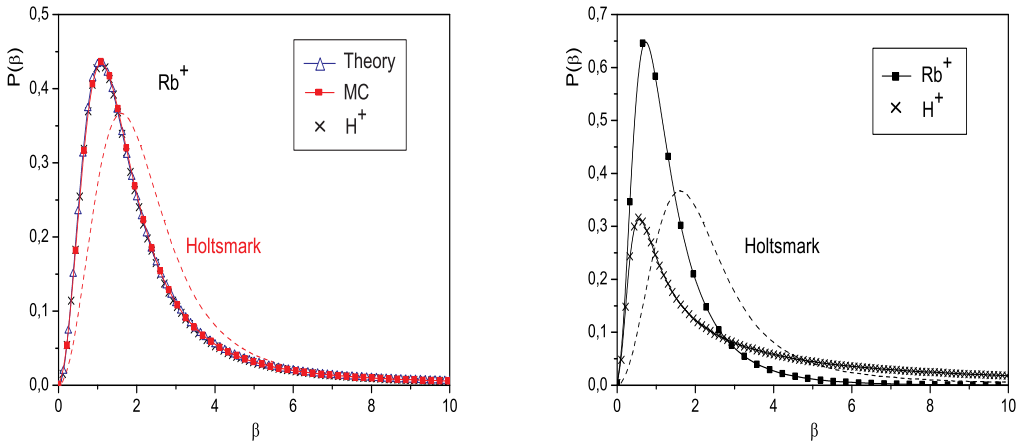

a) b)

Figure 4.15: EMDs in the framework of the Hellmann-Gurskii-Krasko pseudopotential model for a Rb^+ and H^+ plasma at $T = 30000$ K and (a) $\Gamma_{ii} = 0.2$, (b) $\Gamma_{ii} = 2$ (MC) (Sadykova et al., 2009b).

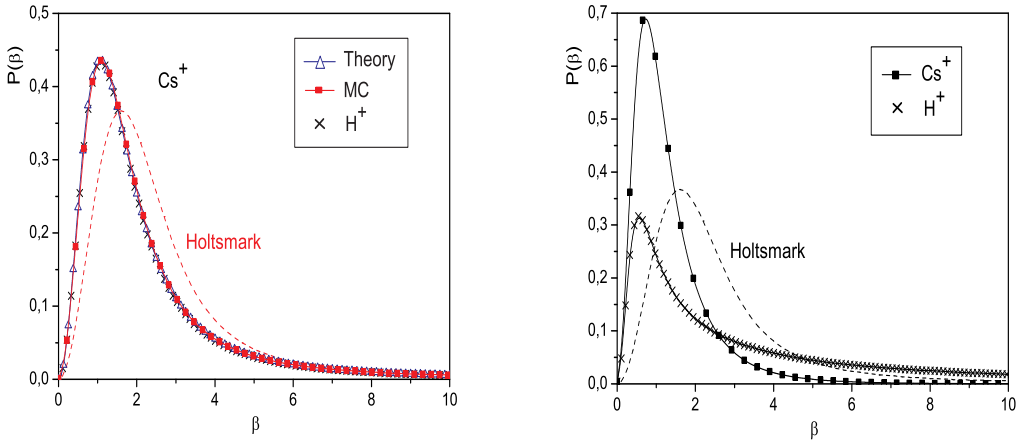

a) b)

Figure 4.16: EMDs in the framework of the Hellmann-Gurskii-Krasko pseudopotential model for a Cs^+ and H^+ plasma at $T = 30000$ K and (a) $\Gamma_{ii} = 0.2$, (b) $\Gamma_{ii} = 2$ (MC) (Sadykova et al., 2009b).

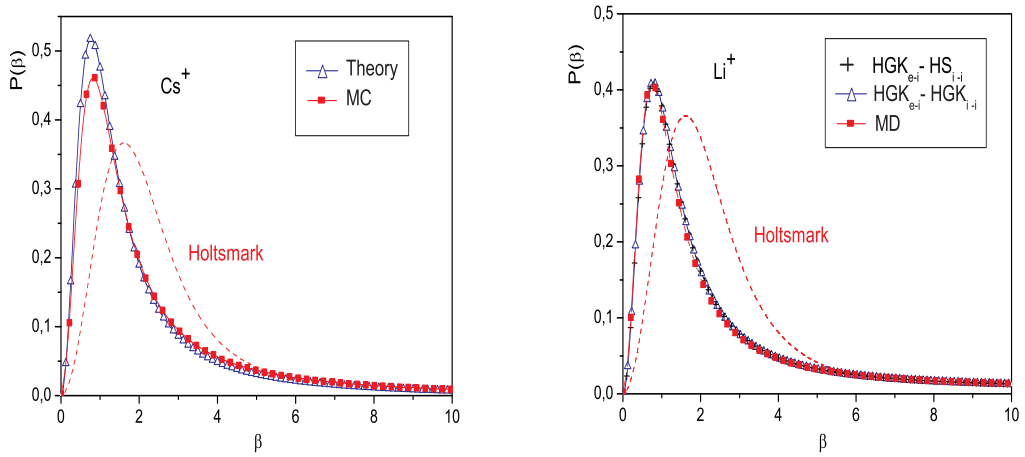

a) b)

Figure 4.17: EMDs in the framework of the Hellmann-Gurskii-Krasko pseudopotential model for a Cs^+ plasma (a) and EMD comparison between Hard-Sphere and HGK models for Li^+ (b) plasma at $T = 30000$ K and $\Gamma_{ii} = 0.8$ (Sadykova et al., 2009b).

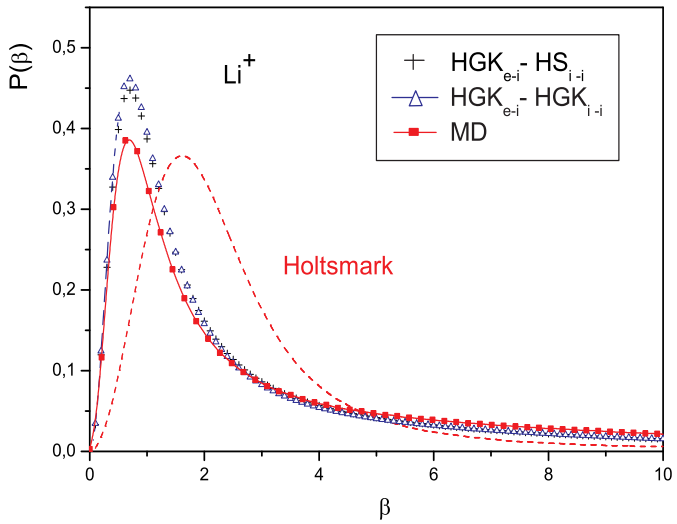

Figure 4.18: Comparison of EMD calculations in the framework of the Hellmann-Gurskii-Krasko pseudopotential model and Hard-Sphere Model for a Li^+ plasma at $T = 30000$ K and $\Gamma = 1.2$ (Sadykova et al., 2009b).

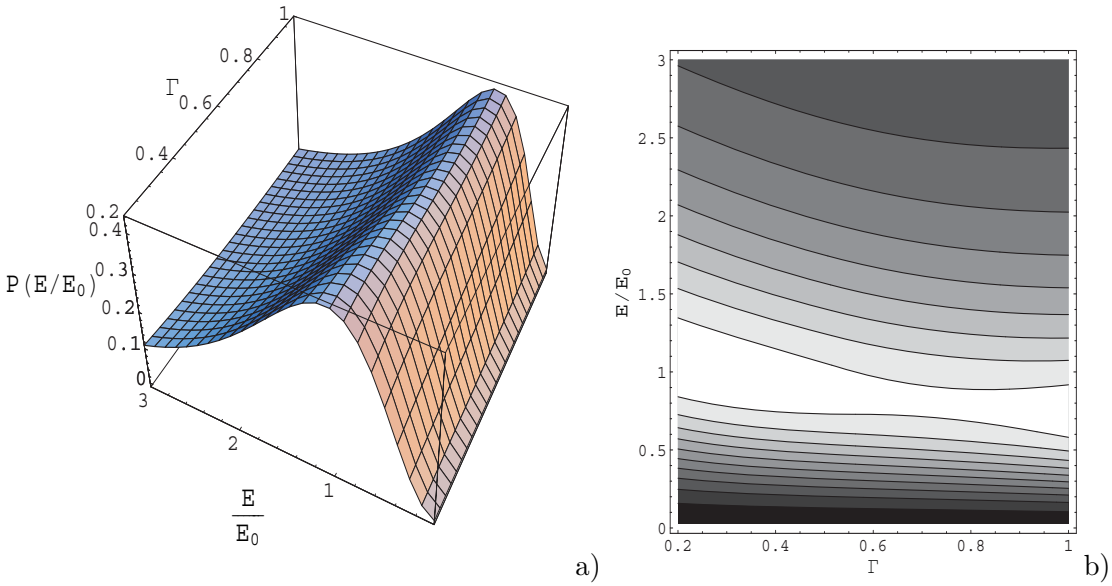

Figure 4.19: EMD in the framework of the Hellmann-Gurskii-Krasko pseudopotential model for a Li^+-plasma at $T = 30000$ K in dependence on Γ_{ii} in a range a) $\Gamma_{ii} = 0.2 \div 1$, b) its contour plot.

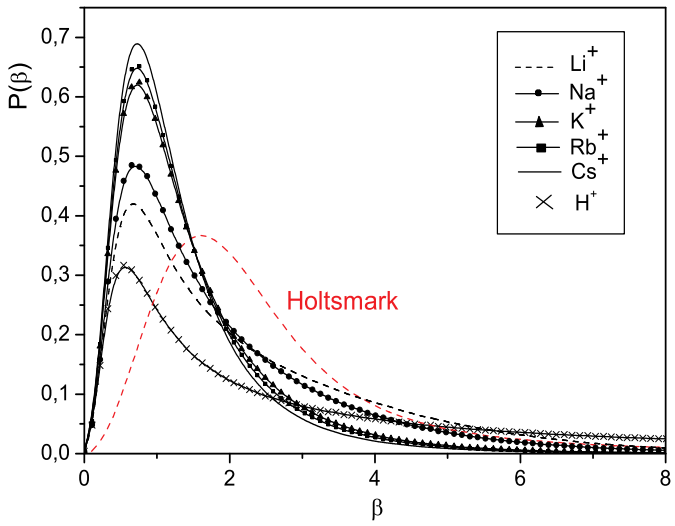

Figure 4.20: Comparison of MC results for EMDs in the framework of the Hellmann-Gurskii-Krasko pseudopotential model for alkali plasmas and H^+ plasma at $T = 30000$ K and $\Gamma_{ii} = 2$ (Sadykova et al., 2009b).

with the so called α Levy exponent found by the Levy stable distribution (Feller, 1970), where the Holtsmark limit, valid at $\Gamma_{ii} \to 0$ with ($\alpha = 3/2$), belongs to, or to the mixed power-exponential law (2.84) obtained by A. Y. Potekhin et al. in (Potekhin et al., 2002),

$$P(\beta) \sim B\beta^{-5/2} \exp(-C\beta^{1/2} - \beta^{-3/2})$$

depending on whether the field is measured at a charge (ion) or a neutral point and which plasma parameters are considered. When the field is measured at a neutral point or charge (ion) at low value of Γ_{ii} then the EMD obeys to the power law (4.34) with an exponent $\alpha \simeq 3/2$ for EMD at a neutral point, whereas when Γ_{ii} is moderate and the field is measured at an ion then the distribution obeys to the Potekhin form (2.84). In the opposite limit of extremely strong correlations ($\Gamma_{ii} \to \infty$), Potekhin et al. derived a more accurate asymptotic expression (2.84) compared to the Mayer model for the charged test particle, which yields (2.83) (Mayer, 1947)

$$P(\beta) = \frac{1}{2\sqrt{\pi}A^{3/2}} {\Gamma_{ii}}^{3/2} \beta^2 \exp\left(-\frac{\beta^2\Gamma_{ii}}{4A}\right),$$

where $A = \frac{15}{4}\sqrt{\frac{2}{\pi}}\frac{1}{3!}$. The Mayer model (2.83) fails in the strong-field limit, because in this case one should include also a test ion that lies at a very short distance $r \sim \beta^{-1/2}$ from the nearest perturbing ion. Then the geometrical and Boltzmann factors give $P(\beta) \sim \beta^{-5/2} \exp(-\Gamma_{ii}\beta^{1/2})$. In the recent work a whole spectrum of exponents $\alpha + 1$ has been obtained for electron-positron plasma in dependence on density and temperature (Sadykova et al., 2010a,b). In the present work for alkali and hydrogen plasmas, in a case of EMD at a an ion at $\Gamma_{ii} = 0.2$ we have found that $A = 0.79$, $\alpha \simeq 1.15$ for Na^+, $A = 0.82$, $\alpha \simeq 1.16$ for Cs^+ and $A = 0.75$, $\alpha \simeq 1.14$ for H^+ plasmas with asymptotic errors: ~ 0.2 % for α, ~ 1.3 % for A as it is shown in the Figure 4.21 a, whereas at high value of $\Gamma_{ii} = 2$ we have obtained $B \simeq 497$, $C \simeq 2.17$ for Na^+ plasma and $B \simeq 20.8$, $C \simeq 1.68$ for Cs^+ plasma with asymptotic errors: ~ 3 % for B, ~ 0.5 % for C shown in the Figure 4.21 b. At a neutral point it is compatible with $\alpha = 3/2$ as shown in the Figures 4.21 a, b for Cs^+, H^+ plasmas characterizing the Holtsmark distribution with asymptotic errors: ~ 1 % for A, ~ 0.15 % for α. In a case of hydrogen the tail is even "heavier" as that of the alkali's. The field at a proton shows a different decay pattern, which we call the modified Potekhin law (3.52), defined by

$$P(\beta) \sim B\beta^{\mu} \exp(-C\beta^{1/2} - \beta^{-3/2})$$

with $B \simeq 0.5$, $\mu \simeq -1.06$ and $C \simeq 0.27$ with asymptotic errors: ~ 0.8 % for B, ~ 1 % for μ and ~ 1.8 % for C. This fact can be explained by the stronger Coulomb field created by protons in comparison with alkali ions where the ion charges are screened by the shell electrons. This allows us to make the following conclusion that at high density, when Γ_{ii} increases, the ion shell structure starts to play a big role and should be thoroughly taken into account.

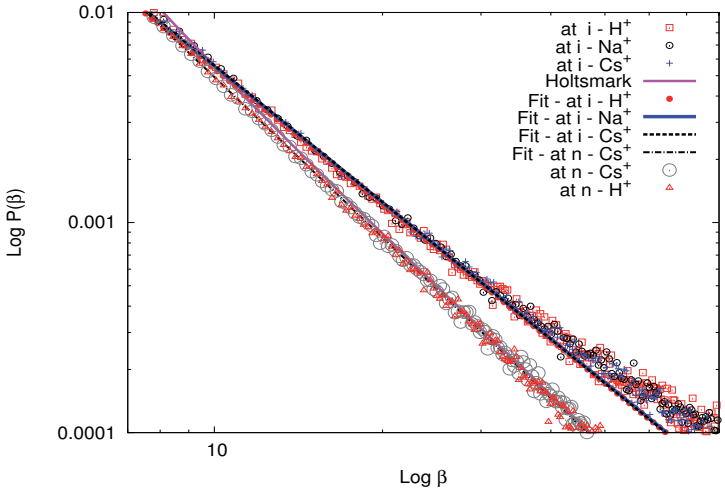

a)

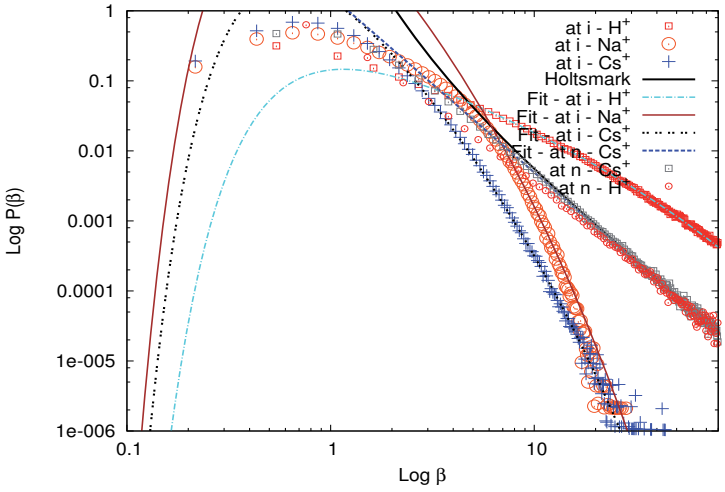

b)

Figure 4.21: The EMD tails for a Cs^+, Na^+ and H^+ plasma at $T = 30000$ K and **a)** $\Gamma_{ii} = 0.2$. The data are clustered in two groups: (i) The data for H^+ and alkali plasmas: H^+ plasma at an ion with the fitted *Levy* parameters of about $A = 0.75$, $\alpha \simeq 1.14$; alkali plasmas at an ion with the fitted *Levy* parameters $A = 0.82$, $\alpha \simeq 1.16$ for Cs^+ and $A = 0.79$, $\alpha \simeq 1.15$ for Na^+ plasmas. (ii) H^+ , Cs^+ plasmas at a neutral point with almost the same *Levy* parameters - $A = 1.7$, $\alpha \simeq 1.54$; **b)** $\Gamma_{ii} = 2$. The data are clustered in three groups: (i) H^+ plasma at an ion with a fitted to the modified *Potekhin* form (3.52) parameters of $B \simeq 0.5$, $\mu \simeq -1.06$ and $C \simeq 0.27$; (ii) Alkali plasmas at an ion with fitted to the *Potekhin* form (2.84) parameters $B \simeq 497$, $C \simeq 2.17$ for Na^+ plasma and $B \simeq 20.8$, $C \simeq 1.68$ for Cs^+ plasma. (iii) H^+ plasma at a neutral point with the fitted *Levy* parameters of about $A = 0.83$, $\alpha \simeq 1.37$, Cs^+ plasma -$A = 1.66$, $\alpha \simeq 1.52$ (Sadykova et al., 2009b). The tail of the Holtsmark distribution (2.25) which is between the cases (i) and (ii) is demonstrated for comparison.

4.3 Electric microfield distributions in a moderately coupled plasma approximation

We consider the two-component electron-ion Li^+, Na^+, K^+, Cs^+ thermally equillibrium and isotropic plasma ($Ze_- = -e_+$ $(Z = 1)$ and masses $m_i >> m_e$) consisting of $N = N_e + N_i + N_R$ $(N_e = N_i, N_R = 1)$ charged particles and a radiator (ion) at a temperature T in a volume Ω. The method which is used for the calculation is the generalized coupling-parameter integration technique for two-component plasmas introduced by Ortner et al. (Ortner et al., 1999). The final calculation formula for the microfield probability distribution function at an ion is the following (2.49)

$$P(\beta) = \frac{2\beta}{\pi} \int_0^\infty k^* T_i(k^*) \sin(\beta k^*) dk^*$$

Here $T_i(k)$ is the Fourier transform of the electric microfield distribution $Q =< \exp(\imath\vec{k} \cdot \vec{E}) >$ with $\vec{E}$ being the total electric microfield, $\beta = \epsilon/\epsilon_0$, $k^* = k\epsilon_0$, $\epsilon_0 = e/(4\pi\varepsilon_0 r_{ei}^2) = en^{2/3}/((36\pi)^{1/3}\varepsilon_0)$ with $r_{ei} = (3/(4\pi n))^{1/3}$ being the $e-i$ interparticle distance, where $n = N/\Omega$, $n = n_e + n_i$.

In the recent work (Sadykova et al., 2009b) on a base of the Ortner et al. method the EMDs for alkali plasmas at low and moderate Γ_{ii} have been calculated. There the RDFs have been determined in the Debye screening approximation (4.24) (weakly coupled regime). Here we use a better approximation for RDF, namely the RDF in a moderately coupled plasma approximation obtained with the help of the screened HGK (4.15), (4.17), (4.19).

The EMD studied in the work (Sadykova et al., 2011a) is considered in *the higher order screening approximation* given by the RDF $g_{\alpha R}(r)$ (2.70) where for determination of the RDFs the expressions (4.15), (4.17), (4.19) (Sadykova et al., 2009a) compared to the Debye screening approximation given by (4.24) on the page 66 are used. The generalized two-body correlation function $\mathcal{G}(\vec{r}, \vec{k})$ is determined as described in previous chapters as (2.71). The Fourier transform of the electric microfield distribution $T_i(l)$ is calculated using Eq. (2.61) or (2.69) with Debye-Hückel effective fields (2.67).

As one can see in the Fig. 4.22a, b, there is a good agreement between the EMD in the moderately coupled approximation and the Monte Carlo (MC) simulations, whereas there is a big discrepancy between the EMD in Debye screening approximation and MC. In a case of Li^+ the curves almost coincide. This can be explained by that fact that the screening effects in equations (4.15), (4.17), (4.19) are better taken into account than in equations (4.24) for a weakly coupled plasma (Sadykova et al., 2009a). It is worth to note that with an increase of number of band electrons in a closed shell from Li^+ till Cs^+ the discrepancy between the present theory and MC grows. This demonstrates again the significant role of ion shell structure at high values of Γ_{ii}. For comparison the corresponding EMDs (MC data) for H^+-plasmas were given too. In this case no ion shell exists and we may see clearly the influence of the ion shell structure. This allows us to conclude that the present moderately coupled plasma approximation provides a considerable improvement in the EMD calculation at moderate Γ_{ii} and should be studied further in a future.

However, we see a wide field of study of EMD in a moderately and strongly coupled

TCP plasmas in the framework of the screened Hellmann-Gurskii-Krasko pseudopotential model on a base of potential-of-mean-force exponential (PMFEX) method proposed by Nersisyan et al. in (Nersisyan et al., 2005). With an increasing value of Γ_{ii} the ion shell structure starts to play a significant role. In a strongly coupled regime the screened HGK pseudopotentials and corresponding RDFs can be determined with the help of the hypernetted-chain (HNC) integral equation technique with the HGK pseudopotentials as micro-pseudopotentials (Hansen and McDonald, 1990).

4.4 Conclusions

The electric microfield distributions have been calculated for Hydrogen H^+, singly ionized alkali plasmas (Li^+, Na^+, K^+, Rb^+, Cs^+) at the location of an ion using the generalized coupling-parameter integration technique for two-component plasmas introduced by Ortner et al. in comparison with MC simulations. The distributions are studied in the framework of the Hellmann-Gurskii-Krasko pseudopotential model which takes into account the ion shell structure. Our models take into account both the quantum-mechanical, ion shell structure and screening field effects. We used the screened Hellmann-Gurskii-Krasko pseudopotential in the Debye screening approximation as well as in a higher-order screening HGK approximation valid also for a moderately coupled plasma, both described in Subsec. 4.1.2. The influence of the coupling parameter along with the ion shell structure on the EMD shape and position was investigated. With an increasing value of Γ_{ii} the ion shell structure starts to play a significant role. High density as well as the coupling parameter causes a shifting of the maximum of probability to lower fields and changing the tails this way significantly modifying the electric microfield distributions. For comparison the corresponding EMDs for H^+-plasmas were given too. In this case no ion shell exists and we may see clearly the deviation of H^+-curve from alkali curves and consequently the influence of the shell structure. For RDFs of Li^+, Na^+, K^+, Cs^+ plasmas we used the screened Hellmann-Gurskii-Krasko pseudopotential in a moderately coupled plasma approximation. The moderately coupled plasma approximation compared to the Debye screening approximation makes a considerable improvement in the EMD calculation at moderate Γ_{ii} leading to a much better agreement with the Monte-Carlo simulations. However, we see a wide field of study of EMD in a moderately and strongly coupled TCP plasmas in the framework of the screened Hellmann-Gurskii-Krasko pseudopotential model on a base of PMFEX method proposed by Nersisyan et al. . With an increasing value of Γ_{ii} the ion shell structure starts to play a significant role. In a strongly coupled regime the screened HGK pseudopotentials and corresponding RDFs can be determined with the help of the hypernetted-chain (HNC) integral equation technique with the HGK pseudopotentials as micro-pseudopotentials. The theoretical results were compared with Monte-Carlo simulations. We have derived a new type of screened HGK pseudopotential described in Subsec. 4.1.3, where for electron-electron interaction we used the corrected Kelbg micro-pseudopotential instead of earlier applied Deutsch pseudopotential.

Summarizing our main results:

(i) The shapes of EMD of the alkali plasmas at moderate values of Γ_{ii} are different. We observe large differences compared to the Holtsmark distribution and to the EMD distribution of hydrogen plasma. This allows us to say that the ion shell structure

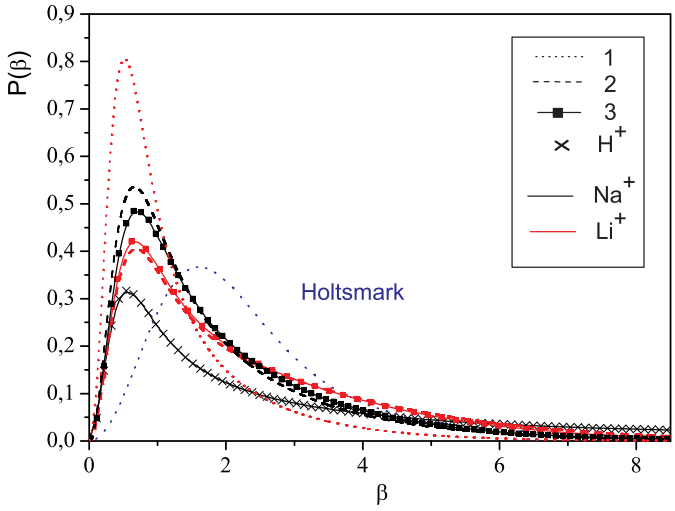

a)

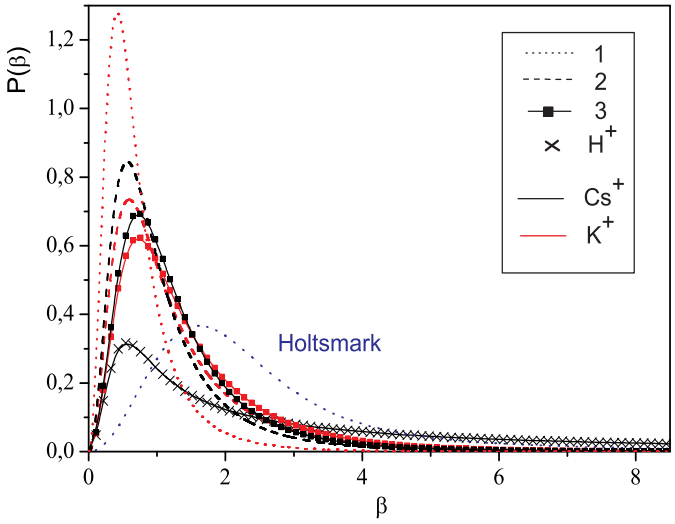

b)

Figure 4.22: Comparison of EMD calculations in the framework of the Hellmann-Gurskii-Krasko pseudopotential model in a moderately coupled plasma approximation (Sadykova et al., 2011a) for H^+, **a)** Li^+, Na^+ and **b)** K^+, Cs^+ plasmas at $T = 30000$ K and $\Gamma_{ii} = 2$. 1: EMD with RDF (2.70) obtained from the screened HGK in Debye screening approximation (4.24) or (20) in (Sadykova et al., 2009a); 2: EMD with RDF obtained from the screened HGK in the moderately coupled plasma approximation (4.15), (4.17), (4.19); 3, H^+: Monte Carlo simulations, which were obtained in (Sadykova et al., 2009b).

influences the EMD strongly;
(ii) The peak of the EMD distribution of alkali plasmas is positioned in between the peak for hydrogen, which is located at lower fields and the Holtsmark distribution which is located at higher fields;
(iii) The tails of the EMD at the location of an ion or neutral point at $\Gamma_{ii} = 0.2$, $T = 30000K$ shown in Figure 4.21 a are in all cases of Levy type $P(\beta) \sim \beta^{-\alpha-1}$ with $\alpha \simeq 3/2$ for EMD at a neutral point. When the field is measured at an ion at moderate $\Gamma_{ii} = 2$ the tails obey to the power-exponential Potekhin form $P(\beta) \sim B\beta^{-5/2} \exp(-C\beta^{1/2} - \beta^{-3/2})$ whereas in Hydrogen plasma it obeys to the modified Potekhin form shown in Figure 4.21 b. In the Figure 4.21 b the Holtsmark limit with the exponent $\alpha = 1.5$ is again in the middle, between the hydrogen plasma with $B \simeq 0.5$, $\mu \simeq -1.06$ and $C \simeq 0.27$ and relatively fast Potekhin power-exponential decay with $B \simeq 497$, $C \simeq 2.17$ for Na^+ plasma and $B \simeq 20.8$, $C \simeq 1.68$ for Cs^+ plasma. The relatively fast decay of the microfield distribution of alkali plasmas is due to the weakening of strong fields due to the screening by the ion cores. This prevents very high fields. We leave a detailed study of this remarkable effect to future work;
(iv) The moderately coupled plasma approximation compared to the Debye screening approximation makes a considerable improvement in the EMD calculation at moderate Γ_{ii} leading to a much better agreement with the Monte-Carlo simulations.
(v) In the parameter range of weakly coupled plasmas considered here the theory by Ortner et al. with Debye screening gives a reasonable approximation which is in a good agreement with MC simulations.

5 Comparison of electric microfield distributions with the experimental optic Li^{2+} and Li^{+} data

Stark broadening of spectral lines, an effect widely applied in plasma diagnostics to evaluate plasma densities in stellar atmosphere or in laboratory (Griem, 1974). In this section we would like to compare our theoretical results for the EMDs with the measured spectra of hydrogen-like lithium Li^{2+} spectra irradiated by a nanosecond laser pulse of moderate intensities ($I \approx 10^{11} - 10^{13}$ W/cm^2) (Schriever et al., 1998b,a) using the results of spectral line theory obtained in (Lorenzen et al., 2008) and of Li^{+} spectra irradiated by a laser pulse ($\lambda = 1064$ nm) of moderate intensity ($I \approx 10^{10}$ W/cm^2) (Doria et al., 2006) using the results of spectral line theory obtained by M. Koubiti on a base of formalism of Stark broadening (Koubiti et al., 2010) [1].

In the work (Lorenzen et al., 2008) pressure broadening of Lyman-lines in dense hydrogen-like lithium plasmas is studied using a quantum statistical approach to the line shape in dense plasmas. The Lyman series is the series of transitions and resulting ultraviolet emission lines of the hydrogen atom as an electron goes from $n \geq 2$ to $n = 1$ (where n is the principal quantum number referring to the energy level of the electron). The transitions are named sequentially by Greek letters: from $n = 2$ to $n = 1$ is called Lyman-alpha, 3 to 1 is Lyman-beta, 4 to 1 is Lyman-gamma, etc. The series is named after its discoverer, American physicist Theodore Lyman. An interest in Lyman-α emission of hydrogen-like lithium is triggered by the search for next-generation light sources for EUV (extreme ultraviolet) lithography.

We also present results obtained by M. Koubiti for the Stark broadening of Li^{+} plasma using the standard Stark broadening theory (Griem, 1974) on a base of the semi-classical approach where the radiator and perturbers are respectively considered as a quantum system and classically moving particles (Koubiti et al., 2010), (Talin et al., 1997).

In both works, Koubiti and Lorenzen et al., the authors study a hot and dense plasma created by irradiating lithium with a high-intensity laser ($I > 10^{10}$ W/cm^2). Under these conditions strong modifications of spectral line features as compared to isolated lines are observed. Stark broadening as well as Doppler shift and broadening play an important role. Due to the sensitivity of these spectral line features to plasma parameters and composition, optical spectroscopy serves as a powerful diagnostic tool for the plasmas (Griem, 1997).

Since the classical description of broadening of absorption lines by collisions with surrounding atoms in 1906 by Lorentz (Lorentz, 1906), the calculation of pressure broadening has evolved drastically (Griem, 1997). The most widely used approach is due to Griem (Griem, 1974) and utilizes an impact approximation together with a

[1] PIIM, UMR 6633 CNRS/Université de Provence, centre Saint-Jérôme, service 232, F-13397 Marseille Cedex 20, France; *mohammed.koubiti@univ-provence.fr*

semi-classical description of perturber-radiator interaction.

5.1 Theory of line broadening for Li^{2+} plasma

Here we would like to describe briefly the spectral line broadening approach used in (Lorenzen et al., 2008). Pressure broadening comprises all shift and broadening effects caused by the medium that surrounds the emitting ion. Here, we outline a microscopic approach to include the most important one. We consider a plasma at a electron density n_e being in a thermal equilibrium at a fixed temperature T. We consider a radiator with nuclear charge Z_N. For simplicity, we restrict our presentation to one ion species with charge $Z = 2$ in the medium. Due to the different masses of ions and electrons, the broadening caused by ions is calculated in quasi-static approximation whereas the broadening of the electrons is considered in binary collisions approximation (Griem, 1974). Lorenzen et al. applied a quantum-statistical approach based on thermodynamic Green's function (Kraeft et al., 1986). This approach has been successfully applied to diagnose experimental hydrogen plasma (Günter, 1995).

In these approximation, the pressure-broadened line profile $I^{pr}(\Delta\omega)$ is given by (Günter, 1995)

$$I^{pr}(\Delta\omega) = \frac{{\omega_0}^4}{8\pi^3 c^3} \exp\left[-\frac{\hbar\omega_0}{k_B T}\right] \left(1+\frac{\Delta\omega}{\omega_0}\right)^4 \exp\left[-\frac{\hbar\Delta\omega}{k_B T}\right] \times \sum_{i,i',f,f'} \left\{ < i|\vec{r}|f >< f'|\vec{r}|i' > \int_0^\infty dE P(E) < i| < f|L^{-1}(\Delta\omega, E)|f' > |i' > \right\}, \tag{5.1}$$

where $\Delta\omega = \omega - \omega_0$ is the difference between the considered frequency ω and the frequency of the unperturbed electronic transition ω_0. $P(E)$ is the ionic electric microfield distribution, i.e. the probability distribution to find the electric field E at the location of the ionic radiator (emitter) due to the surrounding ions immersed in a uniform neutralizing background, see Secs. 4.2, 4.1.2. Medium modifications enter also the line profile operator

$$L^{-1}(\Delta\omega, E) = \hbar\Delta\omega - Re[\Sigma_i(\omega, E) - \Sigma_f(\omega, E)] - \imath\, \mathrm{Im}[\Sigma_i(\omega, E) + \Sigma_f(\omega, E)] + \imath\Gamma_{if}^V \tag{5.2}$$

via self-energies $\sum_i(\omega, E)$ of initial ($n = i$) and final states ($n = f$ = ground state). The vertex correction Γ_{if}^V contains the coupling between the upper and the lower state and vanishes for the Lyman series (Günter, 1995). Following the argument above, the self-energy is approximated by an electronic part which is independent of the ionic microfield and a frequency-independent ionic part

$$\Sigma_n(\omega, E) = {\Sigma_n}^{el}(\omega) + {\Sigma_n}^{ion}(E) \tag{5.3}$$

Furthermore, the thermal motion of the ions leads to Doppler broadening and is accounted for by a convolution of the pressure broadened profile, Eq. (5.1), with a Maxwellian

velocity distribution

$$I(\Delta\omega) = \frac{c}{\omega_0}\sqrt{\frac{m_{ion}}{2\pi k_B T}} \int\limits_{-\infty}^{\infty} d\Delta\omega' I^{pr}(\Delta\omega') \exp\left[-\frac{m_{ion}c^2}{2k_B T}\left(\frac{\Delta\omega - \Delta\omega'}{\omega_0 + \Delta\omega'}\right)^2\right]. \tag{5.4}$$

Here, m_{ion} is the mass of the emitting ion. Finally, the normalized line profile is defined by

$$P(\Delta\omega) = \frac{I(\Delta\omega)}{\int I(\Delta\omega) d\Delta\omega} \tag{5.5}$$

The self-energy of the electrons has been derived within a quantum-statistical many-particle approach using thermodynamic Green's functions (Kraeft et al., 1986). Accounting for dynamical screening, the emitter-electron interaction reads

$$V^s(k, \omega_\nu) = V(k)\left(1 + \int\limits_{-\infty}^{\infty} \frac{d\omega}{\pi} \frac{\mathrm{Im}\,\epsilon^{-1}(k, \omega + \imath\delta)}{\omega - \omega_\nu}\right) \tag{5.6}$$

depending on the bosonic Matsubara frequency ω_ν

$$\hbar\omega_\nu = \frac{\pi\nu}{-i\beta} + \mu,\ \nu = \begin{cases} \pm 1, & \pm 3, \cdots \quad for\ fermions, \\ 0, \pm 2, & \pm 4, \cdots \quad for\ bosons. \end{cases}$$

with μ being the chemical potential, and the wave vector k. The electronic self-energy can be evaluated in Born approximation as

$$\Sigma_n{}^{el}(\Delta\omega) = -\int \frac{d^3k}{(2\pi)^3} V(k) \sum_\alpha |M^0_{n\alpha}(k)|^2 \int_{-\infty}^{\infty} \frac{d\omega}{\pi}(1 + n_B(\omega)) \frac{\mathrm{Im}\,\epsilon^{-1}(k, \omega + \imath\delta)}{\Delta\omega + \omega_{n\alpha} - (\omega + \imath\delta)}. \tag{5.7}$$

Here, the first term in Eq. (5.6) (Fock exchange) is neglected and the Born approximation takes into account only weak collisions which are justified within the parameter range used in the work.

For evaluation of Eq. (5.7) the frequency-independent case $\Delta\omega = 0$ has been considered. The dielectric function ϵ is approximated in the random phase approximation (RPA). $M^0_{n\alpha}(k)$ is the vertex contribution for virtual transitions from n to α. $V(k) = Z_{ion}e^2/\varepsilon_0 k^2$ is the Fourier transformed Coulomb potential and $n_B(\omega) = (\exp[\hbar\omega/(k_B T)] - 1)^{-1}$ is the Bose function.

Assuming a quasi-static approximation, the ionic contribution to the self energy of the ions is given by level perturbations due to the electric field of the ions (Stark effect) and due to the field gradients (quadrupole effect). In (Lorenzen et al., 2008) the Stark effect for hydrogen and hydrogen-like ions has been evaluated using the perturbation theory (Landau and Lifschitz, 1977) while for the quadrupole effect the Halenka's expression has been used (Halenka, 1990). For further details we refer a reader to (Lorenzen et al., 2008).

5.2 Formalism of Stark broadening for Li^{+} plasma

When an atomic or ionic emitter is embedded in a plasma the spectral line it emits is affected by the electric microfield created by the plasma electrons and ions. This is known as Stark effect. Stark broadening theory describes the effect of charged particles on line profiles. The so-called standard theory of Stark broadening (Griem, 1974) is based on a semi-classical picture, i.e. the emitter and the perturbers are respectively considered as a quantum system and classically moving particles whose movement is governed by Newton's equations. In the framework of the dipole approximation, the profile $I(\Delta\omega)$ of a line is the one-side Fourier transform of the dipole autocorrelation function $C_{dd}(t)$:

$$I(\Delta\omega) = \frac{1}{\pi}\,\mathrm{Re}\int_0^\infty C_{dd}(t)\; e^{i\Delta\omega t}dt, \tag{5.8}$$

where $\Delta\omega = (\omega - \omega_0)$ is the detuning from the unperturbed angular frequency ω_0 of the line and Re designates the real part of the integral. In the Liouville space which is a direct product of two Hilbert spaces, the dipole autocorrelation function takes the following form:

$$C_{dd}(t) = \langle\langle \vec{d}^{*}|\{U(t)\}|\vec{d}\rho_0\rangle\rangle, \tag{5.9}$$

where $\vec{d}$ and ρ_0 are respectively the dipole and the density matrix of the emitter while $U(t)$ represents the emitter evolution operator and the brackets $\{\dots\}$ denote an ensemble average over the states of the perturbers. The emitter evolution operator U obeys the following stochastic Liouville equation:

$$\frac{\partial U}{\partial t} = -iLU, \tag{5.10}$$

where the Liouvillian operator $L = L_0 + l(t)$ is the sum of two terms L_0 and $l(t)$ representing respectively the Liouvillian of the unperturbed emitter (including the fine structure term) and that of the time-dependent emitter-perturber interaction. The latter may be written as follows:

$$l(t) = -\vec{d}\cdot\vec{E}(t),$$

where $\vec{E}(t)$ represents the electric field due to the charged perturbers composing the plasma. The line profile (5.8) can be expressed as follows:

$$I(\Delta\omega) = \frac{1}{\pi}\,\mathrm{Re}\int_0^\infty P(E)dE \cdot \sum_{\alpha,\beta,\alpha',\beta'} d_{\alpha\beta}\langle\langle\alpha\beta\left|\left[i\Delta\omega - \frac{i(H_a(E) - H_b(E))}{\hbar} + \mathcal{Q}_{ab}\right]^{-1}\right|\alpha'\beta'\rangle\rangle d^{*}_{\alpha'\beta'}, \tag{5.11}$$

where $P(E)$ represents the ionic EMD, the electron broadening is represented by the collision operator $\mathcal{Q}_{ab}$, H is the Hamiltonian, the a set of emitter states α and α' correspond to the upper levels of the line which are ion-field dependent; the b set of the states, β and β', to the lower levels which are assumed to be unperturbed. Transitions occur from one level of the subsystem a to a level of the subsystem b. H_a and H_b have eigenstates $|a\rangle$ and $|b\rangle$ respectively.

Since electrons and ions in a plasma have typical velocities differing by more than

an order of magnitude their interactions with the emitter are characterized by different timescales and this justifies the natural separation of their interactions with the emitter. If $t_s = 1/\Delta\omega_S$ designates the time of interest of the Stark broadening mechanism ($\Delta\omega_S$ being the Stark width), the main contribution to the integral in Eq. (5.8)-(5.10) comes from interactions over times smaller than t_s. It results from the comparison of the time of interest t_s with the characteristic times of the interactions of the emitter with ions (τ_i) and electrons (τ_e) respectively that we have $t_s >> \tau_e$ near the line center and $t_s << \tau_i$ at angular frequencies corresponding to the line wings. This means that the main contributions to Stark line broadening come from electrons near the line center and from ions in the line wings. Hence generally two approximations are used: the quasi-static approximation for the ions and the impact approximation for the electrons. The former considers the ions as static particles during the radiation process while the latter is a binary collisional approach. The standard model of Stark broadening is based on these two approximations. The lineshape code PPP (Talin et al., 1997) which used for the present calculations relies on these two approximations. The PPP needs as an input atomic data such as energy levels, reduced matrix elements of dipole transitions, level populations and the statistical properties of the electric microfield e.g. the electric microfield distribtion which is either calculated by the code itself or provided by the user. The energies can be taken from the National Institute of Standards and Technology (NIST) (Ralchenko et al., 2010), many reduced matrix elements of dipole transitions are missing in the NIST database and can be calculated as a square root of the line strength (oscillator strength) which is directly related to the Einstein coefficients (measure of the probability of occurring emission) (Koubiti et al., 2010), level population densities are assumed to be at equilibrium. The theoretical profiles are calculated using the EMD calculations obtained in the present work in the framework of the Hellmann-Gurskii-Krasko pseudopotential. The atomic data were calculated using the Cowan's code (Cowan, 1981).

5.3 Comparison with measurements from laser-produced plasmas

Li^{2+} plasma

The authors of (Lorenzen et al., 2008) used experimental data of (Schriever et al., 1998b,a). In this experimental setup, a pulsed laser beam of a Nd:YAG laser (wavelength $\lambda = 1064$ nm) with a maximum energy of 1300 mJ per pulse was focused on the surface of a lithium target. Finding a spot size of 30 μm, intensities between 10^{10} and $1.1 \cdot 10^{13}$ W/cm^2 were realized by attenuating the laser beam at an angle of 45°. The resulting spectra are time and space-integrated. The emission time was measured to be as long as the laser pulse (13 ns).

The Lyman-spectrum has been measured in (Schriever et al., 1998a) with a spectral resolution of $\lambda/\Delta\lambda^I = 300$. A laser intensity of $I_L = 1.1 \cdot 10^{13}$ W/cm^2 was used to generate the plasma. The high intensity leads to an electron temperature of $k_B T_e > 100$ eV. Within the assumption of complete local thermodynamic equilibrium (LTE), the Li^{2+}-fraction reduces to less than 0.1% at these tempeartures. In comparison, the authors apply a linear rescaling of the wavelength axis by 1.1% centered at 13.5 nm,

thus shifting the measured L_β and L_γ to their unperturbed positions. According to the authors (Lorenzen et al., 2008) assumption of LTE is justified by the optical plasma thickness.

To generate the full synthetic Lyman spectrum from Eq. (5.1) - (5.7) (and Refs.) we need an ionic electric microfield distribution function as one of the main inputs entering the equation (5.1). Having known the plasma density and temperature we can easily determine it using C. A. Iglesias method for ionic Li^{2+} OCP plasma in a framework of the Hellmann-Gurskii-Krasko pseudopotential model (Iglesias, 1983; Sadykova et al., 2009a) using the equations (2.42), (2.43) and (2.38) described in Sec. 2.2. The authors of (Lorenzen et al., 2008) used the relative intensities of L_β to L_γ to deduce the temperature which is evaluated to $T = 3 \cdot 10^5$ K. The electron density was fitted to the line width of L_γ as shown in Fig. 5.1 a. Here, an electron density $4 \cdot 10^{25}$ m^{-3} gave the best fit. Comparison of a synthetic Li^{2+} - Lyman spectrum at $T = 300\,000$ K and $n_e = 4 \cdot 10^{25}$ m^{-3} in (Lorenzen et al., 2008) with experimental data (Schriever et al., 1998a) has shown that the EMD, as an input value of the pressure broadened profile, obtained in (Lorenzen et al., 2008) provides a good agreement with the experiment as shown in Fig. 5.1 a. In Fig. 5.2 comparison among the EMDs obtained in the present work on a base of C. A. Iglesias method, Molecular Dynamics with HGK micro-pseudopotential and the EMD curve obtained in (Lorenzen et al., 2008) is presented (Lorenzen et al., 2009). As one can easily see in Fig. 5.2, the curves coincide within the high accuracy demonstrating the validity of the EMD theoretical approach and good accuracy of EMD calculations. By adjusting the plasma layer of thickness the correct ratio between L_α- and L_γ- peak values can be obtained. Fig.5.1 b shows the full spectrum using a plasma layer of thickness 180 μm. For comparison, the spectrum without the self absorption is given too. However, there are clear discrepancies when comparing the line wings. The authors assume that improvements to the microfields and account of strong collisions seem not to overcome this shortcoming and it appears to be connected to the transient nature of laser produced plasmas. In opposite, the presented approach considers mean values for temperatures and density. Adding the line emission of an estimated earlier stage of the plasma, with $n_e = 2 \cdot 10^{27}$ m^{-3} and $l = 2\mu$m, and assuming that these conditions prevail only 0.1% of the time, the line wings can be synthezised, too. This is also shown in Fig. 5.1 b.

Li^{+} plasma

In the experimental apparatus by Doria et al. (Doria et al., 2006) a $Q-$ switched Nd:YAG laser ($\lambda = 1064$ nm, pulse duration 15 ns and 10 Hz repetition rate) was focused onto a pure Li target surface placed inside a vacuum chamber ($5 \cdot 10^{-5}$ mbar) generating a plasma that expands normal to the target surface. The laser irradiance was kept constant at an average of $1.3 \cdot 10^{10}$ W$\cdot$ cm^{-2}. The authors obtained spatially and temporally resolved laser plasma spectra with an instrumental resolution $\lambda/\Delta\lambda^I \approx 2000 \div 2500$. The spectrum of our interest was recorded at a time delay of 60 ns from plasma breakdown. The authors report precise spatial electron temperature distribution, density distribution and population ratio between atoms and ions measurements for different times during the plasma plume expansion. Plasma parameters such as the electron density and temperature as well as the plume velocity were deduced from spectroscopic measurements. Under the assumption of LTE, the electron temperature and its spatial

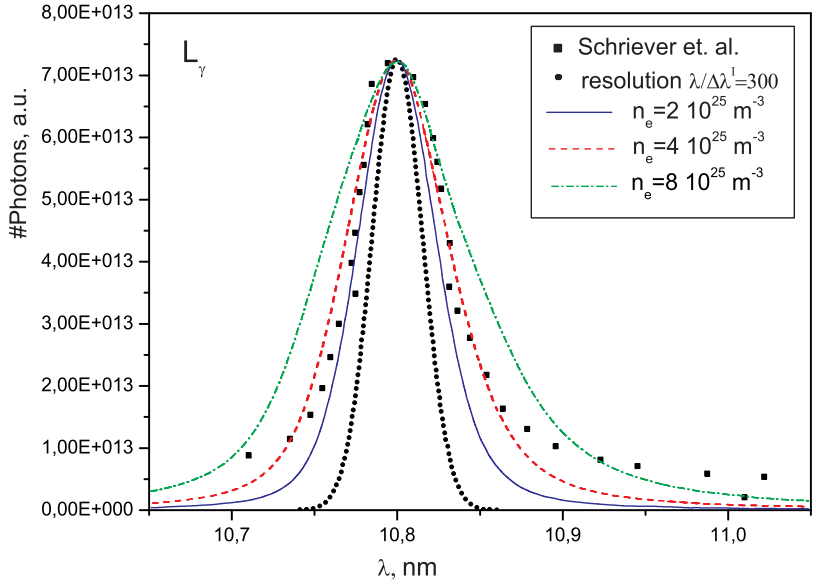

a)

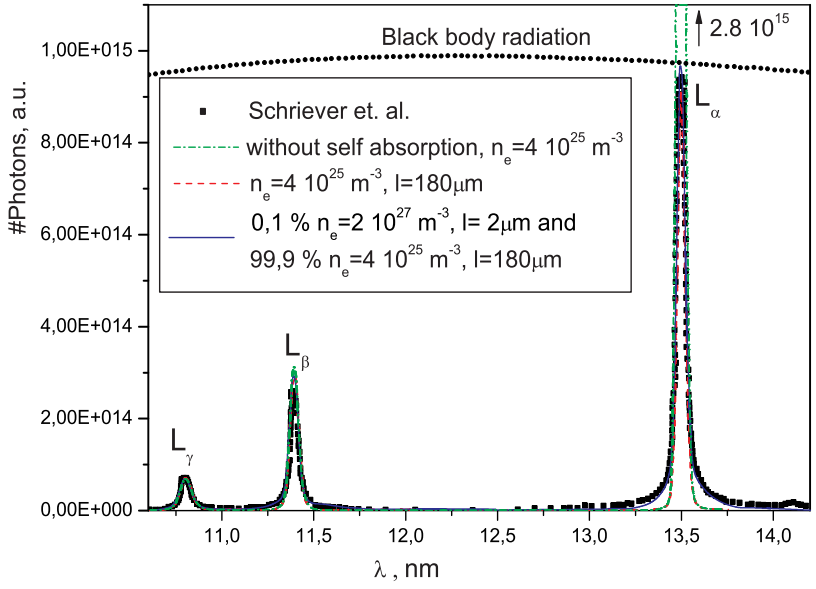

b)

Figure 5.1: Comparison of a synthetic Li^{2+} -Lyman spectrum with the experimental data at $T = 300\,000$ K and $n_e = 4 \cdot 10^{25}$ m^{-3} with the instrumental resolution $\lambda/\Delta\lambda^I = 300$: **a)** the line width is reproduced best with an electron density of $n_e = 4 \cdot 10^{25}$ m^{-3}; **b)** with and without the radiative transport through $l = 180\mu$m, respectively. The blue line corresponds to a spectrum synthesized from two plasma regions.

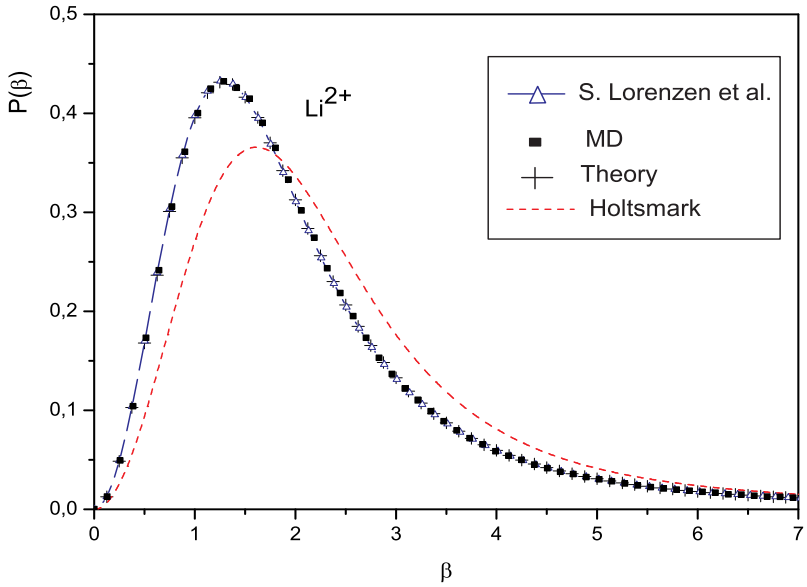

Figure 5.2: Comparison among the electric microfield distributions obtained in the present work (theory and MD) and by (Lorenzen et al., 2009) of Li^{2+} plasma at $T = 300\,000$ K and $n_e = 4 \cdot 10^{25}$ m^{-3}, ionic coupling parameter $\Gamma_{ii} = 0.097$ (Lorenzen et al., 2008). Note that in (Lorenzen et al., 2008) the EMD was scaled: $P(\beta) \cdot 2$ and $\beta/2$.

distribution in the plasma were obtained from relative line intensity measurements. For that purpose, two *Li* II lines were used: $2p\ ^3P_{2,1,0} \rightarrow 2s\ ^3S_1$ ($\lambda = 548$ nm) and $4f\ ^3F_{4,3,2} \rightarrow 3d\ ^3P_{3,2,1}$ ($\lambda = 467$ nm). The Stark broadening of the *Li* II 548 nm line was used to obtain the electron density. From the measured *Li* II 548 nm spectra, it was possible to obtain the spatial distribution of the electron density along the plasma plume expansion direction.

To generate the synthetic *Li* II 548 nm line profile from (5.11) M. Koubiti has used an ionic electric microfield distribution as one of inputs entering the expression for the line profile which was determined in the present work in the framework of the HGK pseudopotential model (Koubiti et al., 2011). Having known the plasma density and temperature we can easily determine it using C. A. Iglesias method for ionic OCP Li^{+} plasma in the framework of the Hellmann-Gurskii-Krasko pseudopotential model (Iglesias, 1983; Sadykova et al., 2009a) using the equations (2.42), (2.43) and (2.38) described in Sec. 2.2. The calculations were obtained for equal ion and electron temperatures $T_i = T_e = 3.32\ eV$ ($T = 38\,527$ K), the latter being obtained using the *Li* II line intensity ratio technique as mentioned above. Profiles of the *Li* II 548 nm line were calculated for $T_i = T_e = 3.32$ eV and different electron densities n_e. A good agreement was found for $n_e = 0.22 \times 10^{24}$ m^{-3}. The results of calculations shown in the figure 5.3 have been compared with experimental spectra taken from the experiment carried out at the Dublin City University (Doria et al., 2006). Many broadening mechanisms affect the *Li* II 548 nm line: Stark effect, Doppler effect and the instrumental function which is a Gaussian with a full width at half maximum FWHM of 0.22 nm. Therefore the measured profiles

are the convolution of a Gaussian (Doppler and instrumental function) and generally a Lorentzian profile (Stark broadening) as shown in Fig. 5.3. Comparison of a synthetic Li^+ (Li II 548 nm) line profile at $T = 3.32$ eV K and $n_e = 0.22 \cdot 10^{24}$ m^{-3} (Koubiti et al., 2011) with the experimental data (Doria et al., 2006) has shown that the EMD, as one of input values of the line profile, obtained by M. Koubiti, provides a good agreement with the experiment as shown in Fig. 5.3. In Fig. 5.4 the EMD obtained in the present work on a base of C. A. Iglesias method for ionic Li^{2+} OCP plasma within the HGK pseudopotential model is presented in comparison with MD and Holtsmark distribution. MD data have been obtained by H. B. Nersisyan using the regularized Coulomb potential (Nersisyan et al., 2005) at the same plasma parameters. The curves are found in a good. agreement with each other.

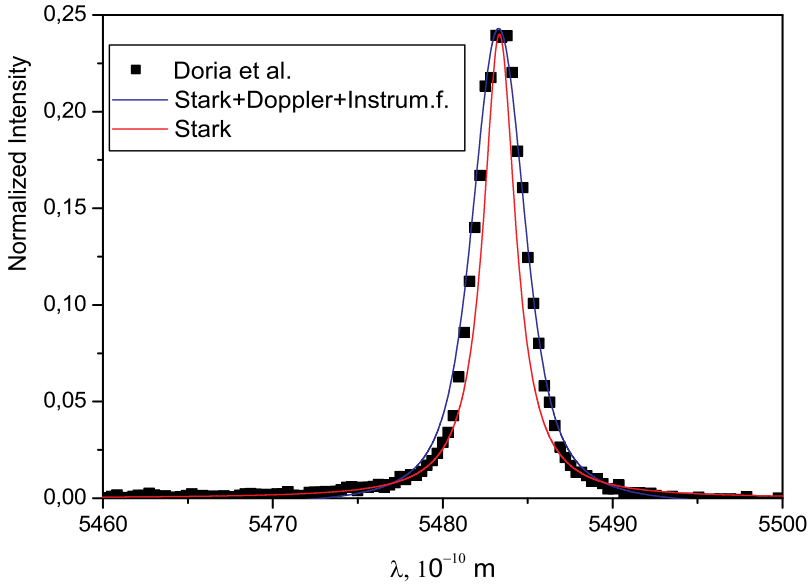

Figure 5.3: Comparison of a synthetic Li II 548 nm line obtained by M. Koubiti (Koubiti et al., 2011) with the experimental data (Doria et al., 2006) at $T = 38\,527$ K and $n_e = 0.22 \cdot 10^{24}$ m^{-3} with a FWHM of 0.22 nm. The line width is reproduced best with an electron density of $n_e = 0.22 \cdot 10^{24}$ m^{-3}.

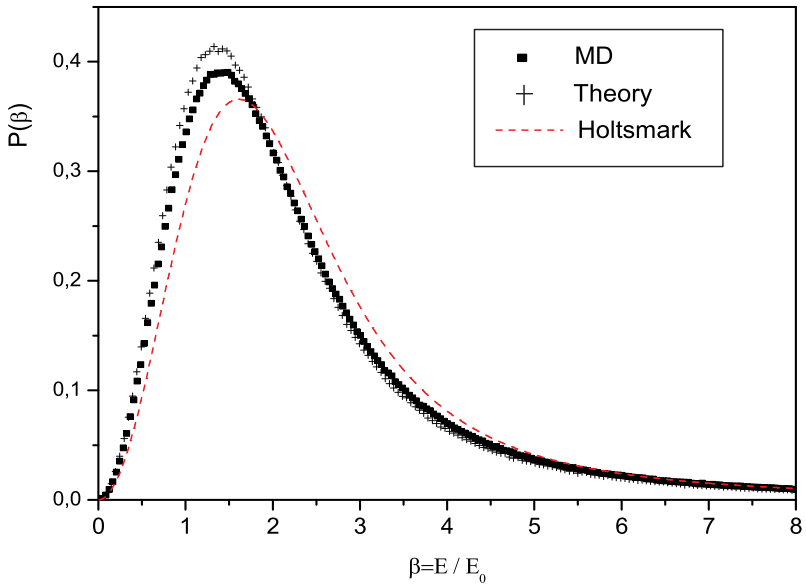

Figure 5.4: The electric microfield distribution obtained in the present work for Li^{+} plasma at $T = 38\,527$ K and $n_e = 0.22 \cdot 10^{24}$ m^{-3} in comparison with MD obtained by Nersisyan and Holtsmark distribution, ionic coupling parameter $\Gamma_{ii} = 0.042$.

6 Static and dynamic structure factors with an account of the ion shell structure for high-temperature alkali and alkaline earth plasmas

As one of possible applications of our new screened Hellmann-Gurskii-Krasko pseudopotentials we see the structure factors because for determination of the static and dynamic structure factors one needs to have a screened pseudopotential as an essential input value. The structure properties of Alkali and earth-alkali plasmas are of basic interest and of importance for high-temperature technical applications. For instance, X-ray scattering experiments have proven to be a powerful technique in measuring densities, temperatures and charge states. The structure factor is the fundamental quantity that describes the plasma X-ray scattering cross-section.

6.1 Static structure factors

6.1.1 Thermal equilibrium plasmas

The partial static structure factors of the system are defined as the equilibrium (equal-time) correlation functions of the Fourier components of the microscopic partial charge densities (Hansen and McDonald, 1981; Hansen et al., 1974):

$$S_{rs}(k) = \frac{1}{N} < \rho^r(\vec{k})\rho^s(-\vec{k}) >, \tag{6.1}$$

where N number of ions and

$$\rho^r(\vec{k}) = \sum_{i=1}^{N} \exp\left(\imath\vec{k}\cdot\vec{r}_i^r\right). \tag{6.2}$$

A linear combination of the partial structure factors which is of high importance, is the charge-charge structure factor defined as

$$\begin{aligned} S_{zz}(k) &= \frac{1}{N_e + zN_i} < \rho^z(\vec{k})\rho^z(-\vec{k}) > \\ &= \frac{S_{ee}(k) - 2\sqrt{z}S_{ei}(k) + zS_{ii}(k)}{2}, \end{aligned} \tag{6.3}$$

where z is the ion charge and $\rho^z = \rho^i(\vec{k}) - \rho^e(\vec{k})$.

We calculate the screened HGK interaction pseudopotentials described above using the semiclassical approach suggested in (Arkhipov et al., 2000). In difference to (Arkhipov

et al., 2000), our approach is based on the HGK pseudopotential model for the interaction between the particles (charged spheres) to account for ion shell structure. Quantum diffraction effects i.e., the Pauli exclusion principle and symmetry, are represented in the electron-electron interactions by the thermal de Broglie wavelength $\lambda_{ee} = \hbar/\sqrt{\pi m_e k_B T}$. The partial static structure factors $S_{rs}(k)$ ($r, s = e$ (electrons) or i (ions)) are defined as the Fourier transform of the pair distribution functions $h_{rs}(r) = g_{rs}(r) - 1$ (Arkhipov and Davletov, 1998):

$$S_{rs}(k) = \delta_{rs} - \frac{\sqrt{n_r n_s}}{k_B T}\Phi_{rs}(k), \tag{6.4}$$

where for for Φ_{rs} the expression (4.15-4.18) are used.

The effective response of the medium is described by the charge-charge correlation function S_{zz}. Gregori et al. used the following definition (Gregori et al., 2007):

$$S^G_{zz}(k) = \frac{S_{ee}(k) - 2\sqrt{z}S_{ei}(k) + zS_{ii}(k)}{1+z} \tag{6.5}$$

In Figures 6.1 (a) - (d) we compare our results on the charge-charge SSF (6.3) using (6.4) for alkali plasmas within the screened HGK pseudopotential model with the corresponding results obtained for alkali (hydrogen-like point charges (HLPC)) plasmas found within the screened Deutsch model for various values of density and temperature (Sadykova et al., 2011b). All curves obtained within the screened Deutsch model converge to each other due to the negligible influence of the alkali ion mass on the wavelength scale $\lambda_{rs} = \hbar/\sqrt{2\pi\mu'_{rs}k_B T}$ with $\mu'_{rs} = \frac{m_r m_s}{m_r + m_s}$ being the reduced mass of the interacting pair $r - s$ in (Arkhipov et al., 2000). The growth of coupling makes the peaks more pronounced and the difference among the curves becomes significant. We see that moderate coupling and the onset of short-range order manifest themselves in S_{zz} as a first localized peak, shown in an amplified scale, for different values of k' for every alkali species; as the number of shell electrons increase (from Li^+ to Cs^+), the position of the peaks shifts in the direction of smaller values of k'. This phenomenon was also reported in (Gregori et al., 2007). Strictly speaking, our approach is valid only for weakly and moderately coupled plasmas with $\Gamma_{ii} \lesssim 1$. The results we present here for $\Gamma_{ii} > 1$ have to be considered as extrapolations to a region where the Bogoljubov expansions should include more terms.

6.1.2 Static structure factors for two temperature plasmas

While for solid density plasmas, obtained with the help of laser-solid density Be or Li interactions, at relatively high temperatures, the condition of LTE is closely approached due to the fast relaxation between ions and electrons, at lower temperatures it is complicated by quantum effects (e.g. degeneracy). The fluctuation-dissipation theorem for solid density plasmas at lower temperatures , as observed by Gregori et al. in (Gregori et al., 2006b), may still be a valid approximation even under nonequilibrium conditions if the temperature relaxation is slow compared to the electron density fluctuation time scale and temperatures are treated in a special way. A common condition in experimental plasmas for this to occur is when $m_i >> m_e$ so that the coupling between the two-components takes place at sufficiently low frequencies. Using a two-component hypernetted-chain (HNC) approximation scheme, Seuferling et al. (Seuferling et al., 1989)

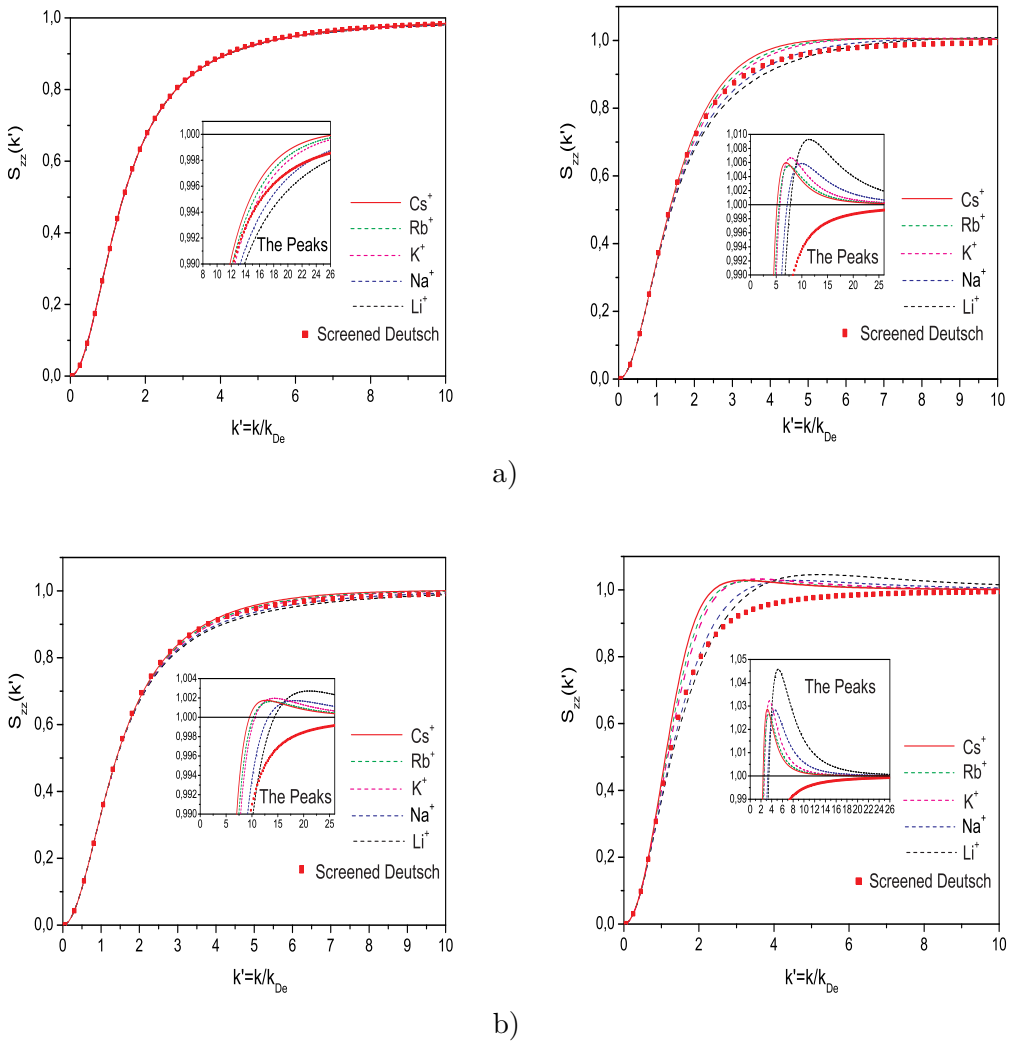

Figure 6.1: The charge-charge static structure factors S_{zz} (6.3) for alkali plasmas (Li^+, Na^+, K^+, Rb^+, Cs^+) within the HGK pseudopotential model as compared to our results obtained in the present work for hydrogen-like plasmas within the Deutsch model on a basis of Gregori et al.(Gregori et al., 2006b) at $T_e = T_i = T_e' = T_i'$. (a) $T_e = 60000$ K, $\Gamma_{ee} = 0.398$, $\Gamma_{ii} = 0.399$; (b) $T_e = 30000$ K, $\Gamma_{ee} = 0.789$, $\Gamma_{ii} = 0.8$; (c) $T_e = 30000$ K, $\Gamma_{ee} = 1.14$, $\Gamma_{ii} = 1.2$; (d) $T_e = 30000$ K, $\Gamma_{ee} = 1.58$, $\Gamma_{ii} = 2$. As scale of the k-vector we use the inverse electron Debye radius k_{De} (Sadykova et al., 2011b).

have shown in this case that the static response under the conditions of the non-LTE (two-temperature) takes the form:

$$S_{rs}(k) = \delta_{rs} - \frac{\sqrt{n_r n_s}}{k_B T'_{rs}} \Phi_{rs}(k) - \delta_{er}\delta_{es}(\frac{T'_e}{T'_i} - 1)\frac{|q(k)|^2}{z} S_{ii}(k) \tag{6.6}$$

where $q(k)$

$$q(k) = \frac{\sqrt{z} S_{ei}(k)}{S_{ii}(k)}, \tag{6.7}$$

and for Φ_{rs} the expressions (4.15-4.19) were used. In order to take into account the quantum plasma effects Gregori et al. suggested to introduce the so called effective ion and electron of Dharma-wardana et al. (Dharma-Wardana and Perrot, 2000) temperatures independently. Definition of the effective temperature T'_{rs} is given by,

$$T'_{rs} = \frac{m_r T'_s + m_s T'_r}{m_r + m_s},$$

allows to extend the fluctuation-dissipation theorem to nonequilibrium (two-temperature) systems and to interpolate between the classical and quantum regimes; in two-temperature systems the de Broglie wavelength becomes $\lambda_{rs} = \hbar/\sqrt{2\pi\mu'_{rs} k_B T'_{rs}}$.

Here $T'_e = (T_e^2 + T_q^2)^{1/2}$ with $T_q = T_F/(1.3251 - 0.1779\sqrt{r_s})$, where $r_s = r_a/r_B$ is the Brueckner parameter, $T_F = \hbar^2(3\pi^2 n_e)^{2/3}/(2k_B m_e)$ and $T'_i = (T_i^2 + \gamma_0 T_D^2)^{1/2}$, $T_D = \Omega_{pi}\hbar/k_B$, $\gamma_0 = 0.152$ is the Bohm-Staver definition for the Debye temperature with $\Omega_{pi}^2 = \omega_{pi}^2/(1 + k_{De}/k^2)$, $\omega_{pi} = \sqrt{ze^2 n_e/(\varepsilon_0 m_i)}$, m_i is the ion mass, $k_{De} = \sqrt{e^2 n_e/(\varepsilon_0 k_B T'_e)}$ is the electronic Debye wavenumber ($T_D \approx 0.16eV$, $T_F \approx 14.5eV$ for Be^{2+}). The main objective of introduction of such quantum temperatures T_q depending on the density r_s by Dharma-wardana et al. (Dharma-Wardana and Perrot, 2000) was to construct a classical Coulomb fluid at some temperatures T'_e such that its correlation energy and spin-dependent distribution functions are those of a quantum electron gas at a given temperature $T_e \to 0$. This approach proved to reproduce finite temperature static properties, e.g. correlation function, of an electron fluid for arbitrary degeneracy (Dharma-Wardana and Perrot, 2000). Similarly, the ion effective temperature T'_i was introduced by Gregori et al. which accounts for ion degeneracy (i.e. phonon coupling) al low temperatures (Gregori et al., 2006b). Since, in the Debye model, the phonon modes with wavelengths up to a fraction of the lattice spacing are considered, in (Gregori et al., 2006b) it is set $k \equiv k_{max} = (2/z)^{1/3} k_F$ with $k_F = (3\pi^2 n_e)^{1/3}$ being the Fermi wavenumber. Due to the large mass difference between ions and electrons, $T'_{ei} = T'_{ee}$. All the parameters considered here are beyond the degeneration border ($n_e \lambda_{ee}^3 < 1$).

Notice that when $T'_e = T'_i = T_e = T_i$ the equation (6.6) turns into the eq. (6.4) in (Arkhipov and Davletov, 1998). The factor $q(k)$ represents the screening cloud of free (and valence) electrons that surround the ion. Since the equation (6.6) corresponds the HNC-approximation, we will use this approximation to treat two-temperature and stronger (moderately) coupled plasmas and to carry out the comparison with the corresponding results of Gregori et al. (Gregori et al., 2006b), (Gregori et al., 2007).

In Figures 6.2 (a), (b), (c), (d) the static structure factors $S_{rs}(k)$ and the screening charge $q(k)$ are shown for a beryllium plasma for different temperatures $T_i = T_e$, $T_i = 0.5 \cdot T_e$, $T_i = 0.2 \cdot T_e$ and the coupling parameters $\Gamma_{ee} = e^2/(4\pi\varepsilon_0 k_B T_e' r_{ee})$, $\Gamma_{ii} = z^2 e^2/(4\pi\varepsilon_0 k_B T_i' r_{ii})$ with $r_{ii} = (3/4\pi n_i)^{1/3}$, $r_{ee} = (3/4\pi n_e)^{1/3}$ are shown. For the conditions typical for laser plasma experiments with solid density beryllium, we have $n_e \approx 2.5 \cdot 10^{23}$ cm^{-3} and $z \approx 2$. This gives $T_F \approx 14.5eV$ and $T_D \approx 0.17eV$. In Fig. 6.2 (c), a minimum arises which defines the size of the ion core. Notice that this minimum becomes less pronounced when the coupling increases.

It is of high interest to study the influence of the ion shell structure on the static structure factors. For this reason in Figures 6.2 (a)-(d) and further we compare the SSF, screening charge obtained from equations (6.6) and (6.7) with the screened HGK pseudopotentials (4.15-4.18) and the corresponding SSF obtained using the screened Deutsch pseudopotential (Arkhipov et al., 2000). In the Figure 6.2 (d) the screening charge $q(k)$ becomes at some k negative and the minimum arises which is due to character of the screened electron-ion interaction.

In Fig. 6.3 the static charge-charge structure factor (6.5) for a beryllium plasma with $n_e \approx 2.5 \cdot 10^{23}$ cm^{-3}, $z \approx 2$, $T_e = 20eV$ and $T_i = T_e$, $T_i = 0.5 \cdot T_e$, $T_i = 0.2 \cdot T_e$ is displayed.

6.2 The dynamic structure factor: the moment approach

In this section we carry out a preliminary study of the charge-charge dynamic structure factor of model plasmas whose static characteristics were determined above. To this end we employ the method of moments suggested in (Adamyan and Tkachenko, 1983; Adamyan et al., 1985) and whose applicability to the investigation of the dynamic properties of one- and two-component plasmas is demonstrated in (Arkhipov et al., 2010) and references therein, particularly by a successful comparison with the numerical simulation data of (Hansen and McDonald, 1981; Hansen et al., 1974).

In this section we consider plasmas in a complete thermal equilibrium. Besides, the HLPC potential model, except the static characteristics determined within the HGK pseudopotential model, is applied to determine the moments or the sum rules. Let

$$\rho^r(\vec{k}, t) = \sum_{i=1}^{N} \exp\left(\imath \vec{k} \cdot \vec{r}_i^{\,r}(t)\right). \tag{6.8}$$

be the Fourier transform of the time dependent microscopic density of species r (Ebeling and Ortner, 1998; Ortner et al., 1997). The corresponding partial dynamic structure factors are the Fourier transforms of the density-density time correlation functions given by

$$S_{rs}(k, \omega) = \frac{1}{2\pi N} \int e^{\imath\omega t} < \rho^r(\vec{k}, t)\rho^s(-\vec{k}, 0) > dt. \tag{6.9}$$

The charge-charge dynamic structure factor $S_{zz}(k, \omega)$ is defined via the fluctuation-dissipation theorem (FDT) (Adamjan et al., 1993; Adamyan and Tkachenko, 2003) as

$$S_{zz}(k, \omega) = -\frac{\hbar \operatorname{Im} \varepsilon^{-1}(k, \omega)}{\pi\Phi(k)[1 - \exp\left(-\beta\hbar\omega\right)]}, \tag{6.10}$$

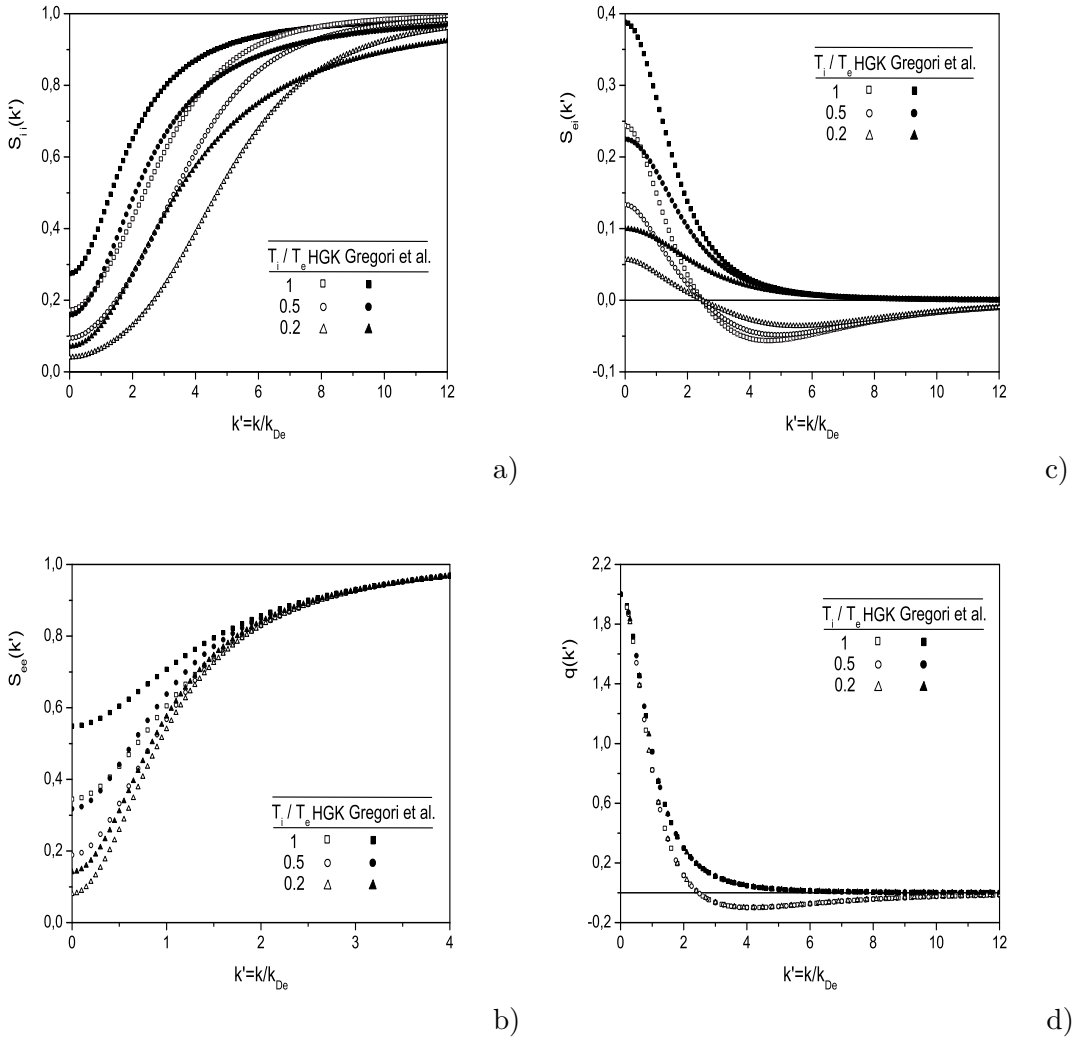

Figure 6.2: Static structure factors and the screening charge $q(k')$ for Be^{2+} plasma at $T_e = 20$ eV, $T_e' = 24.06$ eV, $z = 2$ and $n_e = 2.5 \times 10^{23}$ cm^{-3}. The filled symbols represent the screened Deutsch pseudopotential model obtained by Gregori et al. (Gregori et al., 2006b), (Gregori et al., 2007), while the empty symbols correspond to the screened HGK pseudopotential model. Squares: $T_i/T_e = 1$ ($\Gamma_{ii} = 2.31$, $\Gamma_{ee} = 0.61$). Circles: $T_i/T_e = 0.5$ ($\Gamma_{ii} = 4.63$, $\Gamma_{ee} = 0.61$). Triangles: $T_i/T_e = 0.2$ ($\Gamma_{ii} = 11.57$, $\Gamma_{ee} = 0.61$) (Sadykova et al., 2011b).

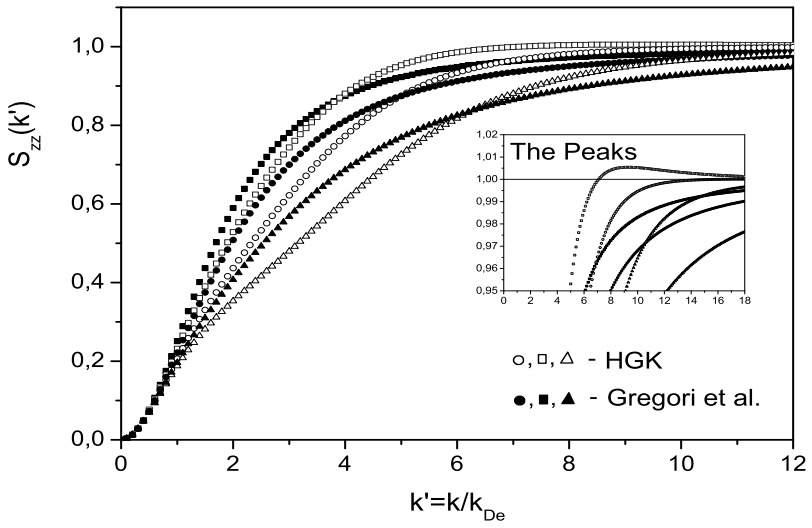

Figure 6.3: The charge-charge static structure factors S_{zz} (6.5) for a beryllium plasma with $n_e \approx 2.5 \cdot 10^{23}$ cm^{-3}, $z \approx 2$, and $T_e = 20$ eV, $T_e' = 24.06$ eV. The filled symbols represent the screened Deutsch pseudopotential model obtained on the basis of (Gregori et al., 2007) , while the empty symbols correspond to the screened HGK pseudopotential model. Squares: $T_i/T_e = 1$ ($\Gamma_{ii} = 2.31$, $\Gamma_{ee} = 0.61$). Circles: $T_i/T_e = 0.5$ ($\Gamma_{ii} = 4.63$, $\Gamma_{ee} = 0.61$). Triangles: $T_i/T_e = 0.2$ ($\Gamma_{ii} = 11.57$, $\Gamma_{ee} = 0.61$) (Sadykova et al., 2011b).

where $\Phi(k) = e^2/\varepsilon_0 k^2$ and $\varepsilon^{-1}(k,\omega)$ is the inverse longitudinal dielectric function of the plasma. The charge-charge dynamic structure factor is directly related to the charge-charge static structure factor as follows :

$$\begin{aligned} S_{zz}(k) &= \frac{1}{n_e + z n_i} \int_{-\infty}^{\infty} S_{zz}(k,\omega) d\omega \\ &= \frac{S_{ee}(k) - 2\sqrt{z} S_{ei}(k) + z S_{ii}(k)}{2}, \end{aligned} \tag{6.11}$$

where $T_e' = T_i' = T_e = T_i$, $T_{ei}' = T_{ee}' = T_e'$, $n_e = z n_i$ ($z = 1$ for hydrogen-like plasmas).

In order to construct the inverse longitudinal dielectric function within the moment approach one has to consider the frequency moments of the loss function $-\operatorname{Im}\varepsilon^{-1}(k,\omega)/\omega$:

$$C_\nu(k) = -\pi^{-1} \int_{-\infty}^{\infty} \omega^{\nu-1} \operatorname{Im}\varepsilon^{-1}(k,\omega) d\omega, \tag{6.12}$$

here with $\nu = 0, 2, 4$. Observe that the odd-number moments vanish due to the parity of the loss function and that the moment $C_2 = \omega_p^2$ expresses the f-sum rule, ω_p being the plasma frequency.

Then the Nevanlinna formula of the classical theory of moments (Akhieser, 1965; Krein

and Nudel'man, 1977) expresses the response function

$$\varepsilon^{-1}(k,\omega) = 1 + \frac{{\omega_p}^2(\omega+q)}{\omega(\omega^2-{\omega_2}^2)+q(\omega^2-{\omega_1}^2)}, \tag{6.13}$$

in terms of a Nevanlinna-class $q = q(k,\omega)$ such that

$$\lim_{z\to\infty}\frac{q\,(k,z)}{z} = 0 \quad , \quad \mathrm{Im}\, z \geq 0.$$

The frequencies ω_1 and ω_2 are defined as respective ratios of the moments C_ν:

$$\begin{aligned} {\omega_1}^2 &= C_2/C_0 = {\omega_p}^2[1-\varepsilon^{-1}(k,0)]^{-1}, \\ {\omega_2}^2 &= C_4/C_2 = {\omega_p}^2[1+Q(k)], \end{aligned} \tag{6.14}$$

where $\varepsilon^{-1}(k,0)$ can be determined from the classical form ($\hbar \to 0$) of the FDT (thermal equillibrium) eq. (6.10) and the Kramers-Kronig relation (Landau and Lifschitz, 2000):

$$\mathrm{Re}\,\varepsilon^{-1}(k,\omega) = 1 + \frac{1}{\pi}P.V.\int_{-\infty}^{\infty}\frac{\mathrm{Im}\,\varepsilon^{-1}(k,\omega)}{\omega'-\omega}d\omega' \tag{6.15}$$

In this way, we get the following expression :

$$\mathrm{Re}\,\varepsilon^{-1}(k,0) = 1 - 2S_{zz}(k)\frac{{k_{De}}^2}{k^2}, \tag{6.16}$$

where $\mathrm{Re}\,\varepsilon^{-1}(k,0) = \varepsilon^{-1}(k,0) = \varepsilon^{-1}(k)$, $S_{zz}(k)$ is defined by (6.11). The function defining the fourth moment is given in the Coulomb HLPC approximation except the static characteristics, given within the HGK pseudopotential model, by (Adamjan et al., 1993; Adamyan and Tkachenko, 2003):

$$Q(k) = K(k) + L(k) + H. \tag{6.17}$$

It contains the kinetic contribution, particularly, for a classical system:

$$K(k) = 3\left(\frac{k}{k_D}\right)^2, \tag{6.18}$$

where ${k_D}^2 = {k_{De}}^2$.

We approximate here the contribution due to the electron-ion correlations by the expression obtained in (Corbatón and Tkachenko, 2008; Adamyan et al., 2009) for hydrogen within the modified RPA:

$$H = \frac{4}{3}r_s\sqrt{\Gamma}_{ee}[3\Gamma_{ee}^2 + 4r_s + 4\Gamma_{ee}\sqrt{6r_s}]^{-1/2} \tag{6.19}$$

Finally, the contribution $L(k)$ takes into account the electronic correlations, we calculated it for the Coulomb potential:

$$L(k) = \frac{1}{2\pi^2 n_e}\int_0^\infty p^2[S_{ee}(p)-1]f(p,k)dp, \tag{6.20}$$

where

$$f\left(p,k\right)=\frac{5}{12}-\frac{p^2}{4k^2}+\frac{\left(k^2-p^2\right)^2}{8pk^3}\ln\left|\frac{p+k}{p-k}\right|. \tag{6.21}$$

In (6.20) the static structure factor is the one defined in (6.6) with the pseudopotentials given in (4.15-4.18).
The authors of (Adamjan et al., 1993; Adamyan and Tkachenko, 2003) suggested to approximate $q(k,\omega)$ by its static value $q(k,0)=\imath h(k)$, connected to the static value $S_{zz}(k,0)$ of the dynamic structure factor through eq. (6.10):

$$h(k)=\frac{({\omega_2}^2-{\omega_1}^2){\omega_p}^2}{\pi\beta\phi(k){\omega_1}^4S_{zz}(k,0)}>0, \tag{6.22}$$

with

$$S_{zz}(k,0)\simeq S^0_{zz}(k,0), \tag{6.23}$$

where $S^0_{zz}(k,0)=\frac{n_e}{k}\sqrt{\frac{m}{2\pi k_BT}}$ (Ichimaru, 1992) so that the relative dynamic structure factor takes the following form:

$$\begin{aligned}\frac{S_{zz}(k,\omega)}{S_{zz}(k,0)}&=\frac{\beta\hbar}{\left[1-\exp\left(-\beta\hbar\omega\right)\right]}\\&\times\frac{\omega h^2(k){\omega_1}^4}{\omega^2(\omega^2-{\omega_2}^2)+h^2(k)(\omega^2-{\omega_1}^2)},\end{aligned} \tag{6.24}$$

with the more simplified expressions for $h(k)$:

$$h(k)=\frac{\varepsilon_0\sqrt{2\pi k_BT}k^3{\omega_p}^2({\omega_2}^2-{\omega_1}^2)}{\pi\beta\sqrt{m}n_ee^2{\omega_1}^4}, \tag{6.25}$$

and the characteristic frequencies $\omega_1(k)$, $\omega_2(k)$:

$$\begin{aligned}{\omega_1}^2&=C_2/C_0=\frac{{\omega_p}^2k^2}{2{k_{De}}^2S_{zz}(k)},\\{\omega_2}^2&=C_4/C_2={\omega_p}^2[1+K(k)+L(k)+H].\end{aligned} \tag{6.26}$$

In Figures 6.4 and 6.5 we present our results for the DSF at a moderate temperature $T=30000$ K and for the concentrations $n_e=1.741\cdot10^{20}-10^{22}$ cm^{-3} (Sadykova, 2010), i. e. for the values of Γ_{ee} used in (Adamjan et al., 1993; Adamyan and Tkachenko, 2003). As one can see in Figures 6.4, 6.5, the curves for alkali plasmas are different from those given for the HLPC potential model with the Coulomb static characteristics (Adamjan et al., 1993; Adamyan and Tkachenko, 2003). The differences are due to the repulsive parts of the HGK pseudopotential which reflects roughly the internal ion shell structure. In alkali plasmas the ion shell structure influences the dynamic structure factor through the sum rules which we satisfy automatically, independently of the choice of the Nevanlinna parameter function $q\left(k,\omega\right)$. In the Figures, in alkali plasmas the

position, heights of the central peaks coincides, except the Fig. 6.4b, with those of the Coulomb potential HLPC potential model, while the positions of the plasmon peaks are slightly shifted. Notice, in alkali plasmas at higher Γ_{ee} the curves split and the plasmon peaks are more pronounced. We observe that the curves shift in the direction of lower values of k compared to the corresponding results of (Adamjan et al., 1993; Adamyan and Tkachenko, 2003). In Fig. 6.4 (b) the curves split into three very sharp peaks. This could be explained by some coupling between bound electrons and the plasmon mode. In Fig. 6.5 the position of the plasmon peaks shift in the direction of higher absolute value of ω, as compared to those in Fig. 6.4. Observe that as the number of shell electrons increases from Li^+ to Cs^+, the curves shift in the direction of low absolute value of ω/ω_p and their heights diminish. The difference is due to the short range forces which we take into account within the HGK pseudopotential model compared to the HLPC pseudopotential model. One should also take into account that we employed different plasma parameters because at the high densities and temperatures studied in (Adamjan et al., 1993; Adamyan and Tkachenko, 2003) the inner electron shells of the alkali plasmas are destroyed.

6.2.1 Taking into account the ion shell structure

In the framework of the Adamyan's et al. HLPC potential model (Adamjan et al., 1993; Adamyan and Tkachenko, 2003) one can include the ion shell structure through the function defining the fourth moment:

$$Q^{HGK}(k) = K(k) + L^{HGK}(k) + H^{HGK}. \tag{6.27}$$

Here, the kinetic distribution is taken the same as in (6.18). We approximate here the contribution due to the electron-ion HGK correlations by the following expression:

$$H^{HGK} = \frac{h_{ei}(r=0)}{3} = \frac{g_{ei}(r=0)-1}{3} \simeq -\frac{1}{3}. \tag{6.28}$$

Within the screened HGK pseudopotential model, the H^{HGK} in eq. (6.28) can be approximated by $-1/3$ because we consider the ion shell structure, that means that the electron cannot approach the ion at $r = 0$ distance. Note that $g_{ei}(r = 0) = 0$ is not exactly true, it is just a good approximation.

The contribution $L^{HGK}(k)$ takes into account the electronic correlations, we calculated it for the HGK pseudopotential:

$$L^{HGK}(k) = \frac{1}{2\pi^2 n_e}\int_0^\infty p^2[S_{ee}(p)-1]f^{HGK}(p,k)dp, \tag{6.29}$$

where

$$f^{HGK}(p,k) = \int_{-1}^{1}\frac{(ps-k)^2}{p^2-2psk+k^2}\zeta_{ee}(\sqrt{p^2-2pks+k^2})\frac{ds}{2} - \frac{\zeta_{ee}(p)}{3} \tag{6.30}$$

where $\zeta_{ee}(p)$ is to be determined from the Deutsch pseudopotential $\varphi_{ee}(p) = \Phi(p)\zeta_{ee}(p)$, where $\Phi(p) = 4\pi e^2/4\pi\varepsilon_0 p^2$ - Fourier transform of the Coulomb potential.

In (6.29) the static structure factor is the one defined in (6.6) with the pseudopotentials

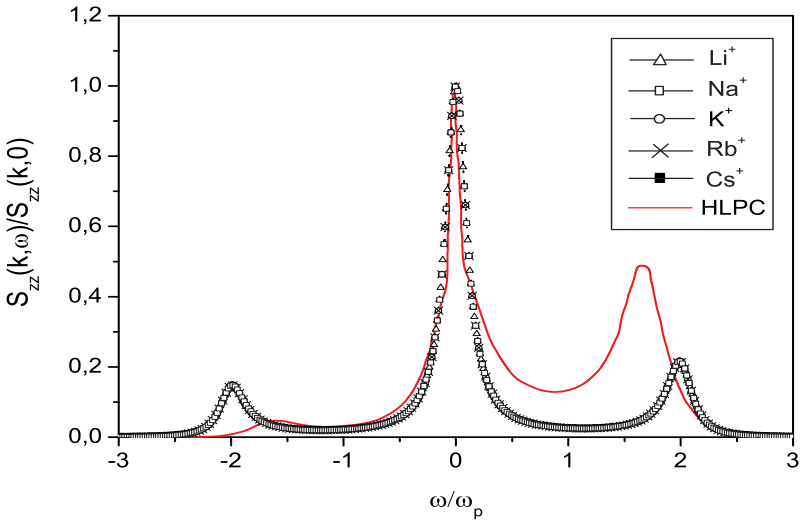

a)

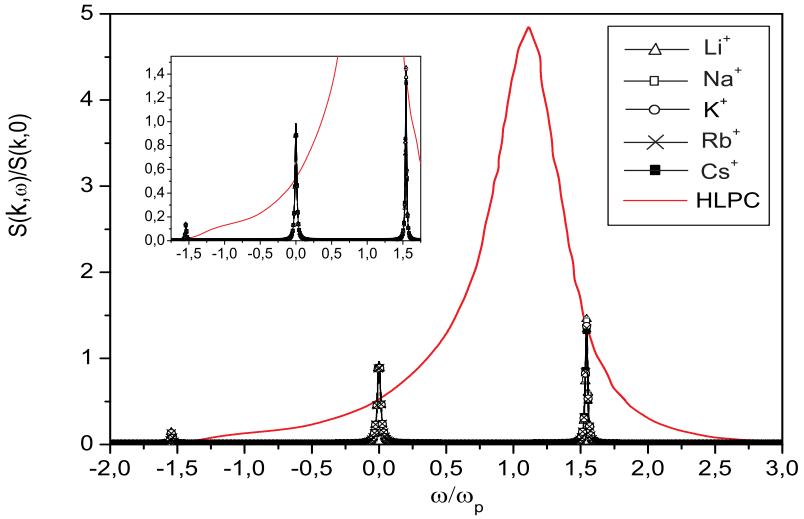

b)

Figure 6.4: The dimensionless dynamic charge-charge structure factor of alkali plasmas (Li^+, Na^+, K^+, Rb^+, Cs^+) determined within the HLPC potential model but with the HGK static characteristics in comparison with the results of (Adamjan et al., 1993) obtained within the same HLPC potential model but with the Coulomb static characteristics at $k = 0.767/r_{ee}$, (a) $\Gamma_{ii} = 0.5$, Present results: $T = 30000$ K, $n_e = 1.741 \cdot 10^{20}$ cm^{-3}, Adamjan et al.: $T = 1574573$ K, $n_e = 2.5 \cdot 10^{25}$ cm^{-3} and (b) $\Gamma_{ii} = 2$, Present results: $T = 30000$ K, $n_e = 1.11 \cdot 10^{22}$ cm^{-3}, Adamjan et al.: $T = 157457$ K, $n_e = 1.61 \cdot 10^{24}$ cm^{-3}. As the frequency scale we use the electron plasma frequency $\omega_p = \sqrt{n_e e^2/\varepsilon_0 m_e}$ (Sadykova et al., 2011b).

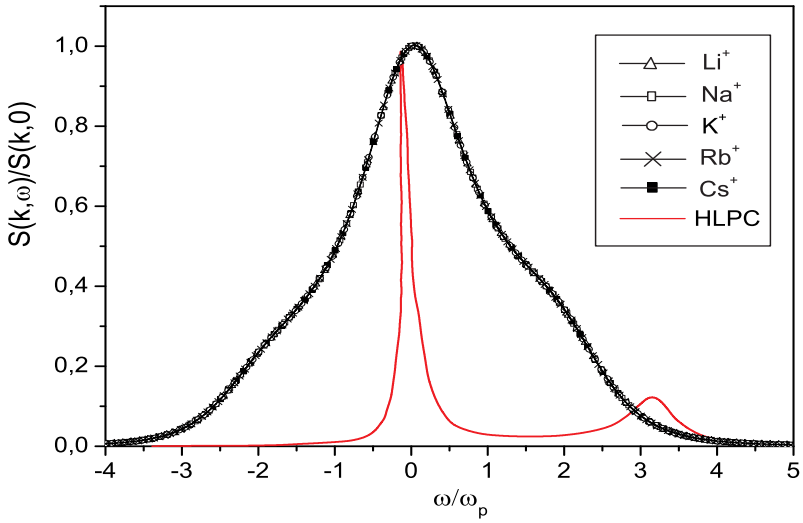

a)

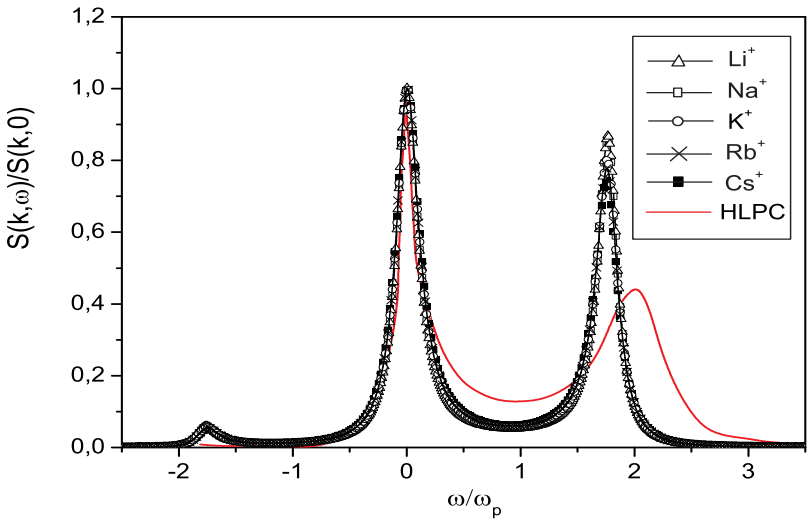

b)

Figure 6.5: The dimensionless dynamic charge-charge structure factor of alkali plasmas (Li^+, Na^+, K^+, Rb^+, Cs^+) determined within the HLPC potential model but with the HGK static characteristics in comparison with the results of (Adamjan et al., 1993) obtained within the same HLPC potential model but with the Coulomb static characteristics at $k = 1.534/r_{ee}$, (a) $\Gamma_{ii} = 0.5$, Present results: $T = 30000$ K, $n_e = 1.741 \cdot 10^{20}$ cm^{-3}, Adamjan et al.: $T = 1574573$ K, $n_e = 2.5 \cdot 10^{25}$ cm^{-3} and (b) $\Gamma_{ii} = 2$, Present results: $T = 30000$ K, $n_e = 1.11 \cdot 10^{22}$ cm^{-3}, Adamjan et al.: $T = 157457$ K, $n_e = 1.61 \cdot 10^{24}$ cm^{-3}. As the frequency scale we use the electron plasma frequency $\omega_p = \sqrt{n_e e^2/\varepsilon_0 m_e}$ (Sadykova et al., 2011b).

given in (4.15-4.18).

The equations (6.22-6.25) and ${\omega_1}^2$ in the equation (6.26) remain the same. But the ${\omega_2}^2$ will turn into :

$$ {\omega_2}^2 = C_4/C_2 = {\omega_p}^2[1 + K(k) + L^{HGK}(k) + H^{HGK}]. \tag{6.31} $$

In Figures 6.6 and 6.7 the DSF with the different definitions of H, L in the Eq. (6.19) with (6.20), (6.21) and H^{HGK}, L^{HGK} in the Eqs. (6.28), (6.29) with (6.30) respectively, are shown for comparison with the HLPC potential model in (Adamjan et al., 1993). As one can see in the Figures the curves for alkali plasmas are different from those given for the HLPC potential model (Adamjan et al., 1993) as well as they are in comparison with each other. The differences are again due to the repulsive parts of the HGK potential, compared to the HLPC potential model, which reflects roughly the internal ion shell structure. In the case of alkali plasmas at higher Γ_{ii} the curves split. This can be explained by that fact that at higher Γ_{ii} alkali ion shell structure influences the dynamic structure factor significantly. In the Figures 6.6 (a) and 6.7 (a) the position and heights of the central peaks coincides but positions of the plasmon peaks are slightly shifted . In alkali plasmas the plasmon peaks are more pronounced especially in the Fig. 6.7 (a), (b) where the ion shell structure is better taken into account through H^{HGK}, L^{HGK}. We observe that the plasmon peaks in the Fig. 6.7 (a), (b) are more pronounced and shifted in the direction of smaller absolute value of ω/ω_p, the heights of the plasmon peaks are higher especially at higher Γ_{ii} than in the Fig. 6.6 (a), (b). All this could be explained by some coupling between bound electrons and the plasmon mode. Observe that at higher Γ_{ii} with an increase of number of shell electrons from Li^+ to Cs^+ the curves shift in the direction of low absolute value of ω/ω_p and their heights diminish. The difference is due to the short range forces which we took into account by the HGK pseudopotential model in comparison with the HLPC potential model. One should also take into account that we employed different plasma parameters because at the high densities and temperatures studied in (Adamjan et al., 1993) inner electron shells of the alkali plasmas are destroyed.

6.3 Conclusions

X-ray scattering experiments has proven to be a powerful technique in measuring densities, temperatures and charge states. The structure factor (SF) is the fundamental quantity that describes the X-ray scattering plasma cross-section. To date, there is still a substantial amount of discrepancy between X-ray scattering data and the theoretical models for the quasi-static scattering component. This motivates this our study of static and dynamic properties of metal plasmas.

The electron-electron, electron-ion, ion-ion and charge-charge static structure factors have been calculated for alkali and Be^{2+} plasmas using the method described and discussed by Gregori et al. . The dynamic structure factors for alkali plasmas have been calculated using the moment approach developed by V. M. Adamyan et al. . The new screened Hellmann-Gurskii-Krasko pseudopotential with the soft ion core, obtained in the present work on the basis of Bogoljubov's method (BBGKY), has been used taking into account not only the quantum-mechanical effects but also the ion shell structure. The results obtained within the screened HGK pseudopotential model for the static

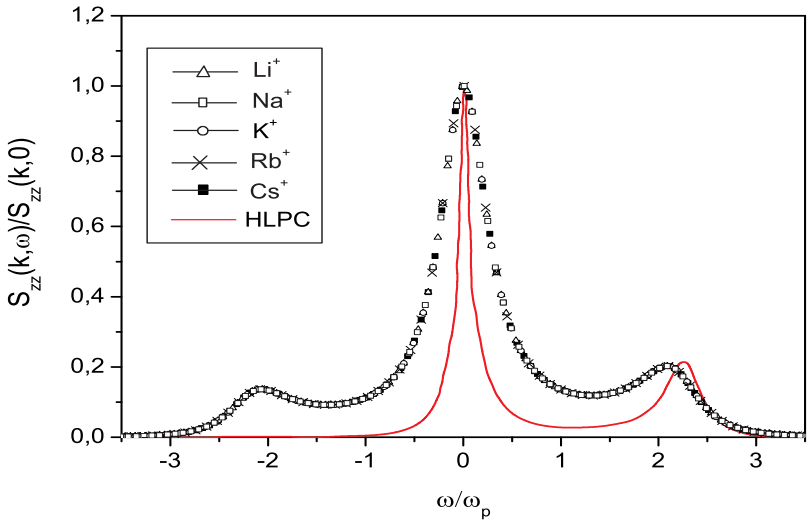

a)

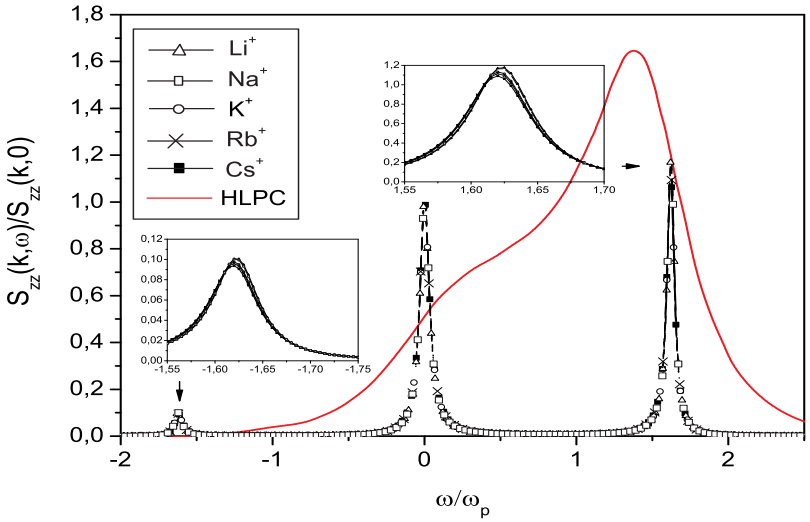

b)

Figure 6.6: The dimensionless dynamic charge-charge structure factor of alkali plasmas (Li^+, Na^+, K^+, Rb^+, Cs^+) determined within the HLPC potential model but with the HGK static characteristics in comparison with the results of (Adamjan et al., 1993) obtained within the same HLPC potential model but with the Coulomb static characteristics at $k = 1.074 \cdot r_{ee}$. (a) $\Gamma_{ii} = 0.5$, Present results: $T = 30000$ K, $n_e = 1.741 \cdot 10^{20}$ cm^{-3}, Adamjan et al.: $T = 1574573$ K, $n_e = 2.5 \cdot 10^{25}$ cm^{-3} and (b) $\Gamma_{ii} = 2$, Present results: $T = 30000$ K, $n_e = 1.11 \cdot 10^{22}$ cm^{-3}, Adamjan et al.: $T = 157457$ K, $n_e = 1.61 \cdot 10^{24}$ cm^{-3}, where the H, L are defined as (6.19) and (6.20), (6.21). As the length scale we use the electron plasma frequency $\omega_p = n_e e^2/\varepsilon_0 m_e$ (Sadykova, 2010).

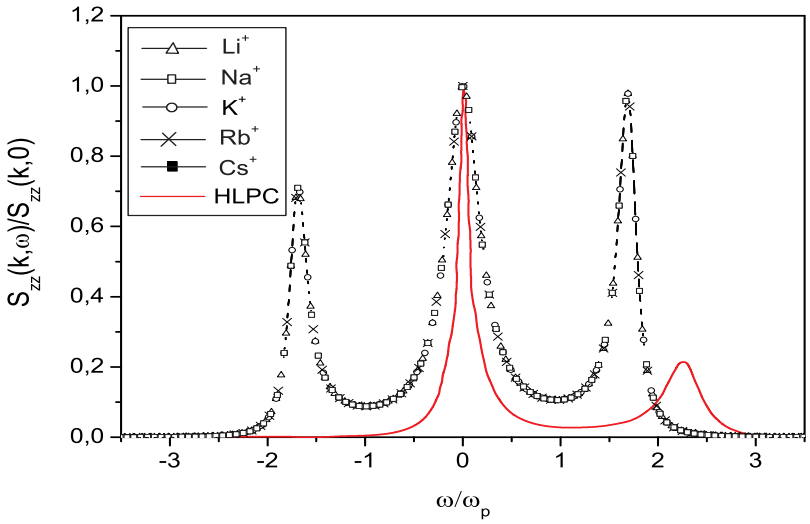

a)

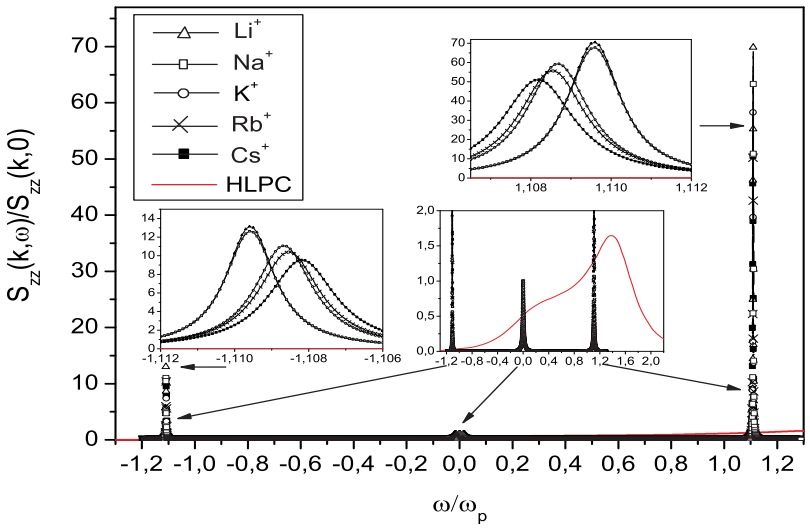

b)

Figure 6.7: The dimensionless dynamic charge-charge structure factor of alkali plasmas (Li^+, Na^+, K^+, Rb^+, Cs^+) determined within the HGK pseudopotential model with the HGK static characteristics in comparison with the results of (Adamjan et al., 1993) obtained within the HLPC potential model with the Coulomb static characteristics at $k = 1.074 \cdot r_{ee}$. (a) $\Gamma_{ii} = 0.5$, Present results: $T = 30000$ K, $n_e = 1.741 \cdot 10^{20}$ cm^{-3}, Adamjan et al.: $T = 1574573$ K, $n_e = 2.5 \cdot 10^{25}$ cm^{-3} and (b) $\Gamma_{ii} = 2$, Present results: $T = 30000$ K, $n_e = 1.11 \cdot 10^{22}$ cm^{-3}, Adamjan et al.: $T = 157457$ K, $n_e = 1.61 \cdot 10^{24}$ cm^{-3}, where the H^{HGK}, L^{HGK} are defined as (6.28) and (6.29), (6.30). As the length scale we use the electron plasma frequency $\omega_p = n_e e^2/\varepsilon_0 m_e$ (Sadykova, 2010).

structure factors have been compared with those obtained by Gregori et al. , while the dynamic structure factors calculated within the HLPC and HGK (pseudo-)potential models, where the HGK pseudopotential model was considered completely within the properties of the HGK pseudopotential (through the fourth moment of the loss function) and the HGK static characteristics, whereas HLPC potential model was treated in a part within the HGK pseudopotential model through the HGK static characteristics, were compared to those of S. V. Adamjan et al. defined within the HLPC potential model as well but with the Coulomb properties and Coulomb static characteristics. We have detected deviations (in the values of the SSFs) from results obtained by Gregori et al. while we have noticed that the present dynamic results are in a reasonable agreement with those of S. V. Adamjan et al.: at higher values of k and with increasing k the curves damp while at lower values of k, and especially at higher Γ_{ee}, we observe sharp peaks also reported by S. V. Adamjan et al. . At lower Γ_{ee} the curves for Li^+, Na^+, K^+, Rb^+ and Cs^+ do not differ while at higher Γ_{ee} the curves split. In alkali plasmas the plasmon peaks are more pronounced especially at higher Γ_{tt} and shifted in the direction of lower ω/ω_p than those considered within the Coulomb HLPC potential model with the Coulomb static characteristics. As the number of shell electrons increases from Li^+ to Cs^+ the curves shift in the direction of low absolute value of ω/ω_p and their heights diminish. The difference is due to the short range structure which we took into account by the HGK pseudopotential model compared to the hydrogen-like point charges model where no ion shell structure is considered. One should also take into account that we employed different plasma parameters because at the high densities and temperatures studied by S. V. Adamjan et al. the inner electron shells of the alkali plasmas are destroyed.

7 Summary

EMDs in electron OCP and electron-positron TCP

We have calculated the electric microfield distributions (EMDs) at an electron and at a neutral point using a coupling-parameter integration technique for electron one-component plasmas developed by C. A. Iglesias (Iglesias, 1983) and the generalized coupling-parameter integration technique for electron-positron two-component plasmas proposed by J. Ortner et al. (Ortner et al., 2000). We study the EMDs in the framework of the Kelbg pseudopotential model, taking into account quantum-mechanical (diffraction, quantum symmetry effects, Pauli blocking effects) and screening effects (Sadykova and Ebeling, 2007). The screening effects were introduced on a base of Bogoljubov's works (Bogoljubov-Born-Green-Kirkwood-Yvon (BBGKY)) described in (Falkenhagen, 1971), (Bogoljubov, 1946, 1962). The screened pseudopotential is represented in a numerically approximated form.

We performed the Molecular Dynamics (MD) simulations of electron-positron TCP and high-frequency OCP plasma and determined the EMDs measured at an electron and at a neutral point as depending on the coupling parameter Γ_{ee} in the range $0.2 \leq \Gamma_{ee} \leq 1.2$ at $T = 30000K$. We show that with an increase of Γ_{ee} the most probable field shifts toward the lower fields. The height of the peak of the corresponding probability density in a case of EMD at an electron decreases with Γ_{ee} for $\Gamma_{ee} > 0.3$. The height of the peak of the corresponding probability density in a case of EMD at a neutral point increases monotonically with Γ_{ee}. We show that at low Γ_{ee} the tails of the EMDs at an electron in OCP, TCP follow a pattern compatible with the Levy-type of distribution ($P(\beta) \sim \beta^{-\alpha-1}$) . The tails of the EMDs measured at a neutral point at $\Gamma_{ee} \leq 2$ follow a pattern compatible with the Holtsmark one ($\alpha = 3/2$) also belonging to the Levy-type of distribution. At higher values of Γ_{ee} and higher fileds $\beta >> 1$ the tails of EMD at an electron are considerably fatter and follow the modified Potekhin law ($P(\beta) = B\beta^{\mu} \exp(-C\beta^{1/2} - \beta^{-3/2})$). At values $0.2 \leq \Gamma_{ee} \leq 1.2$ the tails measured at an electron in electron-positron plasma can be roughly approximated by the decay exponents $\alpha' = \alpha + 1$ corresponding to the Levy-type of distribution changing from -2.2 to -1.8 with increasing Γ_{ee}. The TCP curves referred to either an electron or neutral point are less pronounced than the OCP one and their tails are fatter. This can be explained by that fact that in TCP case two components (electron and ion) are taken into account leading to the attraction between the opposite charges and stronger fields in average. The results were found in a good agreement with the Molecular Dynamics simulation results. These results can serve as a benchmark for our further theoretical work.

EMDs in electron-ion TCP with an account of the ion shell structure

In order to correctly describe alkali plasmas at moderate temperatures one needs to take into account the ion shell structure. For example, for the behaviour of alkali plasmas the short range forces between the charged particles are of great importance (Ebeling et al., 1979). For alkali plasmas at small distances between the particles deviations from Coulomb law are observed which are mainly due to the influence of the core (shell) electrons. In this work we use Hellmann-Gurskii-Krasko (HGK) pseudopotential model for electron-ion interactions and its modified version of ion-ion interactions which take into account the ion shell structure (Krasko and Gurskii, 1969). We have calculated the EMDs for Hydrogen H^+, singly ionized alkali plasmas ($Li^+, Na^+, K^+, Rb^+, Cs^+$) at the location of an ion using Ortner et al. method (Ortner et al., 2000) in comparison with Monte-Carlo (MC), MD simulations. We study the distributions in the framework of the HGK model. Notice also that there is a high interest in the construction of a pseudopotential model of particle interactions in *dense plasmas*; this model is to take into account not only the quantum-mechanical effects including the ion shell structure at short distances, but also the screening field effects. Our models take into account both the quantum-mechanical, ion shell structure and screening field effects. We used the screened HGK pseudopotential in the Debye screening approximation as well as in a higher order screening approximation valid also for a moderately coupled plasma, both were derived in the present work (Sadykova et al., 2009a). In the present work the influence of the coupling parameter along with the ion shell structure on the EMD shape and position was investigated. With an increasing value of Γ_{ii} the ion shell structure starts to play a significant role. High density as well as the coupling parameter causes a shifting of the maximum of probability toward the lower fields and changing the tails this way significantly modifying the electric microfield distributions. For comparison the corresponding EMDs for H^+-plasmas were given too. In this case no ion shell exists and we may see clearly the deviation of alkali curves from H^+ one and consequently the influence of the shell structure. For Radial Distribution Functions (RDF) of Li^+, Na^+, K^+, Cs^+ plasmas we used the screened HGK pseudopotential in a moderately coupled plasma approximation (Sadykova et al., 2011a). The moderately coupled plasma approximation compared to the Debye screening approximation makes a considerable improvement in the EMD calculation at moderate magnitudes of Γ_{ii} leading to a much better agreement with the MC simulations. However, we see a wide field of study of EMD in a moderately and strongly coupled TCP plasmas in the framework of the screened HGK pseudopotential model on a base of potential-of-mean-force exponential (PMFEX) method proposed by Nersisyan et al in (Nersisyan et al., 2005). In a strongly coupled regime the screened HGK pseudopotentials and corresponding RDFs can be determined with the help of the hypernetted-chain (HNC) integral equation technique with the HGK pseudopotentials as micro-pseudopotentials (Hansen and McDonald, 1990). The theoretical results were found in general in a good agreement with MC, MD simulations. We have derived a new type of screened HGK pseudopotential, where for electron-electron interaction we used the corrected Kelbg micro-pseudopotential instead of earlier applied Deutsch micro-peudopotential (Sadykova et al., 2011a). We have also obtained the analytical expressions for the screened Deutsch pseudopotentials (Arkhipov et al., 2000)

through the inverse Fourier transformation in "r" -space neglecting the symmetry effects and ionic screening.

Summarizing briefly our main results:

(i) The shapes of EMDs of the alkali plasmas at moderate magnitudes of Γ_{ii} are different. We observe large differences compared to the Holtsmark distribution and to the EMD distribution of Hydrogen plasma. This allows us to say that the ion shell structure influences the EMD strongly;
(ii) The peaks of the EMD distributions of alkali plasmas is positioned in between the peak of hydrogen, which is located at lower fields and the Holtsmark distribution which is located at higher fields;
(iii) The tails of the EMDs at the location of an ion at $\Gamma_{ii} = 0.2$, $T = 30000K$ or neutral point at any Γ_{ii} are in all cases of Levy-type $P(\beta) \sim \beta^{-\alpha-1}$ with $\alpha \simeq 3/2$ for EMD at a neutral point. When the field is measured at an ion in alkali plasmas at moderately high $\Gamma_{ii} = 2$ the tails obey to the power-exponential Potekhin form $P(\beta) \sim B\beta^{-5/2}\exp(-C\beta^{1/2} - \beta^{-3/2})$ whereas in Hydrogen plasma it obeys to the modified Potekhin form $P(\beta) = B\beta^{\mu}\exp(-C\beta^{1/2} - \beta^{-3/2})$. The Holtsmark limit with the exponent $\alpha = 3/2$ is located in the middle, between the hydrogen plasma with $B \simeq 0.5$, $\mu \simeq -1.06$ and $C \simeq 0.27$ and relatively fast Potekhin power-exponential decay with $B \simeq 497$, $C \simeq 2.17$ for Na^+ plasma and $B \simeq 20.8$, $C \simeq 1.68$ for Cs^+ plasma. The relatively fast decay of the microfield distribution of alkali plasmas is due to the weakening of strong fields due to the screening by the ion cores. This prevents very high fields. We leave a detailed study of this remarkable effect to future work;
(iv) In the parameter range of weakly coupled plasmas the theory by Ortner et al. with Debye screening gives a reasonable approximation which is in a good agreement with MC, MD simulations.
(v) The moderately coupled plasma approximation compared to the Debye screening approximation makes a considerable improvement in the EMD calculation at moderately large Γ_{ii} leading to a much better agreement with the MC, MD simulations.

Comparison with measurements from laser-produced plasmas

Li^{2+} plasma

The Li^{2+} Lyman-spectrum was measured in (Schriever et al., 1998a) with a spectral resolution of $\lambda/\Delta\lambda^I = 300$. A pulsed laser beam of a Nd:YAG laser (wavelength $\lambda = 1064$ nm) with a maximum energy of 1300 mJ per pulse and intensity of $I_L = 1.1 \cdot 10^{13}$ W/cm^2 was focused on the surface of a lithium target to generate the plasma. The high intensity lead to an electron temperature of $k_B T_e > 100$ eV. Comparison of a synthetic Li^{2+}-Lyman spectrum at $T = 300000$ K and $n_e = 4 \cdot 10^{25}$ m^{-3}, obtained using a quantum statistical approach in dense plasmas in (Lorenzen et al., 2008), with experimental data (Schriever et al., 1998a) has shown that the EMD, as one of the main input values of the pressure broadened profile, obtained in the present work provides a good agreement with the experiment. The EMD obtained in the present work for Li^{2+} plasma at $T = 300000$ K and $n_e = 4 \cdot 10^{25}$ m^{-3} on a base of C. A. Iglesias method for ionic Li^{2+} OCP within the HGK pseudopotential model, Molecular Dynamics and the EMD curve obtained in (Lorenzen et al., 2008) coincide within the high accuracy demonstrating the validity of the

EMD theoretical approach and good accuracy of EMD calculations (Lorenzen et al., 2009).

Li^+ plasma

The Li II spectra of Li^+ plasma was measured in (Doria et al., 2006). In the experimental apparatus by Doria et al. (Doria et al., 2006) a $Q-$ switched Nd:YAG laser ($\lambda = 1064$ nm) was focused onto a pure Li target surface placed inside a vacuum chamber ($5 \cdot 10^{-5}$ mbar) generating a plasma that expands normal to the target surface. The laser irradiance was kept constant at an average of $1.3 \cdot 10^{10}$ W$\cdot$ cm^{-2}. The authors obtained spatially and temporally resolved laser plasma spectra with an instrumental resolution $\lambda/\Delta\lambda^I \approx 2000 \div 2500$. The spectrum of our interest was recorded at a time delay of 60 ns from plasma breakdown. Comparison of a synthetic Li^+ (Li II 548 nm) line profile at $T = 3.32$ eV K and $n_e = 0.22 \cdot 10^{24}$ m^{-3}, obtained by M. Koubiti (Koubiti et al., 2011) using the standard theory of Stark broadening on a base of a semi-classical picture, with the experimental data of Doria et al. has shown that the EMD, as one of input values of the line profile, obtained in the present work provides a good agreement with the experiment. The EMD obtained in the present work on a base of C. A. Iglesias method for ionic Li^+ OCP at $T = 38\,527$ K and $n_e = 0.22 \cdot 10^{24}$ m^{-3} within the HGK pseudopotential model and MD data obtained by H. B. Nersisyan using the regularized Coulomb potential have been found in a good agreement with each other.

Static and dynamic structure factors with an account of the ion shell structure for high-temperature alkali and alkaline earth plasmas

X-ray scattering experiments has proven to be a powerful technique in measuring densities, temperatures and charge states. The structure factor is the fundamental quantity that describes the X-ray scattering plasma cross-section. To date, there is still a substantial amount of discrepancy between X-ray scattering data and the theoretical models for the quasi-static scattering component. This motivates this our study of static and dynamic properties of metal plasmas.

We have calculated the electron-electron, electron-ion, ion-ion and charge-charge static structure factors (SSFs) for alkali and Be^{2+} plasmas using the method described and discussed by G. Gregori et al. in (Gregori et al., 2006b, 2007). We have calculated the dynamic structure factors (DSFs) for alkali plasmas using the moment approach developed by V. M. Adamyan et al. (Adamyan and Tkachenko, 1983; Adamjan et al., 1993; Adamyan et al., 1985). The new screened HGK pseudopotential with the soft ion core, obtained on the basis of Bogoljubov's method (BBGKY) in the present work, has been used taking into account not only the quantum-mechanical effects but also the ion shell structure (Sadykova et al., 2009a). The results obtained within the screened HGK pseudopotential model for the SSFs have been compared with those obtained by Gregori et al. (Gregori et al., 2006b, 2007), while the DSFs calculated within the Hydrogen-like point charges (HLPC) and HGK (pseudo-)potential models, where the HGK pseudopotential model was considered completely within the properties of the HGK pseudopotential (through the fourth moment of the loss function) and the HGK

static characteristics, whereas the HLPC potential model was treated in a part within the HGK pseudopotential model through the HGK static characteristics, were compared to those of S. V. Adamjan et al. defined within the HLPC model as well but with the Coulomb properties and Coulomb static characteristics. We have detected deviations (in the values of the SSFs) from results obtained by Gregori et al., while we have noticed that the present DSFs are in a reasonable agreement with those of S. V. Adamjan et al. (Adamjan et al., 1993): at higher values of k and with increasing k the curves damp while at lower values of k, and especially at higher Γ_{ee}, we observe sharp peaks also reported in (Adamjan et al., 1993). At lower Γ_{ee} the curves for Li^+, Na^+, K^+, Rb^+ and Cs^+ do not differ while at higher Γ_{ee} the curves split. In alkali plasmas the plasmon peaks are more pronounced especially at higher Γ_{ii} and shifted toward the lower ω/ω_p than those considered within the Coulomb HLPC potential model with the Coulomb static characteristics. As the number of shell electrons increases from Li^+ to Cs^+ the curves shift toward the low absolute value of ω/ω_p and their heights diminish. The difference is due to the short range structure which we took into account by the HGK pseudopotential model compared to the HLPC. One should also take into account that we employed different plasma parameters because at the high densities and temperatures studied in (Adamjan et al., 1993) the inner electron shells of the alkali plasmas are destroyed.

Appendix

The derivation of the Holtsmark distribution

$$
\begin{aligned}
\ln T(k) =& n\int_0^{\infty}\int_0^{\pi}\int_0^{2\pi}\left[e^{\imath k\phi(r)\cos\theta}-1\right]\sin(\theta)d\varphi d\theta r^2 dr,\\
&\text{where } \phi(r)=ze/(4\pi\varepsilon_0 r^2)\\
=&2\pi n\int_0^{\infty}\int_{-1}^{1}\left[e^{\imath k\phi(r)\cos\theta}-1\right]d\cos\theta r^2 dr\\
=&2\pi n\int_0^{\infty}\left[\frac{e^{\imath k\frac{ze}{4\pi\varepsilon_0 r^2}\cos\theta}}{\imath k\frac{ze}{4\pi\varepsilon_0 r^2}}\Big|_{-1}^{1}-\cos\theta\Big|_{-1}^{1}\right]r^2dr\\
=&2\pi n\int_0^{\infty}\left[\frac{e^{\imath k\frac{ze}{4\pi\varepsilon_0 r^2}}-e^{-\imath k\frac{ze}{4\pi\varepsilon_0 r^2}}}{\imath k\frac{ze}{4\pi\varepsilon_0 r^2}}-2\right]r^2dr\\
=&4\pi n\int_0^{\infty}\left[\frac{\sin(k\frac{ze}{4\pi\varepsilon_0 r^2})}{k\frac{ze}{4\pi\varepsilon_0 r^2}}-1\right]r^2dr\\
&\text{let's denote } k\frac{ze}{4\pi\varepsilon_0 r^2}=Z', \text{ hence } r=\sqrt{\frac{kze}{Z'4\pi\varepsilon_0}}\\
=&-4\pi n\int_0^{\infty}\left[\frac{\sin Z'-Z'}{Z'}\frac{kze}{Z'}\frac{\sqrt{kze}}{2(4\pi\varepsilon_0 Z')^{3/2}}\right]dZ'\\
=&-2\pi n\left(\frac{kze}{4\pi\varepsilon_0}\right)^{3/2}\int_0^{\infty}\left[Z'^{-7/2}(\sin Z'-Z')\right]dZ'\\
&\text{Taking into an account: } \int_0^{\infty}\left[Z'^{-7/2}(sinZ'-Z')\right]dZ'=\tfrac{8}{15}\sqrt{\tfrac{\pi}{2}}\\
=&-2\pi n\left(\frac{kze}{4\pi\varepsilon_0}\right)^{3/2}\frac{8}{15}\sqrt{\frac{\pi}{2}}=-\frac{3}{{r_{ii}}^3}\left(\frac{kze}{4\pi\varepsilon_0}\right)^{3/2}\frac{2}{15}\sqrt{2\pi}, \qquad (1)
\end{aligned}
$$

where $n=3/4\pi{r_{ii}}^3$. Finally one can get:

$$lnT(l)=-3(\frac{kze}{4\pi\varepsilon_0{r_{ii}}^2})^{3/2}\frac{2}{15}\sqrt{2\pi}=-k^{*3/2}\frac{2}{5}\sqrt{2\pi},$$

with $k^* = kE_0$ where $E_0 = ze/(4\pi\varepsilon_0 {r_{ii}}^2)$ is an average electric field.
Holtsmark distribution:

$$P(\beta) = \frac{2\beta}{\pi} \int_0^\infty k^* exp(-{k^*}^{3/2} \frac{2}{5}\sqrt{2\pi}) \sin(\beta k^*) dk^* \tag{2}$$

The Deutsch pseudopotential without the symmetry effects and ionic screening

$$\Phi_{ei}(k) = \frac{ze^2}{\varepsilon_0 \Delta} \frac{1}{k^2(1 + k^2\lambda_{ei}^2)}, \tag{3}$$

$$\Phi_{ee}(k) = \frac{e^2}{\varepsilon_0 \Delta} \frac{1}{k^2(1 + k^2{\lambda_{ee}}^2)}, \tag{4}$$

$$\begin{aligned}\Phi_{ii}(k) =& \frac{z^2e^2}{\varepsilon_0\Delta} \left\{ \frac{1}{k^2(1 + k^2{\lambda_{ii}}^2)} \right. \\ &\left. + \frac{1}{k^4{r_{De}}^2} \left[\frac{1}{(1 + k^2{\lambda_{ee}}^2)(1 + k^2{\lambda_{ii}}^2)} - \frac{1}{(1 + k^2{\lambda_{ei}}^2)^2} \right] \right\}. \end{aligned} \tag{5}$$

Here r_{De} is the Debye radius of electrons with $1/{r_{De}}^2 = e^2 n_e/(\varepsilon_0 k_B T)$, $b = ({\lambda_{ee}}^2 \pi \ln 2)^{-1}$, $A = k_B T \ln 2 \pi^{3/2} b^{-3/2} \varepsilon_0 / e^2$ and

$$\Delta = 1 + \frac{1}{k^2 {r_{De}}^2 (1 + k^2{\lambda_{ee}}^2)}. \tag{6}$$

The pseudopotential $\Phi_{ab}(r)$ can be restored from (3-6) by Fourier transformation

$$\Phi_{ab}(r) = \frac{1}{2\pi^2 r} \int \Phi_{ab}(k) k \sin(kr) dk \tag{7}$$

Let us consider the limiting cases of the expressions (3-4).

A. If $r_{De} \to \infty$, then

$$\Phi_{ab}(r) = \varphi_{ab}(r) \tag{8}$$

When the screening effects are negligible, the pseudopotential $\Phi_{ab}(r)$ coincides with the potentials (3.5).

B. If λ_{ee}, λ_{ei}, $\lambda_{ii} \to 0$, then

$$\Phi_{ab}(r) = \frac{e_a e_b}{4\pi\varepsilon_0} \frac{e^{-r/r_{De}}}{r}. \tag{9}$$

Eq. (9) means when quantum-mechanical effects are negligible, then the pseudopotential $\Phi_{ab}(r)$ coincides with the Debye-Hückel one.

C. If $r_{De} \to \infty$, λ_{ee}, λ_{ei}, $\lambda_{ii} \to 0$, then

$$\Phi_{ab}(r) = \frac{e_a e_b}{4\pi\varepsilon_0 r}. \tag{10}$$

When the quantum-mechanical and screening field effects are negligible, then the pseudopotential $\Phi_{ab}(r)$ coincides with the Coulomb potential.

D. If $\lambda_{ee}, \lambda_{ei}, \lambda_{ii} \ll r_{De}$, then for $e-i$ and $i-i$

$$\Phi_{ab}(r) = \frac{e_a e_b}{4\pi\varepsilon_0 r}\left[e^{-r/r_{De}} - e^{-r/\lambda_{ab}}\right]. \tag{11}$$

The derivation of the asymptote of the Holtsmark distribution

$$\lim_{\beta\to\infty} P(\beta) = \lim_{\beta\to\infty} \frac{2\beta}{\pi} \int\limits_0^\infty k^* \exp(-k^{*3/2}\frac{2}{5}\sqrt{2\pi}) \sin(\beta k^*) dk^*$$

$$= \lim_{\beta\to\infty} -\frac{2\beta}{\pi} \int\limits_0^\infty \frac{\partial}{\partial\beta} \exp(-k^{*3/2}\frac{2}{5}\sqrt{2\pi}) \cos(\beta k^*) dk^*$$

Taking into an account that at $\beta \to \infty \Longrightarrow k^* \to 0$, we get:

$$= \lim_{\beta\to\infty} -\frac{2\beta}{\pi}\frac{\partial}{\partial\beta} \int\limits_0^\infty (1 - k^{*3/2}\frac{2}{5}\sqrt{2\pi}) \cos(\beta k^*) dk^*$$

$$= \lim_{\beta\to\infty} -\frac{2\beta}{\pi}\frac{\partial}{\partial\beta} (\delta(\beta) - \frac{2}{5}\sqrt{2\pi} \int\limits_0^\infty k^{*3/2} \cos(\beta k^*) dk^*)$$

$$= \left| \beta k^* = x, -\frac{2}{5}\sqrt{2\pi}\frac{\partial^2}{\partial\beta^2}\frac{\sqrt{\beta}}{\beta} \int\limits_0^\infty x^{-1/2} \cos x dx \right.$$

$$= -\frac{2}{5}\sqrt{2\pi}\frac{\partial^2}{\partial\beta^2}\frac{1}{\sqrt{\beta}}\Gamma(1/2)\cos\left(\frac{\pi}{4}\right)$$

$$= \left. -\frac{2}{5}\sqrt{2\pi}\beta^{-5/2}\sqrt{\pi}\frac{\sqrt{2}}{2}\frac{3}{4} \right|$$

$$= \lim_{\beta\to\infty} -\frac{2\beta}{\pi}\frac{\partial}{\partial\beta}(\delta(\beta) + \frac{2}{5}\sqrt{2\pi}\beta^{-5/2}\sqrt{\pi}\frac{\sqrt{2}}{2}\frac{3}{4})$$

at$\beta \to \infty \Longrightarrow \delta(\beta) \to 0$, then we have

$$= \underline{\frac{3}{2}\beta^{-5/2}} \qquad (12)$$

Abbreviations

Table 1: Abbreviations

Abbreviations	Description
EMD(s)	Electric Microfield Distribution(s)
OCP	One-component plasma
TCP	Two-component plasma
RDF	Radial distribution function
PMF	Potential-of-mean-force
MC	Monte Carlo
MD	Molecular Dynamics
HGK	Hellmann-Gurskii-Krasko pseudopotential model
HC (HS)	Hard-Core pseudopotential model (Hard spheres)
HLPC	Hydrogen-like point charges model
PBC	Periodic boundary conditions
BBGKY	Bogoljubov-Born-Green-Kirkwood-Yvon method
SSF(s)	Static structure factor(s)
DSF(s)	Dynamic structure factor(s)
RPA	Random-phase approximation
HNC	Hypernetted-chain approximation
LTE	Local thermodynamic equilibrium
APEX	Adjustable-parameter approximation model

Bibliography

S. V. Adamjan, I. M. Tkachenko, J.L. Muñoz Cobo González, and G. Verdú Martín. Dynamic and static correlations in model Coulomb systems. *Phys. Rev. E*, 48:2067, 1993.

V. M. Adamyan and I. M. Tkachenko. High-frequency electric conductivity of a collisional plasma. *High Temp. (USA)*, 21:307, 1983.

V. M. Adamyan and I. M. Tkachenko. Sum rules and exact relations for quantal Coulomb systems. *Contrib. Plasma Phys.*, 43:252, 2003.

V. M. Adamyan, T. Meyer, and I. M. Tkachenko. Rf. dielectric constant of a collisional plasma. *Sov. J.Plasma Phys.*, 11:481, 1985.

V. M. Adamyan, A. A. Mihajlov, N. M. Sakan, V. A. Srećković, and I. M. Tkachenko. The dynamic conductivity of strongly non-ideal plasmas: is the drude model valid? *J. Phys. A: Math. Theor.*, 42:214005 (5pp), 2009.

N. I. Akhieser. *The classical Moment Problem.* Oliver and Boyd, London, 1965.

H. C. Andersen and D. Chandler. Optimized cluster expansions for classical fluids. I. general theory and variational formulation of the mean spherical model and hard sphere percus-yevick equations. *J. Chem. Phys.*, 57:1918, 1972.

E. M. Apfelbaum. The calculation of Cs and Rb conductivities in the region of liquid-plasma transition. *Phys. Chem. Liq.*, 48(4):534–545, 2010.

Yu. V. Arkhipov and A.E. Davletov. Screened pseudopotential and static structure factors of semiclassical two-component plasmas. *Phys. Lett. A*, 247(4-5):339–342, 1998.

Yu. V. Arkhipov, F.B. Baimbetov, and A.E. Davletov. Thermodynamics of dense high-temperature plasmas: Semiclassical approach. *Eur.Phys. J. D*, 8:299–304, 2000.

Yu. V. Arkhipov, A. Askaruly, D. Ballester, A. E. Davletov, G. M. Meirkhanova, and I. M. Tkachenko. Collective and static properties of model two-component plasmas. *Phys. Rev. E*, 76:026403, 2007.

Yu. V. Arkhipov, A. Askaruly, D. Ballester, A. E. Davletov, I. M. Tkachenko, and G. Zwicknagel. Dynamic properties of one-component strongly coupled plasmas: The sum-rule approach. *Phys. Rev. E*, 81:026402, 2010.

N. W. Ashcroft. Electron-ion pseudopotentials in the alkali metals. *J. Phys. C: Solid State Phys.*, 1:232–243, 1968.

F.B. Baimbetov, Kh. T. Nurekenov, and T. S. Ramazanov. Pseudopotential theory of classical non-ideal plasmas. *Phys. Lett. A*, 202:211, 1995.

M. Baranger and B. Mozer. Electric field distributions in an ionized gas. *Phys. Rev.*, 115:521–525, 1959.

B. Bernu and D. Ceperley. NATO ASI Series, Mathematical and Physical Sciences. In *Quantum Monte Carlo Methods in Physics and Chemistry*, C-525, Boston, 1999. Kluwer Academic Publishers.

D.B. Boercker and J.W. Dufty. *In Spectral Line Shapes.* W. de Gruyter, Berlin/New York, 1983.

N.N. Bogoljubov. *Problemy Dinamicheskoii Teorii v Statisticheskoii Fizike (in Russ.).* Gostekhizdat, Moscow-Leningrad, 1946.

N.N. Bogoljubov. *Studies in Statistical Mechanics.* North-Holland, Amsterdam, 1962.

H. P. Bonzel, A. M. Bradshaw, and G. Ertl. *Physics and Chemistry of Alkali Metal Adsorption (Materials Science Monographs).* Elsevier, Amsterdam, 1989.

A. A. Broyles. Stark fields from ions in a plasma. *Phys. Rev.*, 100:1181, 1955.

A. A. Broyles. Fields on plasma ions by collective coordinates. *Phys. Rev.*, 105:347, 1957.

S. Chandrasekhar. Stochastic problems in physics and astronomy. *Rev. Mod. Phys.*, 15: 1–89, 1943.

M.J. Corbatón and I.M. Tkachenko. Static correlation functions in hydrogen-like completely ionized plasmas. In *Int. Conference on Strongly Coupled Coulomb Systems*, Book of Abstracts, page 90, Camerino, Italy, 2008. University of Camerino.

R. D. Cowan. *The theory of Atomic Structure and Spectra.* University of California Press, Berkeley, CA, Berkeley, CA, 1981.

S.S. Dalgic, S. Dalgic, and G. Tezgor. Transferable pair potentials for liquid iron, cobalt and nickel. *Phys. Chem. Liq.*, 40(5):539, 2002.

P. Debye and E. Hückel. Zur theorie der elektrolyte. I. gefrierpunktserniedrigung und verwandte erscheinungen. *Physik. Z.*, 24(185), 1923.

C. Deutsch. Nodal expansion in a real matter plasma. *Phys. Lett. A*, 60:317, 1977.

M. W. C. Dharma-Wardana and F. Perrot. Simple classical mapping of the spin-polarized quantum electron gas: distribution functions and local-field corrections. *Phys. Rev. Lett.*, 84:959, 2000.

D. Doria, K. D. Kavanagh, J. T. Costello, and H. Luna. Plasma parametrization by analysis of time-resolved laser plasma image spectra. *Meas. Sci. Technol.*, 17:670–674, 2006.

T. Dunn and A. A. Broyles. Method for determining the thermodynamic properties of the quantum electron gas. *Phys. Rev.*, 157:156, 1967.

W. Ebeling and J. Ortner. Quasiclassical theory and simulations of strongly coupled plasmas. *Physica Scripta*, T75:93–98, 1998.

W. Ebeling, W-D. Kräft, and D. Kremp. *Theory of Bound State and Ionization Equilibrium in Plasmas and Solids*. Akademie-Verlag, Berlin, 1976.

W. Ebeling, C.-V. Meister, and R. Sändig. . In *Proceedings of the XIII. Conference on "Phenomena in Ionized Gases"*, page 725, Berlin, 1977.

W. Ebeling, C.-V. Meister, R. Sändig, and W-D. Kraeft. Pressure ionization in nonideal alkali plasmas. *Ann. Phys. (Leipzig)*, 36:321, 1979.

W. Ebeling, A. Förster, W. Richert, and H. Hess. Thermodynamic properties and plasma phase transition of xenon at high pressure and high temperature. *Physics A*, 150:159, 1988.

W. Ebeling, G.E. Norman, A.A. Valuev, and I. Valuev. Quasiclassical theory and molecular dynamics of two-component nonideal plasmas. *Contr. Plasma Phys.*, 39:61, 1999.

H. Ebert. *Physikalisches Taschenbuch*. F. Vieweg & Sohn, Braunschweig, 1967.

G. Ecker. Das mikrofeld in gesamtheiten mit Coulombscher wechselwirkung. *Z. Physik*, 148:593, 1957.

G. Ecker. *Theory of Fully Ionized Plasmas*. Academic Press, New York, 1972.

G. Ecker and K.G. Müller. Plasmapolarisation und trägerwechselwirkung. *Z. Physik*, 153:317, 1958.

H. Falkenhagen. *Theorie der Elektrolyte*. S. Hirzel Verlag, Leipzig, 1971.

W. Feller. *An Introduction to the probability theory and its applications*. J. Wiley and Son., New York, 1970.

A.V. Filinov, M. Bonitz, and W. Ebeling. Improved Kelbg potential for correlated Coulomb systems. *J. Phys. A.: Math. Gen.*, 36:5957–5962, 2003.

C. Fiolhais, J. P. Perdew, S. Q. Armster, J. M. MacLaren, and M. Brajczewska. Dominant density parameters and local pseudopotentials for simple metals. *Phys. Rev. B*, 51: 14001–14011, 1995.

W. Freyland. Magnetic susceptibility of metallic and nonmetallic expanded fluid cesium. *Phys. Rev. B*, 20:5104–5110, 1979.

D. O. Gericke, K. Wünsch, and J. Vorberger. Modelling the scattering of X-rays in warm dense matter. *Nuclear Instruments and Methods in Physics Research A*, 606:142, 2009.

S.H. Glenzer. Observations of plasmons in warm dense matter. *Phys. Rev. Lett.*, 98: 065002, 2007.

S.H. Glenzer, G. Gregori, R.W. Lee, F.J. Rogers, S.W. Pollaine, and O.L. Landen. Demonstration of spectrally resolved X-ray scattering in dense plasmas. *Phys. Rev. Lett.*, 90:175002, 2003.

R. E. Goldstein and N. W. Ashcroft. Origin of the singular diameter in the coexistence curve of a metal. *Phys. Rev. Lett*, 55:2164, 1985.

M.-M. Gombert. Temperature-dependent pseudopotential between two pointlike electrical charges. *Phys. Rev. E*, 66:066407, 2002.

I. S. Gradstejn and I. M. Ryzhik. *Tablicy Integralov, Summ, Rjadov i Proizvedenij (Tables of Integrals, Sums, Series and Products).* Nauka, Moscow, 1971.

G. Gregori, S.H. Glenzer, H.-K. Chung, D.H. Froula, R.W. Lee, N.B. Meezan, J.D. Moody, C. Niemann, O.L. Landen, B. Holst, R. Redmer, S.P. Regan, and H. Sawada. Measurement of carbon ionization balance in high-temperature plasma mixtures by temporally resolved X-ray scattering. *J. Quant. Spectrosc. Radiat. Transf.*, 99:225–237, 2006a.

G. Gregori, S.H. Glenzer, and O.L. Landen. Generalized X-ray scattering cross section from nonequilibrium plasmas. *Phys. Rev. E*, 74:026402, 2006b.

G. Gregori, A. Ravasio, A. Höll, S.H. Glenzer, and S. J. Rose. Derivation of the static structure factor in strongly coupled non-equilibrium plasmas for X-ray scattering studies. *High Energy Density Phys.*, 3:99–108, 2007.

H. R. Griem. *Spectral Line Broadening by Plasmas.* Academic Press, New York, 1974.

H. R. Griem. *Principles of Plasma Spectroscopy.* Cambridge University Press, Cambridge, 1997.

S. Günter. *Optische eigenschaften dichter plasmen.* Rostoker Universität, Rostock, 1995.

Z. A. Gurskii and G. L. Krasko. Model'nyj psevdopotenzcial i nekotorye atomnye svojstva sh'elochnyh i sh'elochnozemel'nykh metallov. *Doklady Akademii Nauk SSSR (in Russ.)*, 197:810, 1971.

J. Halenka. Asymmetry of hydrogen lines in plasmas utilizing a statistical description of ion-quadrupole interaction in mozer-baranger limit. *Z. Phys. D*, 16:1, 1990.

J.-P. Hansen and I. R. McDonald. *Theory of Simple Liquids.* Academic Press, London, 1990.

J.-P. Hansen and I.R. McDonald. Microscopic simulation of a strongly coupled hydrogen plasma. *Phys. Rev. A*, 23:2041, 1981.

J.-P. Hansen, E. L. Polock, and I.R. McDonald. Velocity autocorrelation function and dynamical structure factor of the classical one-component plasma. *Phys. Rev. Lett.*, 32:277, 1974.

W. A. Harrison. *Pseudopotentials in the Theory of Metals.* Benjamin, New York, 1966.

V. Heine. The pseudopotential concept. *Solid State Physics*, 24:1–36, 1970.

V. Heine and I. V. Abarenkov. A new method for the electronic structure of metals. *Phil. Mag.*, 9:451, 1964.

V. Heine, M.L. Cohen, and D. Weaire. *Psevdopotenzcial'naya Teoriya (in Russ.)*. Mir, Moscow, 1973.

B. Held, C. Deutsch, and M.-M. Gombert. Quantum diffraction corrections to the high-frequency thermal microfield in a dense electron plasma. *Phys. Rev. A*, 25:585, 1982a.

B. Held, C. Deutsch, and M.-M. Gombert. Quantum corrections to the high-frequency thermal microfield in a dense plasma. *J. Phys. A*, 15:3845, 1982b.

B. Held, M.-M. Gombert, and C. Deutsch. Diffraction and symmetry corrections to the high-frequency thermal microfield in a dense electron plasma. *Phys. Rev. A*, 31:921, 1985.

H. Hellmann. A new approximation method in the problem of many electrons. *Acta Physicochimica URSS*, 1:913, 1935a.

H. Hellmann. A new approximation method in the problem of many electrons. *J. Chem. Phys.*, 3:61, 1935b.

H. Hellmann. A new approximation method in the problem of many electrons. *Acta Physicochimica URSS*, 4:225, 1936.

H. Hellmann and W. Kassatotschkin. Metallic binding according to the combined approximation procedure. *J. Chem. Phys.*, 4:324, 1936.

F. Hensel. *Liquid Metals*. IOP Conf. Ser. No. 30, IPPS, London, 1977.

F. Hensel, S. Jüngst, F. Noll, and R. Winter. *In Localisation and Metal Insulator Transitions*. Plenum Press, New York, 1985.

H. Hess. *Physics of nonideal plasmas*. B.G. Teubner Verlagsgesellschaft, Stuttgart-Leipzig, 1992.

H. Hess. Critical data of metals-estimations for tungsten. *Phys. Chem. Liq.*, 30:251, 1995.

H. Hess, A. Kloss, A. Rakhel, and H. Schneidenbach. Determination of thermophysical properties of fluid metals by wire-explosion experiments. *Intern. J. Thermophys*, 20: 1279, 1999.

A. Höll, Th. Bornath, L. Cao, T. Döppner, S. Düsterer, E. Föster, C. Fortmann, S.H. Glenzer, G. Gregori, T. Laarmann, K.-H. Meiwes-Broer, A. Przystawik, P. Radcliffe, R. Redmer, H. Reinholz, G. Röpke, R. Thiele, J. Tiggesbäumker, S. Toleikis, N.X. Truong, T. Tschentscher, I. Ushmann, and U. Zastrau. Thomson scattering from near-solid density plasmas using soft X-ray free electron lasers. *High Energy Density Phys.*, 3:120, 2007.

J. Holtsmark. Über die verbreiterung von spectrallinien. *Ann. Phys.*, 58:577, 1919.

C. F. Hooper. Electric microfield distributions in plasmas. *Phys. Rev.*, 149:77, 1966.

S. Ichimaru. *Statistical Plasma Physics, Vol. I: Basic Principles*. Addison-Wesley, Redwood City, Calif., 1992.

C.A. Iglesias. Integral-equation method for electric microfield distributions. *Phys. Rev. A*, 27:2705, 1983.

C.A. Iglesias and Jr. C. F. Hooper. Cluster expansion for the electric microfield distribution in a plasma. *Phys. Rev. A*, 25:1049, 1982.

C.A. Iglesias and J. L. Lebowitz. Electric microfield distributions in multicomponent plasmas. *Phys. Rev. A*, 30:2001–2004, 1984.

C.A. Iglesias, J. L. Lebowitz, and D. MacGowan. Electric microfield distributions in strongly coupled plasmas. *Phys. Rev. A*, 28:1667–1672, 1983.

C.A. Iglesias, H. E. DeWitt, J. L. Lebowitz, D. MacGowan, and W. B. Hubbard. Low-frequency electric microfield distributions in plasmas. *Phys. Rev. A*, 31:1698–1702, 1985.

S. Juengst, B. Knuth, and F. Hensel. Observation of singular diameters in the coexistence curves of metals. *Phys. Rev. Lett.*, 55:2160, 1985.

G. Kelbg. Quantenstatistik der gase mit Coulomb-wechselwirkung. *Ann. Physik*, 12:354, 1964a.

G. Kelbg. Klassische statistische mechanik der teilchen-mischungen mit sortenabhängigen weitreichenden zwischenmolekularen wechselwirkungen. *Ann. Physik*, 14:394, 1964b.

D. Klakow, C. Töpffer, and P.-G. Reinhard. Semiclassical molecular dynamics for strongly coupled Coulomb systems. *J. Chem. Phys.*, 101:10766–10774, 1994a.

D. Klakow, C. Töpffer, and P.-G. Reinhard. Hydrogen under extreme conditions. *Phys. Lett. A*, 192:55, 1994b.

Yu.L. Klimontovich. *The kinetic theory of electromagnetic processes*. Springer, Berlin, Heidelberg, New York, 1983.

A.N. Klyucharev, N.N. Bezuglov, A.A. Matveev, A.A. Mihajlov, Lj.M. Ignjatović, and M.S. Dimitrijević. Rate coefficients for the chemi-ionization processes in sodium- and other alkali-metal geocosmical plasmas. *New Astronomy Reviews*, 51:547–562, 2007.

M. Koubiti, H. Capes, L. Godbert-Mouret, Y. Marandet, J. Rosato, and R. Stamm. Stark broadening of high-members of the helium diffuse series in divertor plasmas. *J. Phys. B.:At. Mol. Phys.*, 43:144022, 2010.

M. Koubiti, S. P. Sadykova, and W. Ebeling. Stark broadening of Li^+ plasma and study of influence of the Li^+ ion shell structure on the spectral lines. *The article will soon be submitted*, 2011.

N. P. Kovalenko, Yu. P. Krasnyj, and U. Krey. *Physics of Amorphous Metalls*. Wiley-VCH, Weinheim, 2001.

W-D. Kraeft, D. Kremp, W. Ebeling, and G. Röpke. *Quantum Statistics of Charged Particle Systems*. Akademie-Verlag, Berlin, 1986.

G. L. Krasko and Z. A. Gurskii. Concerning one model pseudopotential. *JETP letters*, 9:363, 1969.

M. G. Krein and A. A. Nudel'man. *The Markov Moment Problem and External Problems*. American Mathematical Society, Translations, New York, 1977.

Yu. K. Kurilenkov and V. S. Filinov. Funkzcii raspredeleniya mikropolya v neideal'noj plazme. *Teplofizika vicokih temperatur*, 18(4):657–667, 1980.

L. D. Landau and E. M. Lifschitz. *Quantum Mechanics:non-relativistic theory*. Pergamon Press, Oxford, 1977.

L. D. Landau and E. M. Lifschitz. *Electrodynamics of continuous media*. Butterworth-Heinemann, Oxford, 2000.

M. Lewis and H. Margenau. Statistical broadening of spectral lines emitted by ions in a plasma. *Phys. Rev.*, 109(3):842–845, 1958.

H. A. Lorentz. The absorption and emission lines of gaseous bodies. *Proc. R. Acad. A. Sci. Amsterdam*, 8 II:591, 1906.

S. Lorenzen, A. Wierling, H. Reinholz, and G. Röpke. Pressure broadening of lyman-lines in dense Li^2+ plasmas. *Contr. Plasma Phys.*, 48:657, 2008.

S. Lorenzen, A. Wierling, H. Reinholz, and G. Röpke. Pressure broadening of spectral lines in dense Lithium plasmas. In *Proceedings to the XIII-th International Conference on "the Physics of Non-ideal Plasmas" (PNP 13 in Chernogolovka)*, Book of abstracts, page 55, URL: http://summa.physik.hu-berlin.de/∼sadykova/pnp13Lorenzen.pdf (poster) and private communications, 2009. Russian Academy of Sciences.

H. Mayer. *Methods of opacity calculations.* Los Alamos Scientific Laboratory Report LA-647, Los Alamos, 1947.

J.E. Mayer and M.G. Mayer. *Statistical Mechanics*. John Wiley & Sons, New York, 1940.

H. Minoo, M.-M. Gombert, and C. Deutsch. Temperature-dependent Coulomb interactions in hydrogenic systems. *Phys. Rev. A*, 23:924, 1981.

N. F. Mott. *Metal-Insulator Transitions*. Taylor and Francis, London, 1974.

B. Mozer and M. Baranger. Electric field distributions in an ionized gas. *Phys. Rev.*, 118:626, 1960.

H. B. Nersisyan, C. Töpffer, and G. Zwicknagel. Microfield distributions in strongly coupled two-component plasmas. *Phys. Rev. E*, 72:036403, 2005.

H. B. Nersisyan, D. A. Osipyan, and G. Zwicknagel. Renormalized cluster expansion of the microfield distribution in strongly coupled two-component plasmas. *Phys. Rev. E*, 77:056409, 2008.

J. Ortner, F. Schautz, and W. Ebeling. Quasiclassical molecular-dynamics simulations of the electron gas: Dynamic properties. *Phys. Rev. E*, 56:4665, 1997.

J. Ortner, I. Valuev, and W. Ebeling. Semiclassical dynamics and time correlations in two-component plasmas. *Contrib. Plasma Phys.*, 39:311, 1999.

J. Ortner, I. Valuev, and W. Ebeling. Electric microfield distribution in two-component plasmas. theory and simulations. *Contrib. Plasma Phys.*, 40:555–568, 2000.

J.I. Penman, J. Clérouin, and P. G. Zérah. Equation of state of a hydrogen plasma by density functional molecular dynamics. *Phys. Rev. E*, 51:R5224–R5227, 1995.

C. Pierleoni, D.M. Ceperley, B. Bernu, and W.R. Magro. Equation of state of the hydrogen plasma by path integral monte carlo simulation. *Phys. Rev. Lett.*, 73:2145, 1994.

A. Y. Potekhin, G. Chabrier, and D. Gilles. Electric microfield distributions in electron-ion plasmas. *Phys. Rev. E.*, 65:036412, 2002.

Yu. Ralchenko, A.E. Kramida, and J. Reader. Nist atomic spectra database. In *NIST Atomic Spectra Database*, http://www.nist.gov/pml/data/asd.cfm, 2010. National Institute of Standards and Technology.

D. Riley, N.C. Woolsey, D. McSherry, I. Weaver, A. Djaoui, and E. Nardi. X-ray diffraction from a dense plasma. *Phys. Rev. Lett.*, 84:1704, 2000.

M. Yu. Romanovsky and W. Ebeling. Microfields and fusion rates for dense plasmas. *Physica A*, 252:488–504, 1998.

M. Yu. Romanovsky and W. Ebeling. Fluctuations of electric microfields in laser-produced ion clusters: Enhancement of nuclear fusion. *Laser Physics*, 14(6):850–856, 2004.

M. Yu. Romanovsky and W. Ebeling. Elementary many-particle processes in plasma microfields. *Contrib. Plasma Phys.*, 46:195–260, 2006.

M. J. Rosseinsky and K. Prassides. Hydrocarbon superconductors. *Nature*, 464:39–41, 2010.

S. Sadykova and W. Ebeling. Electric microfield distributions in dense one- and two-component plasmas. *Contr. Plasma Phys.*, 47:659, 2007.

S. Sadykova, G. Fussmann, and W. Ebeling. Microfield distributions in a dense high-temperature plasma. In *Proceedings of the Conference of the German Physical Society (DPG) on Plasma Physics (The talk at the DPG 2005 in Berlin)*, URL: http://www.dpg-verhandlungen.de/2005/p25.pdf, 2005. DPG.

S. Sadykova, W. Ebeling, I. Valuev, and I. Sokolov. Electric microfield distributions in Li^+ plasma with account of the ion structure. *Contr. Plasma Phys.*, 49:76–89, 2009a.

S. P. Sadykova. Static and dynamic structure factors with an account of the ion structure for high-temperature alkali and alkaline earth plasmas. In *Proceedings of the XXXVII European Physical Society Conference on Plasma Physics in Dublin*, pages 1–4, URL: http://ocs.ciemat.es/EPS2010PAP/pdf/P1.318.pdf, 2010.

S. P. Sadykova, Yu. V. Arkhipov, and A.E. Davletov. Raspredelenie mikropolej v plotnoj vysokotemperaturnoj plazme. *Izvestiya Nazcianal'noj Akademii Nauk Respubliki Kazakhstan (phizika)*, 6:39–49, URL: http://summa.physik.hu-berlin.de/∼sadykova/NANRK.pdf 2004.

S. P. Sadykova, W. Ebeling, I. Valuev, and I.M. Sokolov. Electric microfield distributions in alkali plasmas with account of the ion structure. *Contr. Plasma Phys.*, 49:388–402, 2009b.

S. P. Sadykova, I. Valuev, W. Ebeling, and I. M. Sokolov. Raspredelenie elektricheskikh mikropolej v neideal'noj elektron-pozitronnoj plazme. molekulyarno-dinamicheskoe modelirovanie. *Prikladnaja Phizika*, 1:37–43, URL: http://www.vimi.ru/applphys/appl-10/10-1/10-1-7r.htm 2010a.

S. P. Sadykova, I. Valuev, W. Ebeling, and I. M. Sokolov. Molecular dynamic simulations of electric microfield distributions in a nonideal electron-positron plasma. *Plasma Physics Reports:Nauka/Interperiodica-Pleiades Publishing Ltd.*, 36(13):1161–1166, 2010b.

S. P. Sadykova, W. Ebeling, and I.M. Sokolov. Electric microfield distributions in alkali plasmas with account of the ion structure in a moderately coupled approximation. *Contr. Plasma Phys.*, 51(4):386–390, 2011a.

S. P. Sadykova, W. Ebeling, and I.M. Tkachenko. Static and dynamic structure factors with account of the ion structure for high-temperature alkali and alkaline earth plasmas. *Eur. Phys. J. D*, 61:117–130, 2011b.

G. Schriever, K. Bergmann, and R. Lebert. Narrowband laser produced extreme ultraviolet sources adapted to silicon/molybdenum multilayer optics. *J. Appl. Phys.*, 83: 4566, 1998a.

G. Schriever, S. Mager, A. Naweed, A. Engel, K. Bergmann, and R. Lebert. Laser-produced lithium plasma as a narrow-band extended ultraviolet radiation source for photoelectron spectroscopy. *Applied Optics*, 37:1243, 1998b.

V. Schwarz, B. Holst, T. Bornath, C. Fortmann, W-D. Kraeft, R. Thiele, R. Redmer, G. Gregori, H. Ja Lee, T. Döppner, and S. H. Glenzer. Static ion structure factor for dense plasmas: Semi-classical and ab initio calculations. *High Energy Density Physics*, 6:305–310, 2009.

W. H. E. Schwarz. Das kombinierte näherungsverfahren. I. theoretische grundlagen. *Theor. Chim. Acta (Berl.)*, 11:307, 1968a.

W. H. E. Schwarz. Das kombinierte näherungsverfahren. III. rechnungen an atomaren zweivalenzelektronensystemen. *Theor. Chim. Acta (Berl.)*, 11:377, 1968b.

W. H. E. Schwarz. Die alkalimetallmoleküle nach dem kombinierten näherungsverfahren (kn). *Theor. Chim. Acta (Berl.)*, 15:235, 1969.

P. Seuferling, J. Vogel, and C. Toepffer. Correlations in a two-temperature plasma. *Phys. Rev. A*, 40:323, 1989.

U. Seydel, W. Frucke, and H. Wadle. *Die Bestimmung thermophysikalischer Daten flüssiger hochschmelzender Metalle mit schnellen Pulsaufheizeksperimenten.* Verlag Dr. P. Mannhold, Düsseldorf, 1980.

J. Sheffield. *Plasma Scattering of Electromagnetic Radiation.* Academic Press, New York, 1975.

V. Sizyuk, A. Hassanein, and T. Sizyuk. Three-dimensional simulation of laser-produced plasma for extreme ultraviolet lithography applications. *J. Appl. Phys.*, 100:103106, 2006.

L. Szasz. *Pseudopotential Theory of Atoms and Molecules.* Wiley-Intersc., New York, 1985.

B. Talin, A. Calisti, S. Ferri, M. Koubiti, T. Meftah, C. Mosse, R. Stamm, S. Alexiou, R. W. Lee, and L. Klein. Ground work supporting the codes based upon the frequency fluctuation model. *J. Quant. Spectrosc. Radiat. Transfer*, 58:953–964, 1997.

H. J. Tighe and C. F. Hooper. Stark broadening in hot, dense laser-produced plasmas. *Phys. Rev. A*, 14:1514, 1976.

H. J. Tighe and C. F. Hooper. Low-frequency electric microfield distributions in a plasma containing multiply-charged ions: Extended calculations. *Phys. Rev. A*, 15:1773, 1977.

V. G. Vaks, S. P. Kravchuk, and A. V. Trefilov. Uravnenie sostoyaniya i ob'emnaya zavisimost' termodinamicheskikh svojstv sh'elochnykh metallov. *Fizika Tverdogo Tela (Sov. Phys. Solid State)*, 19:1271, 1977.

H. Wagenknecht, W. Ebeling, and A. Förster. Effective potentials, energies, and pair-distribution functions of plasmas by monte-carlo simulations. *Contrib. Plasma Phys.*, 41:15–25, 2001.

R. Winter, F. Hensel, T. Bodensteiner, and W. Glaeser. Structure and forces in expanded liquid cesium. *J. Phys. Chem.*, 92:7171–7174, 1988.

X.-Z. Yan and S. Ichimaru. Theory of interparticle correlations in dense, high-temperature plasmas. VI. probability densities of the electric microfields. *Phys. Rev. A*, 34:2167, 1986.

V.M. Zamalin, G.E. Norman, and V.S. Filinov. *Metod Monte-Carlo v Statisticheskoii Mekhanike (in Russ.).* Nauka, Moscow, 1977.

W. Zimdahl and W. Ebeling. Theory of the ionization equilibrium in nonideal alkali plasmas. *Ann. Phys. (Leipzig)*, 34:9, 1977.

R. W. Zwanzig. High-temperature equation of state by a perturbation method. I. nonpolar gases. *J. Chem. Phys.*, 22:1420, 1954.

List of Figures

1.1 Density-temperature diagram for various plasmas 5

2.1 The Holtsmark electric microfield distribution for hydrogen-like plasma $z = 1$ 16

2.2 The Holtsmark electric microfield distribution and its asymptote at $\beta \to \infty$ for hydrogen-like plasma $z = 1$ in a double decadic logarithmic scale . . 19

3.1 Comparison between the Coulomb (3.1) and Debye (3.4) potentials of semiclassical Hydrogen-like point charges plasma against the dimensionless distance $R = r/r_B$ at $T = 30000$ K, $1 \cdot 10^28$ m^{-3}, $\Gamma_{ii} = 2$. 34

3.3 Comparison between the Debye and Screened Deutsch pseudopotentials of semiclassical Hydrogen-like point charges plasma against the dimensionless distance $R = r/r_B$ at $T = 5248578$ K and $n_e = 0.2 \cdot 10^{27}$ cm^{-3}. 39

3.4 Comparison between the Kelbg (3.27), Corrected Kelbg 3.28 and Screened Kelbg (3.45) pseudopotentials of semiclassical Hydrogen-like point charges plasma against the dimensionless distance $R = r/r_L$ at $T = 30000$ K and various concentrations. 45

3.5 Electric microfield distributions an electron for OCP plasmas at $T = 394\,000$ K and $\Gamma_{ee} = 0.1, 0.2, 0.4$. The EMD curve measured at an electron at $\Gamma_{ee} = 0.4$ and $T = 394\,000$ K (Sadykova and Ebeling, 2007) is compared to MD results at an electron and neutral point obtained in the present work. The Holtsmark distribution is also shown for comparison. 48

3.6 Electric microfield distributions at an electron for TCP electron-positron plasmas at $T = 30000$ K and a) $\Gamma_{ee} = 0.2$, b) $\Gamma_{ee} = 0.8$. MD results have been taken from (Ortner et al., 2000). The Holtsmark distribution is also shown for comparison. 50

3.7 Electric microfield distribution at an electron for TCP electron-positron plasma at $T = 30000$ K, $\Gamma_{ee} = 1.2$ (Sadykova and Ebeling, 2007). MD results have been taken from (Ortner et al., 2000). The Holtsmark distribution is also shown for comparison. 51

3.8 Electric microfield distributions obtained with the help of MD for TCP electron-positron plasmas at $T = 30000$ K and various Γ. EMD are measured at a) an electron, b) a neutral point (Sadykova et al., 2010b,a). In both figures the EMDs are compared to the high-frequency OCP case at $\Gamma_{ee} = 0.9$ obtained in the present work. The Holtsmark distribution is also shown for comparison. 53

3.9 The tails of electric microfield distributions at electron in a electron-positron plasma, neutral point at $\Gamma_{ee} = 0.9$, $T = 30000$ K, $n_e = 10^{27}$ m^{-3} in comparison with Margenau-Lewis (2.81), Baranger-Mozer (2.82), Holtsmark (2.25) and modified Potekhin approximations (3.52) (Sadykova et al., 2010b,a). 57

4.1 Comparisons among the $e-i$ HGK, Hellmann and Coulomb potentials at $T = 30000$ K for (a) Na^+ and (b) Cs^+ plasmas. 63
4.2 The HGK potential for different alkali plasmas (in atomic units). 63
4.3 Comparisons among the $e-i$ HGK, Fiolhais et al. and Coulomb potentials for Be^{2+} (in atomic units). 64
4.4 The $i-i$ HGK, hard core, soft core and Coulomb potentials for (a) Na^+ and (b) Cs^+ plasmas (in atomic units). 65
4.5 Comparison among the different $e-e$ pseudopotentials of semiclassical Li^+ plasma against the dimensionless distance $R = r/r_L$ at $T = 30000$ K, $\Gamma_{ii} = 0.2$ and $\Gamma_{ii} = 0.8$. 71
4.6 Comparison between the different $e-i$ pseudopotentials of semiclassical Li^+ plasma against the dimensionless distance $R = r/r_L$ at $T = 30000$ K, $\Gamma_{ii} = 0.2$ and $\Gamma_{ii} = 0.8$. 71
4.7 Comparison among the different $i-i$ pseudopotentials of semiclassical Li^+ plasma against the dimensionless distance $R = r/r_L$ at $T = 30000$ K, $\Gamma_{ii} = 0.2$ and $\Gamma_{ii} = 0.8$. 72
4.8 Electron-ion screened Hellmann-Gurskii-Krasko pseudopotentials of semiclassical Li^+ plasma against the dimensionless distance $R = r/r_L$, here $r_L = e^2/(4\pi\varepsilon_0 k_B T)$ at (a) $\Gamma_{ii} = 0.3$, $T = 1049715$ K, $n_e = 1.6 \cdot 10^{24}$ cm^{-3} and (b) $\Gamma_{ii} = 2$, $T = 40000$ K, $n_e = 0.26 \cdot 10^{23}$ m^{-3}. 72
4.9 Electron-electron, ion-ion (a) and electron-ion (b) Radial distribution functions of the screened Hellmann-Gurskii-Krasko pseudopotential of semiclassical Li^+ plasma against the dimensionless distance $R = r/r_L$ at $T = 30000$ K, $\Gamma_{ii} = 0.8$. 73
4.10 Comparison among the different $e-i$ HGK pseudopotentials and the different $i-i$ pseudopotentials for beryllium plasmas (Be^{2+}) (in atomic units). 74
4.11 Comparison among the various $e-i$ **(a)**, $e-e$ **(b)**, $i-i$ **(c)** pseudopotentials at $\Gamma_{ii} \approx 1.56$, $T = 8000$ K, $n_e = 10^{26}$ m^{-3} and $e-i$ pseudopotential **(d)** at $\Gamma_{ii} \approx 0.335$, $T = 8000$ K, $n_e = 10^{24}$ m^{-3} of Cs^+ plasma against the dimensionless distance $R = r/r_L$. 77
4.12 EMDs in the framework of the Hellmann-Gurskii-Krasko pseudopotential model for a K^+ and H^+ plasma at $T = 30000$ K and (a) $\Gamma_{ii} = 0.2$, (b) $\Gamma_{ii} = 2$ (MC) (Sadykova et al., 2009b). 79
4.13 EMDs in the framework of the Hellmann-Gurskii-Krasko pseudopotential model for a Na^+ and H^+ plasma at $T = 30000$ K and (a) $\Gamma_{ii} = 0.2$, (b) $\Gamma_{ii} = 2$ (MC) (Sadykova et al., 2009b). 80
4.14 EMDs in the framework of the Hellmann-Gurskii-Krasko pseudopotential model for a K^+ and H^+ plasma at $T = 30000$ K and (a) $\Gamma_{ii} = 0.2$, (b) $\Gamma_{ii} = 2$ (MC) (Sadykova et al., 2009b). 80

4.15 EMDs in the framework of the Hellmann-Gurskii-Krasko pseudopotential model for a Rb^+ and H^+ plasma at $T = 30000$ K and (a) $\Gamma_{ii} = 0.2$, (b) $\Gamma_{ii} = 2$ (MC) (Sadykova et al., 2009b). 81
4.16 EMDs in the framework of the Hellmann-Gurskii-Krasko pseudopotential model for a Cs^+ and H^+ plasma at $T = 30000$ K and (a) $\Gamma_{ii} = 0.2$, (b) $\Gamma_{ii} = 2$ (MC) (Sadykova et al., 2009b). 81
4.17 EMDs in the framework of the Hellmann-Gurskii-Krasko pseudopotential model for a Cs^+ plasma (a) and EMD comparison between Hard-Sphere and HGK models for Li^+ (b) plasma at $T = 30000$ K and $\Gamma_{ii} = 0.8$ (Sadykova et al., 2009b). 82
4.18 Comparison of EMD calculations in the framework of the Hellmann-Gurskii-Krasko pseudopotential model and Hard-Sphere Model for a Li^+ plasma at $T = 30000$ K and $\Gamma = 1.2$ (Sadykova et al., 2009b). 82
4.19 EMD in the framework of the Hellmann-Gurskii-Krasko pseudopotential model for a Li^+-plasma at $T = 30000$ K in dependence on Γ_{ii} in a range a) $\Gamma_{ii} = 0.2 \div 1$, b) its contour plot. 83
4.20 Comparison of MC results for EMDs in the framework of the Hellmann-Gurskii-Krasko pseudopotential model for alkali plasmas and H^+ plasma at $T = 30000$ K and $\Gamma_{ii} = 2$ (Sadykova et al., 2009b). 83
4.21 The EMD tails for a Cs^+, Na^+ and H^+ plasma at $T = 30000$ K and $\Gamma_{ii} = 0.2$ and $\Gamma_{ii} = 2$. 85
4.22 Comparison of EMD calculations in the framework of the Hellmann-Gurskii-Krasko pseudopotential model in a moderately coupled plasma approximation for H^+, a) Li^+, Na^+ and b) K^+, Cs^+ plasmas at $T = 30000$ K and $\Gamma_{ii} = 2$. 88

5.1 Comparison of a synthetic Li^{2+}-Lyman spectrum with the experimental data at $T = 300000$ K and $n_e = 4 \cdot 10^{25}$ m^{-3}. 97
5.2 Comparison among the electric microfield distributions obtained of Li^{2+} plasma at $T = 300\,000$ K and $n_e = 4 \cdot 10^{25}$ m^{-3} (Lorenzen et al., 2009). 98
5.3 Comparison of a synthetic Li II 548 nm line (Koubiti et al., 2011) with the experimental data (Doria et al., 2006) at $T = 38\,527$ K and $n_e = 0.22 \cdot 10^{24}$ m^{-3}. 99
5.4 The electric microfield distribution obtained in the present work for Li^+ plasma at $T = 38\,527$ K and $n_e = 0.22 \cdot 10^{24}$ m^{-3} in comparison with MD obtained by Nersisyan and Holtsmark distribution. 100

6.1 The charge-charge static structure factors S_{zz} (6.3) for alkali plasmas (Li^+, Na^+, K^+, Rb^+, Cs^+) within the HGK pseudopotential model as compared to our results obtained in the present work for hydrogen-like plasmas within the Deutsch pseudopotential model on a basis of Gregori et al.(Gregori et al., 2006b). 103
6.2 Static structure factors and the screening charge $q(k')$ for Be^{2+} plasma at $T_e = 20$ eV, $T_e' = 24.06$ eV, $z = 2$ and $n_e = 2.5 \times 10^{23}$ cm^{-3}. 106
6.3 The charge-charge static structure factors S_{zz} (6.5) for a beryllium plasma with $n_e \approx 2.5 \cdot 10^{23}$ cm^{-3}, $z \approx 2$, and $T_e = 20$ eV, $T_e' = 24.06$ eV. 107

6.4 The dimensionless dynamic charge-charge structure factor of alkali plasmas (Li^+, Na^+, K^+, Rb^+, Cs^+) determined within the HLPC potential model but with the HGK static characteristics in comparison with the results of (Adamjan et al., 1993) obtained within the same HLPC potential model but with the Coulomb static characteristics at $k = 0.767/r_{ee}$. 111
6.5 The dimensionless dynamic charge-charge structure factor of alkali plasmas (Li^+, Na^+, K^+, Rb^+, Cs^+) determined within the HLPC potential model but with the HGK static characteristics in comparison with the results of (Adamjan et al., 1993) obtained within the same HLPC potential model but with the Coulomb static characteristics at $k = 1.534/r_{ee}$. 112
6.6 The dimensionless dynamic charge-charge structure factor of alkali plasmas (Li^+, Na^+, K^+, Rb^+, Cs^+) determined within the HLPC potential model but with the HGK static characteristics in comparison with the results of (Adamjan et al., 1993) obtained within the same HLPC potential model but with the Coulomb static characteristics at $k = 1.074 \cdot r_{ee}$. 114
6.7 The dimensionless dynamic charge-charge structure factor of alkali plasmas (Li^+, Na^+, K^+, Rb^+, Cs^+) determined within the HGK pseudopotential model with the HGK static characteristics in comparison with the results of (Adamjan et al., 1993) obtained within the same HLPC potential model but with the Coulomb static characteristics at $k = 1.074 \cdot r_{ee}$. 115

List of Tables

1.1 The ionisation energies (eV) of alkali atoms (Ebeling et al., 1976) . . . 10

3.1 Plasma Parameters of consideration . . . 47
3.2 Plasma Parameters of consideration . . . 49
3.3 Nonideality parameter Γ_{ee}, magnitude of the most probable electric field measured at an electron and neutral point in TCP and power of the tail asymptote $\beta^{-\alpha}$ (Sadykova et al., 2010b,a). . . . 55

4.1 The parameters of the Hellmann-Gurskii-Krasko potential in atomic units (Gurskii and Krasko, 1971). . . . 65
4.2 Plasma Parameters of consideration . . . 70

1 Abbreviations . . . 128

Contribution to the Work

1. S. P. Sadykova, I. Valuev, W. Ebeling and I. M. Sokolov. *Plasma Physics Reports*:Nauka/Interperiodica-Pleiades Publishing Ltd., 36, No. 13, 1161-1166, 2010.

2. S. P. Sadykova, W. Ebeling and I. M. Tkachenko. *Eur. Phys. J. D.*, 61, 117-130, 2011.

3. S. P. Sadykova. Static and Dynamic Structure Factors with Account of the Ion Structure for High-temperature Alkali and Alkaline Earth Plasmas. *In Proceedings of the XXXVII European Physical Society Conferences on Plasma Physics*, pages 1-4, Dublin, 2010. (URL: http://ocs.ciemat.es/EPS2010PAP/pdf/P1.318.pdf).

4. S. P. Sadykova, W. Ebeling and I. M. Sokolov. *Contr. Plasma Phys.*, 51, 386-390, 2011.

5. S. P. Sadykova, I. Valuev, W. Ebeling and I. M. Sokolov. *Prikladnaja Phizika*, 1: 37-43, 2010.

6. S. P. Sadykova, W. Ebeling, I. Valuev and I. M. Sokolov. *Contr. Plasma Phys.*, 49: 388-402, 2009.

7. S. Sadykova, W. Ebeling, I. Valuev and I. M. Sokolov. *Contr. Plasma Phys.*, 46: 76-89, 2009.

8. S. Sadykova and W. Ebeling. *Contr. Plasma Phys.*, 47: 659, 2007.

9. S. P. Sadykova, W. Ebeling, et al. . *In the Conference of the German Physical Society on Plasma Physics* (The talk at the DPG 2005 in Berlin), Berlin, 2005. (URL: http://www.dpg-verhandlungen.de/2005/p25.pdf).

10. S. P. Sadykova, Y. V. Arkhipov and A. E. Davletov. *Izvestiya Nazcianal'noj Akademii Nauk Respubliki Kazakhstan* (phizika) , 6: 39-49, 2004.

Acknowledgements

I would like to express my sincere thanks first of all to my Father, Sadykov Polat Sadykovich, who all the way was inspiring and supporting me for my Ph. D. work with all his strong Spirit. My Ph. D. work would not have been possible without his financial support of my Ph. D. work at the Humboldt University at Berlin. I am tremendously thankful to him knowing the fact at which cost he was sacrificing everything to fulfill my dreams. I would like also to thank my mother, Sadykova Saule Baizhanovna, and sister, Sadykova Karlygash Polatovna, for giving me a permanent moral support and precious advices at the different life circumstances, and who accepted that we would not be seeing much of one another for the past few years.

I would like to thank Prof. Werner Ebeling for having been my supervisor and giving me a scientific, organizational support. It has been always for me a great honor and high responsibility to be his Ph. D. student. Prof. Werner Ebeling was helping me a lot by giving valuable scientific advices and suggestions. The most part of the work done I owe to his interest to my work, his patience he showed in answering my many questions and his diligent work as a supervisor and co-author of the number of articles, essays, projects that needed to be reviewed.

I would like to thank Prof. Igor Michajlovich Sokolov for being so kind to become my supervisor too. I am very grateful to him for providing me with the facilities to make a Ph. D. work, and also for financial, organizational support of my scientific conferences. I also thank him for precious advices about the fundamental Holtsmark distribution, Hertz theory and number of interesting lectures.

I would like to express my gratitude to Academician Prof. Anri Amvros'evich Rukhadze for his consultation and precious advices about the electric microfield theory. It was a great honor for me to have private communications with him !

My acknowledgement goes to Prof. Lutz Schimansky-Geier for being alway kind to me and providing a friendly working atmosphere in the group. I also would like to thank Prof. Lutz Schimansky-Geier and Prof. I. M. Sokolov for their scientific seminars which were not only interesting but also allowed to gain new insights into various disciplines and methodologies.

I further owe a debt of gratitude to PD. Dr. Bernd Esser for being always very nice to me, for his scientific advices and series of valuable books which he kindly granted to me for broadening of my scientific horizons.

I would like to express my gratitude to the ERASMUS-MUNDUS foundation for the scholarship which I was privileged to benefit from during the last two years of my research, which also made doing of my Ph. D. at the Humboldt university at Berlin possible.

My sincere thanks go to Dr. Mohammed Koubiti, from CNRS/Université de Provence, centre Saint-Jérôme, for his diligent work on the theoretical optic L^+ spectra which allowed to get more comparisons with experiments and in this way increased the value of my Ph.D. work.

My acknowledgement goes to Prof. Costello, from the Dublin City University, the National Centre for Plasma Science and Technology, and Prof. H. Luna, from Federal University of Rio de Janeiro, Institute for Physics, for their quick aid in getting the experimental data for comparison.

I further owe my gratitude to Prof. Wolfgang Nolting for his valuable lectures on : "Many-particle Physics" which allowed to deep my knowledge in this discipline.

I would like to thank Dr. G. Motz for always being a great support for me in difficult situations, for her precious suggestions which helped me to overcome different problems.

I would like to thank Evi Poblenz, who was helping me a lot in a search for a financial support, for her dedication to her voluntary work on promotion of women in science which she used to do from the bottom of her heart.

I would like to express my deepest gratitude to the city secondary school specialized for physics and mathematics in Alma-Ata, Kazakhstan where I had an honor to be graduated from, all my teachers, especially to A. A. Chernobaj, who were inspiring us for the science and gave us a high hope for the best future!

I would like to thank all my close friends: Vladislav Sechin who studied with me at the city secondary school specialized for physics and mathematics in Alma-Ata and who has been backing me all the way, Emmanuell Schmieder, Valentina Forini, Gergana, David Sperber, Federico Camboni, Martin Mamach for being very kind, generous and supportive to me, and who always provided open ear for my ramblings on different topics.

I would like to express my sincere thanks to Dipl. Phys. Michael Happ for help and always welcoming a great number of my questions related to computers and software.

Our diploma student, Bernard Sonnenschein, also was so kind as to help with the translation of the abstract into the scientific German language.

My sincere thanks go to Dipl.-Ing. Josephine Auerbach for her dedication to her work and her readiness to help every one.

Selbständigkeitserklärung

Ich erkläre, dass ich die vorliegende Arbeit selbständig und nur unter Verwendung der angegebenen Literatur und Hilfsmittel angefertigt habe.

Berlin, den 03.01.2010 Saltanat Polatovna Sadykova